# HYDRODYNAMICS AND MORPHOLOGY AROUND BRIDGE PIERS IN SEEPAGE AFFECTED ALLUVIAL CHANNEL

*Thesis submitted in partial fulfilment of the requirements*

*for the award of the degree of*

**Doctor of Philosophy**

in

Civil Engineering

by

**Rutuja Chavan**


DEPARTMENT OF CIVIL ENGINEERING

INDIAN INSTITUTE OF TECHNOLOGY GUWAHATI,

GUWAHATI-781039, INDIA

JANUARY 2018

*Dedicated to*

***my Family***

# Declaration

I, Rutuja Chavan, declare that this thesis titled, “Hydrodynamics and Morphology around Bridge Piers in Seepage affected Alluvial Channel” and the work presented in it are my own. I Confirm that:

• The work contained in this thesis is original and has been done by myself and under the general supervision of my supervisor(s).

• The work reported herein has not been submitted to any other Institute for any degree or diploma.

• Whenever I have used materials (concepts, ideas, text, expressions, data, graphs, diagrams, theoretical analysis, results, etc.) from other sources, I have given due credit by citing them in the text of the thesis and giving their details in the references.

• I also affirm that no part of this thesis can be considered plagiarism to the best of my knowledge and understanding and take complete responsibility if any complaint arises.

• I am fully aware that my thesis supervisor(s) are not in a position to check for any possible instance of plagiarism within this submitted work.

Date: Rutuja Chavan

Department of Civil Engineering
Indian Institute of Technology Guwahati
Guwahati - 781039 Assam India

Dr. Bimlesh Kumar
Associate Professor
0361-2582420
bimk@iitg.ernet.in

# Certificate

This is to certify that this thesis entitled "Hydrodynamics and Morphology around Bridge Piers in Seepage affected Alluvial Channel " submitted by Rutuja Chavan, in partial fulfilment of the requirements for the award of the degree of Doctor of Philosophy, to the Indian Institute of Technology Guwahati, Assam, India, is a record of the bonafide research work carried out by her under my guidance and supervision at the Department of Civil Engineering, Indian Institute of Technology Guwahati, Assam, India. To the best of my knowledge, no part of the work reported in this thesis has been presented for the award of any degree at any other institution.

Date:

Place: IIT Guwahati

(Dr. Bimlesh Kumar)

# Publications

**Journals**

- Rutuja Chavan, Anurag Sharma and Bimlesh Kumar- Effect of Downward seepage on Turbulent characteristics and Bed Morphology around Bridge piers, Journal of Marine Science and Application, 16, 1, 60-72, 2017.
- Rutuja Chavan, and Bimlesh Kumar- Experimental Investigation on Flow and Scour Characteristics around Tandem Piers in Sandy Channel with Downward Seepage, Journal of Marine Science and Application, 16, 3, 313-322, 2017.
- Anurag Sharma, Rutuja Chavan and Bimlesh Kumar- Multi-Scale Statistical Characterization of Migrating Pier Scour Depth in Non-Uniform Sand Bed channel, The International Journal of River Basin Management, 15, 3, 265-276, 2017.
- Rutuja Chavan, B. Venkataramana, P. Acharya and Bimlesh Kumar- Comparison of Scour and Flow characteristics around Circular and Oblong Bridge piers in Seepage affected Alluvial Channel, Journal of Marine Science and Application (accepted for publication).
- Rutuja Chavan, and Bimlesh Kumar- Prediction of Scour Depth and Dune Morphology around Circular Bridge Piers in Seepage Affected Alluvial Channel, Environmental Fluid Mechanics (accepted for publication).

*Communicated*

- Rutuja Chavan, and Bimlesh Kumar- Suction Effects on Dynamics of Migrating Scour Depth and Dune- Like Bedforms at Tandem Piers, Canadian Journal of Civil Engineering, (Revision sent).
- Rutuja Chavan, and Bimlesh Kumar- Hydrodynamics and Morphology around Tandem Piers of Different Diameters in Alluvial Channel with Downward Seepage, Environmental Fluid Mechanics, (Under review ).
- Rutuja Chavan and Bimlesh Kumar- Turbulent Flow Structures and Scour Hole Characteristics around Circular Bridge Pier over Non-uniform Sand Bed Channel with Downward Seepage, Sediment Research, (Under review).

**Conferences**

- Rutuja Chavan and Bimlesh Kumar Development of Incipient Motion Criteria for Alluvial Channel, National Conference On Water and its Sustainability in mining and Other Environment: Vision 2050 on March 28-29, 2014, Department of Civil Engineering, Indian School of Mines, Dhanbad.
- Rutuja Chavan, Pratik Acharya and Bimlesh Kumar -Experimental investigation of turbulent flow structures and scour depth around bridge pier in an alluvial channel with downward seepage, IBMS 2016 Conference on 4th & 5th October 2016 at NDMC Convention centre, New Delhi.
- Rutuja Chavan, B. Venkataramana and Bimlesh Kumar -Investigation of turbulent flow statistics and bed morphology around circular bridge pier, Proceedings of International Conference on Hydraulics, Water Resources and Coastal Engineering (Hydro2016), CWPRS Pune, India, 8th to 10th December 2016, pp 115-119.
- Rutuja Chavan, Nairita Mukhopadhyay, Anurag Singh and Bimlesh Kumar - Comparison of existing equation for scour at bridge piers using laboratory and field data, Proceedings of International Conference on Hydraulics, Water Resources and Coastal Engineering (Hydro2016), CWPRS Pune, India, 8th to 10th December 2016, pp 642-648.
- Rutuja Chavan and Bimlesh Kumar -Flow analysis and scour around piers in tandem arrangement, Proceedings of International Conference on Hydraulics, Water Resources and Coastal Engineering (Hydro2016), CWPRS Pune, India, 8th to 10th December 2016, pp 928-932

# Acknowledgements

Many people have directly or indirectly contributed to my doctoral work. This thesis could not be completed without assistance, understanding and counselling of several people throughout the research. Before presenting my research work, I would like to take the opportunity to humbly acknowledge all of them for their constant support and guidance.

First and foremost, I would like to express my sincere gratitude to my supervisor **Dr. Bimlesh Kumar** for his support and guidance during my PhD study. He showed tremendous confidence in me and was very patient, for which I shall always be indebted to him. I appreciated all his contributions of time and ideas to make my doctoral research experience productive and stimulating. I feel fortunate to have him as a mentor of my thesis. I also owe to his wife **Dr. Jaishree Karan Prabha** for her love and care as a family.

I would also like to give my sincere thanks to the members of my doctoral committee: **Dr. Ajay Kalamdhad** (Chairman), **Dr. Manish Kumar Goyal**, **Dr. Nanda Kishore and Dr. Rishikesh Bharti** for their insightful comments, encouragement, guidance and valuable time through this research.

I owe sincere thanks to the Ministry of Human Resources and Development, Govt. of India for providing fellowship for the duration of my PhD. I would like to thank Indian Institute of Technology for such a pleasant atmosphere and the advanced facilities like a central workshop, central library and state of art facilities to carry out the research.

I am indebted to my Lt. **Aaji** (grandma) for her blessings, my **Baba** (grandpa) for his unconditional support and belief in me because of which I could reach up to this level. I gained a lot from my grandparents, when I was a child my mind was like a raw material, and those were your wrists, which moulded this raw material in some useful shape.

I will always be grateful to my parents, **Aai** (Prof. Jyoti Chavan) and **Pappa** (Prof. M. D. Chavan) for supporting and believing me throughout my studies. The sacrifice you did for me cannot be repaid ever. Much obliged to you for enabling me to settle on my own

choices at each phase of life. Special thanks to my lovely brother **Darshan**, who always stood for me in every situation. The long chats and discussions with him regarding society, current affairs, politics, life and so forth are brain boosting for me.

Most importantly, I am incredibly indebted to my husband **Mr. Sagar Pawar** for his great love, kind patience and invaluable support. Thank you for being a vital source of encouragement when I feel lack of faith and energy. Without his help, it would not be possible for me to complete this work and write the thesis. The bond of friendship and love between us made me far more grounded which I could have never envisioned. He made me laugh countless times and consistently helped me when I was in torment and my mind got blank. I would like to acknowledge my **in-laws** (Aai and Pappa) for their understanding, love and affection throughout my PhD research.

Before starting my research, it was my first step to be in well verse with the sophisticated instruments that would be needed in my research. I would like to express my gratitude towards **Dr. Bebina Devi** and **Anurag Sharma** for introducing me to the instruments.

I am indebted to **Bazal Da** for his assistance and guidance to conduct the experiments. He was always available whenever I required, without him these experiments were not possible to perform smoothly. I would like to acknowledge the security guards of the civil engineering department at IITG who have always been very helpful when we were performing experiments in the night.

My sincere gratitude to my two M.Tech juniors cum younger brothers **Bonu** and **Pratik** without their support and help it would not be easy for me to carry such a huge number of experiments. Both of them have provided extreme help in my experimental work and always motivated me when I felt so down. Besides, I would like to thank my juniors **Barsharani**, **Ashok**, **Shubham** and **Anurag** for giving me their time and helping me in the experiments. Additionally, the help extended by summer interns Nairita, Vindhya and Mrigakshee cannot be left unmentioned.

I would like to thank my friends cum family Shivani, Abhishek and Ankita for all the cherish moments we had together. I am thankful to Varsha, Shravani, Bala, Siddhartha and MH Civil @ IITG group as their presence on campus brought lots of fun. I also thank IITG Maharashtra Mandal.

I thankfully acknowledge the Physiotherapist at IITG Hospital, Mr. Kandarpa Jyoti Das, because of his consistent efforts I could manage to bend for a couple of hours and carry heavy instruments when I have even lost the hope of sitting at one place for a couple of hours.

I gratefully acknowledge Dr. Sandeep Mali and Dr. Bajad (Dept. of Civil Engineering, SCOE- Pune) for their support and advice, which were very helpful in the journey.

Providence brought in touch with many helpful people. I could not name everyone, but I am indeed thankful to all of them for their help.

Finally, I bow my head to the **Supreme Lord** in deepest gratitude and seek blessings.

# Abstract

The scour around bridge piers is a contributor to the waterway bridges failure. Prediction of scour depth is one of the most significant problems in designing of bridges. Due to the complexity of scour phenomenon, available empirical equations do not always offer accurate scour depth prediction. For proper estimation of scour depth, deep understanding of flow structures around bridge piers is essential. The present research work experimentally investigates the flow field and its consequences on scour geometry around bridge piers. The experiments were carried out in a straight flume with the bed made up of non-uniform sands. Two different diameters of piers and two different types of sands used for experimentation. Experimentation has been done for single pier and tandem piers. An important feature of sand bed channels, downward seepage, was considered in the present work. The present work focuses on the effect of downward seepage on flow statistics and bed morphology around piers. Two different seepage percentages, 10% and 15%, were considered for exploring the change in flow characteristics with respect to no seepage case.

Turbulent structures of the flow around single piers and tandem piers have been analysed for with and without downward seepage through channel boundaries. From the measurements of turbulent characteristics such as time-averaged streamwise velocity, Reynolds stresses; a strong reversal flow near the bed at upstream of piers and near the free surface at downstream of piers have been observed. The turbulent kinetic energy, Reynolds normal stresses are found to be increased near the edge of the scour hole. The flow field around tandem piers is more complex than single pier as the rear pier hinders the wake region behind the front pier. Analysis of bursting events shows that sedimentation effect prevails within the scour hole whereas outside the scour hole erosive forces become more dominant. However, with downward seepage the reversal flow at upstream and downstream of piers due to flow separation is decreased. The decreased magnitude of turbulent statistics like velocity, Reynolds stresses, TKE, third order moments at upstream of pier on the application of seepage shows the hindered erosive capacity of flowing stream.

The scour depth at pier with larger diameter is greater than the pier with smaller diameter in all the experimental runs. In case of tandem piers, the scour depth at front pier is greater than the scour depth at rear pier due to sheltering effect of front pier. The scour depth at both single and tandem piers is reducing with increasing seepage percentages. The rate of development of scour depth is more in case of no seepage runs than with seepage runs. The scoured material is deposited behind piers, forming a dune like structures. Empirical relationships have been developed for estimation of scour depth and dune morphology around single piers in the presence of downward seepage.

The multi-scale statistical characterization of migrating scour depth at piers and dune like bedforms forming behind the piers has been carried out. The celerity of migrating scour depth is decreasing with time as well as decreasing with increasing downward seepage. Probability density function (pdf) of bedform elevation has positive tail slightly thicker than the Gaussian. We quantified the presence of rich multiscale statistical structure, using wavelet decomposition and estimated scale dependant celerity of migrating dune like bedforms occurring behind the piers. The decreasing celerity of migrating dune like structure with respect to time and downward seepage shows the faster movement of smaller bedforms relative to larger one at downstream of tandem piers.

***Keywords:*** Celerity, Downward seepage, Reversal flow, Scour, Turbulent structures, Wake, Wavelet decomposition

# Content

# List of figures

# List of Tables

# Abbreviations

| | |
|---|---|
| $Al$ | Alignment factor |
| $b$ | Width of pier |
| $B$ | Distance between consecutive piers |
| $ds$ | Scour depth |
| $D$ | Diameter of pier |
| $Fd$ | Froude number |
| $Fd_c$ | Critical Froude number |
| $h$ | Flow depth |
| $H_D$ | Height of dune |
| $K_I$ | Flow intensity factor |
| $K_s$ | Pier shape factor |
| $K_\alpha$ | Pier alignment factor |
| $K_{bed}$ | Bed condition factor |
| $R$ | Hydraulic radius |
| $Re$ | Reynolds number |
| $Re_s$ | Seepage Reynolds number |
| $Sh$ | Shape factor |
| $U$ | Average velocity |
| $U_{cr}$ | Critical velocity |
| $X_D$ | Streamwise distance of dune crest from pier |
| $d_{50}$ | Median sand diameter |
| $Vs$ | Seepage velocity |
| $\sigma_g$ | Standard deviation |
| $g$ | Gravitational acceleration |
| $\upsilon$ | Kinematic viscosity |
| $\alpha$ | Blockage ratio |

# Chapter 1

# Introduction

## 1. 1 Overview

In the field of hydraulic engineering, river flow and problems associated with it such as sediment transport, deformation of the riverbed, flooding and scouring are considered as the significant issues in the development of a country. Deformation of the riverbed at bridge site is critical and has been the subject of intrest to hydraulic engineers and designers. The main reason behind the changes in bed elevation at bridge sites are aggradation and degradation of the riverbed; temporary scour due to changes in river condition and presence of hydraulic structures like bridge piers, which obstruct the flow and resulting in constriction of stream that leads to scouring around piers (Melville, 1975).

Bridges are one of the most important hydraulic structures as they facilitate rapid and safe movement of goods and personnel across the rivers (Kothyari, 2008). While flood damages typically involve widespread inundation of agricultural land, destruction of homes and businesses and disruption of economic activity, a less obvious threat is the existence of bridges over waterways that cause flow obstruction and scour around the bridge foundations with the possible failure of the bridges. Major damage to bridge crossings occurs during floods which can endanger the lives of travelling public and causes costly disruptions to traffic flow. Thus, bridge failure will result in disaster and has profound social and economic impact. In the history of bridge failure, scour around bridge piers has been identifying as the primary cause of concern on the stability of bridges (Smith, 1976; Jones et al., 1995; Melville and Coleman, 2000). Statistical studies of last few decades show that scour around bridge piers is a significant reason behind major damage to bridges. Since 1950 in the United States, 60% of 823 bridges have been damaged or collapsed due to riverbed scour (Shirhole and Holt, 1991). Railway bridge RDG1 in England failed in November 2009 due to undetermining. According to their study, U.S. Federal Highway Association reported that every year about 50 bridges have failed in the US annually and out of this number 50% bridges have failed due to scour around piers which results in higher cost of maintenance.

The hydrodynamic forces of flow, transport sediments from resting position to new location in the bed. Because of the erosive action of the flowing water, there is a tendency for the pier foundation to be exposed by this action. With the prospect of more severe and more frequent floods due to climatic change, reducing the risk of bridge failure is increasingly becoming important. Bridge damage has deep social and economic implications due to the costs of reconstruction, maintenance and monitoring of existing structures, the disruptions of traffic flow circulation and in some cases the costs of human lives. Analysis on the failure risk of bridges affected by scouring that include economic feasibility study of possible countermeasures to prevent bridge collapse with appropriate bridge foundation design are useful for engineers to make assesment on the proposed intervention plans and define new design approach. Scouring around piers has been a concern as it affects stability of the bridge foundation. Melville and Coleman (2000) have made emphasis on the impacts of scour around piers on bridge stability.

## 1.2 State of art

The previous studies and investigations are summarised in this section. The explanations are followed by types of scour, mechanism of scour, factors affecting scouring, scour depth prediction methods and description of flow around bridge piers.

### 1.2.1 Scour at Bridge Piers

Scour is the removal of sediment particles around the structures constructed in path of flowing stream due to the erosive action of flowing stream such that there is a tendency to expose the foundation of the structure, which may result in structural collapse (Elsabaie, 2013). Scour at a pier is caused due to the forces exerted on the bed by the complex, highly three-dimensional and unsteady flow field generated by the pier (Kirkil et al., 2008). Scour is a worldwide phenomenon and of great concern especially to civil engineers as any structure constructed in a flowing stream, will tend to advance scour around pier due to a sudden change in the flow pattern. Scour is the natural phenomenon brought about by the erosive action of flowing stream in alluvial channels (Breusers et al., 1977). Scour is the lowering of the streambed, which takes place around a structure constructed in flowing water (Garde and Kothyari, 1998). Lowering of bed can be attributed to the three-dimensional flow separation and sediment transport around piers (Garde and Raju, 2000). The extent of reduced bed level from the initial bed level of the

stream is the scour depth (Melville and Coleman, 2000), Cheremisinoff et al., (1987) affirmed that scour can either be caused by normal flows or flood events. The higher flow velocity may lead to increase the rate of scouring during flood events than normal flow conditions. According to Melville and Coleman, (2000), the total scour at bridge crossing comprised of general scour, contraction scour and local scour.

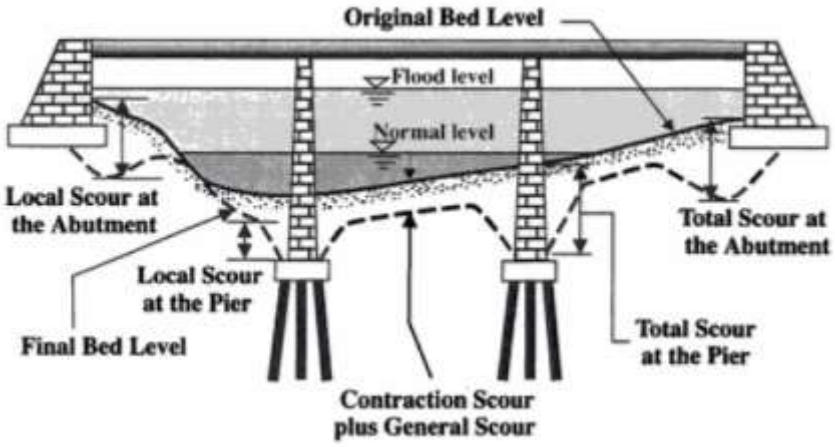


Figure 1.1 Types of scour that can occur at bridge (Melville and Coleman, 2000)

#### 1.2.1.1 General Scour

General scour forms due to natural process and is the general removal of bed material from river bed that corresponds to the change in river characteristics. This type of scour occurs irrespective of any structural obstruction. It can be referred as bed aggradation/degradation and is categorized as short-term scour and long-term scour according to the time it takes to reach the scour. Short-term general scour occurs during single or sequential floods (daily, weekly, monthly or seasonally). Scour at channel confluences, scour at bends, scour arising from a shift in the channel thalweg and bed-form migration are included in short-term general scour (Coleman and Melville, 2001). Because of the fact that formation of contraction scour and local scour dominate over that of short-term scour, it is tough to anticipate it at the structure; hence, short-term scour is not included in the design computations. Long-term general scour forms naturally or develops with some modifications at watershed and stream and undoubtedly occurs over the years and has a relatively longer timescale. Human causes of long-term general scour are channel alterations, streambed mining and dam/reservoir construction. In addition,

channel straightening, tectonic activities, fire and climate change develop long-term scour naturally.

#### 1.2.1.2 Contraction Scour

Contraction scour tends to occur at entire bridge section due to contraction of flow. Construction of piers across channel will result in the reduction of the channel flow area. Reduction in channel flow area will result in the increase in velocity and shear stress and subsequent increase in the erosive forces. In respond to the above actions the removal of bed material from the contracted reach will be further induced which can cause lowering of the bed elevation. This process continues until the equilibrium is reached. Bed elevation is lowered, average velocity and bed stress decrease at the reach and the amount of bed material removed from the reach becomes equal to that of bed material transported to the reach.

#### 1.2.1.3 Local Scour

According to Melville and Coleman (2000), localized scour is a collective term of contraction scour and local scour. Local scour occurs when an obstruction is introduced into the flow (Melville, 1994). Presence of manmade structures like piers, abutments in rivers, alters the flow patterns and accelerates the flow around structures consequently erode the bed material around the structures. According to the condition of bed load transport, local scour can be divided into clear water scour and live bed scour.

Clear-water scour occurs when the bed material at the upstream of the bridge structure has no motion. Under clear-water conditions, pier foundation is eroded rapidly at the early stages, but subsequently, scour hole development reaches equilibrium as the magnitude of the shear stresses is reduced due to the flow alteration caused by the generation of scour hole. At the equilibrium time, sediment is not transported to or carried away from the hole.

Live bed scour occurs when there is transport of bed material from upstream reach of the channel. In case of live bed scour, the scour hole is continuously supplied with the sediment transported from upstream reach. The equilibrium scour depth is reached when the rate of sediments feed to the scour hole is equal to the rate of sediment transported out from the scour hole.

### 1.2.2 Mechanism of Local Scour

Many researchers have stated that the vortex system around piers is the basic mechanism behind local scour (Melville, 1975; Ettema, 1980; Y M Chiew, 1984; Melville and Coleman, 2000; Qadar, 1981; Richardson and Davis, 2001). Melville (1975)and Chiew (1984) have reported that the vortex system around bridge piers in the primary cause of scour around piers. The increased velocity near bed due to horseshoe vortices around piers results in increasing sediment transport capacity of flow. The wake vortices keep sediment in suspended position and carried the eroded material at downstream side. Melville and Coleman (2000) have stated that down-flow and surface roller at upstream of pier, horseshoe vortex at base of pier and wake vortices at downstream side of pier are the principal features of the flow field around bridge piers. Figure 1.2 shows schematic diagram of scour process around bridge piers.

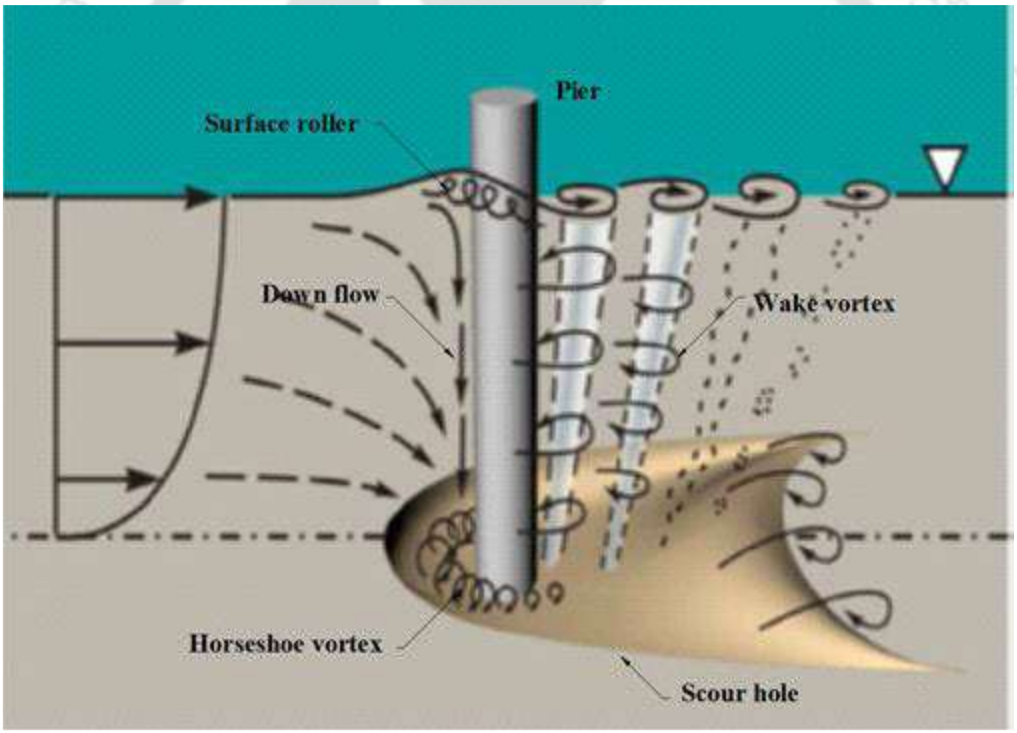


Figure 1.2 Schematic diagram of scour process around bridge piers, (Ettema and Melville, 2011)

For fully turbulent flow stagnation line form at the upstream face of the pier with decreasing pressure towards the bed. This decreasing pressure gradient occurs due to velocity profile of approaching flow being much slower closure to the bed. The

combination of the downward flow and the incoming flow around the pier results in a flow separation and the formation of a vortex at the bed around the pier. The approaching flow curves down a horseshoe vortex, which resembles a shape of "horseshoe". To take the point, it is of note to express that horseshoe vortex is developed after the scour hole generation. As it is formed as a consequence of a scour, horseshoe vortex takes an important role in transporting material away from the scour hole. Downflow and horseshoe vortex play a major role in scour process. Due to the shear stress gradients at the upstream side of the pier, the wake vortices originate from flow separation at the sides of the pier. With the effect of downflow, wake vortices are transferred downstream by the approach flow and behave like vacuum cleaners picking up and carrying the sediment entrained by the downflow and horseshoe vortex. The strength of wake vortices decreases very quickly as the distance downstream of the pier increases. When compared to horseshoe vortex, the intensity of wake vortices is weaker. Thus, maximum scour depth occurs at the upstream face of the pier. In addition to this, the water surface rises at upstream of pier and forms surface rollers which rotate in the counter direction of horseshoe vortex. The surface rollers influence horseshoe vortex, as long as the flow depth is lesser, the surface rollers affect the horseshoe vortex to become weaker, so the scour depth is reduced for shallow flow (Richardson and Davis, 2001).

### 1.2.3 Factors Affecting Scour Depth

Scour around bridge pier is complex interaction between flow structures and bed material and the extent of scour depends on the fluid properties and geometry of pier. According to Melville and Coleman, (2000) the functional form of scour depth with different parameters can be written as follow:

$$ds = f\{\text{fluid}(\rho, \upsilon, g), \text{flow}(h, U), \text{bed material}(\sigma_g, d_{50}, U_c), \text{pier geometry}(D, Sh, Al)\} \quad (1.1)$$

Where, $ds$ is scour depth at piers, $\rho$ is density, $\upsilon$ is kinematic viscosity, $g$ is gravitational acceleration, $h$ is flow depth, $U$ is average velocity, $\sigma_g$ is standard deviation of sand, $d_{50}$ is median sediment diameter, $U_c$ is critical velocity, $D$ is pier diameter, $Sh$ and $Al$ are pier shape and alignment factors respectively. By applying Buckingham π- theorem, Eq. 1.1 can be reduced to set of non-dimensional variables for dimensionless scour depth as follows:

$$\frac{ds}{D} = f\left\{\frac{U}{\sqrt{gh}}, \frac{Uh}{\upsilon}, \frac{U}{U_c}, \frac{h}{D}, \frac{D}{d_{50}}, \sigma_g,\right\} \tag{1.2}$$

Where, $\frac{U}{\sqrt{gh}}$ is Froude number, which includes the effect of gravity, $\frac{Uh}{\upsilon}$ is Reynolds number that includes the effect of viscosity, $\frac{U}{U_c}$ is ratio of velocity and critical velocity, $\frac{h}{D}$ is ratio of flow depth and pier diameter, $\frac{D}{d_{50}}$ is ratio of pier diameter and median sediment size and $\sigma_g$ is standard deviation. However, many of the prediction methods did not account Reynolds number as similarity requirements posed by the Froude number, and Reynolds number can typically not be satisfied at the same time. Reynolds number effect or viscous effect is not much significant in turbulent flow, and usually, free surface flows are governed by gravity forces. Hence, most of the models have considered Froude number for scaling. $U_c$ is the critical velocity at which incipient motion of sediment will occur. There could be possible relationship between incipient motion and bed material type. When the average velocity exceeds critical velocity ($U/U_c$ >1), sediment particles will be carried by approaching flow and scouring is considered as live bed scour. However, if $U/U_c$ is less than unity then clear water scour occurs and this is typical of flow over alluvial channels (Ettema and Melville, 2011). According to previous studies, it has been noted that the effect of $U/U_c$ is indistinct in comparison to the influence of flow shallowness ($h/D$) (Mohamed et al., 2005). Piers are classified as narrow, wide and intermediate pier depending upon the flow shallowness ($h/D$). When 0.2< $h/D$ <1.4, then the piers are classified as intermediate piers where scour depth depends on both water depth and width of the pier. For $h/D$ < 0.2, scour depth is influenced by the height of water. If $h/D$ is, greater than 1.4 then piers are said to be narrow piers where for narrow piers maximum scour depth is found to be at upstream of piers (Ettema and Melville, 2011) and it is dependent on pier width where flow depth no longer influences the scour depth (Johnson and Torrico, 1994). The effect of relative sediment coarseness ($D/d_{50}$) on scour depth is quite inconsistent. Melville and Coleman, (2000) have described that sediment size influence is negligible for $D/d_{50}$ >50. It has been shown that the scour depth decrease with increasing $D/d_{50}$. However, if $D/d_{50}$ > 100, there is limited effect on scour depth due to the scaling of sediment size (Lee and Sturm, 2009). The sediment non-uniformity or geometric standard deviation ($\sigma_g$) is described in several different ways.

Under armouring conditions, the coarser particles can help to reduce the scour depth. In case of non-uniform sand scour depth is influenced by geometric standard deviation ($\sigma_g$) of bed material (Kothyari, Raju and Garde, 1992). For circular piers, the shape factor *Sh* is unity and alignment factor *Al* is not required (Ettema and Melville, 2011). In spite of the fact that there is no extensive documentation on particular arrangement of dimensionless factors ought to be framed thus, it can be contended that the dimensional variables should include all the parameters affecting scour depth and flow interaction around piers.

### 1.2.4 Estimation of Scour Depth

For the safety of bridges, accurate prediction of scour depth is necessary as underestimation may lead to failure of structure and overestimation will lead to increase in the construction cost (Melville and Coleman, 2000). Therefore, proper estimation of scour depth is necessary to determine the optimum foundation depth for bridge piers. Many researchers have focused on estimating maximum scour depth around bridge piers (Breusers, Nicollet and Shen, 1977; Raudkivi and Ettema, 1983; Chiew and Melville, 1987; Melville and Coleman, 2000). Inglis (1949), Ahmad (1953), Chitale (1962) and Blench (1969) have developed regime equations for stable irrigation canals in India.

The methodology adopted in IRC-5 (1998) and IRC-78 (2000) to estimate the scour depth $d_s$ is based on Lacey (1930) regime theory and is given below:

$$d_s = KD_{LQ} \tag{1.3}$$

Where,

$$D_{LQ} = 0.47(Q/f)^{1/3} \tag{1.4}$$

And

$$f = 1.76\sqrt{d} \tag{1.5}$$

Where, $Q$ is discharge in $m^3/s$, $D_{LQ}$ in m and $f$ is Lacey's silt factor related to the median size of bed material $d$ (mm). $K$ varied from 1.76 to 2.59 with an average of 2.09. According to Inglis (1949), $d_s$ is given by equation,

$$d_s = 2D_{LQ} \tag{1.6}$$

Above equations currently being used in most hydraulics engineering applications in India with regards to scour around bridge piers.

Chabert and Engeldinger (1956) have conducted laboratory experiments to investigate the effect of time and velocity on clear water and live bed scour at bridge piers. They have carried 300 experimental runs using different sizes and shapes of the piers in various channels. They have also studied some protective measures of scour.

IAHR Model (Breusers et al., 1977) for clear water scour depth,

$$ds/b = 2.3K_{\sigma}K_{(b/d_{50})}K_dK_sK_{\alpha} \tag{1.7}$$

For live bed scour,

$$ds/b = XK_{(b/d_{50})}K_dK_sK_{\alpha} \tag{1.8}$$

Where, $K_{\sigma}$ is sediment non-uniformity factor, $K_{(b/d50)}$ is sediment coarseness factor, $K_d$ is sediment size factor, $K_s$ and $K_{\alpha}$ are pier shape and alignment factor respectively. $X$ varies from 2 to 2.3 for uniform sands and 0.5 to 2 for non-uniform sands.

Ettema (1980) have reported that the equilibrium scour depth at bridge piers is reached after 14 days. In addition to this, he has classified different phases of development of scour hole as the initial phase when the development of scour hole is very rapid, the erosion phase in which scour depends upon the strength of horseshoe vortex and equilibrium phase which is associated with the equilibrium scour depth.

Yanmaz and Altinbilek (1991) have conducted experimental runs for various durations such as 5min, 20 min, 60 min and 150 min. They have studied the variation in scour geometry with respect to time and developed semi-empirical equation based on sediment continuity equation to determine scour depth as a function of time.

Kothyari et al., (1992) have conducted experiments on temporal variation of scour depth around a circular bridge pier. Kothyari-Garde-RangaRaju (K-G-R) model (1992), for clear water scour:

$$ds/d_{50} = 0.66(b/d_{50})^{0.75}(h/d_{50})^{0.16}\left\{\left(U^2 - U_c^2\right)\rho/\left(\Delta\gamma_s d_{50}\right)\right\}\alpha^{-0.3} \tag{1.9}$$

For live bed scour,

$$ds/d_{50} = 0.88(b/d_{50})^{0.67}(h/d_{50})^{0.4}\alpha^{-0.3} \quad (1.10)$$

Where, $\alpha$ is blockage ratio ( $\alpha = (B-b)/B$ ).

Nazariha (1996) have conducted experiments for 90 hours long duration and stated that 83% of total active scouring occurs within first two hours before the rate of scouring is slowed down.

Parola et al., (1996) investigated that the foundation of bridge pier affects the scour depth. Foundation tends to minimize the scour depth when it is placed below the streambed. Scour depth is more sensitive if the top elevation of the foundation is above the streambed. Foundation extended in length in upstream twice the pier width and placed below the bed level protected the streambed at upstream of the pier from scour.

Melville and Chiew, (1999) have carried out laboratory experiments to determine the time to reach equilibrium scour depth. Estimation of equilibrium scour depth is necessary to avoid inherent difficulty like when to stop the experiment. Thus, they have introduced a definition of equilibrium scour depth as *te* is the time at which scour hole develops to the equilibrium depth, *dse*, at which the rate of increase of scour does not exceed 5% of the pier diameter in succeeding 24 hours.

Melville and Coleman (2000) have developed a mathematical model for estimation of scour depth depending upon various *K* –factors is given as,

$$ds = K_h K_I K_d K_s K_\alpha K_t \quad (1.11)$$

Where, $K_h$ is flow depth –pier size factor, $K_I$ is flow intensity factor, $K_d$ is sediment size factor, $K_s$ is shape factor, $K_\alpha$ is alignment factor, and $K_t$ is the time factor. All *K* -factors are derived from the relationship between various parameters like flow depth, velocity, geometry of pier, sediment size and their significance on scour depth around piers.

HEC-18 (Richardson and Davis, 2001) model is given by,

$$ds/b = 2K_s K_\alpha K_{bed} K_a (h/b)^{0.35} Fr^{0.43} \quad (1.12)$$

Where, $K_{bed}$ is a factor for bed condition, $K_a$ is a factor for armouring of sediments.

Oliveto and Hager (2002) have conducted laboratory to investigate temporal evolution of scour depth at piers and abutments with total six different sediment sizes out of which

three are uniform. The proposed equation depends upon three parameters namely, relative length of pier or abutment, relative time and particle Froude number.

### 1.2.5 Flow around Bridge Piers

Previous research emphasis that scouring around bridge piers is one of the most common reasons behind waterway bridge failure. The mechanism of scour is complex due to the interaction of flow and structure. Thus, the study of flow structure interaction around bridge piers is essential to explore the process of scouring.

Many researchers have divided the horseshoe system into two types namely: a laminar horseshoe vortex system and turbulent horseshoe vortex system (Baker, 1979, 1980; Kirkil et al., 2008; Huang et al., 2014). Baker (1979) conducted laboratory experiments using circular cylinders under turbulent flow condition and reported that the structure in the flowing stream obstruct the stream flow and results in the formation of horseshoe vortex. The horseshoe vortex leads to increase the bed shear stresses, which could erode the bed materials and initiates formation of scour hole around piers. He perceived from experiments that the horseshoe vortex system comprises of two primary vortices. One was observed near the bed, and other was smaller intermittent vortices found near the base of the cylinder.

The role of turbulent flows in sediment transport is of significant importance because the morphodynamical changes are governed by them in the form of entrainment and deposition of the sediment particles. Local scour around the bridge pier results in a complex interaction between turbulent flow and mobile bed sediment particles. Thus, investigating hydrodynamics of the flow structure near the scour and erosion mechanisms can provide a proper insight into the scouring process and aid to predict scour depth precisely (Ahmed and Rajaratnam, 1998). The stochastic nature of turbulent flow around bride pier has been investigated only in a handful studies (Melville, 1975; Istiarto et al., 2001) hence, the precise effect of pier on the flow separation, reattachment and the perturbed shear layer in the turbulent flow responsible for sediment transport is yet unclear.

Izadinia et al., (2013) carried out an experimental investigation on the turbulent flow parameters around a circular pier. They stabilized the scour hole with cement after

reaching the equilibrium scour depth. They found that probability of occurrence of sweep events are dominant at upstream of the pier while at the downstream of the pier both sweep and ejection both are nearly equal. They observed strong reversal flow at upstream of the pier near the bed region.

Mazumder et al. (2011) carried out an experimental investigation to understand the turbulent flow statistics around a circular cylinder placed transverse to flow. They observed that the turbulent characteristics like velocity, Reynolds stress and turbulent intensities are highly fluctuating near the pier. Their work is further extended in the study of (Maity and Mazumder, 2012). Maity and Mazumder (2012) conducted laboratory experiments in the flume with short piers of different diameters placed transverse to the flowing stream. They observed that the magnitude of turbulent kinetic energy (TKE) is higher near the edge of the scour hole. Within the scour hole, both sweep and ejection events are more dominant. However, inward and outward interaction are equally important.

Kothyari and Kumar (2012) carried out sets of experiments using single pier and compound pier and investigated that, measurements of velocity, turbulence intensities and Reynolds shear stress around piers at different vertical planes exhibit almost similar profiles along the flow depth. However, close to the piers the vertical profiles changed significantly due to vortex formation. At downstream of piers, in the wake region reversal flow was observed. They emphasized from the observations made by using compound piers that the foundation of pier should be below the bed level to lessen the scour depth at upstream of piers.

Extensive investigations to date are focused on scouring around the single pier. Very few studies have been made on the group of piers. Group of piers are becoming more popular because of geotechnical and economic reasons (Coleman, 2005). In actual practice, bridge piers in rivers are installed in the form of two or more piers sequentially aligned in the flow direction. Obstruction to flowing stream by a group of piers results in complex flow field around structures. According to Beg (2010), scouring around a group of piers is quite different with one that happens around the single pier. Some researchers have studied most simple and widely used arrangement that is a tandem arrangement of a group of piers (Hannah, 1980; Salim and Jones, 1996; Ataie-Ashtiani and Beheshti, 2006). Hannah

(1980) investigated the scour depth around tandem piers with regards to spacing between the piers. Salim and Jones (1996) reported that the scour depth in case of tandem piers decreases with increasing distance between the piers. Ataie-Ashtiani and Beheshti (2006) experimentally investigated the scour around tandem piers and provided a correction factor to improve the accuracy of existing equations for predicting maximum scour depth. Beg and Beg (2015) conducted laboratory research on two piers of different diameters arranged in tandem manner and suggested that mutual interference effect on scouring may lead to failure of the bridge, if pier group effect is ignored and bridge piers are designed merely as an isolated pier. Keshavarzi et al., (2017) experimentally studied the turbulent flow statistics around in-line piers by changing the spacing between piers. They argued that the flow structure around two in-line bridge piers is very different than the flow structure around the single pier.

A number of researchers performed several qualitative flow-visualizations to investigate the effect of pile spacing on the vortex shedding frequencies (Tanida et al., 1973, Igarshi, 1981; Palau-Salvador et al., 2008). The phenomenon of oscillating the flow behind an obstruction to the flowing stream is known as vortex shedding. When the flow is disrupted by any obstacle like bridge piers; vortices are created behind the obstruction and detach periodically. Sumer and Fredose (1997) stated that the vortex shedding phenomenon is critical in case of bridge piers as the flow regime is changed with increasing *Re*.

Sumner (2010) observed that when two cylinders are placed in a tandem manner, the flow field is very complicated due to the complex interaction of shear layers, vortices and wakes around the cylinders. He stated that the flow regime depends upon the spacing between two piers. Additionally, the downstream cylinder interferes with the wake and vortex formation region of the upstream cylinder. He further reported that the upstream cylinder behaved as a turbulence generator and the downstream cylinder behaved as a wake stabilizer.

According to Lee (2006), the wake vortices at the backside of piers contribute to the movement of the sediment particle through the process of suspending, sliding, jumping and rolling. The approaching stream first hits the pier and separated along the sides of the pier directed towards the centerline and again curl back forming vortices. The vortex shedding frequency is directly proportional to the velocity of flow and inversely

proportional to the characteristic length that is pier diameter. The vortex shedding frequency is related to Strouhal number, given by:

$$St = \frac{fD}{U_0} \tag{1.13}$$

Where, *St* is the Strouhal number, *f* is vortex shedding frequency, *D* is pier diameter, and $U_0$ is flow velocity.

Sumer and Fredsoe (1997) reported that Strouhal number increases gradually with increasing Reynolds number. When the Reynolds number is less (*Re* = 40), *St* was found to be 0.1. However, *St* is 0.2 when Reynolds number is about 300 and becomes nearly constant for Reynolds number higher than 300.

## 1.3 Problem Descriptions

The river bed condition plays a vital role in changing the flow characteristics in natural or manmade alluvial channels. Granular boundaries of alluvial channels in the form of sand particles and gravels are permeable in nature. The permeable boundaries allow transfer of mass and momentum across the interface between the fluids and porous media. Depending upon the level of the surrounding ground water table, water percolates through the boundaries of alluvial channels in the form of seepage in either direction, i.e. upward and downward direction. In case of upward seepage or injection, water seeps into the channel, while with downward seepage or suction water seeps out from the channel (Figure 1.3). The interaction between the flow in the channel and ambient groundwater is very important as it plays an essential role in controlling transportation of contaminants and maintaining healthy ecosystem (Brunke and Gonser, 1997; Jones and Mulholland, 2000). The seepage flow through alluvial channels significantly influence the flow characteristics like velocity, shear stress near the channel bed and consequently leads to morphodynamic changes of channel and sediment transport.

Previous researchers agree that the seepage losses results in reducing the conveyance capacity of the channel (Krishnamurthy and Rao, 1969; Sharma and Chawla, 1975; Raja et al., 1983; Berenbrock, 1999; Carlson and Petrich, 1999; Fipps, 2005; Martin and Gates, 2014).

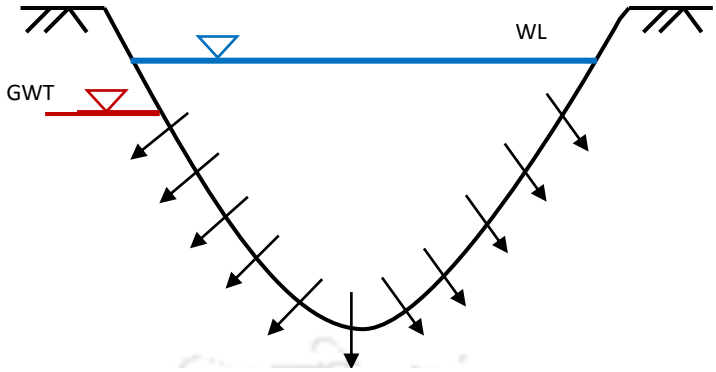


(a) Downward seepage

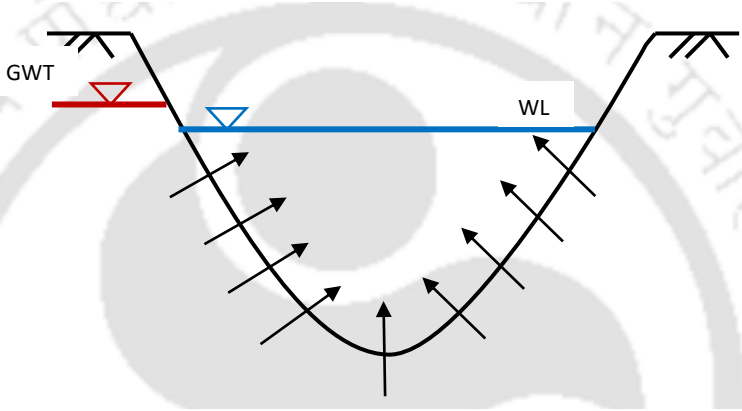


(b) Upward seepage

Figure 1.3 Flow through boundaries of alluvial channels, (a) Downward seepage (b) Upward seepage

Krishnamurthy and Rao (1969) investigated seepage losses on Ganga canal using radioisotopes and estimated the seepage losses of 2.2$m^3$/day/m. Sharma and Chawla (1975) stated that in the earthen irrigation canals, by the time the water reaches the field it undergoes losses of 45% of the water supplied at the head of the canal through bed and sides of the canals. Raja et al. (1983) used nuclear technique and measured seepage loss varying from 1.3 to 4.3 $m^2$ /106 $m^2$ of the wetted surface area. Tanji and Kielen (2002) have estimated seepage losses of 20-50% of the total volume in unlined earthen canals in semiarid regions. Australian National Committee on Irrigation and Drainage (ANCID, 2006) found that 10-30% of water is lost in the form of downward seepage in alluvial channels. Dukker (1994) conducted a field study to measure the seepage losses using inflow and outflow technique on Lower Gugera Branch Canal and observed seepage rate varying from 3.54cm to 62.04cm per day because of errors and uncertainties during measurements. Carlson and Petrich (1999) carried out studies on New York Canal and

estimated cumulative seepage losses of approximately 12% and 20% of the inflow discharge. An analysis of conveyance efficiency of the canal at the diversion of the canal to the field in the Lower Rio Grande Valley in Texas was obtained as 69.7%, indicating loss of water in the form of seepage (Fipps, 2005). Martin and Gates (2014) have calculated water loss around 15% of upstream flow rate due to downward seepage. According to Turner (1995) and Karambas (2003), the situations are very complex in coastal environments, for example, swash zone, where seepage losses vary both temporally and spatially. Seepage affects the hydrodynamic characteristics of alluvial channels by detaching the resting bed particles and enhance the rate of sediment transport. This problem is related to the solution of crucial practical engineering issues such as stability of hydraulic structures, which is substantially affected by the groundwater movement.

Some of the elegant researchers observed that downward seepage results in increasing velocity near the bed (Oldenziel and Brink, 1974; Maclean, 1991; Chen and Chiew, 2004; Singha et al., 2012; Cao and Chiew, 2014; Deshpande and Kumar, 2016). Watters and Rao (1971) conducted laboratory experiments to investigate the effect of seepage on the stability of bed particles. They measured drag and lift forces on bed material in case of injection and suction condition and found that considering the drag forces, injection enhances the stability of bed material, whereas, suction advances the movement of bed material. Regarding the lift forces, injection hinders the bed particle movement and suction holds opposite result.

Oldenziel and Brink (1974) stated that rate of transport of sediment particles increase with an increase in bed shear stress. In addition to this, they suggested that rate of sediment transport decrease in case of downward seepage and increase in evidence of upward seepage.

Willet and Drossos (1975) conducted laboratory experiments in a narrow flume with small seepage zone and observed that downward seepage causes localized scour hole around the seepage affected area. Also, faster grains movement was observed over the length of seepage zone rather than elsewhere in the flume.

Maclean and Willets (1986) measured the bed shear stress with seepage and without seepage conditions by visualizing the initiation of motion of the indicator grains. It was found that the bed shear stress increase with application of downward seepage.

Maclean (1991a) made velocity measurements by performing two sets of experiments in an open channel and in a wind tunnel with a high rate of downward seepage. He observed that velocity decreases toward water surface and increases close to the channel bed under the condition of downward seepage in the open channel.

Maclean (1991b) investigated that downward seepage results in increasing bed shear stress, which leads to erosion of bed material. When the downward seepage velocity was 10% of the mean channel velocity, the increase in bed shear stress is approximately twice the uniform shear stress.

Prinos (1995) explained the Reynolds-average Navier-Stokes equation to study the influence of downward seepage on the boundary shear stress. In the seepage zone, it was found that the bed shear stress increases, while increasing the downward seepage rate. The quantitative analysis have confirmed that the rise in seepage velocity by 9% can causes increase in the bed shear stress by eight times as compared to the without seepage case.

Cheng (1997) conducted laboratory experiments to investigate the effect of upward seepage on open channel flow and observed that the root mean square values of velocity fluctuations and Reynolds shear stress increases near the bed region.

Chang and Chiew (1999) carried out analytical and experimental studies considering additional forces due to seepage and stated that critical velocity decreases with the application of upward seepage.

Rao and Sitaram (1999) carried out laboratory experiments and found that upward seepage increases the stability of bed particles, while it reduced with the application of downward seepage. They concluded qualitatively that turbulence intensities were higher for downward seepage than for upward seepage or without seepage. It was argued by Rao and Sitaram (1999) that in case of upward seepage, the effective weight of bed particles reduces which causes the decrease in the resistance and because of the reduction in the

near-bed velocity as well as turbulence intensity, hydrodynamic forces acting on the bed particles also reduce. Opposite results were observed for the case of downward seepage.

Krogstad and Kourakine (2000) showed the effect of localized upward seepage on turbulent flow structure close to the channel bed in their experimental study. They found that bed shear stresses significantly reduced when water entered through the channel boundary in the form upward seepage.

Chen and Chiew (2004) experimentally investigated that the conventional law of wall is not applicable to open channel flow with downward seepage. In addition to this, they found that the velocity increased near the bed and decreased near the free surface hence, more uniform velocity distribution is observed. The origin displacement, slip velocity, shear velocity and bed shear stress increase with downward seepage.

Rao and Sreenivasulu (2009) stated that injection increase the stability of bed particles and suction reduce the stability and initiates their mobility. They emphasize that seepage in either way affect the resistance and mobility of the channel therefore, the effect of seepage must be considered in canal designing.

Sreenivasulu et al. (2011) pointed out that in the presence of downward seepage stream power varied non-linearly in the channel and it decreased in the downstream direction. Higher stream power prevailed on the upstream end of the channel with downward seepage hence it got eroded. The deposition was observed at the downstream end of the flume. They recommended that the effects of downward seepage should be considered in channel design.

Rao et al. (2011) considered the effect of downward seepage on the geometry of sand bed channels. They found that the presence of seepage alters the stability of the regime channel as well as flow characteristics. They defined that the regime channels are free to adjust section, pattern, geometry, and shape in response to hydraulic changes. The bivariate and trivariate regression relationships were developed for an alluvial channel under the influence of downward seepage.

Cao and Chiew (2014) conducted laboratory experiments to study the influence of downward seepage on the rate of sediment transport in closed conduit. Their results

indicate that the near-bed velocities are closely related to the sediment transport rate with downward seepage and the bed load transport rate increased with the rate of downward seepage. They also carried out a numerical simulation of the closed-conduit flows and noted that the results were similar to their experiments. They emphasized that transportation of bed material is enhanced with the increase in suction zone length.

Deshpande and Kumar (2016a) conducted laboratory experiments in the alluvial channel made of non-cohesive material and observed that downward seepage has altered the channel morphology and increase the bed shear stress. Sediment transport in the form of sheet flow is found when suction is applied to the non-transporting channels designed on incipient motion condition. An empirical relation for the thickness of sheet flow layer was developed by considering downward seepage as an independent parameter.

Lu and Chiew (2007a), Dey et al. (2012), Patel et al. (2015) and Deshpande and Kumar (2016b) investigated the influence of downward seepage on turbulent flow characteristics in open channel flow. They found that velocity, bed shear stress and consequently rate of sediment transport increase with application of downward seepage.

Limited literature can be found on the effect of seepage on scouring around bridge piers. As downward seepage alters the flow characteristics hence, change the morphology of alluvial channel; it significantly affects the scouring around bridge piers. Qi et al. (2012) conducted an experimental study to investigate the effect of point suction with 2% suction flow rate on scouring around a cylindrical bridge pier. They observed a reduction in equilibrium scour depth up to 50% and 30% when the point suction is applied at upstream and downstream of pier respectively and argued that suction can be used as an efficient pier scour countermeasure. Soltani-Gerdefaramarzi et al., (2014) have conducted laboratory experiments with a combined system of bed suction and jet injection through the pier body and found that suction and injection together results in reduction of scour depth. Dey and Sarkar (2007) conducted experiments with injection seepage through river bed downstream of an apron of sluice gate. They observed that equilibrium scour depth and many other scour geometry parameters increased with the increase of injection. Francalanci et al., (2008) experimentally studied that suction caused scour and injection leads to the deposition of bed material.

## 1.4 Objectives

Lateral flow through the boundaries of alluvial channels in the form of seepage affect the flow characteristics of the main stream channel. Because of the presence of seepage through porous boundaries, additional hydrodynamic forces may exert on sediment particles. These additional forces may have a significant impact on sediment transportation. Thus, the occurrence of seepage leads to change bed morphology and hydrodynamic characteristics of alluvial channels. The study of seepage flow is essential to understand its effect on detachment and further transportation of bed material as transportation of sediment results in aggradation and degradation of channel boundaries. Thus, for the management of fluvial system and construction of hydraulic structures, it is necessary to understand groundwater movement and its consequences on sediment transport. To understand the effect of downward seepage on the process of scouring around bridge pier, it is essential to understand the influence of downward seepage on the hydrodynamics of flow around the pier. Most of the previous researchers have studied the change in flow characteristics on the application of downward seepage or upward seepage on either plane or fixed bed. To understand the effect of seepage on the process of scouring and flow statistics around piers, the study must be carried out on an alluvial channel with the installation of piers. Because of practical difficulties in obtaining sufficiently accurate and comprehensive data in actual field experiments, well-designed laboratory studies are preferred as a truthful method to provide information concerning details of the hydraulic parameters. Such information is important in application and development of numerical models that can help to predict flow characteristics and scour around bridge piers in alluvial channels. In addition to this, in the present work, the experimentation was carried out using non-uniform sand bed to replicate the actual field condition as the riverbeds usually comprise of non-uniform bed material (Wu et al., 2004). In this research, two types of pier arrangements namely, single pier and tandem piers are studied. Based on this, following are the objectives of the present research work:

**a. Single Pier**

- Study of effect of pier diameter on scour depth
- Study of effect of sediment size on scour depth
- Investigation of turbulent flow structures around single pier
- Study of change in bed morphology due to local scour around single pier

- Study on time evolution of scour depth
- Development of the relationships for the scour geometry around single bridge pier
- Study on effect of downward seepage

**b. Tandem piers**

**1. Two piers of same diameters arranged in tandem manner**

**2. Two piers of different diameters arranged in tandem manner**

- Investigation of turbulent flow structures around tandem piers
- Study on scour depth and bed morphology around tandem piers
- Study on time evolution of scour depth
- Study on effect of downward seepage

A schematic view of the objectives outlined in the present research work is shown below in Figure 1.4.

## 1.5 Thesis Organisation

The thesis has been organised into six chapters. A brief introduction to the chapters is given below:

Chapter 1 presents an introduction to scour and related problems. Review of the literature of various pioneering researchers on scouring around bridge piers is carried out, and the effect of downward seepage on transportation of sediments is discussed. After a critical review, various objectives of the present study are outlined in this chapter.

Chapter 2 gives a detailed description of the facilities and equipment used for experimental tests. Additionally, this chapter presents the development of flume, the design of the physical model, bed material, experimental procedure used to collect experimental data and its processing with the results is given.

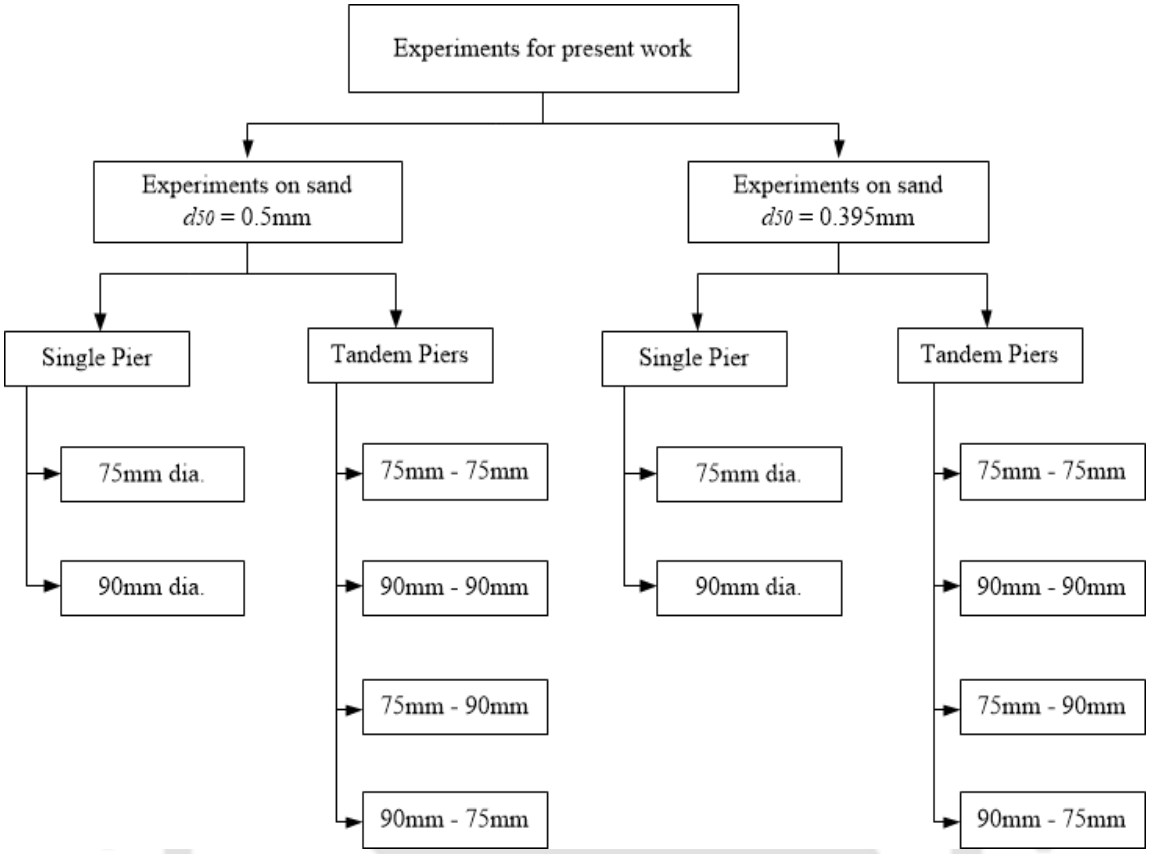


Figure 1.4 Experimental program in the present research work

Chapter 3 provides the results obtained from the laboratory experiments on flow structures around and scour geometry around a single bridge pier. The various results obtained and compared for with seepage and without seepage conditions. In this chapter different empirical approaches for prediction of scour depth are discussed and further, new empirical relationships are developed for prediction scour depth and dune geometry in alluvial channels of non-uniform sand bed considering the effect of downward seepage.

Chapter 4 is concerned with the experimental study of tandem piers in seepage affected alluvial channels. This chapter explores the change in flow characteristics and scour around tandem pier with similar as well as with different diameters. Strouhal number is determined and compared to each arrangement.

Chapter 5 deals with the effect of downward seepage on migrating scour depth and bedforms behind the piers. Temporal and spatial descriptions of migrating scour depth and bedforms around piers are shown.

Chapter 6 concludes the present research work and presents the scope of future work. Various references that have been reviewed for the present thesis work are listed at the end of the dissertation.

Chapter **2**

# Experimental Setup and Methodology

## 2.1 Overview

One of the most important and intriguing approach to solve and understand the problems regarding sediment transports and bed morphology is by conducting laboratory flume experiments, as there is a greater control on the hydraulic condition in the flume. Therefore, hydraulic engineers are relied on the empirical relations, developed based on the experimental measurements and intuitions, for designing the hydraulic structures. Various hydraulic flow conditions can be simulated by performing laboratory experiments through proper dimensional analysis depending upon the fundamental principles of the mechanism.

As discussed in chapter 1, the present work aims to investigate the effect of downward seepage on the mechanism of scouring, flow field and morphodynamic characteristics of alluvial channels around bridge piers. An experimental approach can be used to simulate the behaviour of the channel morphology in different given scenarios. To observe the overall fundamental effect, various hydraulic conditions can be provided by changing bed material, discharge, and seepage velocity. The equipment and laboratory methods used for experimentation are described in the present chapter. All the relevant material related to the methods of operation of this equipment will also be introduced in this chapter. This chapter first illustrates the available apparatus before describing the manner in which it was used for gaining various results. The end of the chapter describes in detail the different series of experiments that were planned and carried out during the course of the research.

## 2.2 Bed Material

River sands used for experimentation were sieved carefully to determine the median sand size ($d_{50}$). From the grain size distribution curves shown in Figure 2.1. The median sand diameters were found to be 0.5mm and 0.395mm and standard deviation 1.65 and 1.85 respectively. Non-uniformity in the particle size distribution for the sand was confirmed

with the value of geometric standard deviation ($\sigma_g$) greater than 1.4 (Marsh et al., 2004). The geometric standard deviation is calculated as:

$$\sigma_g = \sqrt{d_{84}/d_{16}} \tag{2.1}$$

Where $d_{84}$ and $d_{16}$ are defined as the grain for which 84% and 16% of the sample is finer by weight.

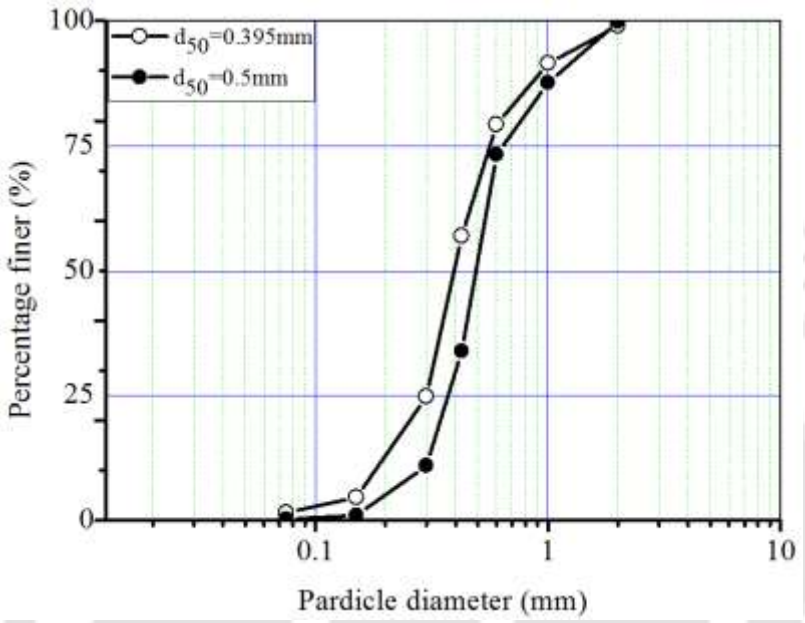


Figure 2.1 Sand size distribution curve

## 2.3 Tilting Flume

The experiments were performed in a glass-walled tilting flume of 20m long, 1m wide and 0.72m deep (Figures 2.2 and 2.3). To collect water from the overhead tank and to straighten the flow before introducing in the flume a collection tank of length 2.8m, width 1.5m and depth 1.5m was provided at upstream of the flume. A couple of baffle walls were installed next to the collection tank to prevent highly turbulent flow from entering into the flume. For the length of 2m at upstream of the flume, gravels were placed in order to ensure smooth entry of the flow. The entire length of the channel, except the 2m length at upstream limit, was made porous by placing a fine mesh (0.1 mm x 0.1 mm aperture), which was supported with the help of steel structure of 0.22m height, placed at the bottom of the channel below the sand bed. Sand was spread on the mesh to prevent its entrance into the bottom chamber. The seepage chamber of length 15.2m from the downstream

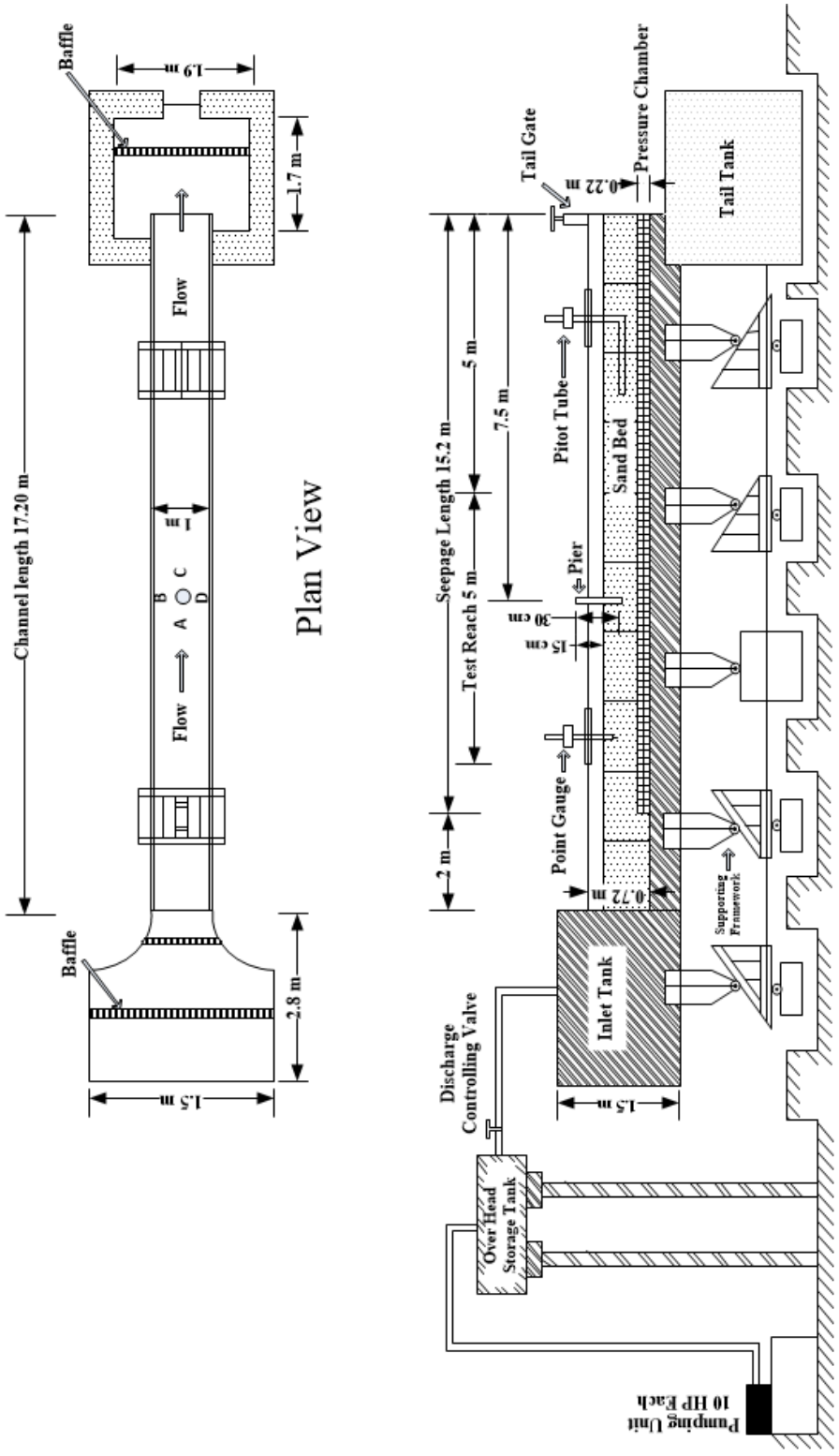


Figure 2.2 Schematic diagram of experimental flume

Figure 2.3 Snapshot of the tilting flume

end of the flume, width 1m and depth 0.22m was provided beneath the main channel as shown in Figure 2.2. The seepage chamber was used to extract water from channel bed (uniformly) in the form of downward seepage. The amount of downward seepage was controlled by valves connected to the seepage chamber. The flow depth in the main channel during the experiments was maintained by adjustable tailgate installed at the downstream of the flume. The flow in the flume is driven by three 10HP centrifugal pumps. The pumps were deployed to supply water to the overhead tank. A regulating valve was used to supply a controlled amount of water in the main channel connected to the overhead tank. A snapshot of flume has been depicted in Figure 2.3.

## 2.4 Test Section

In the flume, the flow is significantly affected by its entry and exit conditions. If the flow is delivered to the flume directly by pipes, it leads to intense circulations in the flow. In the present experiments, the pipe arrangements are made in such a way that the fluctuations could be avoided. First, the water was collected in the upstream collection tank by allowing the flow with the help of controlling valve provided at the overhead tank. The level of water rose gradually in the upstream collection tank prior to its introduction into the channel. To ensure smooth entrance of the flow into the channel, couple of baffle walls were installed in the upstream collection tank just upstream of the channel entrance. Free overfall of flow from the tailgate causes acceleration of flow in the near-bed region just upstream of the tailgate. To minimize the effect of entry and exit conditions in the channel, the test section in the present experiments was considered as a 5m length in the middle of the flume (5m to 10m from tailgate). The length of flume is long enough for the fully developed flow to be established for all the runs. In the present work, the criteria of the length of boundary layer development is equal to 56$h$ where $h$ is flow depth; given by Ardiclioglu and Ozturk (2006) and Kirgoz and Ardiclioglu (1997) is satisfied.

## 2.5 Main Channel Discharge

A regulating valve was connected to the overhead tank to supply a controlled amount of water in the main channel. Discharge in the main channel was measured with the help of a rectangular notch provided at the downstream of flume (Figure 2.4). The coefficient of discharge was calculated by using the following equation:

$$Q = \frac{2}{3} C_d L_n \sqrt{2g} (h_n)^{3/2} \quad (2.2)$$

Where, $L_n$ is length of the notch ($L_n$=0.5m), $g$ is the gravitational acceleration, and $h_n$ is the height of the flow above notch. $C_d$ is the coefficient of discharge for the rectangular notch, and it was obtained to be 0.82.

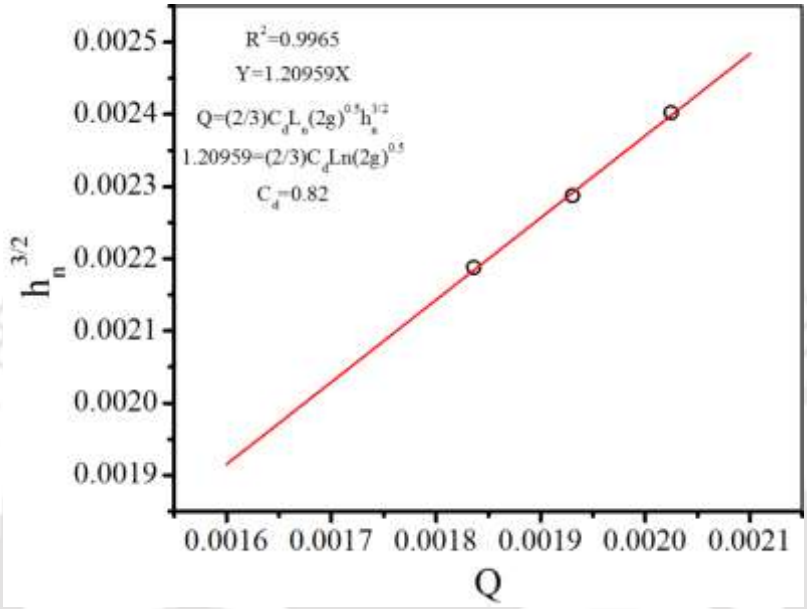


Figure 2.4 Calculation of coefficient of discharge for rectangular notch

Figure 2.5 Measurement of main channel flow discharge over rectangular notch

## 2.6 Seepage Discharge

A pair of electromagnetic flow meters was installed at the downstream of the flume to measure and control the desired seepage discharge. The flow meters were connected to the seepage chamber through pipes. The working principle of electromagnetic flow meters is based on Faraday's law of electromagnetic induction. According to this principle, when a conductive medium passed through a magnetic field *B*, a voltage, *E* was generated which was proportional to the velocity of the conductor, $u_c$, the density of the magnetic field, *B*, and the length of the conductor, *X*. In a flow meter, a current was applied to wire coils on the meter body to generate a magnetic field. The liquid flowing through the pipe acted as the conductor and induced voltage, which was proportional to the average flow velocity. The induced voltage was detected by sensing electrodes mounted in the flow meter body and sent to a transmitter, which calculates the volumetric flow rate based on the pipe dimensions. Mathematically, Faraday's law can be stated as:

$$E \propto u_c BX \tag{2.3}$$

The flow meters had a control valve and a digital display which was used to apply the desired percentage of seepage discharge (Figure 2.6). The seepage discharge can be estimated using the relation given below:

$$q_s = A_p u_c \tag{2.4}$$

Where, $q_s$ is the seepage discharge in $m^3/s$, $A_p$ is the area of pipe in $m^2$ , and $u_c$ is the fluid velocity through the flow meter.

## 2.7 Flow Depth

The flow depth in water was measured using digital point gauge assembled on a moving trolley as depicted in Figure 2.7. This arrangement could cover the full cross-sectional area by moving in a lateral and longitudinal direction. This was a direct indicating gauge, eliminates observation errors caused by Vernier and scale reading. It could be used in different ways as it could set to zero at any place in the operating range in order to get relative measurements. The liquid crystal digital display shows the reading of flow depth in different units, and it has a resolution of $\pm 0.1$ mm. A quick release mechanism allows

smooth changes of positions. Where depth of flow was defined as the difference between the water surface level and the bed level.

Figure 2.6 Electromagnetic flow meters for measuring seepage discharge

## 2.8 Bed slope

The bed slope ($S_0$) of the flume was measured with the help of Total Station. A Total Station is a modern electronic device that combined the ability to measure a position horizontally and vertically simultaneously. It has two components, a machine mounted on a static tripod, and a 'target' prism on a metal staff, which is moved around the site. The machine part of the total station has a lens somewhat like a telescopic rifle-sight with cross-hairs which are focused on the prism. The whole instrument revolves horizontally, and the lens swivels vertically too. The Total Station is partly based on the principle used in traditional theodolites, where angles are calculated from vertical and horizontal 360-degree scales. It combines these with a device known as an Electronic Distance Measurer or EDM.

Figure 2.7 Digital point gauge assembled on moving trolley

## 2.9 Velocity and Turbulence Measurement

To investigate the turbulent characteristics of flow, instantaneous velocities were measured. Velocity measurements were taken by a four-beam down looking Vectrino+ Acoustic Doppler Velocimeter (ADV) probe manufactured by Nortek (Figure 2.8). The instrument allowed data collection at a higher sampling rate up to 200 Hz. The Vectrino used Doppler Effect for measurement of velocity. The Doppler Effect changes in pitch that is heard when either the source of sound or the observer is in motion. The pitch of the horn of vehicle heard by the observer is higher when the vehicle is coming towards the observer, and the pitch is lower when the vehicle is moving away from the observer. This change in pitch tells us how fast the vehicle is moving. The ADV uses this principal to measure the velocity of water in three dimensions.

The device transmits short pairs of acoustic pulses, listens to their echoes and ultimately measures the change in pitch or frequency of the returned sound. The transmitted waves

bounce off from suspended particles or moving particulates present in the water, which move, with the same average speed of water and three receiving probes listened for the change in frequency of returned sound. Consequently, the measured velocity is the velocity of water. The ADV calculates the velocity of water in the *x*, *y* and *z* directions. In addition to this, the ADV allowed measurement of the distance of central transmitter from the boundary. The instrument collects data in a cylindrical remote sampling volume of user adjustable heights located 5cm below the central transmitter (Figure 2.8). The velocity data obtained by ADV was collected in the computer using a software called Vectrino+ developed by Nortek (Figure 2.9). The height of the sampling volume was set at 4mm when the measurement location was away from the bed and 1mm when very near to the bed so that the sampling volume did not touch the particles on the bed surface. The time duration for data acquisition was 5 minutes where 40,000 samples were collected. Special care was taken to collect data with a correlation coefficient greater than 70 and signal to noise ratio (SNR) between 10 to 15. Very near to the bed, slight deviation (± 5%) in the correlation was observed. In order to check the uncertainty associated with the ADV data, 16 pulses of 40000 samples for the duration of 5 minutes each were collected at a location 3 mm above the bed level. The velocity data obtained from ADV included spikes because of interference between transmitted and received signals. These data were needed to be post-processed or filtered. For removing the spikes in the velocity data acceleration threshold method (Goring and Nikora, 2002) was used (Figure 2.10). Threshold values (1-1.5) were selected by trial and error in such a way that Kolmogorov's -5/3 law was satisfied in the inertial subrange of the streamwise velocity (Dey et al., 2012). It can be observed from Figure 2.10 that power spectra $F_{uu}$ at $z \approx 0.01$m for filtered velocity pulses were in good agreement with the Kolmogorov's -5/3 law in the inertial subrange, where $F_{uu}$ is power spectra for a streamwise component of velocity, and $f$ is the frequency in Hz.

In Table 2.1, $\bar{u}$,$\bar{v}$ and $\overline{w}$ are the time averaged velocities in streamwise, spanwise and vertical direction, $u'$,$v'$ and $w'$ are the fluctuations of instantaneous streamwise velocity $U_i$, spanwise velocity $V_i$ and vertical velocity $W_i$, respectively and $(u'u')^{0.5}$, $(v'v)^{0.5}$ and $(w'w')^{0.5}$ are root mean square (rms) of $u'$, $v'$ and $w'$ respectively.


Figure 2.8 Acoustic Doppler Velocimeter for measuring instantaneous velocities

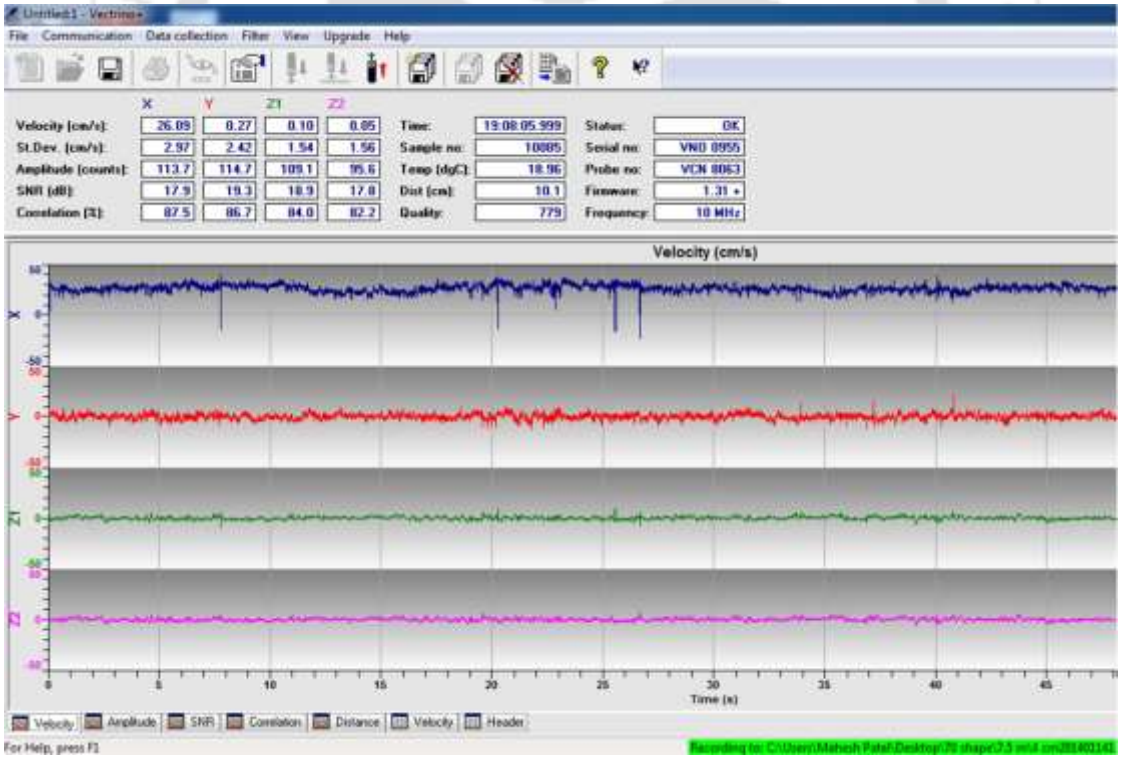


Figure 2.9 Vectrino + software for velocity data collection

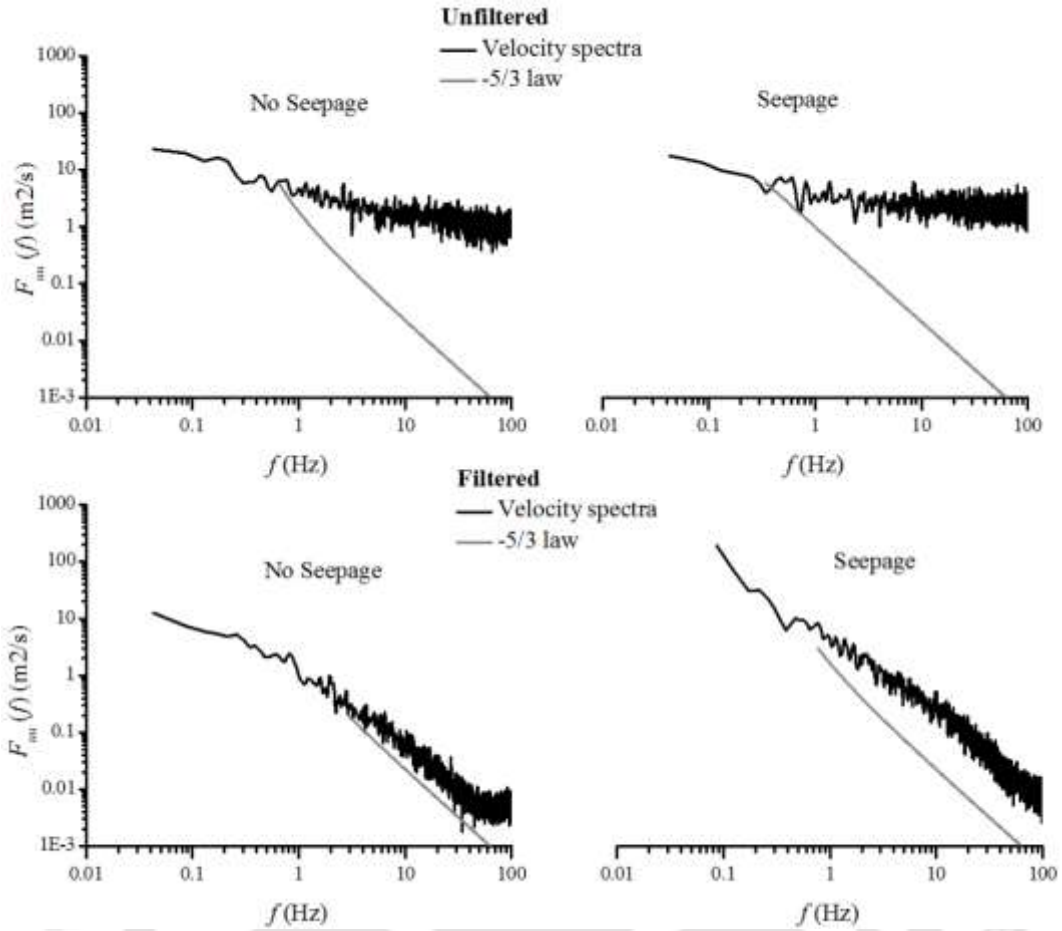


Figure 2.10 Velocity power spectra with Kolmogorov's -5/3 law

The time avaeraged velocities were estimated from the instantaneous velocities as given below:

$$\left.\begin{aligned}\bar{u} &= \frac{1}{N}\sum_{i=1}^{N} U_i \\ \bar{v} &= \frac{1}{N}\sum_{i=1}^{N} V_i \\ \bar{w} &= \frac{1}{N}\sum_{i=1}^{N} W_i\end{aligned}\right\} \tag{2.5}$$

Where, $N$ is total number of samples and,

$$\left.\begin{aligned}u' &= U_i - \bar{u} \\ v' &= V_i - \bar{v} \\ w' &= W_i - \bar{w}\end{aligned}\right\} \tag{2.6}$$

Table 2.1 Uncertainty associated with ADV data

| | $u$(m/s) | $v$(m/s) | $w$(m/s) | $\left(\overline{u'u'}\right)^{0.5}$ | $\left(\overline{v'v'}\right)^{0.5}$ | $\left(\overline{w'w'}\right)^{0.5}$ |
|---|---|---|---|---|---|---|
| **Standard deviation** | $2.15\times10^{-3}$ | $9.94\times10^{-4}$ | $4.44\times10^{-4}$ | $1.09\times10^{-3}$ | $9.06\times10^{-4}$ | $3.24\times10^{-4}$ |
| **Uncertainty %** | 0.14 | 0.08 | 0.03 | 0.09 | 0.08 | 0.03 |

## 2.10 Temperature and Kinematic Viscosity

The average temperature of the water during experiments was recorded by Vectrino+ ADV which has a temperature sensor (thermistor), located inside the probe head. The corresponding value of kinematic viscosity ($cm^2/s$) was determined from standard tables.

## 2.11 Measurements of the Geometry

The topographical changes in the channel bed were measured using 5MHz Ultrasonic Ranging System manufactured by SeaTek. The system contains eight transducers attached to an automated trolley (Figure 2.11). The spacing between two transducers was kept as 25mm. The automatic trolley can move in a longitudinal direction with constant speed. The trolley was designed using four high torque DC geared motor connected to the wheels and speed was controlled with the help of pulse width modulated DC motor speed controller switch in order to match the sampling rate of the transducers. This system can record the samples at a maximum 5 MHz sound frequency to obtain the distance to a target. First, the transducer sent a transmit pulse of 10 microsecond duration. The pulse traveled through water and reflected off of a target. The reflected signal travels back to the transducers and then detected by the electronics. Since the speed of sound in water is known, and the time it took for the pulse to travel from the transducer to the target and back is known, the distance to the target can be calculated. The wavelength of 5 MHz sound waves in water is 0.3mm. The resolution and accuracy (if several pinges are processed per return) is 0.1mm and +/- 0.2 mm respectively.

## 2.12 Uncertainty Analysis

To investigate uncertainty associated with the measured data uncertainty analysis has been carried out before performing the experiments. The uncertainty was measured for the main channel discharge ($Q$), seepage discharge from electromagnetic flow meter ($q_s$)

and the distance measured from the SeaTek Ultrasonic Ranging System ($y$). From each of these instruments, several reading were taken repeatedly. The results are presented in Table 2.2.

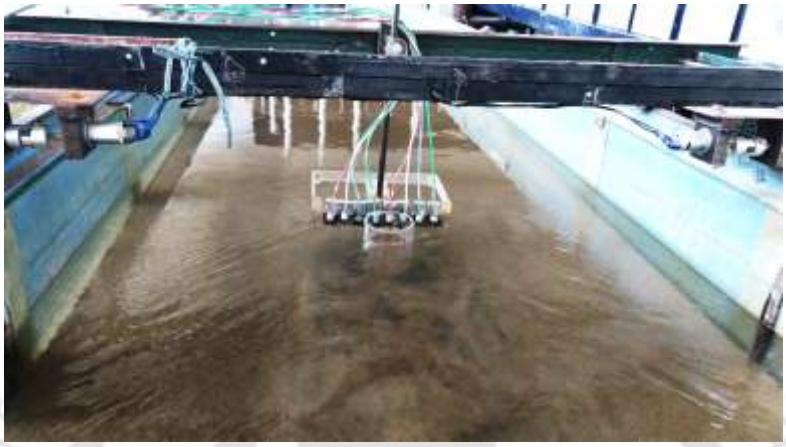

Figure 2.11 Transducers of SeaTek Ultrasonic Ranging System

Table 2.2 Uncertainty analysis of the data collection

| Statistical parameters | $Q$ | $q_s$ | $y$ |
|---|---|---|---|
| Standard deviation | 0.00068 | 0.00037 | 0.00090 |
| Standard uncertainity | 0.03478 | 0.03765 | 0.0189 |

## 2.13 Pier Characteristics

The circular piers of perspex glass material of diameters 75mm (P1) and 90mm (P2) were used for experimentation. The height of piers was 300mm (150 mm above the sand bed). In order to avoid sidewall effect, the diameters of piers were selected in such a way that diameters should not be less than 6% and greater than 10% of channel width, and the ratio $D/d_{50}$ should be greater than 50 to neglect the effect of sediment size around bridge piers (Chiwe and Melville, 1987).

## 2.14 Experimental Program

The experimental program mainly consisted of two test series of two types of piers arrangements namely, single pier and tandem piers. For single pier, the experiments were carried for two different diameters 75mm (P1) and 90mm (P2). In case of tandem piers, experiments were performed on four different types of tandem arrangements. The

arrangements for tandem piers (Figure 2.12) were (i) front pier of diameter 75mm – rear pier of diameter 75mm (P1 – P1) (ii) front pier of diameter 90mm – rear pier of diameter 90mm (P2 – P2) (iii) front pier of diameter 75mm – rear pier of diameter 90mm (P1 – P2) (iv) front pier of diameter 90mm – rear pier of diameter 75mm (P2 – P1).

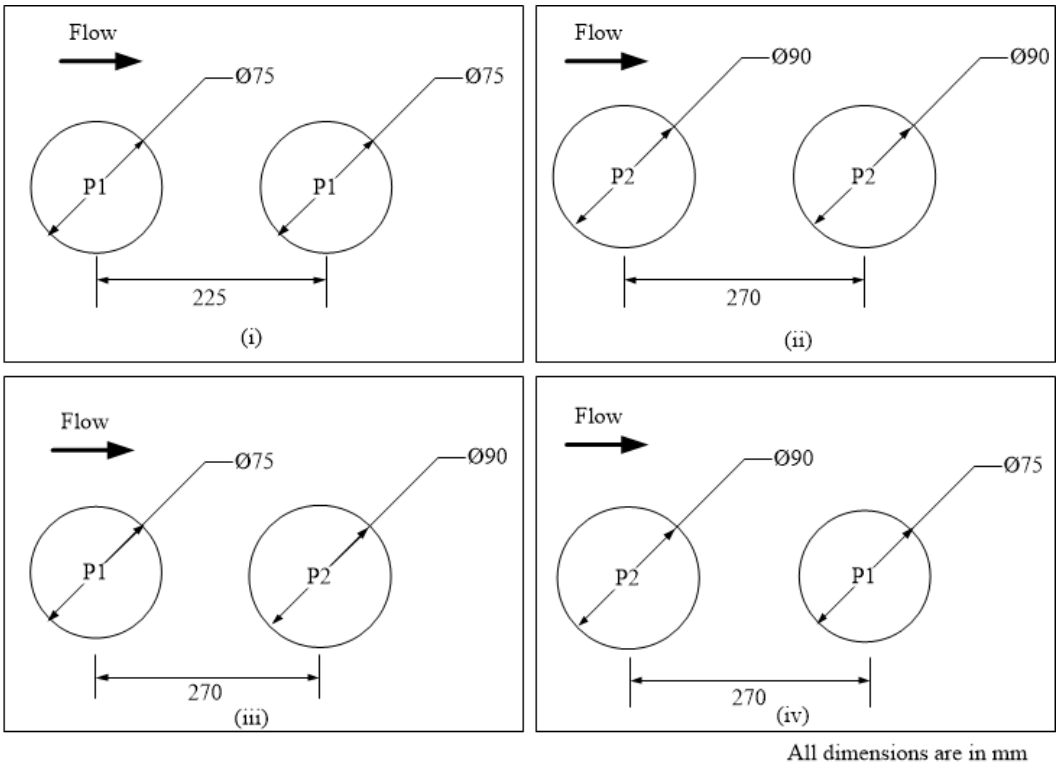


Figure 2.12 Arrangements for tandem piers

The experiments were conducted with five different discharges for no seepage, 10% seepage and 15% seepage conditions. Each experimental run was carried for 24 hours. For every experimental run, the bed was prepared plane (Figure 2.13). After preparation of bed, the pier was installed in the middle of the test section along the centreline. The discharge was slowly introduced in the channel till the desired flow discharge was attained. In case of tandem piers, the centre to centre spacing between piers was maintained as three times (greater) diameter of pier to avoid interference effect of the piers (Ataie-Ashtiani and Baheshti, 2006). Figure 2.14 shows the locations around piers where velocity measurements were taken. Table 2.3 shows experimental conditions of this work.

Figure 2.13 Bed preparation before installation of pier

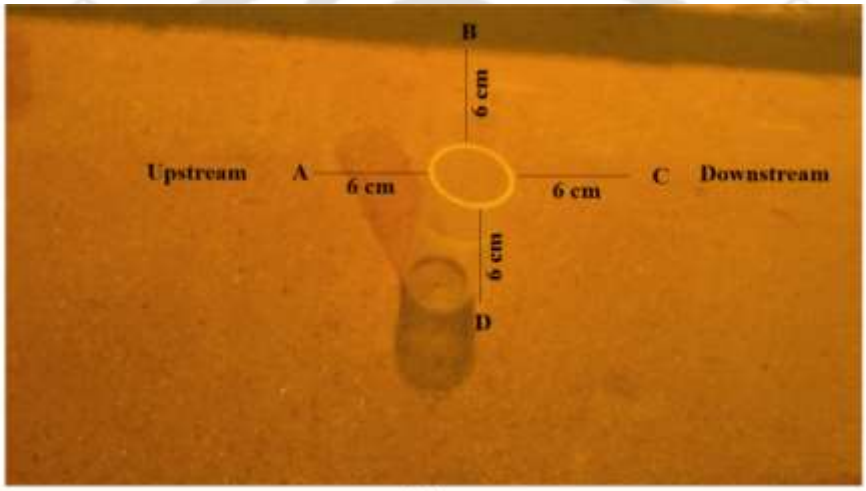


(a)

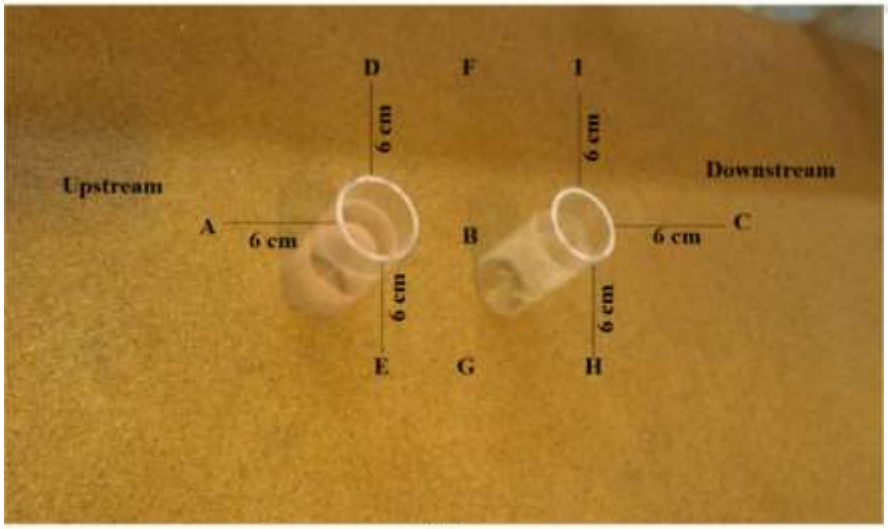


(b)

Figure 2.14 Measurement locations around bridge piers

Table 2.3 Experimental conditions

| No. | Pier arrangements | $\sigma_g$ | Flow depth (h) m | Discharge (Q) $m^3/s$ | Seepage % |
|---|---|---|---|---|---|
| 1 | | | 0.118 | 0.032 | 0 |
| 2 | | | 0.118 | 0.032 | 10 |
| 3 | | | 0.118 | 0.032 | 15 |
| 4 | | | 0.121 | 0.034 | 0 |
| 5 | (a) Single pier | | 0.121 | 0.034 | 10 |
| 6 | (i) 75mm | | 0.121 | 0.034 | 15 |
| 7 | (i) 90mm | | 0.123 | 0.036 | 0 |
| 8 | (b) Tandem piers | (i) 1.65 | 0.123 | 0.036 | 10 |
| 9 | (i) 75mm-75mm | (ii)1.85 | 0.123 | 0.036 | 15 |
| 10 | (ii) 90mm-90mm | | 0.126 | 0.038 | 0 |
| 11 | (iii)75mm-90mm | | 0.126 | 0.038 | 10 |
| 12 | (iv)90mm-75mm | | 0.126 | 0.038 | 15 |
| 13 | | | 0.129 | 0.04 | 0 |
| 14 | | | 0.129 | 0.04 | 10 |
| 15 | | | 0.129 | 0.04 | 15 |

*For each arrangement experiments were carried for all discharges on each type of sand. Total no of experimental runs was 180*

Chapter **3**

# Effect of Downward Seepage on Turbulent Flow Field and Bed Morphology around Bridge Piers[i,ii]

## 3.1 Introduction

The flow field around bridge piers is one of the most important topics to hydraulic engineers. Study of flow characteristics around bridge piers leads to an in-depth understanding of flow and its consequences, also provides more insight into the process of scouring around bridge piers. According to Ahmed and Rajaratnam (1998), a vast amount of study has been carried out since the late 1950s to investigate the flow structure around bridge piers and its influence on the process of scouring. They stated that investigation of hydrodynamics of the flow around piers provides proper understanding of scour and aid to predict the scour depth precisely. Some of the eminent researchers have provided a comprehensive understanding of three-dimensional turbulent flow structures and consequently the mechanism of the process of scouring around the bridge piers and prediction of scour depth. Melville and Raudkivi (1977b) conducted an experimental study to investigate flow around circular piers under flatbed and deformed bed conditions. Many researchers conducted laboratory experiments to explore the interaction between flow fields around pier in terms of horseshoe vortex and its effect in increasing scour depth (Qadar, 1981; Baker, 1981). Some of the researchers have studied the stochastic nature of turbulent flow around piers (Melville 1975; Dey et al. 1995; Istiarto 2001; Dey and Rajkumar 2007b). This chapter explains the precise effect of the pier on flow separation, turbulent flow statistics under the influence of downward seepage.

---

[i] Chavan, R., & Kumar, B. (2017). Experimental investigation on flow and scour characteristics around tandem piers in sandy channel with downward seepage Journal of Marine Science and Application, 16(3), 313-322.

[ii] Chavan R., and Kumar B.- Prediction of Scour Depth and Dune Morphology around Circular Bridge Piers in Seepage Affected Alluvial Channel, Environmental Fluid Mechanics (accepted for publication)

A large number of studies have been conducted to predict the scour depth around piers (Laursen and Toch, 1956; Breusers et al., 1977; Ettema, 1980; Melville and Sutherland, 1988; Kothyari et al., 1992; Melville and Coleman, 2000; Ansari et al., 2002; Chang et al., 2004; Aghaee-Shalmani and Hakimzadeh, 2015). Recently researchers have attempted to reduce the scour depth around bridge piers using flow altering devices such as riprap, bed sills and collars (Chiew and Lim, 2000; Chiew, 2004; Zarrati et al., 2004 and 2006; Grimaldi et al., 2009; Masjedi et al., 2010). The scoured bed material around piers is deposited at downstream of pier along as well as at sides of the centreline and producing hump. Very less information is available about the deposition of bed material or dune like bedforms at the rear side of the pier. Pagliara and Carnacina (2010) have analysed the temporal evolution of dunes forming at rear side of piers in the presence of debris accumulation. Ettema et al. (2011) have stated that dunes behind pier divert the flow to sides which results in reducing erosion of dunes. Around the piers, the flow is highly turbulent and with time gradually erodes the bed material deposited behind piers in the form of dunes, and hence, deepens the scour hole. Euler and Herget (2012) have carried out experimental investigation and studied scour and deposition of bed material at submerged and non-submerged cylindrical bridge piers. The deposition of sand at downstream of piers is troublesome for navigation. Department of the U.S. Army Corps of Engineers (1982) have reported that due to dune formation, the problematic situation occurred for navigation interests in Missouri as well as Mississippi rivers. For a detailed investigation of dunes structures, a model study was conducted at the St. Antony Falls Hydraulic Laboratory (1982), and it was concluded that to avoid deposition of bed material behind piers, the riverbed adjacent to piers need to stabilize. Oliveto and Hager (2014) have studied the morphological features of dune like bedforms occurring at downstream of piers and proposed equations for morphologic dune evolution and their propagation behind piers. This chapter provides new empirical relations for scour depth and dune morphology behind piers in seepage affected alluvial channel.

## 3.2 Velocity

The presence of piers in alluvial channels leads to change the flow characteristics of the approaching stream flow. The velocity profiles with non-dimensional flow depth ($z/h$) around the piers of 75 mm and 90 mm diameter for no seepage and seepage runs are shown in Figures 3.1 and 3.2 respectively, where $z$ is flow depth from bed surface at

which velocity measurements are taken, and *h* is total flow depth. Figures 3.1 and 3.2 show the velocity profiles at upstream (section A), downstream (section C) and at the sides of piers in the transverse direction (section B and Section D) for piers of diameter 75mm and 90mm respectively. As shown in Figures 3.1 and 3.2, a streamwise component of velocity is observed to be negative near the bed and becomes positive as the distance from the bed increases ($z/h > 0.1$). The maximum velocity occurred roughly on the edge of the scour hole ($z/h \approx 0.4$).

The streamflow is obstructed by the pier, and it comes to rest at the face of the pier, which causes adverse pressure gradient. Owing to it, a strong downward flow is being observed at regions close to the bed. The downward flow impinges on the bed, erodes the bed material around the pier and the circulating flow along the sides of the pier carries the eroded bed material further and hence develops the scour hole. Once the scour is initiated, the downflow close to the pier moves in a reverse direction to that of stream flow, near the bed within the developing scour hole and dislodges the material from the slanting slope of the scour hole. Reversal flow can be seen near the bed within the scour hole hence the negative streamwise velocity component at upstream of the pier. The decreasing pressure gradient at the upstream face of the pier accelerates the stream flow along the sides of the pier leads to generate wake vortices at the downstream of the pier which initiates scouring of the bed material at the downstream of the pier. At the downstream of the pier, the streamwise velocity component increases and attains its maximum value near the edge of scour hole ($z/h \approx 0.35$). At free surface, reversal flow can be seen. At sections B and D, the velocity profile follows the universal logarithmic profile as shown in Figure 3.1. The non-dimensional expression of the log law is given as (Deshpande and Kumar, 2016):

$$\frac{u}{u_*} = \frac{1}{k}\ln\left(\frac{z^+ + \Delta z^+}{x^+}\right) \tag{3.1}$$

Where, $u_*$ is shear velocity, $z^+ = z/d_{50}$, $\Delta z^+ = \Delta z/d_{50}$, $x^+ = z_0/d_{50}$, $k$ is Karman's constant, $\Delta$ is virtual bed level and is zero velocity level. A similar trend has been observed for 90 mm pier. Regression equations as shown in Figure 3.1 (e) has resulted in 0.41 as Von-Karman constant, which reduces to 0.34 in case of 10% seepage (0.32 for 15% seepage).

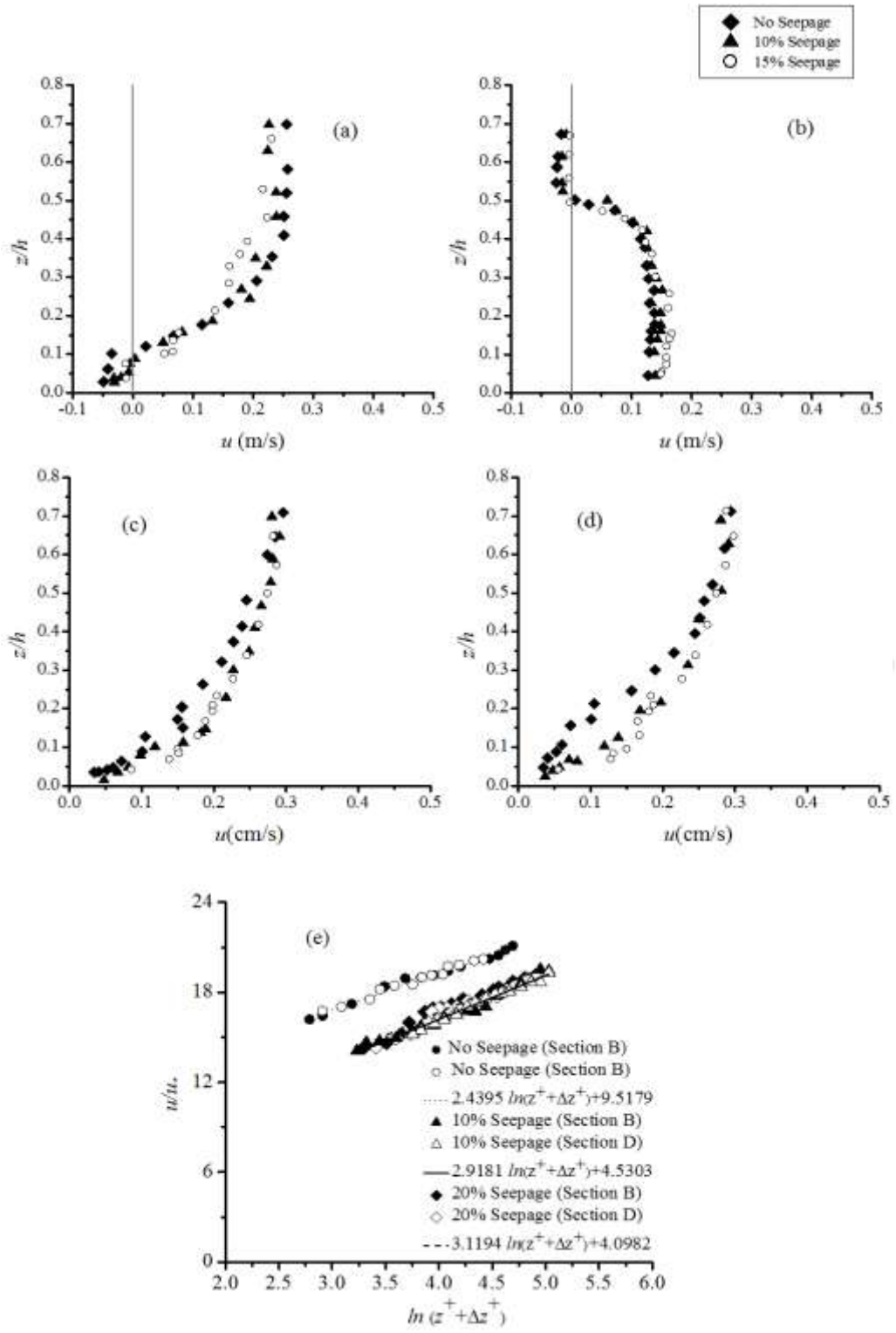


Figure 3.1 Velocity profiles around pier of diameter 75mm (a) Upstream A, (b) Downstream C, (c) Section B, (d) Section D, (e) Logarithmic law for velocity distributions

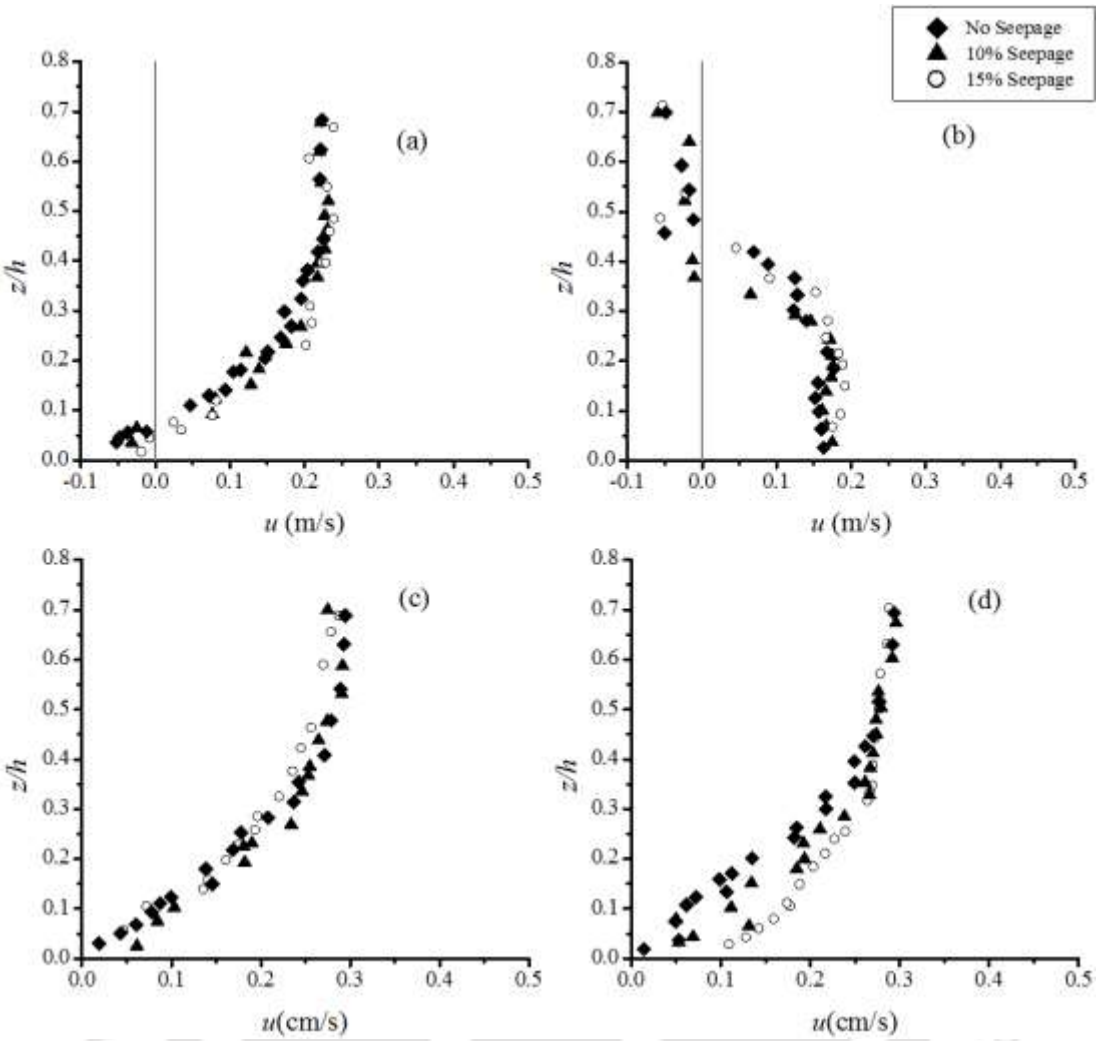


Figure 3.2 Velocity profiles around pier of diameter 90mm (a) Upstream A, (b) Downstream C, (c) Section B, (d) Section D

Downward seepage in channel shifts the velocity profile towards downward which leads to increase in velocity near the bed and boundary shear stress, which results in more sediment movement near the bed. With the application of seepage, at upstream of the pier velocity profiles shifts downwards which limits the flow reversal zone when compared to the no seepage condition. It should be noted here that seepage is applied all along the flume contrary to point suction available in the literature. Thus there is a movement of bed particles from the upstream zone, which reduces the upstream scour hole depth and increases the dune deposition on the downstream side (Sarkar et al., 2015). Application of downward seepage reduces flow reversal near free surface and increases the near-bed velocity. At sections B and D, it can be seen clearly that near the bed, velocity is

increasing on the application of downward seepage. On application of 10% seepage and 15% seepage, velocity is increased on an average value of 15% and 25% respectively.

## 3.3 Reynolds Shear Stress (RSS)

Reynolds shear stress $\left(\tau_{xz} = \overline{u'w'}\right)$ defines the real-time momentum flux of the streamwise velocity in the vertical direction caused by the fluctuating velocity field. Vertical distribution of RSS for no seepage and seepage runs for piers of diameter 75mm and 90mm have been depicted in Figures 3.3 and 3.4 respectively.

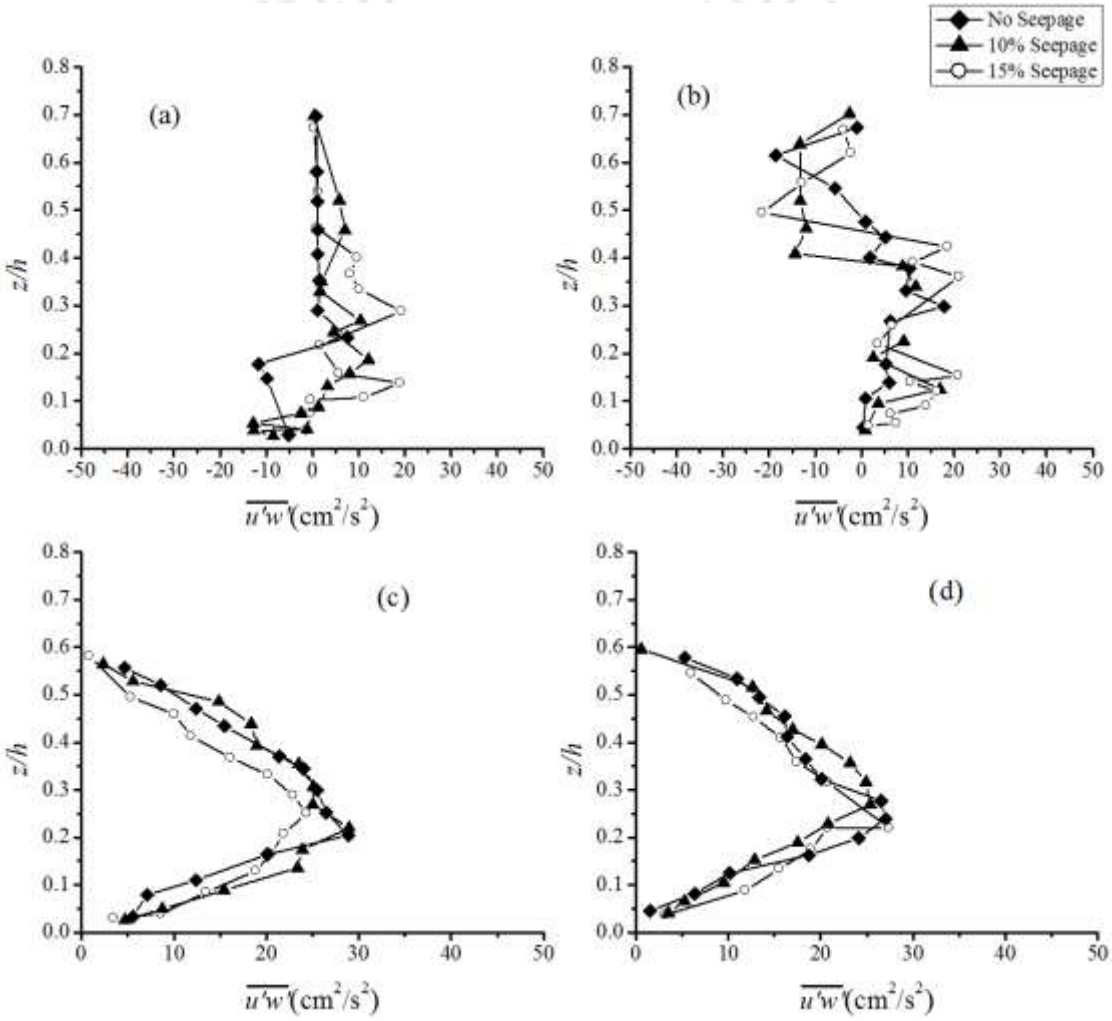


Figure 3.3 RSS profiles around pier of diameter 75mm (a) Upstream A, (b) Downstream C, (c) Section B, (d) Section D

From Figures 3.3 and 3.4, it can be perceived that, at the side sections of the piers (Section B and D), maximum Reynolds shear stress occurs near the bed ($z/h \leq 0.2$).

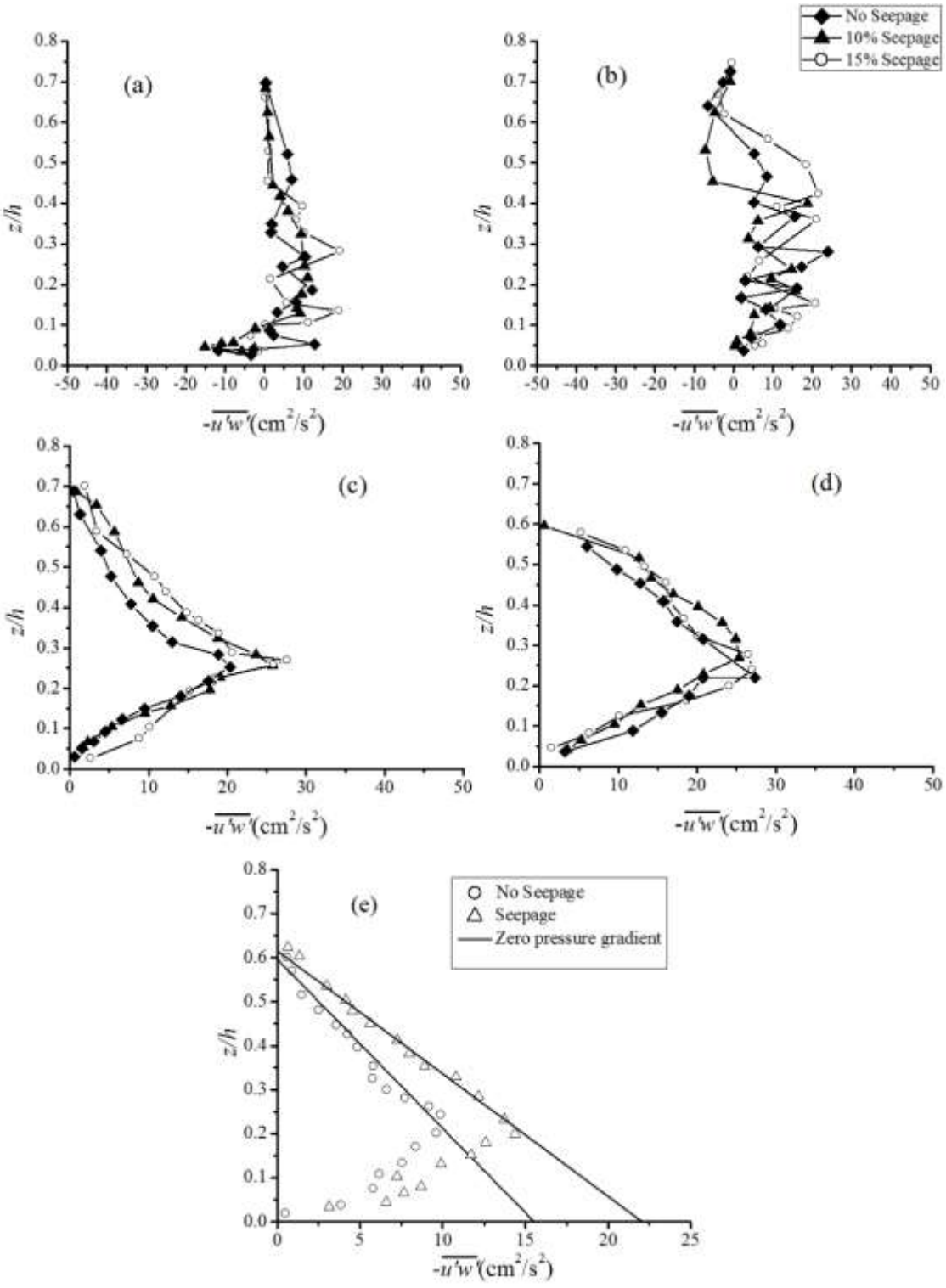


Figure 3.4 RSS profiles around pier of diameter 90mm (a)Upstream A, (b)Downstream C, (c) Section B, (d) Section D (e) Distribution of RSS at zero pressure gradient

Figure 3.4(e), shows that distribution of RSS for both no seepage and seepage runs at side sections B and D are accordance to the linear law of RSS for free surface flow with zero pressure gradient $\left(\left(1-\frac{z}{H}\right)=\frac{-\overline{u'w'}}{u_*^2}\right)$. RSS increase with an increase in distance from the free surface, attains maximum value somewhere between $0.15< z/h < 0.25$ and then again decreases towards the bed because of the presence of roughness sub layer. At the upstream (A) and downstream (C) of the pier RSS fluctuates heavily owing to the continuous development of vortex region (Figures 3.3 and 3.4). Presence of downward seepage increases the Reynolds shear stress and thereby increases in sediment transport. It is found that on the application of downward seepage, Reynolds shear stress $-\overline{u'w'}$ is increased by an average value of 16% with 10% seepage and 25% with 15% seepage as compared to that with no seepage run. At the upstream (A) of the pier, the magnitude of Reynolds shear stress is higher in case of no seepage condition than 10% and 15% seepage condition due to flow reversal within the scour hole. At the downstream (C) of the pier, flow separation occurs results in increasing turbulence; the Reynolds shear stress is more than the upstream (A) of the pier and fluctuates heavily because of wake vortices. At the downstream (C) of the pier near bed Reynolds shear stress increase for 10% seepage than no seepage and again increase in case of 15% seepage, which leads to more erosion due to increase in momentum exchange with respect to the seepage conditions. For seepage runs Reynolds shear stress $-\overline{u'w'}$ becomes negative near the bed and nearly above the scour hole at upstream (A) and downstream (C) of pier respectively because of reversal flow. Upstream and downstream are the controlling section of the hydrodynamics around bridge pier, and thus, these two sections have been considered for detailed investigations of higher order turbulent statistics in the following sections.

## 3.4 Quadrant Analysis

Organized coherent structures play an important role in mass and momentum exchange and hence these structures need to be identified. Quadrant analysis is carried out to study the contribution of different velocity fluctuations to Reynolds stress at a point. The total Reynolds shear stress ($-\overline{u'w'}$) at any given point is the sum of different types of bursting events. In quadrant analysis, the characteristics of bursting events are studied with conditional statistics of *u'* and *w'* by plotting them in a *u'w'* plane (Lu and Willmarth,

1973) to evaluate the total Reynolds stress at a single point as the sum of contribution from different types of events. The bursting events are defined by four quadrants (Maity and Muzumder, 2012) ($q$ = 1, 2, 3 and 4) as, (1) outward interaction $(Q1)(u'>0, w'>0)$, (2) ejection $(Q2)(u'<0, w'>0)$, (3) inward interaction $(Q3)(u'<0, w'<0)$, (4) sweep $(Q4)(u'>0, w'<0)$.

The bursting phenomenon is described by two significant features ejection and sweep. Ejection is upward entrainment of low-speed fluid particles into the main turbulent flow, as instantaneous velocity is lower than time-averaged local velocity. During sweep event, these ejected low-speed fluid particles are brushed away by high-speed fluid particles. Sweep is the downward movement of high-speed fluid particles towards the bed. A parameter H called hole size that represents the threshold level (Nezu and Nakagawa 1993) is given as follow:

$$\left|u'w'\right| = H\sqrt{\overline{u'^2}}\sqrt{\overline{w'^2}} \tag{3.2}$$

The Hole region $H$ = 0 means all data $(u', w')$ are taken into consideration. At any point in a flow, the contribution from events towards the RSS production from events excluding hole size is obtained by (Raupach, 1981):

$$u'w'_{q,H} = \lim_{T\to\infty}\frac{1}{T}\int_0^T u'(t)\,w'(t)\,I_{q,H}(z,t)\,dt \tag{3.3}$$

Where $t$ is time, $T$ is sampling duration, $I_{q,H}$ is the indicator function defined as:

$$I_{q,H}\left[u'(t)\,w'(t)\right] = \begin{cases} 1, \ if\ (u', w')\ \text{is in quadrant}\ q\ \text{and}\ \left|u'w'\right| \geq H\left(\overline{u'^2}\right)^{0.5}\left(\overline{w'^2}\right)^{0.5} \\ 0, \text{otherwise} \end{cases} \tag{3.4}$$

Reynolds shear stress fractional contribution to each event is given by:

$$S_{q,H} = \frac{u'w'_{q,H}}{\overline{u'w'}} \tag{3.5}$$

$S_{q,H}$ is positive in case of sweeps and ejection while it is negative in case of outward and inward interactions. Sweeps and ejection occur when $q$ is even and outward and inward interactions occur when $q$ is odd. For $H$ =0:

$$S_{10} + S_{20} + S_{30} + S_{40} = 1 \tag{3.6}$$

Systematic variation of the hole size $H$ allows the investigation of the contributions of events to the total Reynolds shear stress, whether they are large, small or frequent. Figure 3.5 shows variation of stress fraction against $z/h$ at upstream and downstream of the pier with 75 mm diameter for no seepage, 10% seepage, 15% seepage at $H$ = 0.

From Figure 3.5, the contribution of events Q1 and Q3 is more than Q2 and Q4 within the scour hole region ($z/h$<0.1) at upstream of the pier. As the flow in the scour hole does not have sufficient capacity to move the particles further, the particles near the bed are lifted up by the flow instead of transporting along with flow and returned back to the bed. Sweep and ejection events are more dominant around the edge of scour hole and above. The dominance of sweep results in the arrival of high-speed fluid particles contributing greater $+u'$ in streamwise direction and greater $-w'$ in the vertical direction, which causes the progressive deepening the scour hole at upstream of the pier. Ejection events are pronounced at the downstream side of the pier. It is observed that the fluctuations of stress fraction are increased near the bed in the scour region due to the complexity of flow and decreased towards the surface. The magnitude of events is stronger at downstream of the pier than upstream because of the higher turbulence production at the downstream of the pier. Similar results are obtained for pier with 90 mm diameter. Analysis of bursting events shows that contribution of all events to the Reynolds shear stress are increased in case of seepage as compared to no seepage runs as shown in Figure 3.5. On application of downward seepage, it can be seen that contribution of ejection event is more resulting in the arrival of low-speed fluid particles due to retardation of flow in streamwise direction. The magnitude of stress fraction is increased with the increased of seepage as compared to that with no seepage run. While moving away from the bed, it is observed that contribution of ejection and sweep to the Reynolds shear stress are greater than inward and outward interaction. On application of seepage, contribution of ejection events increased and accompanied by a decrease in sweep events.

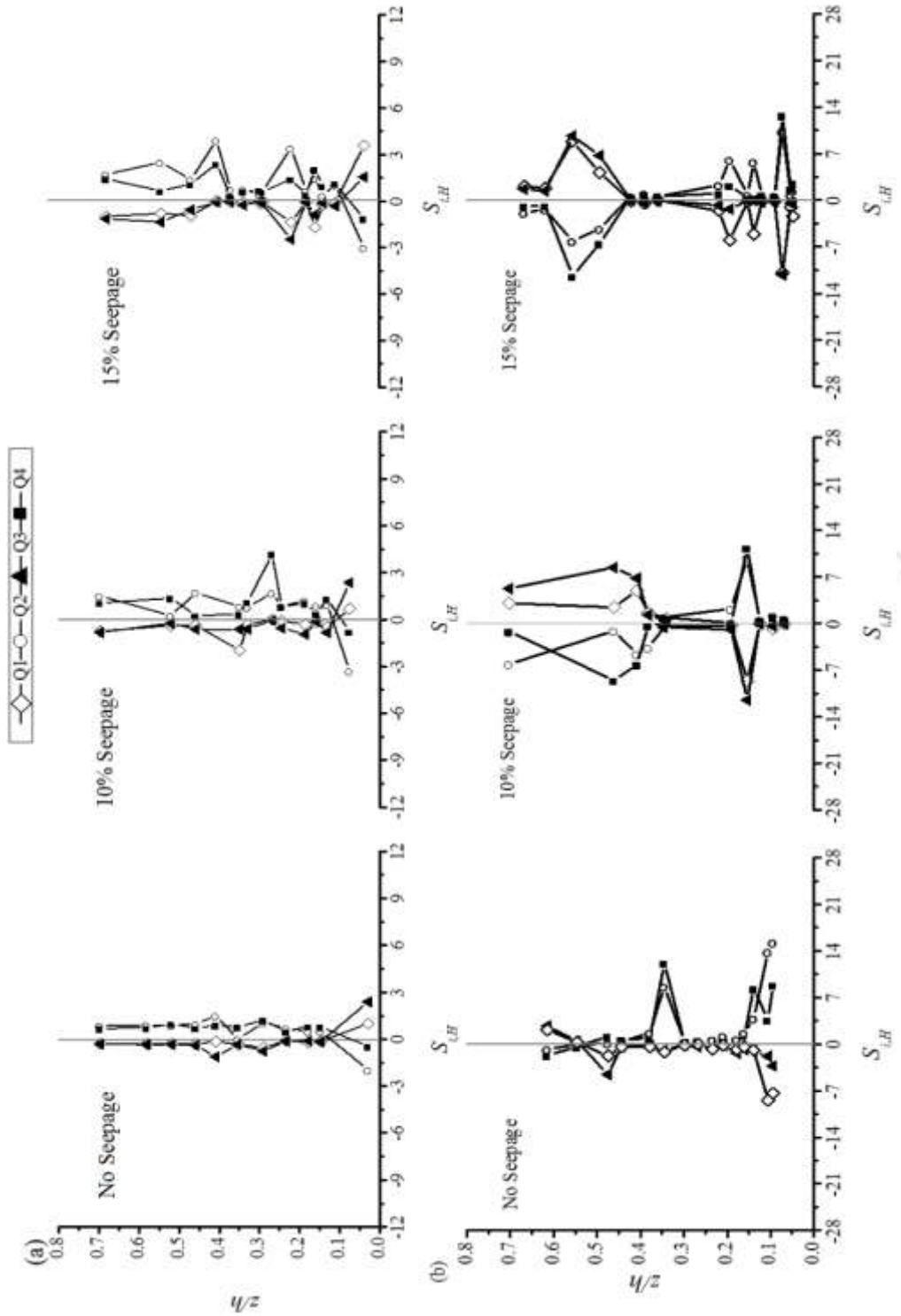


Figure 3.5 Stress fraction $S_{i,H}$ against $z/h$ at (a) Section A (b) Section B

## 3.5 Morphological features around bridge piers

Transportation of sediments leads to change the morphodynamical conditions of the alluvial channel, which can be observed in the form of aggradation and degradation of channel boundaries. Reduction of channel cross-sectional area that arises due to the construction of structures such as bridge piers obstruct the stream flow and leads to excavate and removal of sediments around the structures. The flowing water is impeded by the bridge piers and the flow separated in three directions, the modifications in flow pattern has caused inflation in shear stress which dislodges the stream bed material around piers and resulting in scour.

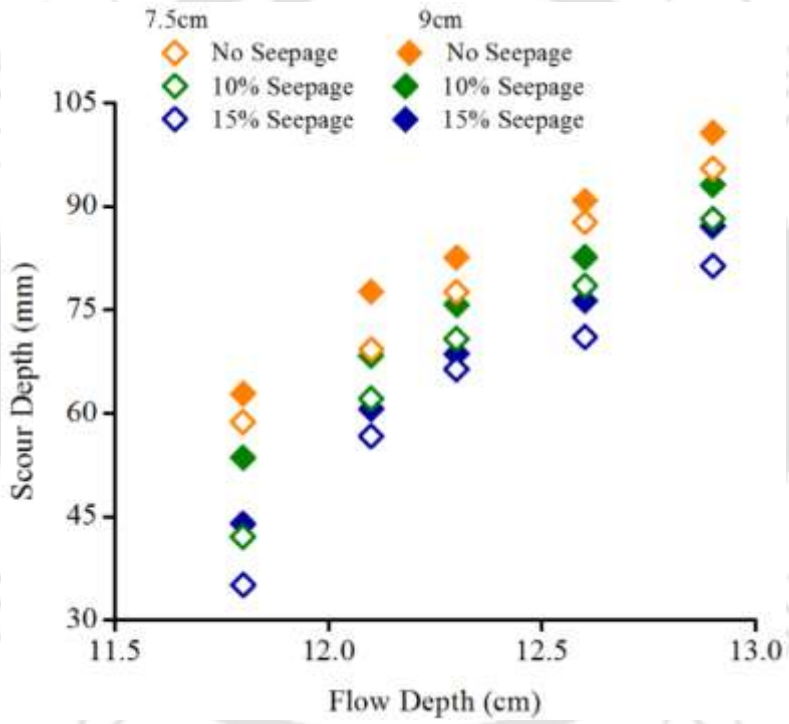


Figure 3.6 Scour depth with respect to flow depth for no seepage, 10% seepage and 15% seepage conditions

Naturally, the boundaries of alluvial channels are porous in nature which permits the flow of water in or out from channel boundaries depending upon the surrounding groundwater table. The downward seepage (outflow from channel boundaries) through channel boundaries, significantly affect the morpho-dynamical condition of alluvial channels as downward seepage enhances transportation of sediments. Downward seepage also affects

the scour depth at bridge piers as it plays an important role in changing the bed morphology of alluvial channel.

Figure 3.6 shows a graph of scour depth against flow depth (of no seepage run) for no seepage, 10% seepage and 15% seepage conditions for both 75mm and 90mm piers. Close observation of graph reveals that the scour depth is more at 90mm diameter pier than 75mm diameter. From the Figure 3.6, it can also be observed that the scour depths are maximum for no seepage runs for every flow depth. For both diameters, 75mm and 90mm; in case of 10% seepage runs scour depths are lesser than no seepage condition and again reduced in case of 15% seepage condition of corresponding discharges.

The scouring around bridge piers is time-dependent phenomenon. The development of vortex around pier with time is being considered as the primary source for scour depth. With increasing time, scour depth increases up to certain limit, later on erosive capability of flowing stream and resistance to the motion of bed material attains equilibrium.

Figure 3.7 shows lateral bed profiles at upstream and downstream of the pier which is measured with Ultrasonic ranging system at different time intervals. The measurements are taken for 20cm transverse distance at upstream and downstream of the pier by considering the centre of the pier as the centre of that transverse distance. The flow obstructed by pier erodes the bed material around the pier in longitudinal and transverse direction for both no seepage and seepage runs. Lateral flow occurs through the boundaries of alluvial channels in the form of seepage, which also affect the flow characteristics of the mainstream flow and rate of sediment transport. With progressing time, the scour depth enlarged at upstream and downstream of the pier. From Figure 3.7, it can be seen that initially the change of scour depth is substantial for both no seepage and seepage conditions, and reduces gradually with time. It can be perceived from Figure 3.7; the rate of scour depth formation decreases by 50% in 12 hours. However, rate of scour depth development in no seepage runs is faster when compared to seepage runs; the reason could be the strength reduction of reserve flow in seepage runs as indicated by velocity profile.

As the approach streamflow hits the pier, strong pressure gradient generated which results in downflow along the face of the pier. The downflow hits the bed and start eroding the

bed material. Within the developing scour hole, downflow moves in reverse direction to that of stream flow along the slanting slope of scour hole. This reversal flow at upstream of the pier is mainly responsible for the growth of scour hole at upstream of pier. Accumulation of eroded bed material at the rear side of pier produces dune like bedforms that significantly changes the bed morphology.

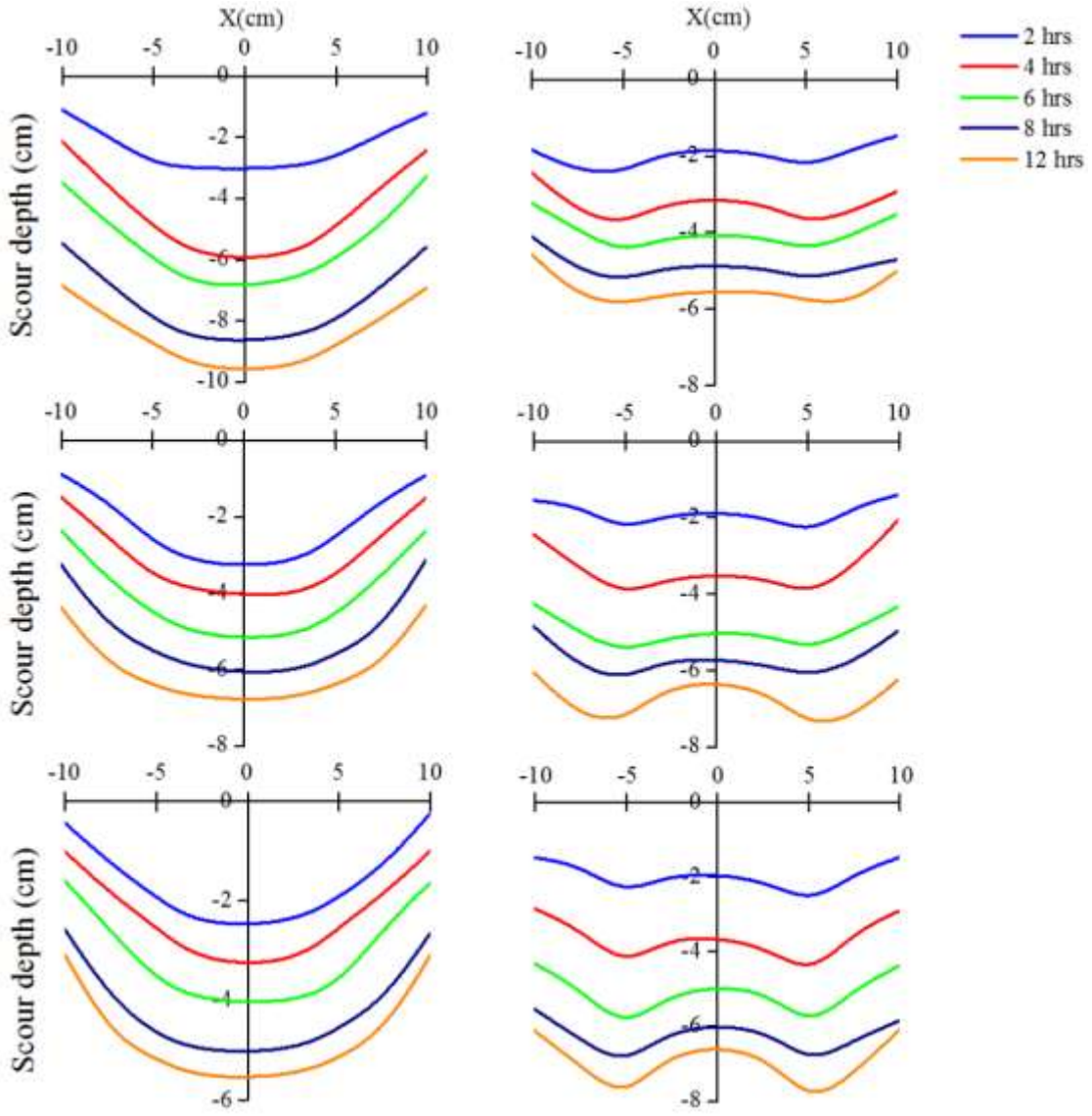


Figure 3.7 Development of scour depth with time at (A) upstream (B) downstream of the pier for (i)No seepage, (ii)10% seepage, (iii)15% seepage

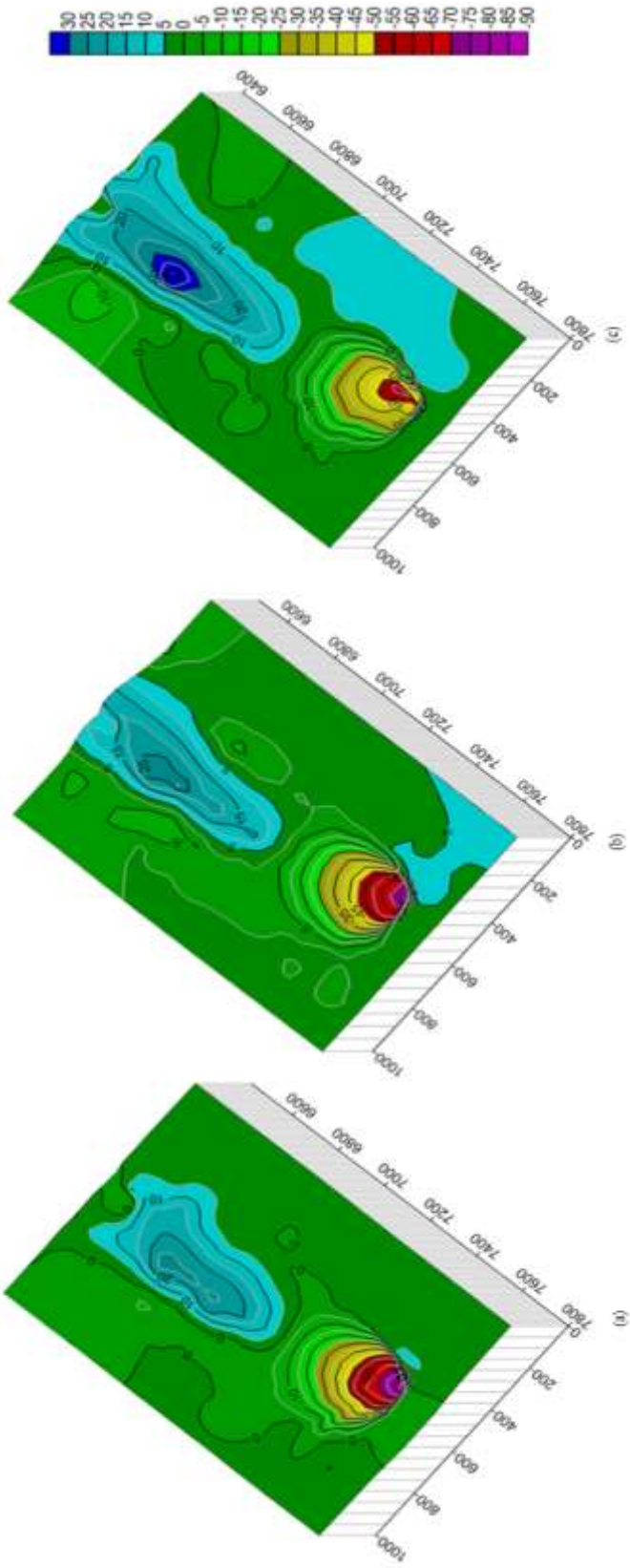

Figure 3.8 Contour profiles around pier for (a) no seepage, (b) 10% seepage and (c) 15% seepage conditions

The bedforms behind pier obstruct the flow at rear side of piers and affect the stream resistance. Therefore, interpretation of bedforms geometry seems important in waterway designing. Figure 3.8 shows contour profiles of scour around the pier for highest discharge for no seepage, 10% seepage and 15% seepage runs. From Figure 3.8, it can be observed that the deposition height is more in case of seepage runs than no seepage condition. Close observation of Figure 3.8 reveals that the scour depth at upstream of pier is more in case of no seepage run and reduced with increasing seepage percentage. Figure 3.9 shows bed morphology along the centreline for all experimental conditions. Close observation of Figure 3.9 shows that the distance of dune crest from the pier is more in case of no seepage condition and reducing with increasing seepage percentage.

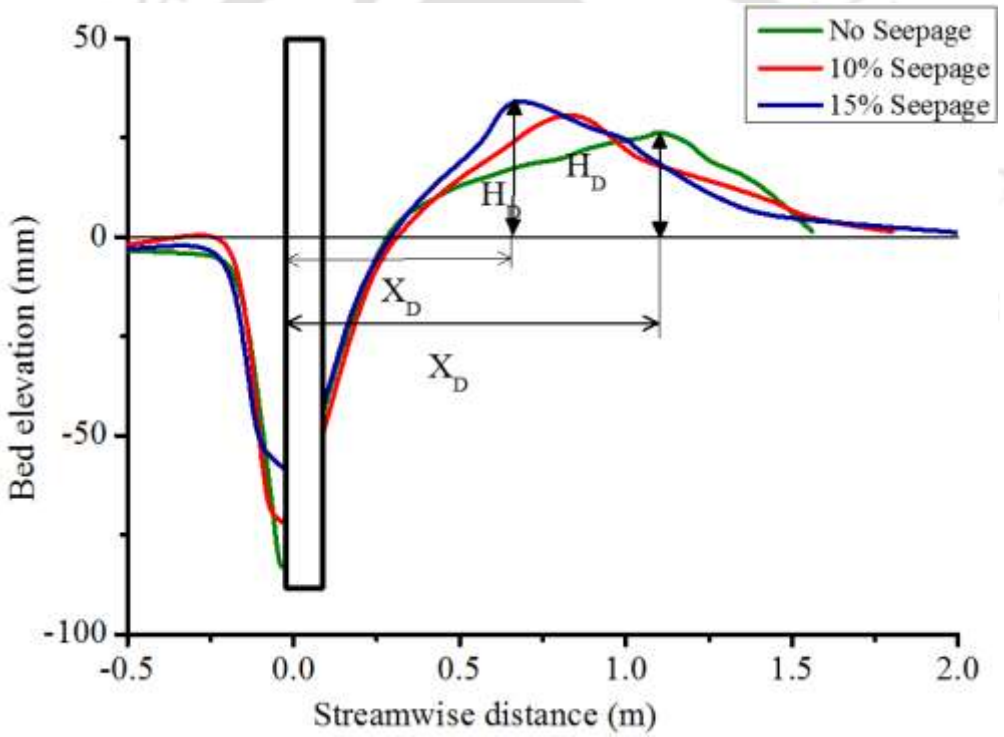


Figure 3.9 Bed elevation profile along the centerline

### 3.5.1 Development of a new Scour depth prediction method

As mentioned in chapter 1 in section 1.2.3 and 1.2.4, the scour depth around bridge piers is the result of the interaction of flow with bed material around piers due to flow separation. The intensity of scour depends upon the fluid and flow properties, characteristics of bed material and geometry of piers as mentioned in Eq.1.1. Many eminent researchers have developed the scour depth prediction methods some of the

methods are discussed in chapter 1 and some are mentioned in table 3.1. However, some of the scour estimation methods are in practice still, there are many challenges in hydraulic modelling as the field conditions are less consistent in comparison with laboratory conditions. For example, in laboratory, the bed material size is purposely uniform, which is contradictory with natural field conditions. In laboratory, the channel aspect ratio tends to be small, which results in strong secondary currents. The river bed condition also plays vital role in influencing the channel geometry.

Table 3.1 Equations of scour depth proposed by different investigators

| Sr. No | Researchers | Equations |
|---|---|---|
| 1 | Laursen and Toch (1956) | $\frac{ds}{D}=1.5\frac{h}{D}$ |
| 2 | Shen et al. (1969) | $ds=0.000223\left(\frac{U\times b}{\nu}\right)$ |
| 3 | Hancu, (1971) | $\frac{ds}{b}=2.42\left(2\frac{U}{U_{cr}}-1\right)\left(\frac{U_{cr}^2}{gD}\right)^{1/3}$ |
| 4 | Breusers et al. (1977) | $\frac{d_s}{b}=2\tanh\left(\frac{h}{b}\right)K_I K_s K_\alpha$ |
| 5 | Jain and Fisher (1980) | $\frac{ds}{D}=1.86\left(\frac{h}{D}\right)^{0.5}\left(Fd-Fd_c\right)^{0.25}$ |
| 6 | Jain (1981) | $\frac{ds}{b}=1.84\left(\frac{h}{b}\right)^{0.3}Fd_c^{0.25}$ |
| 7 | Dey (1999) | $\frac{ds}{b}=1.77\left(\frac{h}{b}\right)^{0.15}$ |
| 8 | Ettema et al., (2011) | $\frac{ds}{D}=\left(\frac{h}{D}\right)^{0.62}\left(\frac{U}{\sqrt{gh}}\right)^{0.2}\left(\frac{D}{d_{50}}\right)^{0.08}$ |
| 9 | HEC-18, (2001) | $\frac{ds}{D}=2k_s k_\alpha k_{bed} k_a\left(\frac{h}{D}\right)^{0.35}\left(Fd\right)^{0.43}$ |

| | | |
|---|---|---|
| 10 | Nordila et al.,(2014) | $\frac{ds}{b} = -0.004\left(\frac{b}{d_{50}}\right)^2 + 0.252\frac{b}{d_{50}} - 0.149; 4 \le b/d_{50} \le 25$<br>$\frac{ds}{b} = \frac{2}{\left(0.027\frac{b}{d_{50}} - 0.6\right)^{1.4} + 1.3} + 1.8; 25 \le b/d_{50} \le 1\times10^4$ |
| 11 | Sheppard, (2014) | $\frac{ds}{D} = 2.5 f_1 f_2 f_3$<br>*where,*<br>$f_1 = \tanh\left[\left(\frac{h}{D}\right)0.4\right], f_2 = 1 - 1.2\left[\ln\left(\frac{U}{U_{cr}}\right)\right]^2,$<br>$f_3 = \frac{D/d_{50}}{0.4\left(D/d_{50}\right)^{1.2} + 10.6\left(D/d_{50}\right)^{-0.13}}$ |

Natural streams or alluvial channels comprise of porous boundaries made up of sand particles or gravels. Hence, water percolates in the form of seepage through granular boundaries. So the essential and well-known feature of alluvial channels have been neglected by previous studies. Scour prediction criteria mentioned above and in table 3.1, have developed without considering downward seepage into account. As discussed earlier, downward seepage shows significant impact on scour depth, so it is essential to incorporate downward seepage as an explicit variable for prediction of scour depth. From the previous literature, it has been observed that, Patel et al. (2015) and Deshpande and Kumar (2016) have used the downward seepage parameters in terms of seepage Reynolds number ($Re_s = V_s d_{50}/\upsilon$, where, $V_s$ seepage velocity, $V_s = q_s/(p_s L)$, $q_s$ is seepage discharge over the reach length L, $p_s$ is wetted perimeter) and seepage intensity ($N = \frac{(2\rho u_s V_s)}{\tau_{c0}}$, where $\tau_{c0}$ is critical bed shear stress) respectively. The seepage intensity parameter is depending upon critical bed shear stress, which is related to the initiation of motion of bed particles. The phenomenon of scour around piers is independent of threshold condition of bed particle, however; it is governed by the turbulence of flow. Hence, in this work seepage Reynolds number is considered as non-dimensional seepage parameter. Therefore, in this study equation 1.1 can be changed to following functional relationship:

$$ds = f(h, d_{50}, \sigma_g, g, \upsilon, U, D, V_s, R) \tag{3.7}$$

Where, $h$ is flow depth, $d_{50}$ is median sediment diameter, $\sigma_g$ is standard deviation of sand, $g$ is gravitational acceleration, $\upsilon$ is kinematic viscosity, $U$ is average velocity, $D$ is pier diameter, $Vs$ is seepage velocity, and $R$ is the hydraulic radius. The dimensional analysis indicated that the non-dimensional scour depth ($ds/D$) is a function of four dimensionless

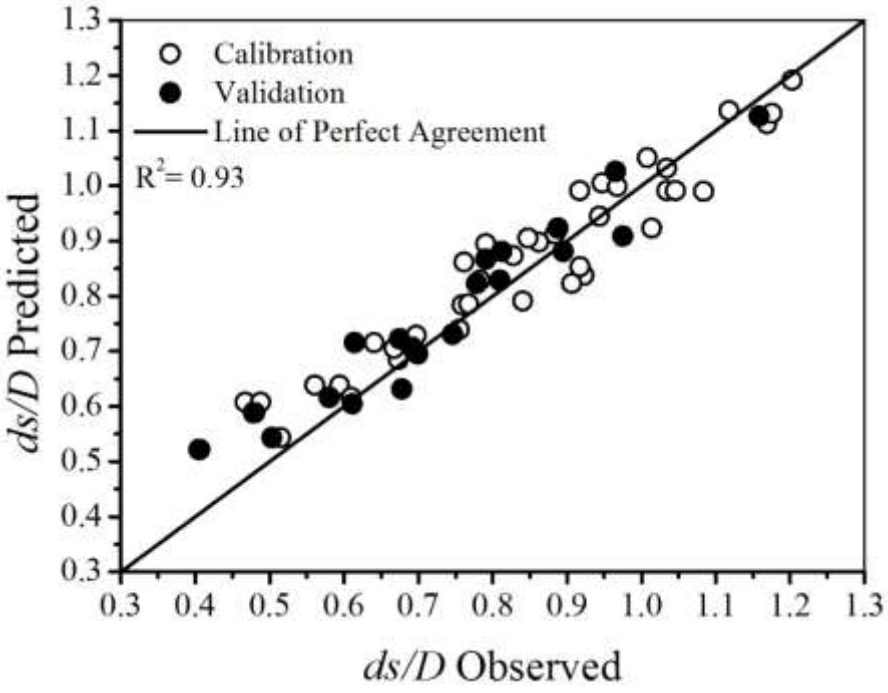


Figure 3.10 Comparison of non-dimensional scour depths obtained from experiments and computed using Equation 3.10

parameters: (1) Froude number $Fd$ ($U/\sqrt{gR}$), (2) Standard deviation ($\sigma_g$), (3) $h/d_{50}$, (4) Seepage Reynolds number $Re_s$.

$$\frac{ds}{D} = f\left(\frac{U}{\sqrt{gR}}, \sigma_g, \frac{h}{d_{50}}, \frac{V_S d_{50}}{\nu}\right) \tag{3.8}$$

The form of the equation is written as:

$$\frac{ds}{D} = Fd^a \sigma_g{}^b \left(\frac{h}{d_{50}}\right)^c \Big/ \exp\left(\mathrm{Re}_s\right)^d \tag{3.9}$$

The coefficients a, b, c and d are obtained by least square fitting procedure with all data points. Seepage Reynolds number is mentioned in exponential form to satisfy no seepage condition of the channel. The final form of the equation is as follows:

$$\frac{ds}{D} = Fd^{4.43}\sigma_g^{-4.71}\left(\frac{h}{d_{50}}\right)^{1.49} \Big/ \exp\left(\mathrm{Re}_s\right)^{0..79} \tag{3.10}$$

The parity plot of equation 3.10 has been shown in Figure 3.10. As shown in the Figure 3.10, the value of $R^2$ (= 0.93) is high thus; it shows that the predictability of the relationship is quite high.

### 3.5.2 Morphological Dune Evolution

Oliveto and Hager (2014) explored the features of the migrating dune like bedforms generated immediately behind piers due to scouring. They proposed equations for prediction of dune crest height and streamwise distance of dune crest from pier as a function of key parameters are given as:

$$\left.\begin{aligned} H^*_D &= \frac{h_{D,\max}}{h_0} = 0.25\left(\frac{D}{h_0}\right)^{0.5}\sigma^{-0.5}F_d^{\,0.2} \\ X^*_D &= \frac{x_{D,\max}}{h_0} = 10\left(\frac{D}{h_0}\right)^{0.5}\frac{1}{1+\Delta F_d} \end{aligned}\right\} \tag{3.11}$$

Where, $H^*_D = h_D/h_0$ is relative maximum dune crest height, $h_D$ is dune crest height, $h_0$ is approach flow depth, $D$ is pier diameter, $\sigma$ is sediment non-uniformity parameter, $F_d$ is densimetric Froude number, $X^*_D = x_D/h_0$ is relative distance of maximum dune crest from pier, $\Delta F_d$ is wash out parameter, $x_{D,max}$ is related to $h_{D,max}$.

Figures 3.11 and 3.12 show the relationship between experimentally measured and predicted values of dimensionless dune crest height ($H_D/h$) and non-dimensional streamwise distance ($X_D/h$) respectively using Oliveto and Hanger (2014) equations. Oliveto and Hanger (2014) equation overpredicts the dune height for no seepage condition and under-predicts in case of seepage experiments. However, the streamwise distance is overpredicted by Oliveto and Hanger (2014) equation in case of no seepage as well as seepage conditions.

In order to find the effect of seepage on dune formation at downstream of the pier, dimensional analysis has been performed to generate empirical relationship for the height of dunes. The non-dimensional height of dunes ($H_D/h$) is considered as a function of Froude number, standard deviation, $D/h$ and seepage Reynolds number.

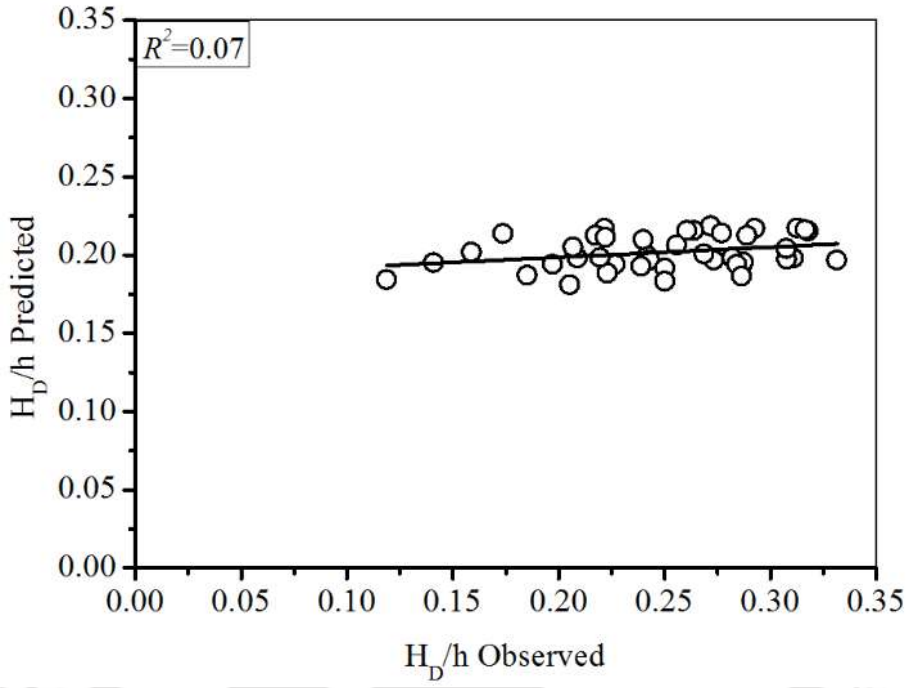


Figure 3.11 Comparison of predicted and observed nondimensional dune crest height for Hager and Oliveto (2014) equation.

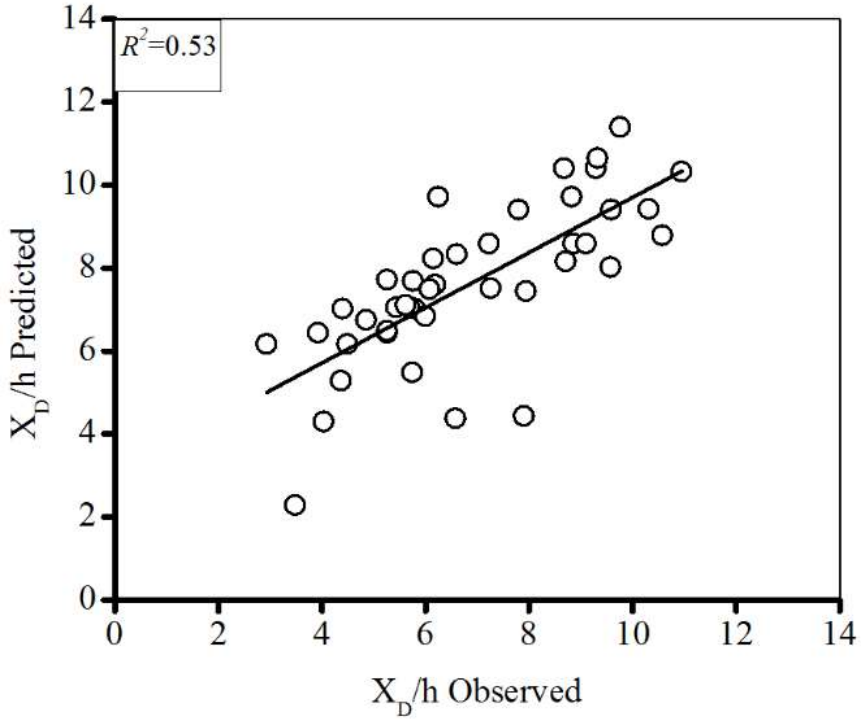


Figure 3.12 Comparison of predicted and observed $X_D$/h for Hager and Oliveto (2014) equation.

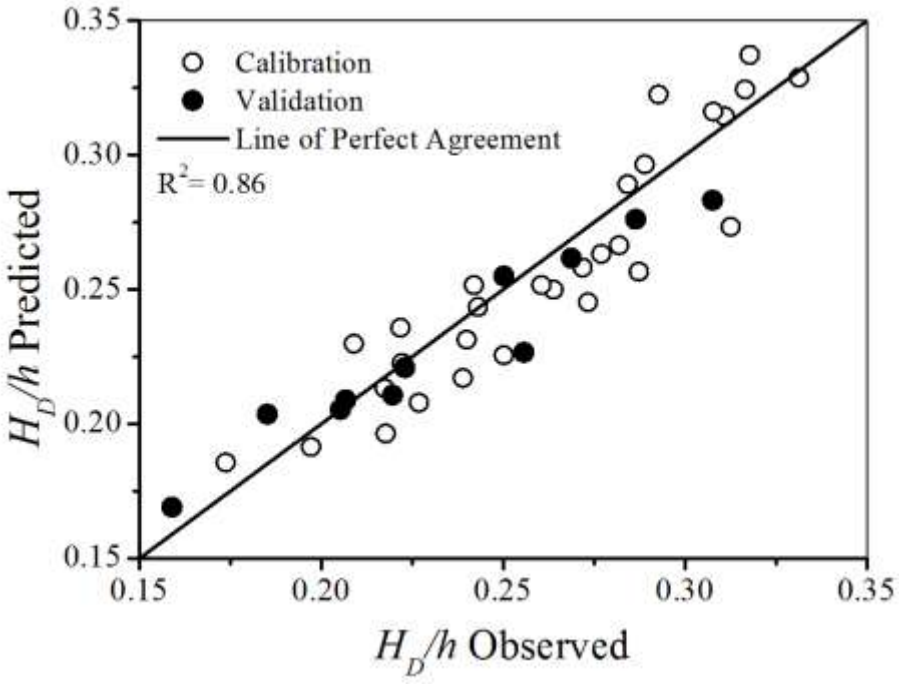


Figure 3.13 Comparison of non-dimensional dune crest heights obtained from experiments and computed using Equation 3.13

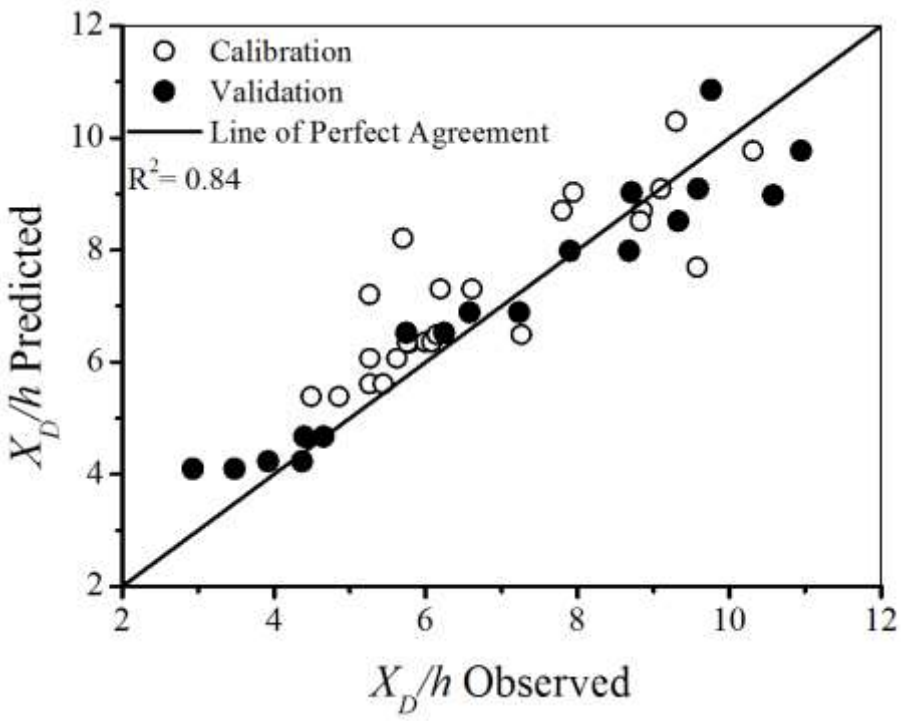


Figure 3.14 Comparison of $X_D/h$ obtained from experiments and computed using Equation 3.15

The equation for the non-dimensional height of dune was assumed to be in the form of:

$$\frac{H_D}{h} = f(Fd, \frac{D}{h}, R_{es}, \sigma_g) = a(Fd)^b \left(\frac{D}{h}\right)^c (\sigma_g)^d \exp(R_{es})^e \quad (3.12)$$

Moreover, the final equation is as follows:

$$\frac{H_D}{h} = 10.45(Fd)^{2.6} \left(\frac{D}{h}\right)^{0.14} (\sigma_g)^{-0.82} \exp(R_{es})^{0.7} \quad (3.13)$$

Similarly, dimensionless streamwise distance of dune crest from pier ($X_D/h$), is expressed by,

$$\frac{X_D}{h} = f(Fd, \mathrm{Re}, \mathrm{R}_{es}, \sigma_g) \quad (3.14)$$

The equation was obtained as,

$$\frac{X_D}{h} = \frac{Fd^{3.93}\,\mathrm{Re}^{0.83}}{\exp(\mathrm{R}_{es})^{0.76}\,\sigma_g^{\,2.69}} \quad (3.15)$$

Figures 3.13 and 3.14 show relationship between experimentally measure and predicted values of $H_D/h$ and $X_D/h$ using equation 3.13 and equation 3.15 respectively.

### 3.5.3 Statistical Criteria

Empirical relationships have been developed with the inclusion of seepage parameter (Equations 3.10, 3.13 and 3.15). In this portion, we will discuss about the performance of newly developed empirical equations. It has been observed that scour depth is reduces with increasing seepage percentage. The new empirical equation for scour depth is compared with various widely used scour depth predictors mentioned in table 3.1. The various equations are compared for no seepage and seepage conditions separately.

Performance of equation 3.10 and scour depth prediction methods mentioned in table 2 is checked by four statistical criteria: coefficient of regression ($R^2$), Root Mean Square Error (RMSE), Nash Sutcliffe efficiency ($E$), Index of Agreement ($d$) and Variance explained by predictive models based on cross-validation ($VEcv$).

$$RMSE = \left[ \frac{\sum_{i=1}^{N} \left( (ds/d)_{i(\mathrm{P})} - (ds/d)_{i(\mathrm{O})} \right)^2}{N} \right]^{1/2} \tag{3.16}$$

$$E = 1 - \frac{\sum_{i=1}^{N} \left( (ds/d)_{i(P)} - (ds/d)_{i(O)} \right)^2}{\sum_{i=1}^{N} \left( (ds/d)_{i(O)} - \left(\overline{ds/d}\right)_{(O)} \right)^2} \tag{3.17}$$

$$d = 1 - \frac{\sum_{i=1}^{N} \left( (ds/d)_{i(\mathrm{P})} - (ds/d)_{i(O)} \right)^2}{\sum_{i=1}^{N} \left( \left| (ds/d)_{i(P)} - \left(\overline{ds/d}\right)_{(\mathrm{O})} \right| + \left| (ds/d)_{i(O)} - \left(\overline{ds/d}\right)_{(\mathrm{O})} \right| \right)^2} \tag{3.18}$$

Where, $(ds/d)_{i(P)}$ and $(ds/d)_{i(O)}$ are *i*th predicted and observed non-dimensional scour depths respectively. $\left(\overline{ds/d}\right)_{(\mathrm{O})}$ is the average value of observed non-dimensional scour depths. *N* is the total number of events. Li (2017) has recommended *VEcv* criteria for accessing the accuracy of the predictive models. It is defined as the proportion of the variation in the validation data explained by predicted data obtained from predictive models based on cross-validation (2016). *VEcv* is accuracy measure based on predicted values derived from cross-validation. *VEcv* is also called G-value or goodness of prediction measures (2001). *VEcv* is computed as:

$$VEcv = \left( 1 - \frac{\sum_{i=1}^{N} \left( (ds/d)_i - (ds/d)_p \right)^2}{\sum_{i=1}^{N} \left( (ds/d)_i - (\overline{ds/d}) \right)^2} \right) 100(\%) \tag{3.19}$$

The statistical comparison for both no seepage and with seepage condition is mentioned in table 3.2 and table 3.4 respectively. From table 3.1 it can be seen that HEC-18(2001), Shen et al. (1969) and Hancu (1971) are better predictors for scour depth in case of no seepage conditions. However, the accuracy of all equations has decreased (table 3.4) with seepage, which suggests that none of the aforementioned scour depth predictors are precise for prediction of scour depth in case of seepage affected channels. From

experimental results, it has been observed that some of the scour depth equations can be pertinent for no seepage condition yet over-predict the scour depth in case of seepage condition. From table 3.5, it appears that equation 3.10 gives a reasonable prediction in case of both no seepage and seepage conditions.

Table 3.2 Evaluation of different methods in prediction of pier scour depth for no seepage condition.

| **Predictors** | **$R^2$** | **RMSE** | **E** | ***d*** | **VEcv (%)** |
|---|---|---|---|---|---|
| Laursen and Toch (1956) | 0.36 | 0.77 | -45.6 | 0.05 | -4560 |
| Ettema et al., (2001) | 0.45 | 0.33 | -7.5 | 0.44 | -750 |
| HEC-18(2001) | 0.68 | 0.29 | -5.83 | 0.45 | -583 |
| Sheppard et al. (2014) | 0.36 | 0.27 | -19.8 | 0.29 | -1980 |
| Shen et al.(1969) | 0.71 | 0.27 | -4.83 | 0.46 | -483 |
| Hancu (1971) | 0.84 | 2.17 | -370 | 0.08 | -37000 |
| Breusers (1977) | 0.35 | 0.5 | -19.25 | 0.29 | -1925 |
| Jain & Fischer (1980) | 0.52 | 0.38 | -10.64 | 0.37 | -1064 |
| Jain (1981) | 0.41 | 0.12 | -0.16 | 0.71 | -16 |
| Dey (1999) | 0.36 | 0.55 | -1.12 | 0.28 | -112 |
| Nordila et al.,(2014) | 0.16 | 0.64 | -31.15 | 0.25 | -3115 |

The performance of the new prediction criteria for dune morphology are mentioned in table 3.5. From the table, it can be perceived that the newly developed prediction criteria with incorporating downward seepage parameters are suitable for both with seepage and without seepage condition.

Table 3.3 Evaluation of different methods in prediction of pier scour depth for seepage condition

| **Predictors** | **$R^2$** | **RMSE** | **E** | **Id** | **VEcv (%)** |
|---|---|---|---|---|---|
| Laursen and Toch (1956) | 0.24 | 1.1 | -39.2 | 0.068 | -3900 |

| | | | | | |
|---|---|---|---|---|---|
| Ettema et al., (2001) | 0.32 | 0.54 | -8.73 | -0.65 | -873 |
| HEC-18(2001) | 0.52 | 0.5 | -7.47 | 0.41 | -747 |
| Sheppard et al. (2014) | 0.24 | 0.84 | -22 | 0.28 | -2200 |
| Shen et al.(1969) | 0.54 | 0.47 | -6.37 | 0.43 | -637 |
| Hancu (1971) | 0.62 | 2.92 | -278.84 | 0.09 | -27884 |
| Breusers (1977) | 0.24 | 0.82 | -21 | 0.29 | -2100 |
| Jain & Fischer (1980) | 0.39 | 0.62 | -11.76 | 0.35 | -1176 |
| Jain (1981) | 0.19 | 0.17 | 0.04 | 0.75 | 4 |
| Dey (1999) | 0.24 | 0.89 | -25.3 | 0.27 | -2530 |
| Nordila et al.,(2014) | 0.11 | 1.03 | -34.1 | 0.24 | -3410 |

Table 3.4 Evaluation of Equation 3.10

| **Condition** | **$R^2$** | **RMSE** | **E** | **Id** | **VEcv (%)** |
|---|---|---|---|---|---|
| No Seepage | 0.90 | 0.07 | 0.90 | 0.93 | 90 |
| With Seepage | 0.93 | 0.06 | 0.89 | 0.93 | 89 |

Table 3.5 Evaluation of Equation 3.13 and equation 3.15.

| **Equations** | **$R^2$** | **RMSE** | **E** | **Id** | **VEcv (%)** |
|---|---|---|---|---|---|
| Eq.3.13 | 0.86 | 0.006 | 0.86 | 0.92 | 86 |
| Eq.3.15 | 0.84 | 0.008 | 0.82 | 0.9 | 82 |

## 3.6 Discussions

The new empirical relationships were developed for prediction of scour depth and dune geometry at circular bridge piers with the inclusion of seepage. Natural streams, rivers often comprise of porous boundaries. The permeable boundaries allow transfer of mass and momentum through it, which results in complex interaction between surface and subsurface flow. Seepage through channels boundaries may exert additional hydrodynamic forces on bed material that results in modification of bed morphology and

hydrodynamic characteristics of alluvial channels. Results showed that the scour depth reduces with downward seepage, which may lead to reduce the cost of construction or protection measures if seepage is included in the design. So understanding the importance of downward seepage, the proposed equations for scour depth, the height of dunes and streamwise distance of dune crest from pier through experimental study are empirical in nature, which can be further modified using data from actual field observations. Because of the typical dimensions of the laboratory flumes and lower limit of sediment size, it is difficult to relate scour in the flume to scour in the rivers. These difficulties limit the use of laboratory flumes in developing accurate predictors of scour at full-scale piers. Generally, the river models are made to be 'distorted' model. Distorted models are those in which one or more terms of the model are not correspondingly identical with its prototype. The distorted models for scour around piers are very helpful in the proper understanding of the likely performance of the prototype. Considering the limitations of the flume, field and mathematical models, further elucidation of scouring at bridge piers depends on the combined use of the three investigative approaches.

Sensitivity analysis for Equations 3.10, 3.13 and 3.15 has been carried out and depicted in Figures 3.15, 3.16 and 3.17. Sensitivity analysis is a widely used technique to determine how different values of an independent variable will influence a particular dependent variable under a given set of assumptions. Sensitivity analysis is helpful to determine the impact of the actual outcome of a particular variable will have when it varies from previously assumed value and the analyst can determine how changes in one variable will affect the target variable. In the present study, sensitivity analysis is carried out by changing one variable for $\pm 5\%, \pm 10\%, \pm 15\%$ while, keeping other variables fixed. Figure 3.14 a, b, c and d shows the sensitivity of Equation 3.10 with the variation in the values of Froude number ($Fd$), standard deviation ($\sigma_g$), Seepage Reynolds number ($Re_s$) and ($h/d50$). From Figure 3.14, it can be observed that the Equation 3.10 is highly sensitive towards standard deviation and Froude number. Similarly, from Figures 3.15 and 3.16, it can be seen that equation 3.13 is highly sensitive towards Froude number whereas Equation 3.15 is highly sensitive to Froude number and standard deviation.

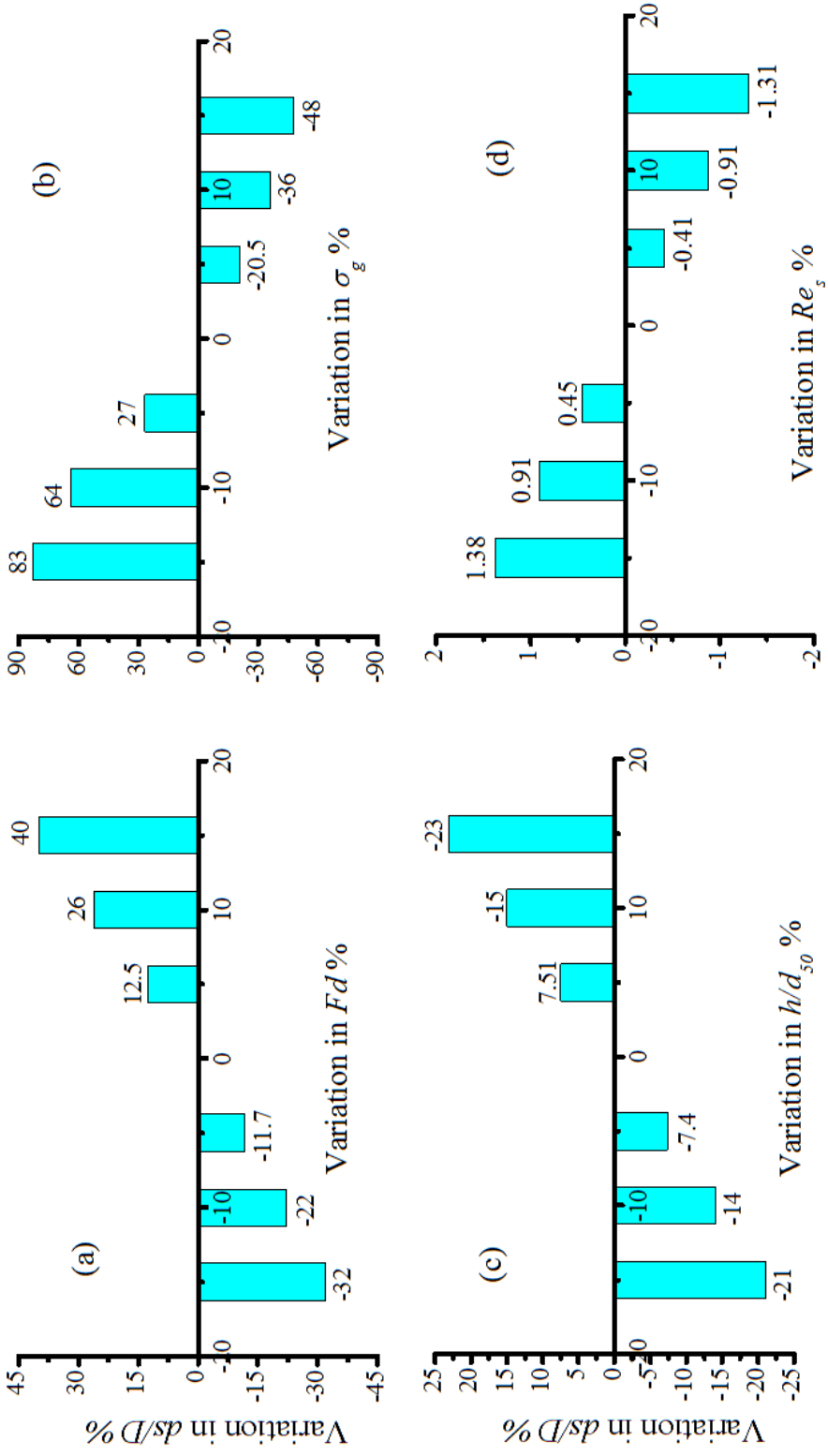


Figure 3.15 Sensitivity analysis for equation 3.10

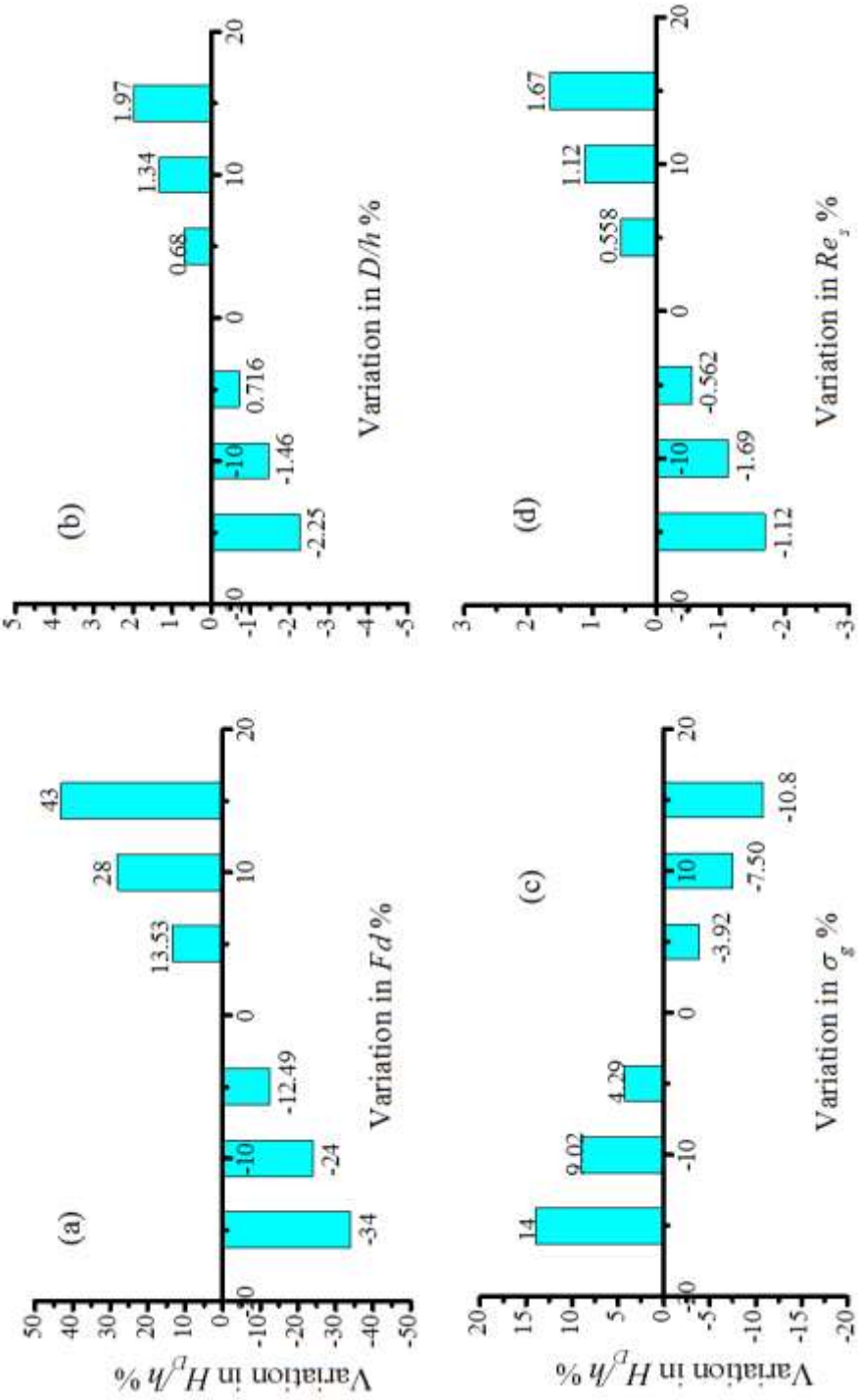


Figure 3.16 Sensitivity analysis for equation 3.13

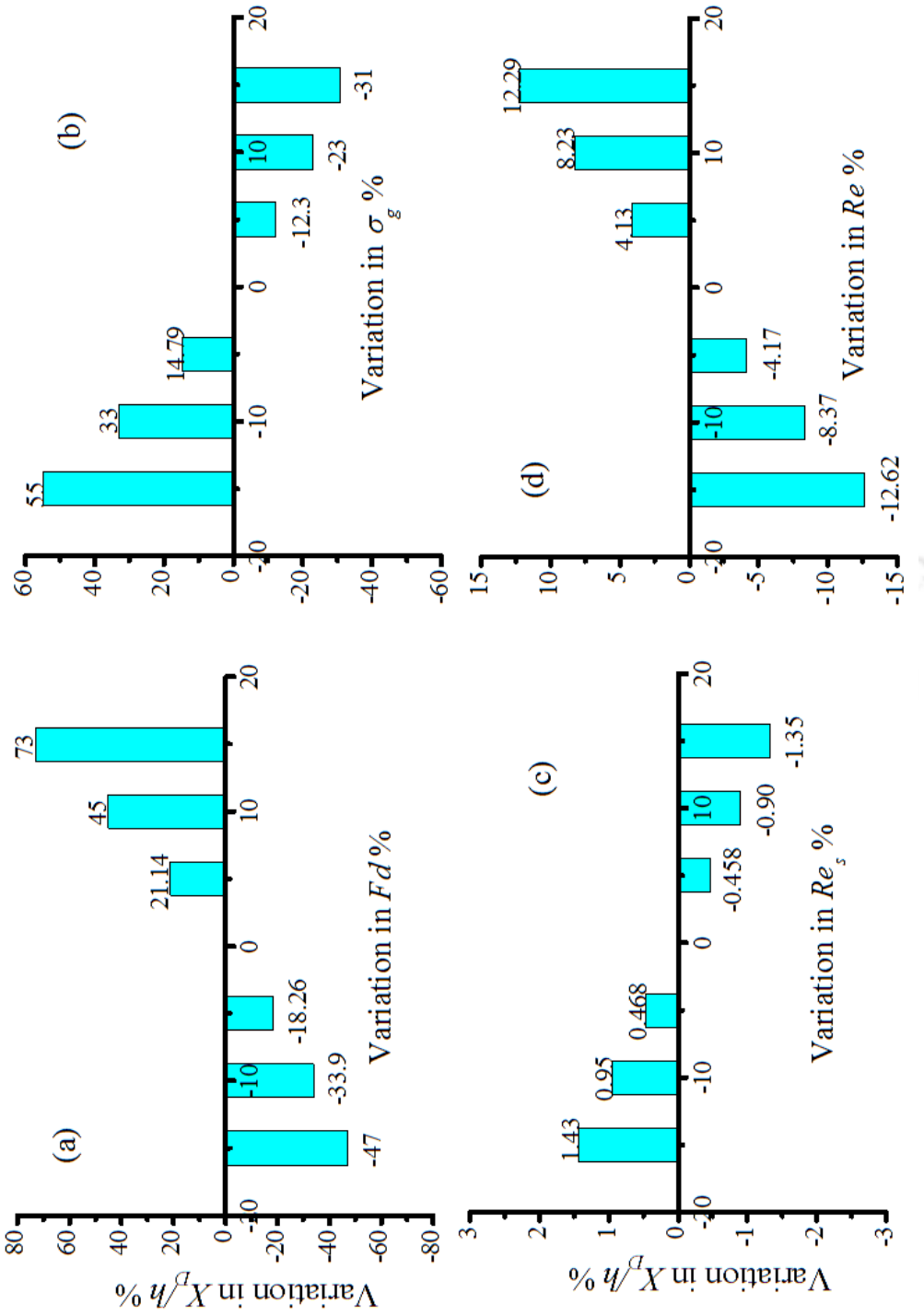


Figure 3.17 Sensitivity analysis for equation 3.15

## 3.7 Conclusion

Upstream and downstream of the pier were observed to be the most critical sections. At the upstream of the pier, maximum velocity occurs near the edge of the scour hole, whereas, it occurs near the bed at the downstream of the pier. Downward seepage obstructs the reversal of flow at upstream of the pier resulting in less momentum transfer, which minimizes the scouring of the bed material. The presence of downward seepage leads to the increase in Reynolds shear stress which is upgraded by separation of the stream flow that leads to vortex shedding at the downstream of the pier. Reynolds shear stress fluctuates heavily on the application of downward seepage. The Reynolds shear stress turns out to be more negative in the vicinity of bed at upstream of the pier while at downstream of the pier, it occurs near the surface. The contribution of sweep events towards Reynolds shear stress increases with downward seepage at the upstream of the pier, whereas, at the downstream of the pier ejection events become more dominant with seepage which induces the sediments in suspension, to get transported further along the flow.

Bridge piers are obstacles in fluvial environments, which cause flow separation and prompt scouring the bed material around piers. The results showed that the scour depth at piers is maximum in case of no seepage experiments and reduces for seepage experiments with increasing seepage percentage. Towards the start of scouring, the rate of expansion in scour depth progressively and gradually diminishes with development in time. The height of dunes at rear side of pier is lesser in case of no seepage runs and increases with increasing seepage percentage.

The new empirical relationship is developed for prediction of scour depth with the inclusion of downward seepage in the form of seepage Reynolds number. The results show that, though Shen et al. (1969), Hancu (1971) and HEC-18(2001) are fairly good compatible with observed scour depth in case of no seepage runs; but not suited for seepage runs. Oliveto and Hager (2014) equations are used to compare experimental findings and observed dune height and streamwise distance of dune crest from the pier, which shows that the equations are not compatible in case of seepage, runs. With the inclusion of seepage parameter, new empirical equations are developed for prediction of dune morphology.

Chapter **4**

# Hydrodynamics and Morphology around Tandem Piers in Alluvial Channel with Downward Seepage[iii]

## 4.1 Introduction

In the alluvial channels, complicated flow structures around bridge piers result in scouring which is the main reason behind the structural collapse. Many researchers have investigated that vortex system developed around bridge pier is responsible for scouring around piers (Melville, 1975; Ettema, 1980; Qadar, 1981; Cheiw, 1984; Melville and Coleman, 2000; Richardson and Davis, 2001; Sheppard, 2004; Pasiok and Stilger-Szydło, 2010). Melville (1975) and Chiew (1984) have stated that the vortex system consisting of horse shoe vortex and wake vortices is the primary reason behind the scouring around piers. Horseshoe vortex increases velocity near the bed, and wake vortices keep the sediment particles in suspension. Qadar (1981), has reported that the flow separates at upstream of the pier and rolls up near the bed region, which causes scouring around piers. According to Melville and Coleman (2000), the principal characteristics of flow field are downflow at the upstream face of pier, horseshoe vortex near the bed, surface roller and wake vortices at downstream of the pier. Izadinia et al. (2013) have investigated flow characteristics around single pier with fixed bed condition. Reviews of previously published researches show that the turbulent flow characteristics around single bridge pier are very complex. Hence, it is more complex around a group of piers.

Nowadays, a group of piers are widely used in bridge designing seeing geotechnical and economical reasons (Ataie-Ashtiani et al., 2010). In crowded cities, it is needful to construct multilane bridges or new bridge beside the old one. Sometimes, in practice, it is observed that many bridges are wide and compromise number of piers aligned in the flow direction to support the structure. In this chapter the tandem arrangement of piers is

[iii] Chavan, R., & Kumar, B. (2017). Experimental investigation on flow and scour characteristics around tandem piers in sandy channel with downward seepage. Journal of Marine Science and Application, 16(3), 313-322.

studied which is one of the simplest arrangements of group of piers. Phenomenon of scouring around single pier is quite different from scouring around group of piers (Beg, 2010). Many researchers have conducted laboratory experiments on tandem arrangement of piers to investigate the effect of spacing between piers on scouring (Salim and Jones, 1998; Ataie-Ashtiani and Beheshti, 2006). Salim and Jones (1998) have found that scour depth decreases with increasing distance between piers. Ashtiani and Beheshti (2006) have conducted laboratory experiments and suggested correction factor for accuracy of existing scour equations for tandem arrangement of piers. Said et al. (2008) have conducted laboratory experiments and obtained velocity data around single pier and two submerged tandem piers and stated that in case of tandem piers flow characteristics vary with distance between piers. Palau- Salvador et al. (2008) have reported that presence of second pier disturb the wake vortices at downstream of front pier. Ataie-Ashtiani and Aslani-Kordkandi (2013) have carried out laboratory experiments to investigate the variation of turbulence flow statistics around single pier and tandem piers. Some of the researchers have conducted experiments on tandem piers in wind tunnels (Okajima et al., 2007; Sumner, 2010; Elhimer et al., 2016). This chapter presents the results of turbulence characteristics of flow around piers of same and different diameters arranged in tandem manner. It discusses the effect of downward seepage on flow characteristics and bed features around tandem piers.

## 4.2 Tandem Piers of Similar Diameter

In the case of tandem piers, approaching flow reaches the front pier and separates in the form of downflow along the face of pier and side circulations, further results in formation of wake vortices at downstream of pier. In between both piers, the flow is noticeably complex due to wake vortices forming at downstream of front pier and obstruction to the flow by rear pier. Behind the rear pier, wake vortices formed due to flow separation and results in reversal flow near free surface. To understand the change in flow characteristics and its influence on scour geometry around piers under no seepage and with seepage conditions the velocity measurements were taken around piers. The experiments are conducted for two piers of diameter 75mm and for two piers of diameter 90mm arranged in tandem manner. The centre-to-centre spacing between two piers is three times the diameter of piers. The trend of turbulent statistics is similar for both the arrangements.

### 4.2.1 Velocity

The velocity profiles were measured by ADV around piers at three sections, upstream (A) of the front pier, in between both the piers (B) and downstream (C) of the rear pier. Figure 4.1 shows velocity profiles around 75mm diameter tandem piers at three sections; A (7.5975, 0.5), B (7.388, 0.5) and C (7.1835, 0.5) respectively for no seepage, 10% seepage and 15% seepage runs. The velocity profiles are plotted with $z/h$ verses $u$, where $z$ is the distance of the point from bed; where velocity measurements were taken, $h$ is the total flow depth and $u$ is time averaged velocity.

At upstream of the front pier that is at section A, as the approach flow is obstructed by the front pier, the reversal velocity can be seen near the bed with in the scour hole where the streamwise component of velocity is found to be negative. With increasing distance from the bed, the stream wise velocity component becomes positive and reached to maximum velocity near the edge of the scour hole at ($z/h \approx 0.45$). At downstream of the pier, at section C, reversal flow can be seen near the free surface and becomes positive with increasing distance from the free surface; the stream wise velocity component attains its maximum value near the bed ($z/h \approx 0.1$). Section B is the most critical section where the velocity profile is influenced by flow circulations at the downstream of the front pier and obstruction to the flow by the rear pier. At section B, near the free surface the velocity is less positive and gradually increasing near the bed. In the case of tandem piers, the flow behaviour between the two piers is noticeably complex. The flow leads to the formation of wake vortices at downstream of the pier by moving further along the sides of the front pier due to flow separation at upstream of the front pier. The velocity of flow decreases while approaching the rear pier because of the wake vortices at front pier (Ataie-Ashtiani and Aslani-Kordkandi, 2013). At downstream of the rear pier, reversal flow can be seen near the free surface and velocity is increasing gradually with moving towards the bed. Downward seepage leads to increase the velocity and shear stress near the bed which enhance rate of sediment transport (Devi and Kumar, 2015). In this study, though the velocity increased on application of downward seepage, downward seepage impedes the

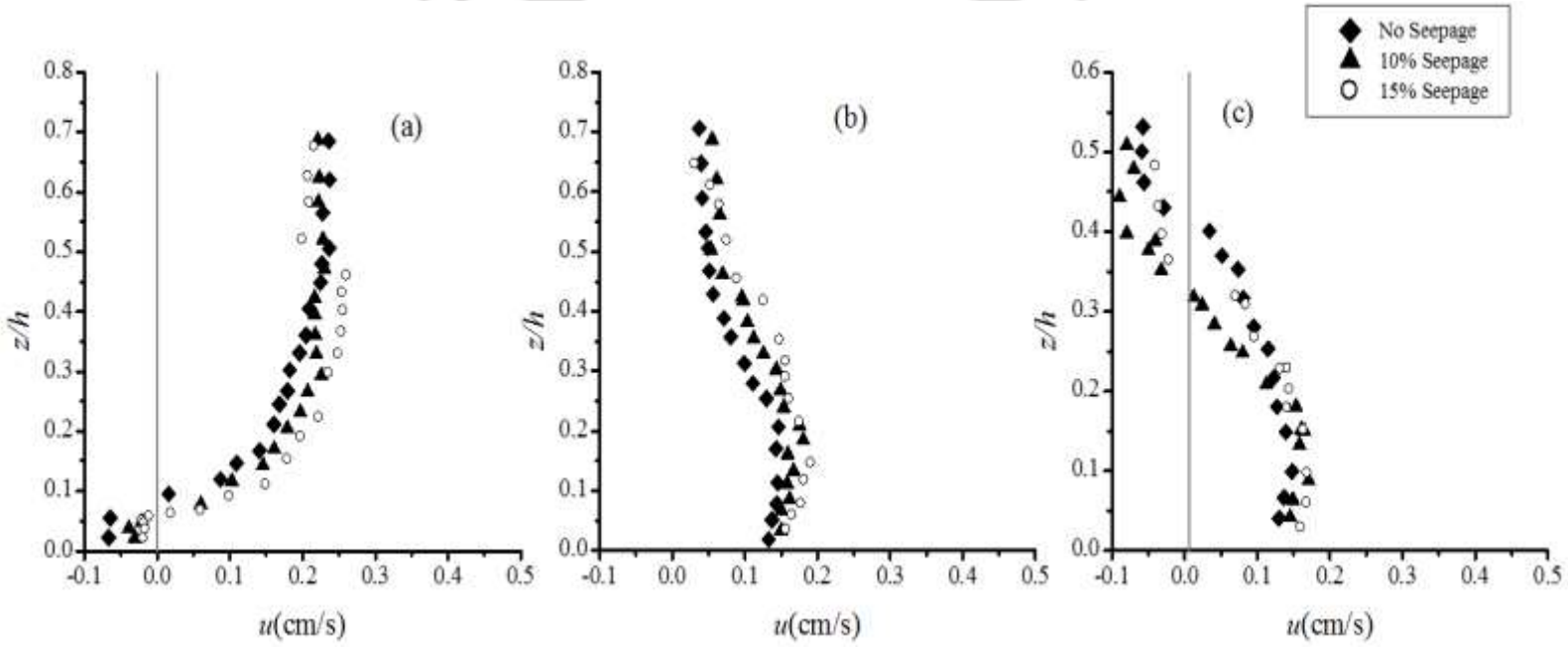


Figure 4.1 Velocity profiles around tandem piers at (a) Upstream A, (b) Section B, (c) Downstream C

reversal flow. Consequently, the velocity of flow is less near the bed at the upstream of the front pier (Section A) and near the surface at Section C in case of seepage runs.

### 4.2.2 Reynolds Shear Stress

Presence of pier diverts the approaching flow at the upstream edge of the pier, leading to create more turbulence around the pier. The flow separation generates higher Reynolds stresses and enhances the momentum exchange owing to scour around piers. Reynolds shear stress becomes negative near the bed at section A and near the free surface at section C. Reynolds stresses are stronger at downstream of piers than those at the upstream of piers due to formation of wake vortices at downstream of piers. At section B, Reynolds shear stress fluctuates heavily due to wake vortices generated at the downstream of the front pier and obstruction to the forwarding flow because of rear pier. From Figure 4.2, it can be perceived that at section A, Reynolds stresses are negative near bed and near free surface at section C. At section A, Reynolds stresses are increasing, with moving away from the bed whereas, at section C Reynolds stresses are increasing with moving towards bed. Downward seepage leads to decrease Reynolds stresses near the bed at upstream of the pier. The Reynolds shear stresses are more in case of no seepage run then decrease in case of 10 % seepage and again decrease in case of 15% seepage run.

### 4.2.3 Quadrant Analysis

At the upstream of the front pier in near bed region, the reversal flow lifts the sediment particles from the scour hole. However; the particles are unable to move forward as flow is not having sufficient capacity to carry the particles. It can be observed visually during the experiments that particles dislodged by the reversal flow from the slanting slope of the scour hole are again settled down on the bed. From Figure 4.3, it can be observed that near the bed within the scour hole ($z/h \leq 0.1$) at the upstream of the pier, Q1 and Q3 events contribute more to the total Reynolds shear stress than Q2 and Q4. Contributions from sweep and ejection events are more than inward and outward interaction at outside the scour hole. Near the edge of the scour hole, sweep events are more dominant. Sweep events are governing mechanism for the threshold condition of mobile bed channel due to arrival of high speed fluid particles which enhance the momentum exchange and lead to the development of the scour depth.

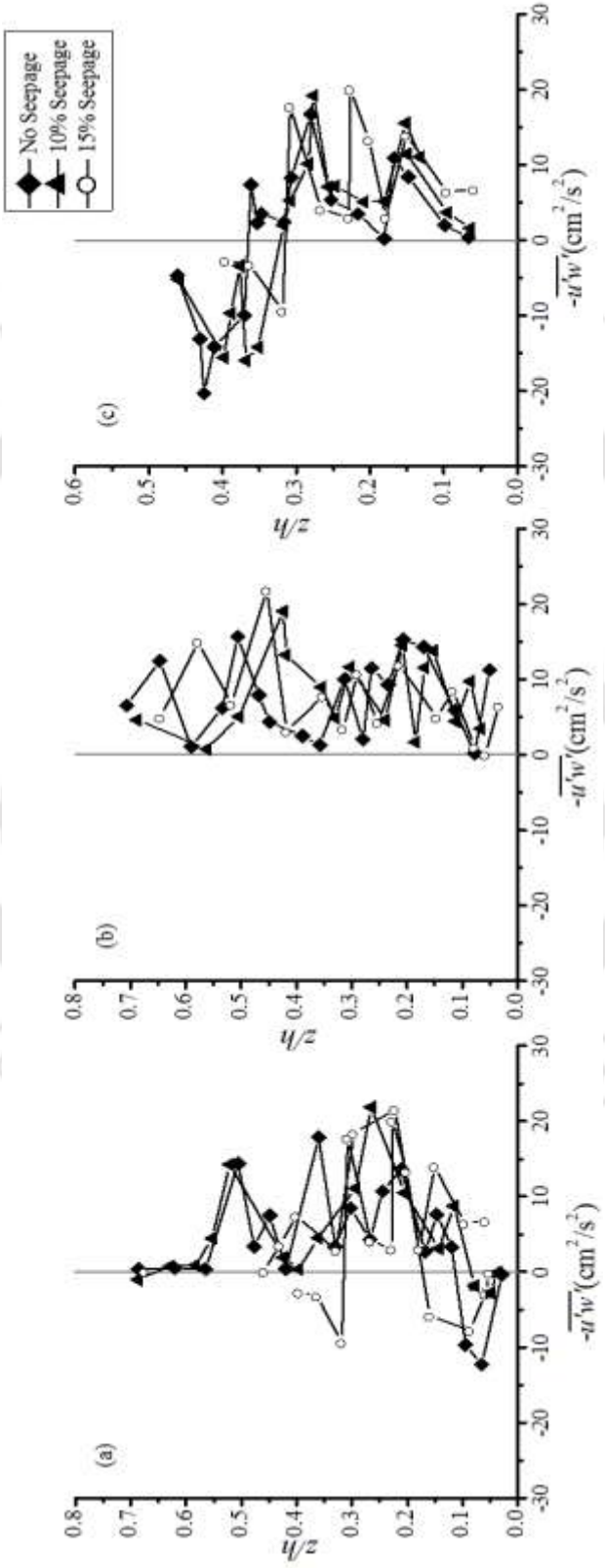


Figure 4.2 RSS profiles around piers at (a) Upstream A, (b) Section B, (c) Downstream C

In the downstream of the piers (section C) within the scour hole ($z/h \leq 0.38$), ejection events are dominant over sweep events as low speed fluid parcels arrive due to reversal flow which is contributing greater $-u'$ in streamwise direction. Ejection events brought the sediment in suspension, which reduces towards the water surface. Whereas, above scour hole ($z/h>0.38$), probability of occurrence of sweep and ejection events is nearly same.

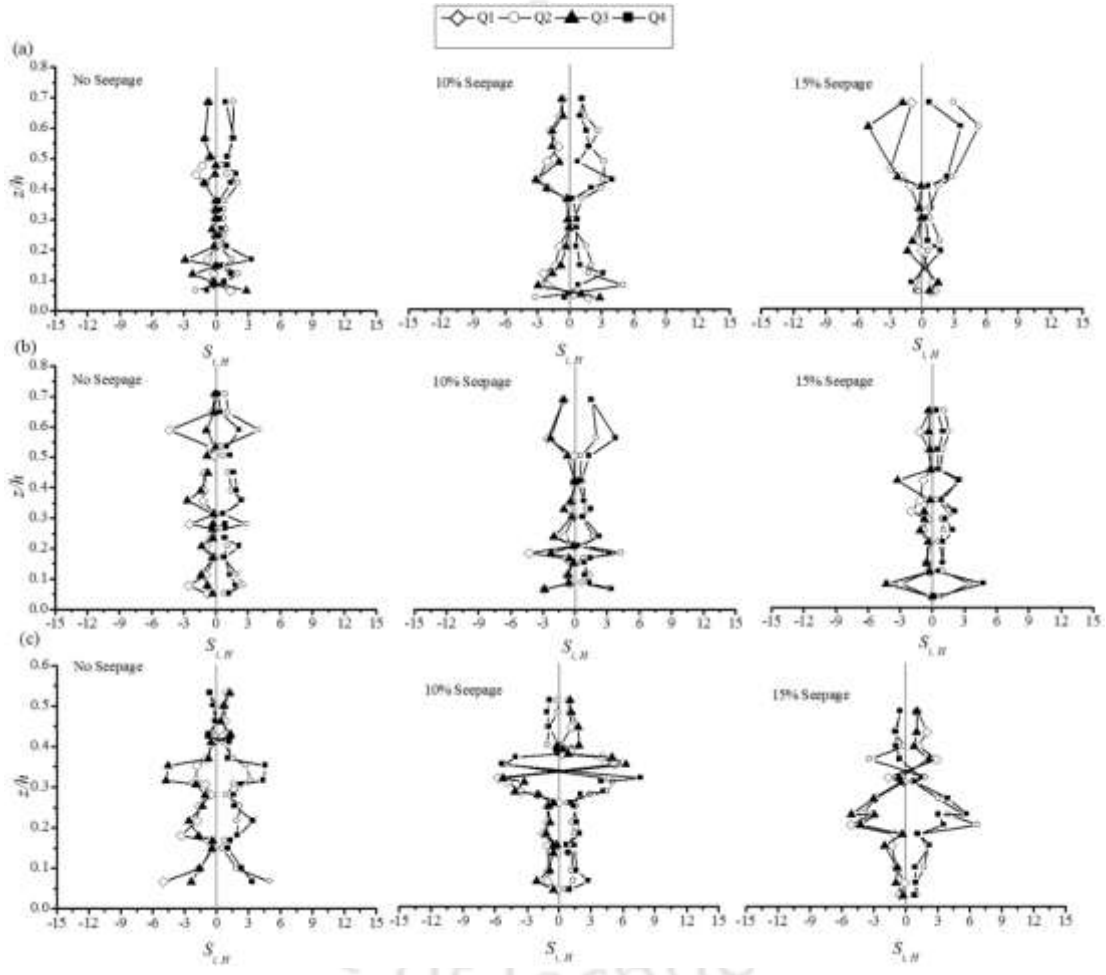


Figure 4.3 Stress fraction $S_{i,H}$ against $z/h$ at (a) Section A (b) Section B (c) Section C

The magnitude of events is greater at this section as the flow is more turbulent due to wake vortices forming at downstream of piers. At section B, throughout the flow depth, contributions coming from sweep and ejection events are more than contributions of inward and outward interaction. At section B, fluctuations of stress fraction are increased. At section A that is upstream of the piers and section C that is downstream of the piers,

stress fraction fluctuates more near the bed due to complex flow structure within the scour hole and fluctuations are reduced gradually towards the surface.

Downward seepage through channel boundaries influences the conditional RSS distribution. The contribution of all four quadrants namely; inward interaction, outward interaction, ejection and sweep to the Reynolds shear stress are increased in case of seepage as compared to no seepage runs. From Figure 4.3, it can be observed that downward seepage results in the arrival of low-speed fluid particles due to retardation of flow, which indicates ejection events. Whereas, above the scour hole contribution of ejection and sweep events are greater, inward and outward interaction contribute weakly to total Reynolds shear stress.

### 4.2.4 Moment Analysis

Third order correlations of velocity fluctuations are studied to procure the information of contribution velocity fluctuations in terms of flux and diffusion of the Reynolds stresses (Simpson et al., 1981). The third order correlation is defined as, $M_{jk} = \overline{\hat{u}^j \hat{w}^k}$ where, j + k = 3, $\hat{u} = u' \Big/ \left(\overline{u'u'}\right)^{0.5}$ and $\hat{w} = w' \Big/ \left(\overline{w'w'}\right)^{0.5}$ (Raupach, 1981). $M_{30}$ ($\overline{\hat{u}^3}$) is skewness of *u'*, also known as the streamwise flux of streamwise Reynolds stress $\overline{u'u'}$ while $M_{03}$ ($\overline{\hat{w}^3}$) is skewness of vertical velocity fluctuations $w'$ and also known as the vertical flux of the vertical Reynolds stress $\overline{w'w'}$. $M_{12}$ ($\overline{u^1 w^2}$) and $M_{21}$ ($\overline{u^2 w^1}$) are diffusions of vertical Reynolds stress in streamwise direction and streamwise Reynolds stress in vertical direction respectively.

The third order correlation of velocity fluctuations ($M_{30}$, $M_{03}$, $M_{12}$ and $M_{21}$) at upstream of piers (section A) and downstream of piers (section C) for with and without seepage conditions are depicted in Figure 4.4. From Figure 4.4, it can be observed that third order moments are fluctuating heavily throughout the flow depth and fluctuations are more near the edge of the scour hole. At the upstream of piers (section A) $M_{30}$ and $M_{12}$ start with positive values near the bed and then changing over to the negative values with increasing *z/h*, which implies that near the bed $\overline{u'u'}$-flux and $\overline{w'w'}$-diffusion occur in streamwise direction while moving away from the bed, $\overline{u'u'}$ -flux and $\overline{w'w'}$- diffusion occur in

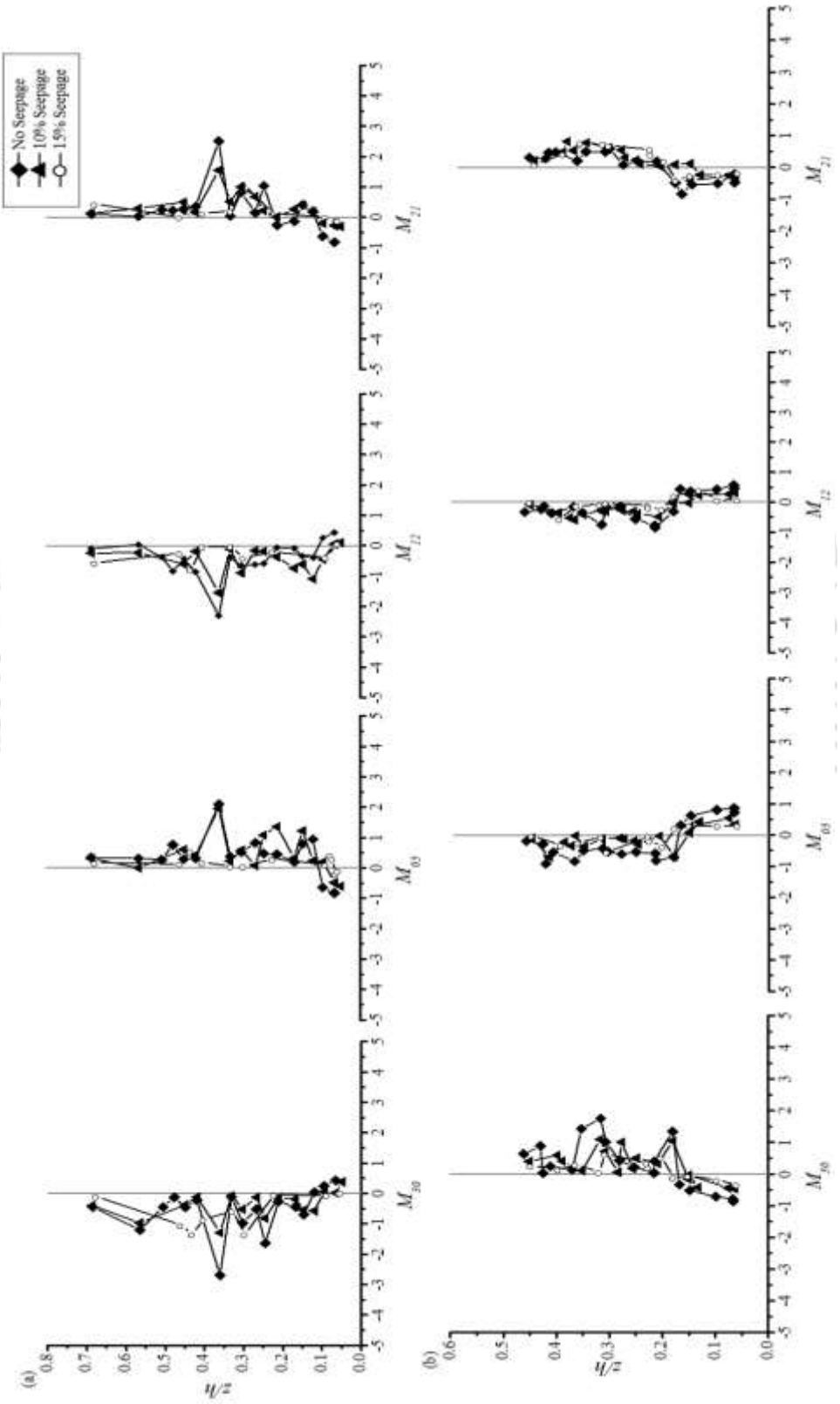


Figure 4.4 Vertical distribution of higher order moments at (a) Upstream A, (b) Downstream C

opposite direction to that of flow direction and become pronounced with an increase in *z/h*. In case of seepage runs, at the upstream of the piers near the bed region, positive values of $M_{30}$ and $M_{12}$ are decreased unlike the plane bed as reversal flow slows down on the application of downward seepage. $M_{03}$ and $M_{21}$ initiate with negative values and then change to positive values; it suggests that $\overline{w'w'}$-flux and $\overline{u'u'}$-diffusion are in downward direction near the bed region. Negative nature of $M_{03}$ and $M_{21}$ decreases on application of downward seepage. At upstream of pier negative values of $M_{03}$ and $M_{21}$ shows that flow is coming towards the bed and is transported along flow direction, which can be observed from positive values of $M_{30}$ and $M_{12}$. At downstream of piers (Section C), $M_{30}$ starts with negative and turns towards positive and $M_{03}$ starts with positive and turns towards negative with increasing distance from bed. Negative $M_{30}$ and positive $M_{03}$ suggest that $\overline{u'u'}$- flux occurs in opposite to streamflow direction and $\overline{w'w'}$- flux in upward direction. Whereas, $M_{12}$ starts with positive values near bed then turn towards negative and $M_{21}$ starts with negative near the bed and change to positive with increasing distance from bed. This shows that, at downstream of piers near the bed, $\overline{w'w'}$ diffusion occurs in the direction of stream and $\overline{u'u'}$ diffusion occurs in downward direction. Near free surface $M_{12}$ is negative and $M_{21}$ is positive that is $\overline{w'w'}$ diffusion and $\overline{u'u'}$diffusion propagate against the flow direction and in upward direction respectively which can be justifiable with enhanced secondary currents due to formation of wake vortices at downstream of piers. At section C, near the bed negative $M_{30}$ and positive $M_{03}$ indicate the arrival of slower moving fluid parcels that represent an ejection motion. At downstream of piers, sediment particles are removed from bed due to ejection and ejection decrease near free surface. With downward seepage negative nature of $M_{30}$ and $M_{21}$ as well as positive nature of $M_{03}$ and $M_{12}$ decrease. At section B, which is at downstream of the front pier trend of higher order moments is nearly same as it is obtained for section C.

### 4.2.5 Flux of the Turbulent Kinetic Energy

The distribution of non-dimensional flux of streamwise ($F_{TKEu} = f_{TKEu}/U_*^3$) and vertical ($F_{TKEw} = f_{TKEw}/U_*^3$) turbulent kinetic energy is shown in Figure 4.5 which can be calculated as (Raupach, 1981),

$$\left.\begin{aligned} f_{TKEu} &= 0.75\left(\overline{u'u'u'} + \overline{u'w'w'}\right) \\ f_{TKEw} &= 0.75\left(\overline{u'u'w'} + \overline{w'w'w'}\right) \end{aligned}\right\} \quad (4.1)$$

The graph of the non-dimensional flux of turbulent kinetic energy against *z/h* for no seepage and seepage conditions at upstream and downstream of piers are shown in Figure 4.5. Presence of piers in flowing stream leads to change the flow pattern around piers and turbulent flow characteristics accordingly. At the upstream of the piers (section A) for no seepage conditions $f_{TKEu}$ begin with small positive and $f_{TKEw}$ start with negative values. With increasing *z/h*, $f_{TKEu}$ turns towards negative and $f_{TKEw}$ turns towards positive. Positive values of $f_{TKEu}$ and negative $f_{TKEw}$ are associated with the streamwise flux of turbulent kinetic energy in streamwise direction and vertical flux of turbulent kinetic energy is in the downward direction. However, away from the bed, negative $f_{TKEu}$ and positive $f_{TKEw}$ imply that streamwise flux of turbulent kinetic energy opposite to flow direction and vertical flux of turbulent kinetic energy in the upward direction. Negative $f_{TKEu}$ and positive $f_{TKEw}$ initiate retardation process with the arrival of low-speed fluid parcels. Though the same pattern is observed in case of seepage runs, close observation of Figure 4.5 shows that near the bed $f_{TKEu}$ and $f_{TKEw}$ have lesser positive and negative values in case of seepage runs than no seepage condition.

At downstream of piers (section C), secondary currents are more dominant due to wake vortices. $f_{TKEu}$ and $f_{TKEw}$ initiate with small negative and positive values respectively. Moving away from the bed, nearly at the edge of the scour hole $f_{TKEu}$ turns towards positive and $f_{TKEw}$ turns towards negative. Near the bed at the downstream of the piers, negative $f_{TKEu}$ and positive $f_{TKEw}$ indicate that streamwise flux of turbulent kinetic energy against flow direction and vertical flux in the upward direction respectively. Negative $f_{TKEu}$ and positive $f_{TKEw}$, signifies retarding effect due to wake vortices forming at the downstream of the piers which result in the arrival of slowly moving fluid parcels. However, near the free surface, positive $f_{TKEu}$ and negative $f_{TKEw}$ corresponds to a streamwise flux of turbulent kinetic energy is in the flow direction and vertical flux of turbulent kinetic energy is in the downward direction that results in the inrush of fluid parcels. In case of downward seepage conditions, near the bed $f_{TKEu}$ becomes less negative and $f_{TKEw}$ becomes more positive. At section B, it is observed that streamwise and vertical

flux of turbulent kinetic energy fluctuates and follows nearly the same trend as it is obtained at section C. On application of the downward seepage, the negative $f_{TKEu}$ and positive $f_{TKEw}$ are decreased near the bed, which results in lesser momentum exchange in case of seepage runs than no seepage condition.

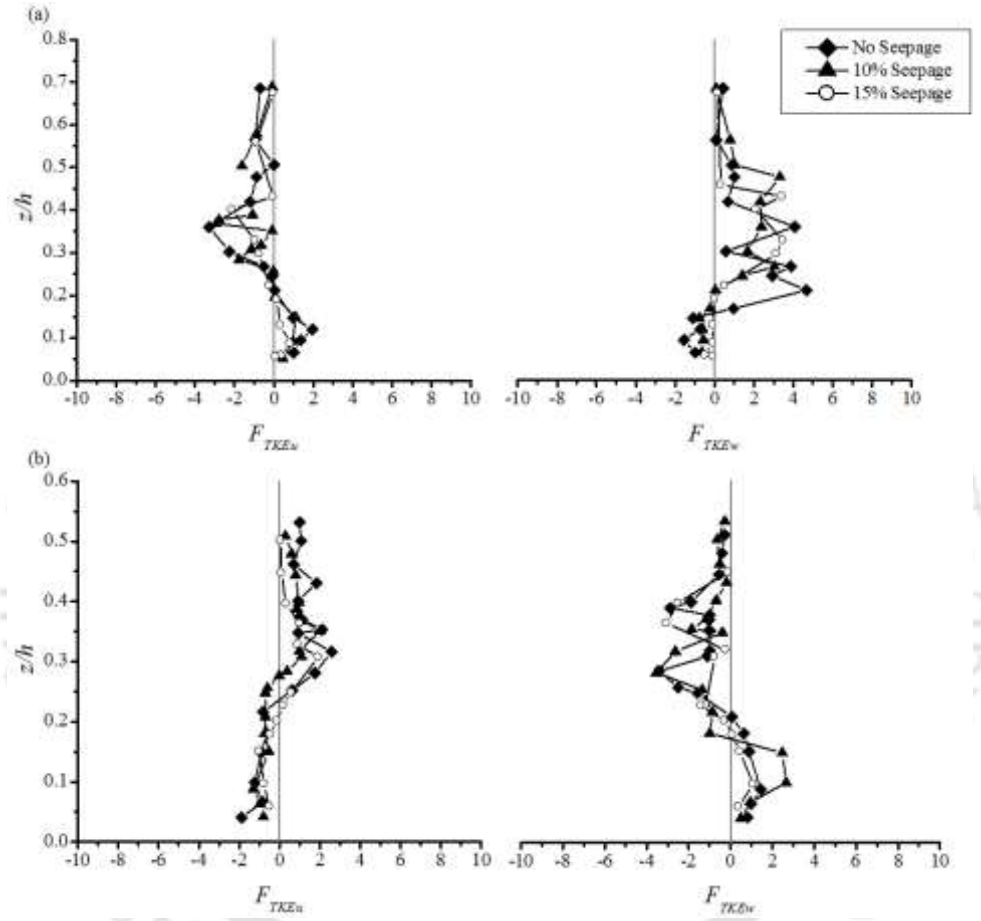


Figure 4.5 Vertical distribution of TKE Fluxes at (a) Upstream A, (b) Downstream C

### 4.2.6 Power Spectra Analysis

The strength of wake vortices has been determined by conducting power spectra analysis. Power spectra were obtained from Fast Fourier Transformation (FFT) of the auto-covariance function of velocity time series data. The resultant power spectra are calculated as, $S(f) = \{S_u(f)^2 + S_v(f)^2 + S_w(f)^2\}^{0.5}$ ; $S_u(f)$, $S_v(f)$ and $S_w(f)$ are power spectra of velocity components in streamwise, transverse and vertical direction respectively. Figure 4.6 shows power spectra plotted against the frequency for velocity components at downstream of piers (section C) for no seepage, 10% seepage and 15% seepage, near free

surface ($z/h \approx 0.4$). In the power spectrum distribution, power related to the peak frequency indicates the strength of wake vortices. Strength of vorticity is associated with the capacity of the wake vortices to move the bed particles. From power spectra analysis, Strouhal number is calculated as, $fD/U_0$ where, $f$ is vortex shedding frequency; which is associated with maximum $S(f)$ in Figure 4.6, $D$ is diameter of pier and $U_0$ is depth average flow velocity. In this study, Strouhal number is calculated at the near free surface ($z/h \approx 0.4$) and near bed region for no seepage ($z/h \approx 0.07$) and seepage conditions and values are mentioned in Table 4.1.

Table 4.1 Strouhal number at downstream of piers

| | **Strouhal number** | |
|---|---|---|
| Case | Near Free Surface | Near Bed |
| **No Seepage** | 0.23 | 0.15 |
| **10% Seepage** | 0.18 | 0.13 |
| **15% Seepage** | 0.16 | 0.11 |

For no seepage condition, the vortex-shedding frequency is 0.927 Hz corresponding vortex shedding period is 185, and Strouhal number ($St$) near the free surface is 0.23, which is comparable with literature (Igarshi, 1981; Sumner et al., 1999; Ataie-Ashtiani and Aslani-Kordkandi, 2013). Inside the scour hole that is near bed region Strouhal number is lesser than it is at the near free surface as the strength of wake vortices is least near the bed (Ataie-Ashtiani and Aslani-Kordkandi, 2013).

It cab be seen in the present study that downward seepage changes the stream flow characteristics and bed morphology around piers. It also shows significant impact on velocity power spectra. From Figure 4.6, it can be observed that at downstream of piers, the resultant power spectrum is shifted towards lower frequency on the application of downward seepage hence, the value of Strouhal number is decreasing. At downstream of piers, reduction in strength of wake vortices or decrement in Strouhal number indicates that lateral flow through channel boundaries diminishes the capacity of wake vortices to move the bed material.

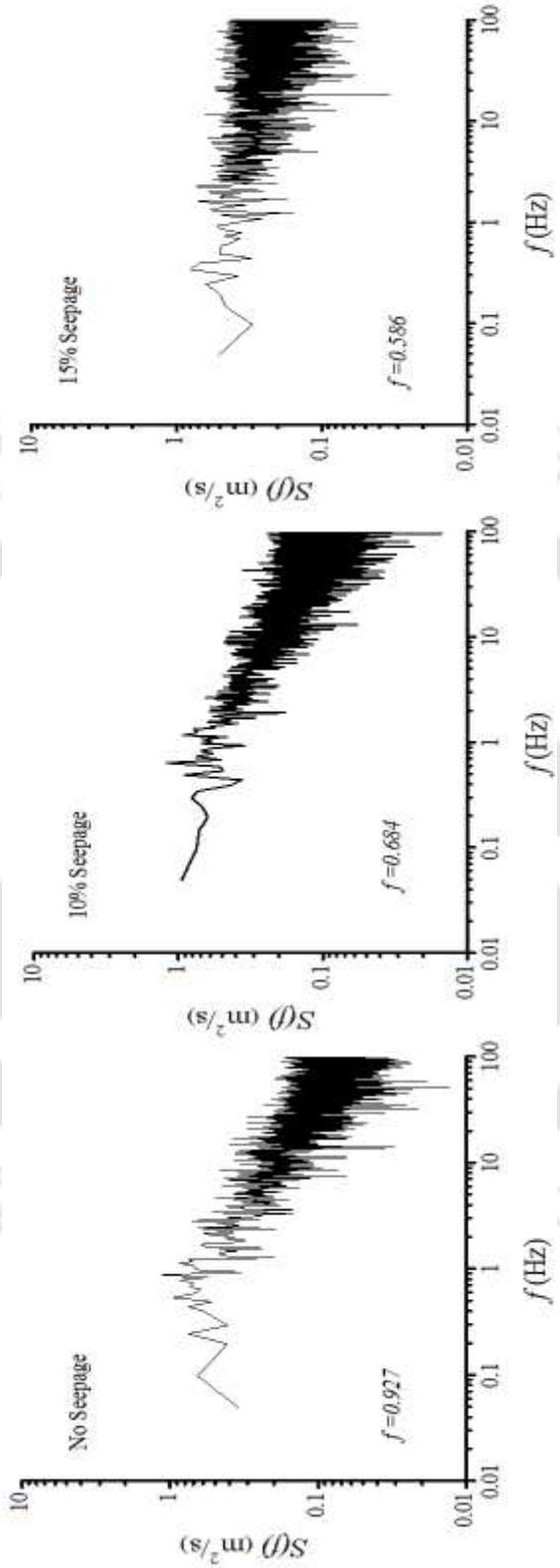


Figure 4.6 Power spectra at downstream of piers

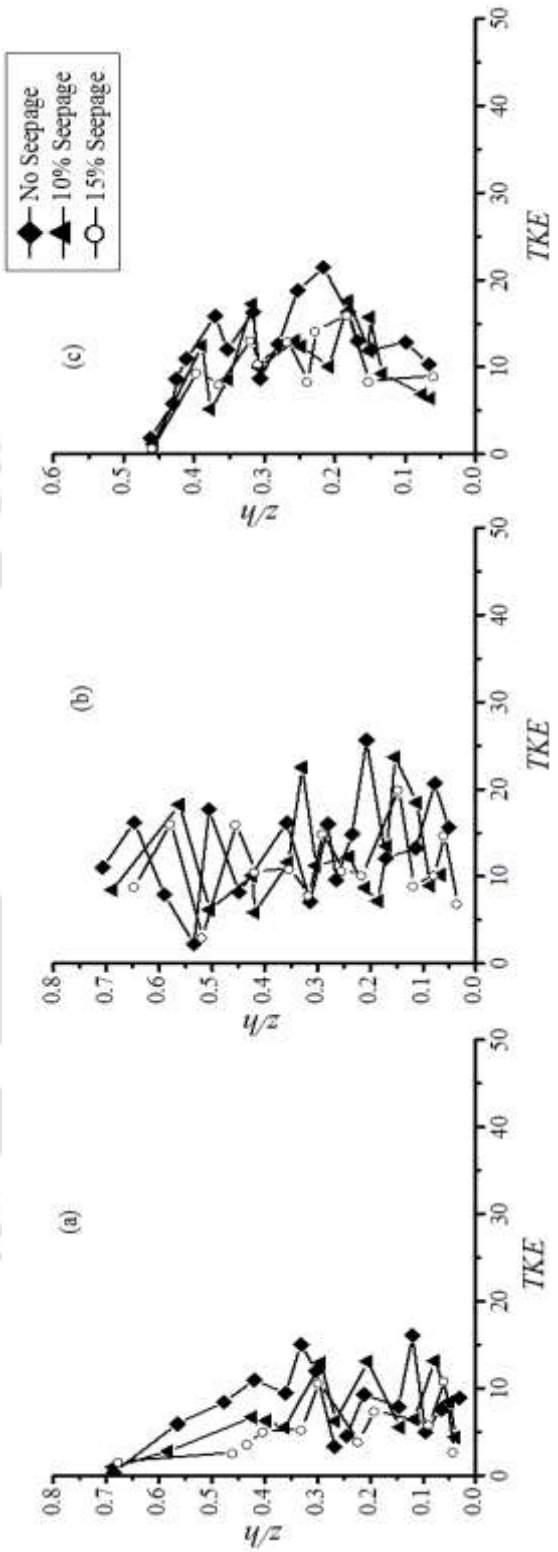


Figure 4.7 Vertical distribution of turbulent kinetic energy at (a) Upstream A, (b) Section B, (c)

### 4.2.7 Turbulent Kinetic Energy

The vertical profiles of turbulent kinetic energy (TKE) $\frac{\rho}{2}(\overline{u'^2}+\overline{v'^2}+\overline{w'^2})$ at sections A, B and C for no seepage, 10% seepage and 15% seepage runs are shown in Figure 4.7. It can be perceived from Figure 4.7, that at section A, near the free surface TKE is lesser and increases with decreasing distance from bed, attained higher value near the scoured region and again decreasing near the bed. Strong pressure gradient and separation of flow at upstream of the piers lead to generate more kinetic energy near the edge of the scour hole (Maity and Mazumder, 2012). A higher magnitude of TKE results in scouring at upstream of the piers. At the downstream of piers (section C), a higher value of TKE is obtained near the free surface and magnitude of TKE is decreasing while moving away from the free surface. At section B, TKE profile is irregular and fluctuates heavily due to chaotic flow behaviour. TKE profile changes significantly on the application of downward seepage. Close observation of Figure 4.7 shows that magnitude of TKE is decreased with the application of downward seepage. In this study, unlike the plane bed, decreased level of turbulence has been seen on the application of downward seepage this might happened due to the reduction in strength of reversal flow with downward seepage.

### 4.2.8 Scour around Piers

The cross-sectional area of the channel is reduced due to the construction of structures like bridge piers in the channel. Presence of piers in the channel, obstruct and divert the path of the flowing stream. Separation of flow due to piers leads to generate higher Reynolds stresses near the bed around piers. Inflation in Reynolds stresses increase the momentum exchange consequently, erodes the bed material around the piers. In this study, two piers are arranged in tandem manner. The approaching flow is obstructed by the front pier, separated in a downward direction along the face of the pier and along sides of the pier in the form of side circulations. At the front of the pier, the downward flow hits the bed and extract the bed material, which is carried forward by the circulating flow along the sides of the pier and deposited just behind the pier. In the gap between two piers, the flow pattern is complicated because of the wake vortices forming at downstream of the front pier and obstruction to flow by the rear pier. In case of the tandem arrangement of bridge piers, the presence of rear pier restrains the wake vortices formed at the downstream of the front pier. The wake vortices are smaller near the bed, as the distance

from the bed increases the wake vortices increase in length (Ataie-Ashtiani and Aslani-Kordkandi; 2013) and moves further along the approaching stream flow, obstructed by the rear pier. Hence, the flow obstructed by rear pier is weaker than the fully developed flow which is obstructed by the front pier. The downflow at the front pier has to have more potential to scour around front pier than the downflow along the face of the rear pier. As flow passes towards rear pier, wake vortices at the downstream of front pier reduces the velocity of flow, which creates less turbulence at the rear pier and consequently lessens the scour depth at the rear pier.

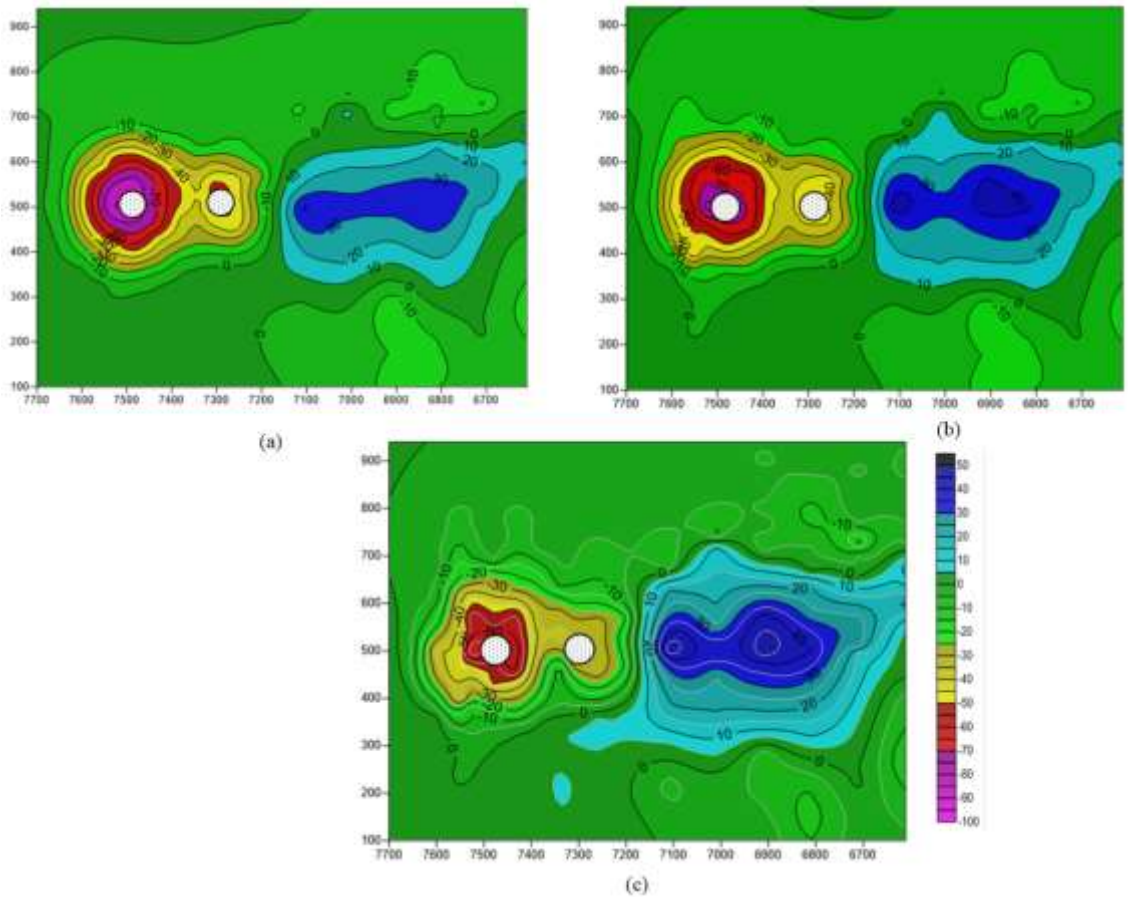


Figure 4.8 Scour around piers (a) No Seepage, (b)10% Seepage, (c)15% Seepage (All dimensions are in mm)

The bed morphology for both no seepage and seepage runs are depicted in Figure 4.8. The scour depth at the rear pier is reduced nearly about 50% than the scour depth occurred at the front pier for all the runs. In case of 10% seepage, scour depth at the front pier is

reduced by 16% and at the rear pier by 14% and for 15% seepage scour depth is decreased by 23% at the front pier whereas by 26% at the rear pier. The extracted bed material is deposited further along the centreline, which produces hump at the downstream of the piers. The height of hump is lesser for no seepage run than the seepage runs. Hump height is increased by 10% for 10%seepage and again increased by 16% for 15% seepage.

Development of scour around bridge piers is depending upon time. Vortex around piers expands in lateral and longitudinal direction with time. At different intervals of time, lateral bed profiles are measured at upstream of piers with Ultrasonic ranging system for 20cm transverse distance at the upstream and downstream of the pier by considering the centre of the pier as the centre of that transverse distance. From Figure 4.9, it can be seen that initially, rate of scouring is greater which reduces gradually and decreased up to 50% within 12 hours. Flowing stream is obstructed by piers hence generates pressure gradient at the face of the piers. Adverse pressure gradient at the face of the piers results in unstable strong downflow (Yong et al., 2015) along the face of the piers. The downflow hits the bed and erode the bed material and moves in a reverse direction to that of the flowing stream. The reversal flow removes the bed material from slanting slope of the scour hole and enlarges the vortex size. Hence, the reversal flow at the upstream of piers is responsible for the development of scour. As the lateral flow in the form of downward seepage through channel boundaries leads to change channel hydrodynamics, consequently modifies the bed morphology around piers. In case of no seepage runs, rate of development of scour depth is more than seepage runs as the downward seepage curtails the reverse flow near the bed at upstream of piers.

### 4.2.9 Conclusions

At upstream of both piers, near the bed region and near the free surface, at downstream of both piers reversal flow is observed. Downward seepage impedes the reversal flow hence controls erosive capacity of reversal flow. A significant decrease in Reynolds shear stress near the bed at upstream of the piers results in lower scour depth in case of seepage runs. In the gap between two piers, wake vortices are forming near the surface due to flow separation at the front pier and reversal flow can be seen near the bed due to obstruction by rear pier.

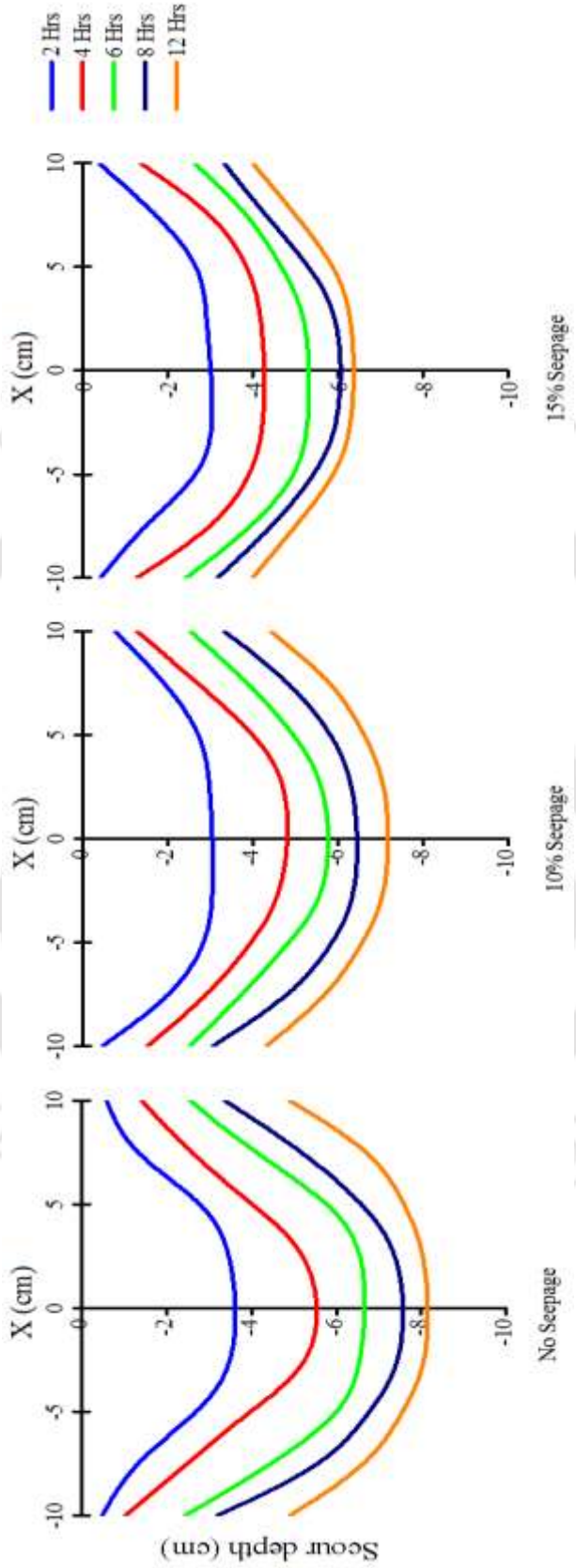


Figure 4.9 Development of scour depth with time at upstream of piers

Therefore, velocity is less near free surface and is increasing with moving towards bed. At the upstream of pier, near the bed, inward interaction and outward interaction contribute more to the Reynolds shear stress whereas away from bed contribution of sweep events are greater.With downward seepage, contribution of all events is increasing. At downstream of piers ejection events are more dominant. Whereas in the gap between two piers, contribution of ejection and sweep are stronger towards Reynolds shear stress. In seepage runs, lesser streamwise flux of streamwise Reynolds stress and lesser vertical flux of vertical Reynolds stress is observed near the bed at upstream of piers. Lesser fluxes of streamwise turbulent kinetic energy in streamwise direction and vertical fluxes of turbulent kinetic energy in vertical direction also been observed. Hence, at upstream of piers lower momentum exchange near the bed leads to minimize the scour depth on application of downward seepage. Turbulent kinetic energy is higher near the edge of the scour hole and is decreasing with downward seepage. Power spectral analysis of velocity components has been carried out at downstream of piers. With downward seepage resultant power spectra shifts towards lower frequency, consequently Strouhal number is decreasing. Hence, downward seepage is responsible for decreased strength of wake vortices. Piers obstruct the flowing stream hence; flow separation around piers leads to erode the bed material, eroded material carried by flowing stream and gets deposited at the downstream of piers. Scour depth at front pier is twice the scour depth at the rear pier for all the runs and with downward seepage; scour depth reduces around both piers. Rate of development of scour depth decreases with downward seepage.

## 4.3 Tandem Piers with Different Diameters

In case of tandem piers with different diameters, experimentation has been done on two types of tandem arrangements (T1 and T2) namely, 75mm front pier - 90mm rear pier (T1) and 90mm front pier- 75mm rear pier (T2). The centre-to-centre distance between piers for both the arrangement was kept as three times the greater diameter. In this section, the change in flow characteristics and consequent changes in scour geometry around the tandem piers of different diameters are discussed. The trends of profiles of turbulent statistics are similar for both the arrangements.

### 4.3.1 Velocity

For both T1 and T2 arrangements, section A is at upstream of front pier and section C is at downstream of rear pier both the sections are measured at distance of 6cm away from the wall of respective piers. Section B is exactly at the middle of the gap between the piers. The trend of velocity profiles is same for both arrangements. Figure 4.10 displays velocity profiles at three sections A, B and C for no seepage and with seepage conditions.

At upstream section A, a streamwise component of velocity is found to be negative near the bed region. However, with moving away from the bed, the streamwise component of velocity becomes positive. The maximum velocity is obtained nearly at the edge of the scour hole and then becomes nearly constant towards free surface. At downstream of the rear pier, at section C, near the free surface, the velocity is found to be negative and moving away from free surface the velocity is becoming positive and attains maximum value near the bed ($z/h \approx 0.1$). At sections A and C, the negative value of streamwise velocity indicates the presence of reverse flow in this region. In between two piers, i.e. at section B the streamwise component of velocity is positive but smaller near free surface and gradually increasing towards the bed. The smaller positive value of streamwise velocity near free surface indicates that the wake vortices behind front pier are weakened due to the presence of rear pier. With the application of downward seepage, the velocity of reverse flow near the bed at upstream of piers and near the free surface at downstream of piers is decreasing. However, as the seepage percentage increases, the velocity is increasing away from the bed at upstream section A and near the bed at downstream section C where there is no reversal flow. The downflow at the upstream face of pier due to flow separation hits the bed. Within the developing scour hole the flow moves along the slanting slope of the scour hole in the reverse direction to that of approaching flow. The negative velocity near the bed at upstream of piers confirms the reversal flow which is mainly responsible for scouring. At downstream of piers the negative velocity is obtained due to wake vortices. However, the downward seepage counters the reverse flow and diminishes its strength to erode the bed material.

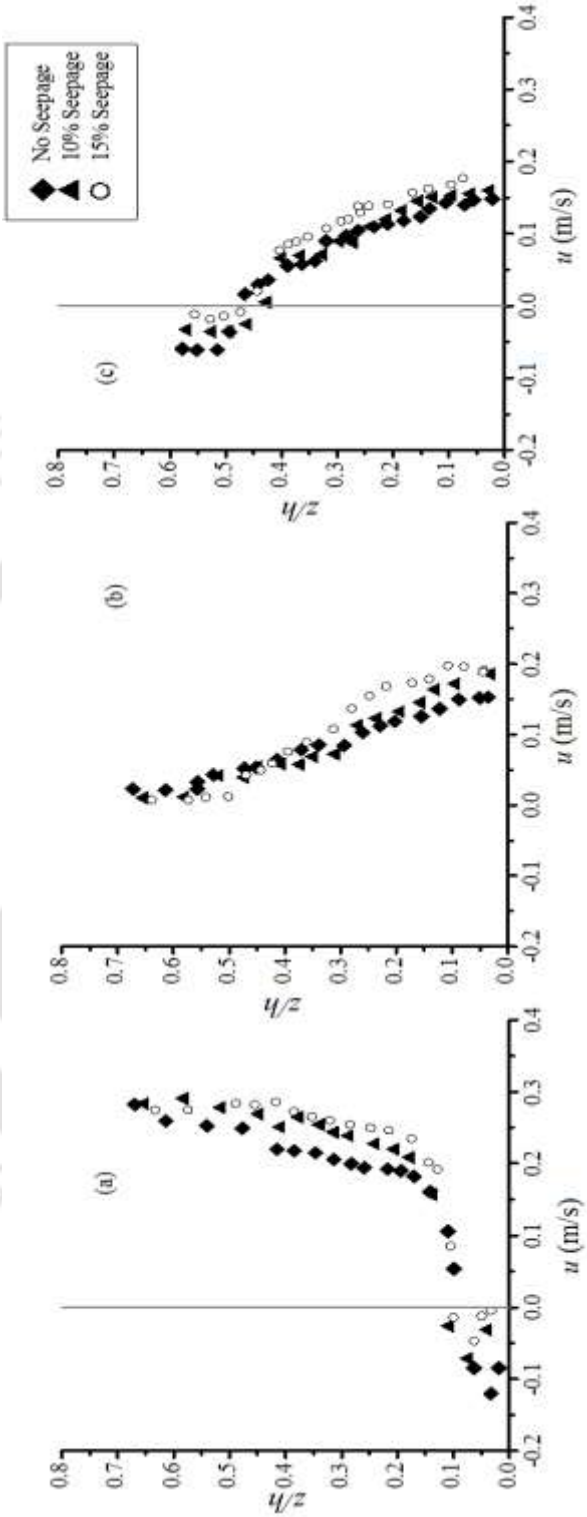


Figure 4.10 Velocity profiles at (a) Upstream A, (b) Section B (c) Downstream C of piers

### 4.3.2 Reynolds Shear Stress

The flow separation at piers results in enhancing the Reynolds stresses near the piers, which leads to scour the bed material. Figure 4.11 shows Reynolds shear stress (RSS) profile at sections A, B and C for no seepage, 10% seepage and 15% seepage condition. Near the bed region within scour hole and near the free surface at upstream section A and downstream section C of piers, the Reynolds stresses are negative. At section B and C, Reynolds stresses are highly fluctuating due to the dominance of wake vortices. It can be observed from Figure 4.11 that, at section A, Reynolds stresses are smaller near free surface and reach to a maximum value near the edge of scour hole and attain negative value towards the bed. At downstream of the rear pier, section C, negative Reynolds stresses turns towards positive while moving towards the bed. The negative value of the Reynolds stresses confirms reversal flow at that region. Keen observation of Figure 4.11 shows that with downward seepage the Reynolds stresses near the bed region at upstream section A and near the free surface at downstream section C are decreasing which reveals that downward seepage reduces the strength of reversal flow. Decreased value of Reynolds stresses on the application of seepage signifies the reduced erosive capacity of flow.

### 4.3.3 Turbulence Intensity

Turbulence intensity provides the information regarding the contribution of fluctuating components of velocity to the turbulence production. It is defined as:

$$\left.\begin{aligned}\sigma_u &= \sqrt{\overline{u'^2}} = \sqrt{\frac{1}{n}\sum_{i=1}^{n}\left(U_i-\bar{u}\right)^2}\\ \sigma_w &= \sqrt{\overline{w'^2}} = \sqrt{\frac{1}{n}\sum_{i=1}^{n}\left(W_i-\bar{w}\right)^2}\end{aligned}\right\} \tag{4.2}$$

Vertical profile of $\sigma_u$ and $\sigma_w$ at sections A, B and C plotted for no seepage, 10% seepage and 15% seepage conditions are shown in Figure 4.12.

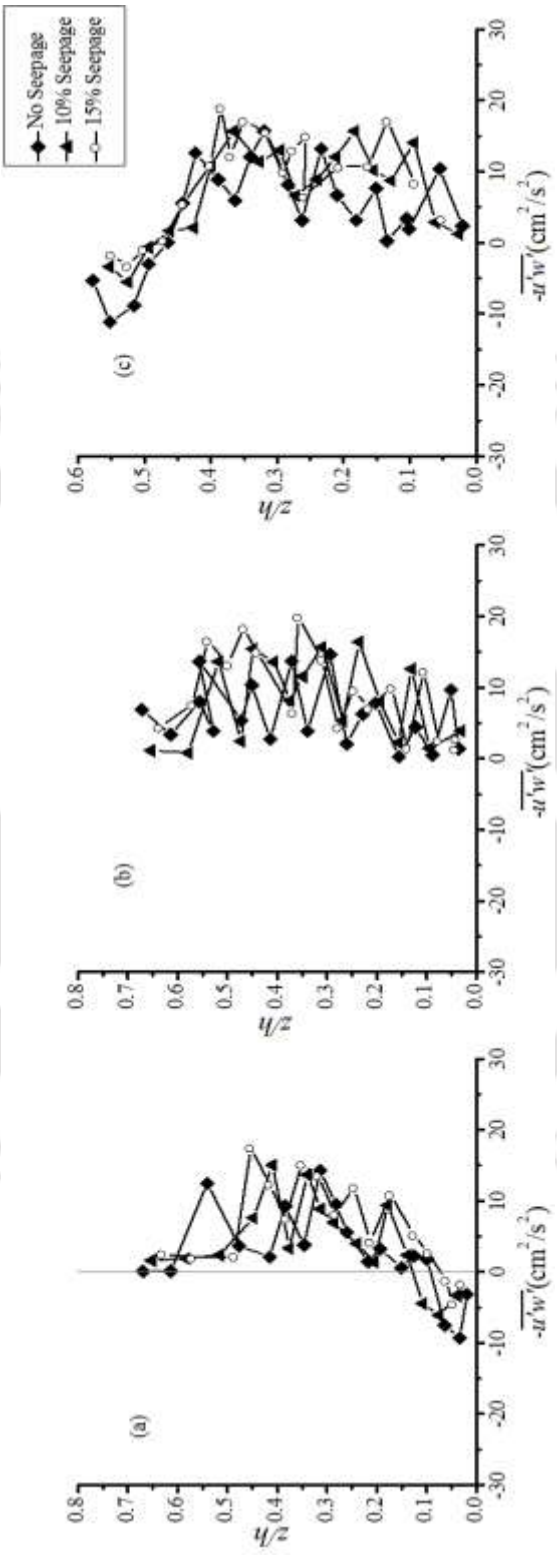


Figure 4.11 RSS profiles at (A) Upstream A, (B) Section B, (C) Downstream C of piers

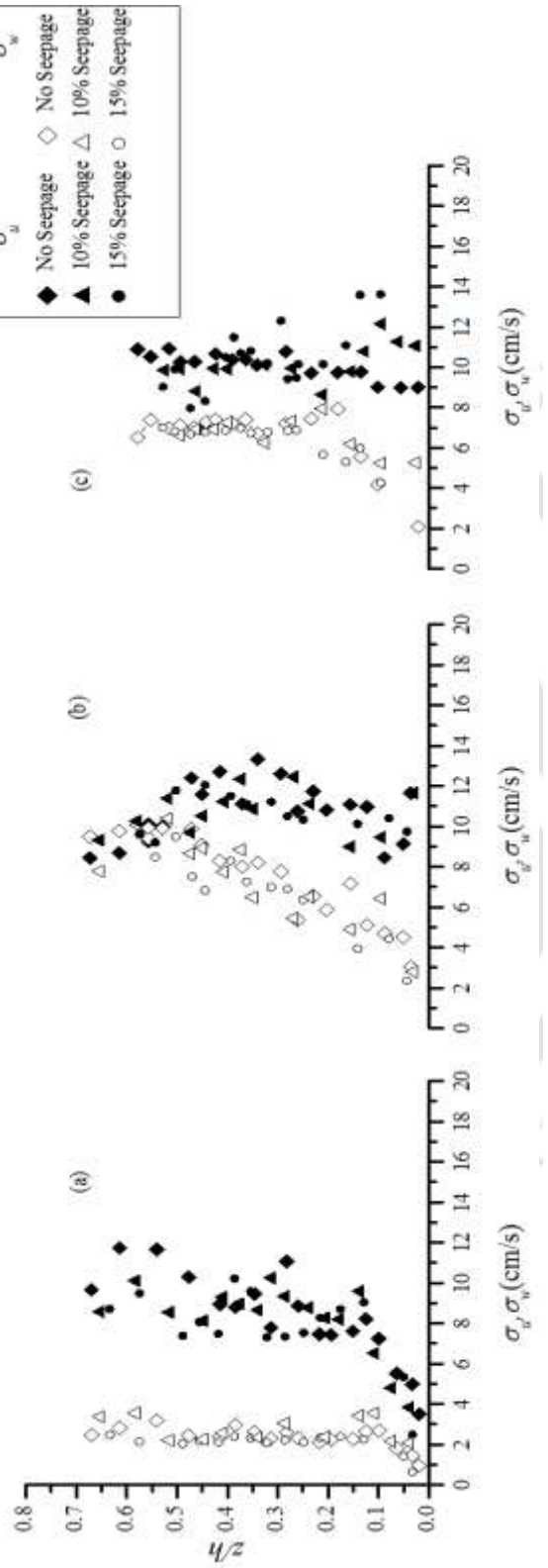


Figure 4.12 Turbulent intensity profiles at (a)Upstream A (b)Section B(c)Downstream C of piers

At the upstream section A, $\sigma_u$ is decreasing towards the bed with increasing seepage, which is different than the case of plane bed without piers where turbulent intensities are increasing with increasing seepage. Vertical turbulence intensities are lesser in magnitude than longitudinal turbulence intensities, which shows that fluctuating components of velocity in streamwise direction are more dominant at upstream of piers. At section B, near the free surface, both longitudinal and vertical turbulent intensities are nearly same in magnitude. However, moving away from free surface, longitudinal turbulent intensities are increasing while vertical turbulent intensities are decreasing, as the wake vortices are diminishing in strengths while moving away from free surface. At section C, the magnitude of vertical turbulence intensities is increased. Higher magnitude of vertical turbulence intensities are evidence of wake vortices forming at downstream of piers as wake formation results in enhancing vertical turbulence intensities at section C. The magnitude of longitudinal turbulence intensities is quite smaller than their magnitudes at upstream section A. At downstream section C, turbulence intensities are decreasing near free surface with downward seepage where they are increasing near the bed. The decreased turbulence intensities near the free surface at downstream of piers signifies the retardation of wake vortices on the application of downward seepage.

### 4.3.4 Moment Analysis

Vertical distribution of third-order correlation of velocity fluctuations ($M_{30}$, $M_{03}$, $M_{12}$ and $M_{21}$) for no seepage, 10% seepage and 15% seepage at upstream of piers (section A) and downstream of piers (section C) is shown in Figure 4.13. From Figure 4.13, it can be observed that at upstream of piers (section A) $M_{30}$ and $M_{12}$ start with positive values near the bed and then changing over to the negative values with increasing *z/h*, which implies that near the bed $\overline{u'u'}$-flux and $\overline{w'w'}$- diffusion occur in streamwise direction while moving away from the bed, $\overline{u'u'}$ -flux and $\overline{w'w'}$- diffusion occur in opposite direction to that of flow direction and become pronounced with an increase in *z/h*.

In case of seepage runs, at upstream of the piers near the bed region, positive values of $M_{30}$ and $M_{12}$ are decreased which is contradictory with the case of plane mobile bed as reversal flow slows down on the application of downward seepage. $M_{03}$ and $M_{21}$ initiate with negative values and then change to positive; it suggests that $\overline{w'w'}$-flux and $\overline{u'u'}$-

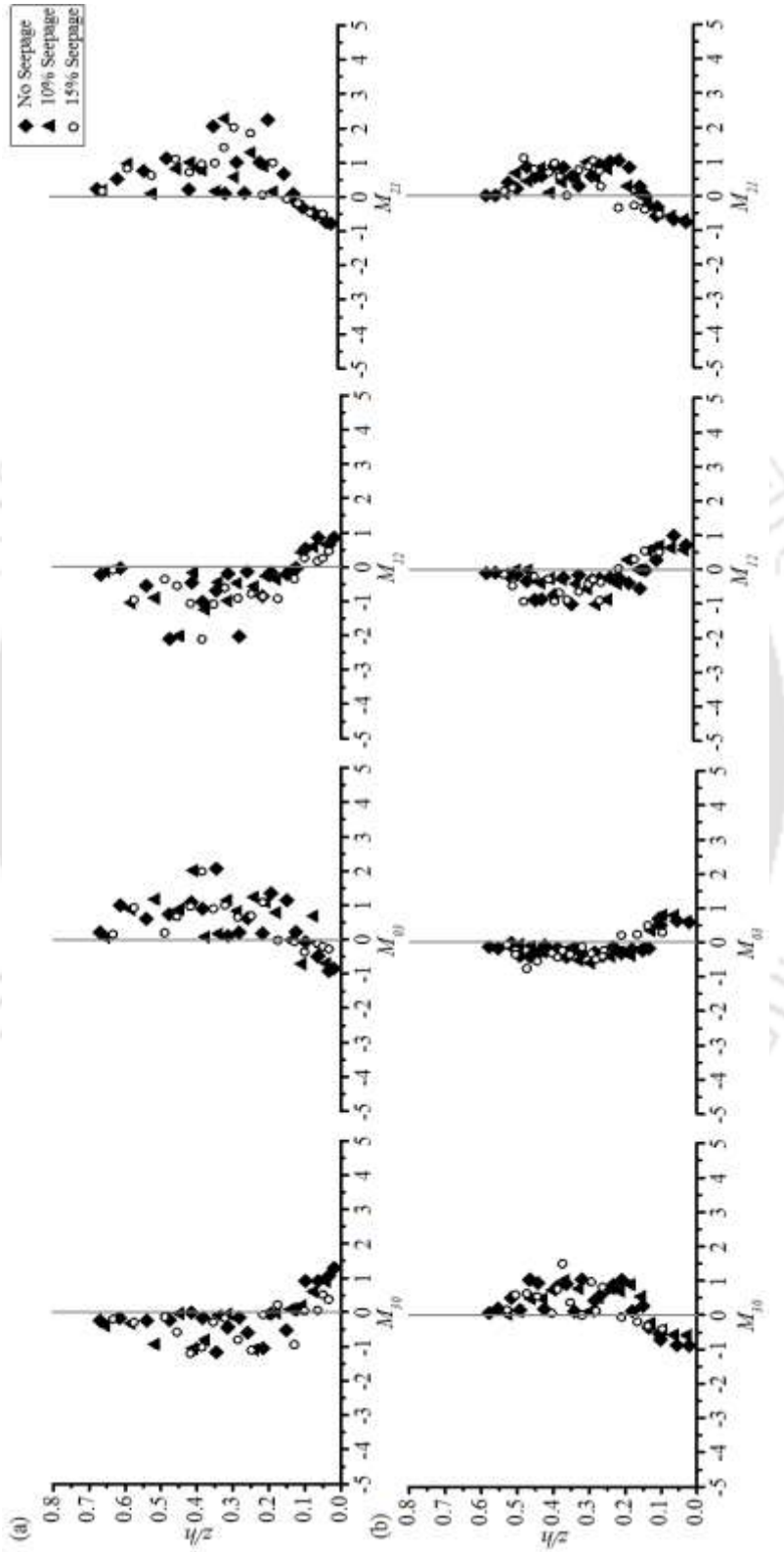


Figure 4.13 Vertical distribution of higher order moments at (a)Upstream A, (b)Downstream C of piers

diffusion are in the downward direction near the bed region. Negative nature of $M_{03}$ and $M_{21}$ decrease on the application of downward seepage. Negative values of $M_{03}$ and $M_{21}$ show that flow is coming towards the bed and is transported along the flow direction, which can be observed from positive values of $M_{30}$ and $M_{12}$. At downstream of piers (Section C), $M_{30}$ starts with negative and turns towards positive, and $M_{03}$ starts with positive and turns towards negative with increasing distance from the bed. Negative $M_{30}$ and positive $M_{03}$ suggest that $\overline{u'u'}$ - flux occurs in opposite to stream flow direction and $\overline{w'w'}$ - flux in an upward direction. Whereas, $M_{12}$ starts with positive values near bed then turn towards negative and $M_{21}$ starts with negative near the bed and change to positive with increasing distance from the bed. It shows that at downstream of piers near the bed $\overline{w'w'}$ diffusion occurs in the direction of the stream and $\overline{u'u'}$ diffusion occurs in a downward direction. Near free surface $M_{12}$ is negative and $M_{21}$ is positive that is $\overline{w'w'}$ diffusion and $\overline{u'u'}$ diffusion propagate against the flow direction and in an upward direction respectively which can be confirming the dominance of secondary current at downstream of piers due to the formation of wake vortices. At section C, near the bed negative $M_{30}$ and positive $M_{03}$ indicate the arrival of slower moving fluid parcels, which represent an ejection motion. With downward seepage negative nature of $M_{30}$ and $M_{21}$ as well as positive nature of $M_{03}$ and $M_{12}$ decrease.

At section B, which is at downstream of the front pier trend of higher order moments is nearly same as it is obtained for section C.

### 4.3.5 Turbulent Kinetic Energy

The vertical distribution of turbulent kinetic energy (TKE) $\frac{\rho}{2}(\overline{u'^2}+\overline{v'^2}+\overline{w'^2})$ at sections A, B and C for no seepage, 10% seepage and 15% seepage runs are depicted in Figure 4.14. At upstream of piers, section A, TKE is lesser near the free surface and increasing gradually towards bed, attained maximum value near the edge of scoured region as strong pressure gradient and separation of flow at upstream of the piers lead to generate more kinetic energy near the edge of the scour hole (Maity and Mazumder, 2012) and again decreasing near the bed. A higher magnitude of TKE results in scouring at upstream of the piers.

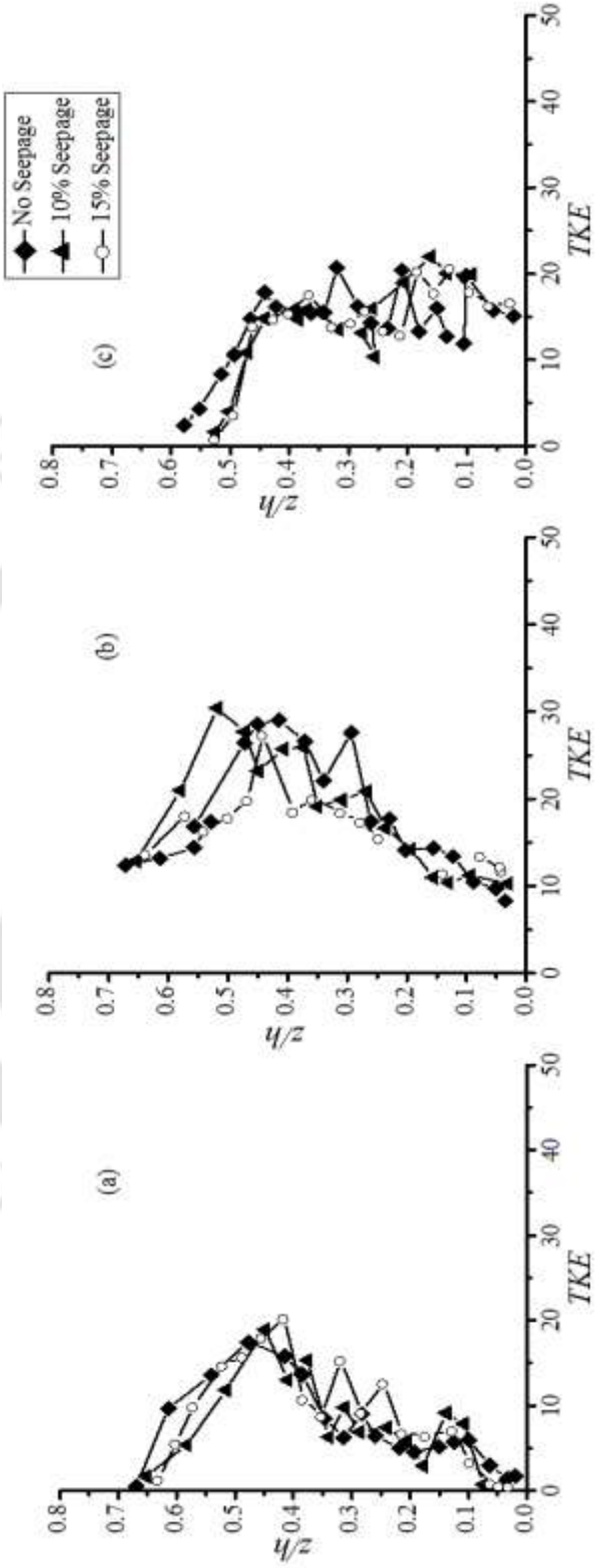


Figure 4.14 Vertical distribution of turbulent kinetic energy at (a)Upstream A, (b)Section B, (c)Downstream C of piers

At section B, TKE profile is irregular and fluctuates heavily due to chaotic flow behaviour. TKE profile changes significantly on the application of downward seepage. Close observation of Figure 4.14 shows that magnitude of TKE is decreases with application of downward seepage. In this study, unlike the plane bed, decreased level of turbulence has been seen on application of downward seepage this might happened due to a reduction in strength of reversal flow with downward seepage.

### 4.3.6 Flux of the Turbulent Kinetic Energy

Presence of piers in flowing stream leads to change the flow pattern around piers and turbulent flow characteristics accordingly.

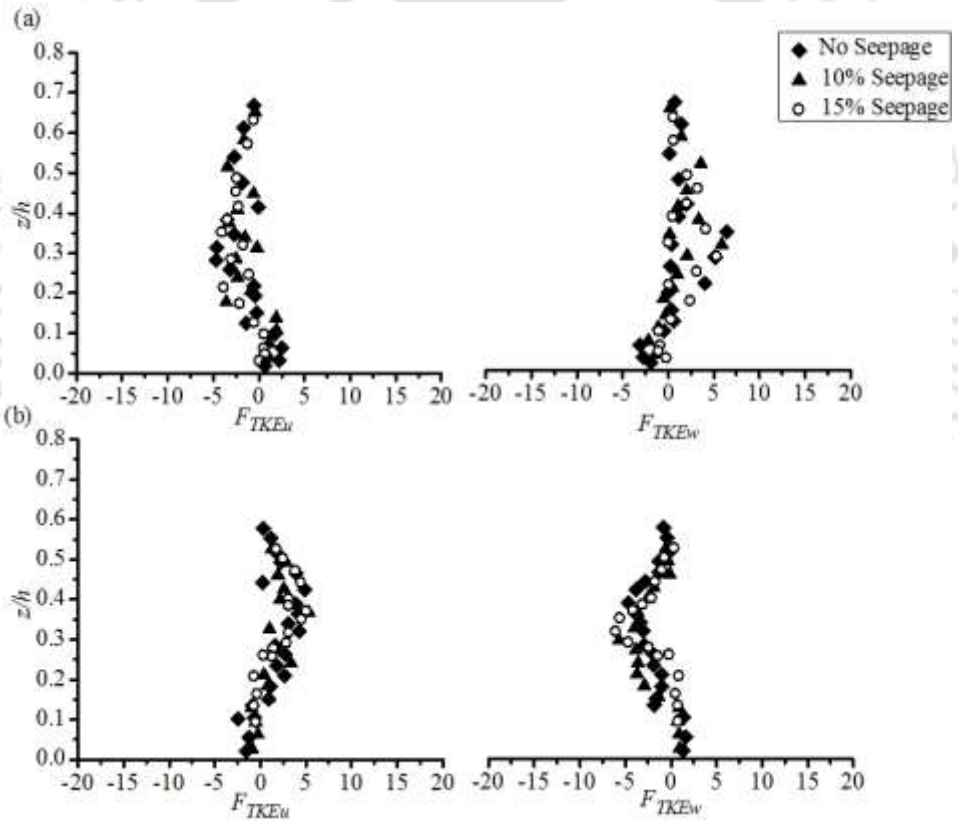


Figure 4.15 Vertical distribution of TKE Fluxes at (a)Upstream A, (b)Downstream C of piers

At upstream of the piers (section A) for no seepage conditions $f_{TKEu}$ begin with small positive and $f_{TKEw}$ start with negative values (Figure 4.15). With increasing $z/h$, $f_{TKEu}$ turns towards negative and $f_{TKEw}$ turns towards positive. Positive values of $f_{TKEu}$ and negative

$f_{TKEw}$ are associated with the streamwise flux of turbulent kinetic energy in streamwise direction and vertical flux of turbulent kinetic energy is in the downward direction. Away from the bed negative $f_{TKEu}$ and positive $f_{TKEw}$ imply that streamwise flux of turbulent kinetic energy opposite to flow direction and vertical flux of turbulent kinetic energy in the upward direction. Negative $f_{TKEu}$ and positive $f_{TKEw}$ originate retardation process with the arrival of low-speed fluid parcels. Though the same pattern is observed in case of seepage runs, close observation of Figure 4.15 shows that near the bed $f_{TKEu}$ and $f_{TKEw}$ have lesser positive and negative values in case of seepage runs than no seepage condition.

At downstream of piers (section C), secondary currents are more dominant due to wake vortices. $f_{TKEu}$ and $f_{TKEw}$ initiate with small negative and positive values respectively. Moving away from the bed, nearly at the edge of the scour hole $f_{TKEu}$ turns towards positive and $f_{TKEw}$ turns towards negative. At downstream of piers near the bed region, negative $f_{TKEu}$ and positive $f_{TKEw}$ indicate that streamwise flux of turbulent kinetic energy against the flow direction and vertical flux in an upward direction respectively. Negative $f_{TKEu}$ and positive $f_{TKEw}$, indicate retarding effect due to wake vortices forming behind the piers, which results in the arrival of slowly moving fluid parcels. However, near the free surface, positive $f_{TKEu}$ and negative $f_{TKEw}$ corresponds to streamwise flux of turbulent kinetic energy is in the flow direction and vertical flux of turbulent kinetic energy in downward direction results in inrush of fluid parcels. In case of downward seepage conditions, near the bed $f_{TKEu}$ becomes less negative and $f_{TKEw}$ becomes more positive. At section B, it was observed that streamwise and vertical flux of turbulent kinetic energy fluctuates and follows nearly same trend as it is obtained at section C. On application of downward seepage, the negative $f_{TKEu}$ and positive $f_{TKEw}$ are decreased near the bed, which results in lesser momentum exchange in case of seepage runs than no seepage condition.

### 4.3.7 Power Spectra Analysis

Strength of wake vortices to erode the bed material has been determined by power spectra analysis. In the power spectrum distribution, power related to the peak frequency indicates strength of wake vortices. The strength of vorticity is associated with the capacity of the wake vortices to move the bed particles. From power spectra analysis,

Strouhal number is calculated. The values of Strouhal number near free surface and near-bed region for no seepage and seepage conditions are mentioned in Table 4.2.

Table 4.2 Strouhal number at downstream of piers

| | **Strouhal Number** | | | |
|---|---|---|---|---|
| | Arrangement T1 (75mm-90mm) | | Arrangement T2 (90mm-75mm) | |
| | Near free surface | Near bed | Near free surface | Near bed |
| **No Seepage** | 0.26 | 0.18 | 0.24 | 0.16 |
| **10% Seepage** | 0.21 | 0.15 | 0.20 | 0.13 |
| **15% Seepage** | 0.18 | 0.13 | 0.16 | 0.11 |

From Table 4.2, it can be observed that Strouhal number is lesser near the bed region for both no seepage and seepage conditions than the Strouhal number near the free surface. Lesser Strouhal number near the bed, shows that the wake vortices are weaker near the bed, however, they are dominant near the free surface. The values of Strouhal number are decreasing with increasing seepage percentage for both the arrangements T1 and T2. As seepage impedes the reversal flow, the strength of wake vortices to scour the bed material diminishes. The Strouhal number at downstream of arrangement T2 is lesser than the Strouhal number at downstream of arrangement T1 for all the conditions. Reduced Strouhal number at arrangement T2 indicates depletion in scouring of bed material in comparison to than arrangement T1.

### 4.3.8 Scour around Piers

Construction of hydraulic structures like bridge piers results in a reduction of cross-sectional area of the alluvial channels. The change in cross-sectional area modifies the stream flow characteristics. Separation of flow due to presence of piers increases the shear stress and correspondingly increases the erosive capacity of the stream. In the case of tandem piers, the stream flow is obstructed by the front pier that results in downflow along the face of the front pier and wake vortices behind the pier due to flow separation. However, the wake vortices behind the front pier are again retrained by the rear pier.

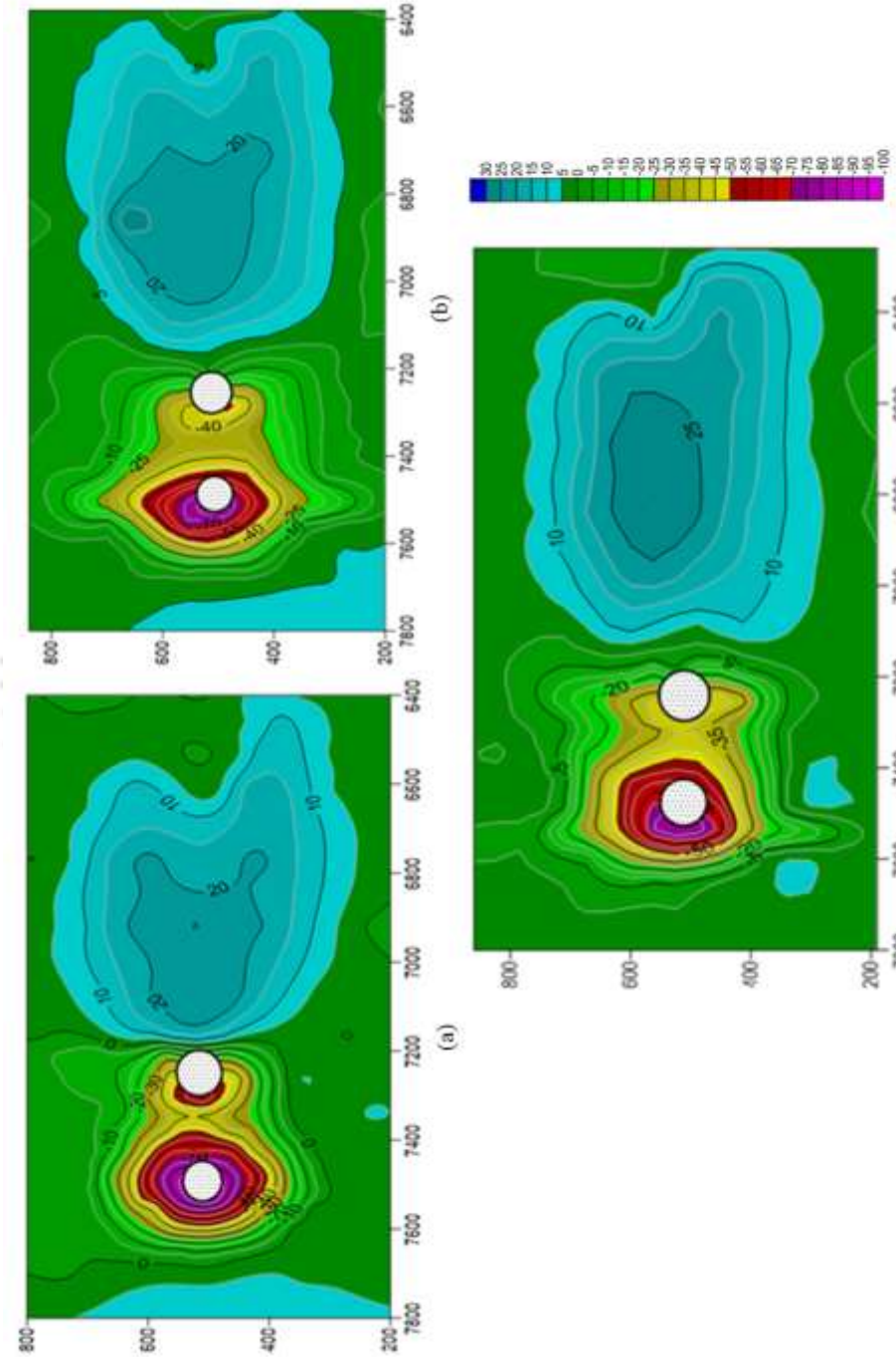


Figure 4.16 Contour profiles of Scour around arrangement T1 for (a)No Seepage, (b)10% Seepage, (c)15% Seepage (All dimensions are in mm)

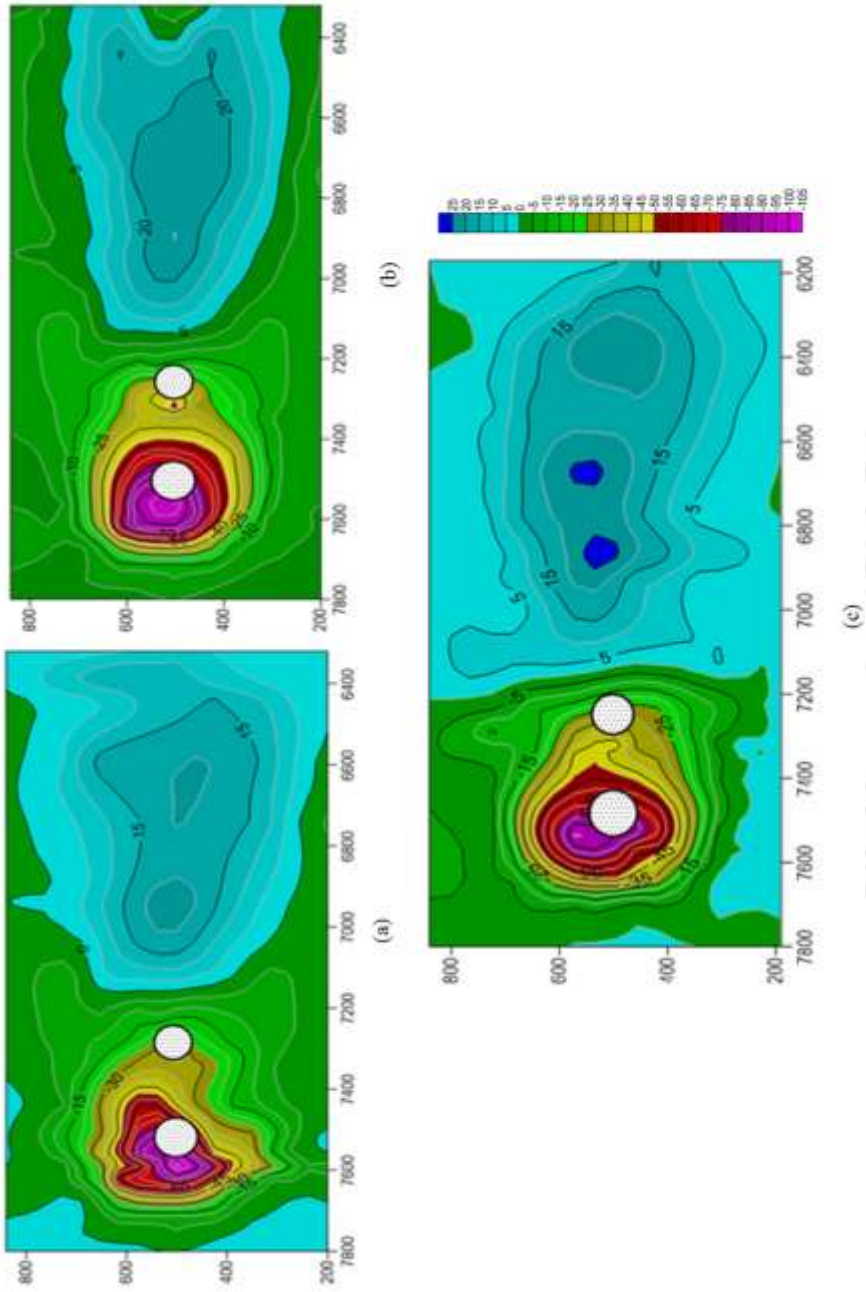


Figure 4.17 Contour profiles of Scour around arrangement T2 for (a)No Seepage, (b)10% Seepage, (c)15% Seepage (All dimensions are in mm)

Again the flow separation occurs at rear pier results in the formation of wake vortices at downstream of rear pier and downflow along the upstream face of pier. In between both piers, the flow is highly complex due to formation of wake vortices behind the front pier and reversal flow near the bed due to obstruction of the rear pier. In case of a tandem arrangement, the front pier always witnesses a deeper scour depth. The front pier works as a shield and protects the rear one. The flow obstructed rear pier is weaker than the flow obstructed by front pier due to wake vortices forming behind the front pier and which might be the reason for lesser scour depth at rear pier than the front one.

Figures 4.16 and 4.17 show contour profile of scoured bed for arrangements T1 and T2 respectively for no seepage, 10% seepage and 15% seepage runs. When two similar piers are arranged in a tandem manner, the scour depth at the rear pier is found to be nearly half of the scour depth at the front pier (Chavan and Kumar, 2017). In this study, two piers with different diameter are placed in a line by two different arrangements T1 and T2 with 75mm front and 90mm rear pier and 90mm front and 75mm rear pier respectively.

Figure 4.18 shows scour depth at the front and rear pier for arrangements T1 and T2 for no seepage, 10% seepage and 15% seepage conditions. It can be observed from Figure 4.18 that the scour depth at the rear pier is lesser than the scour depth at the front pier in both the arrangements. However, the percentage of reduction in scour depth at rear pier than the front pier is more in case of arrangement T2 (nearly 60%) than T1 (nearly 40%). Keen observation of Figure 4.18 shows that the scour depth at both front and rear pier for both the arrangements are decreasing with increasing seepage discharge of the corresponding main channel flow. The scour depth is decreasing on the application of seepage discharge due to a reduction in erosive capacity of reversal flow in case of seepage runs (Figure 4.11). The development of scour depth at bridge piers is a time depending phenomenon. With increasing time, the scour depth is gradually increasing, but after a certain period the erosive capacity of flowing stream and resistance offered by bed material attains an equilibrium condition.

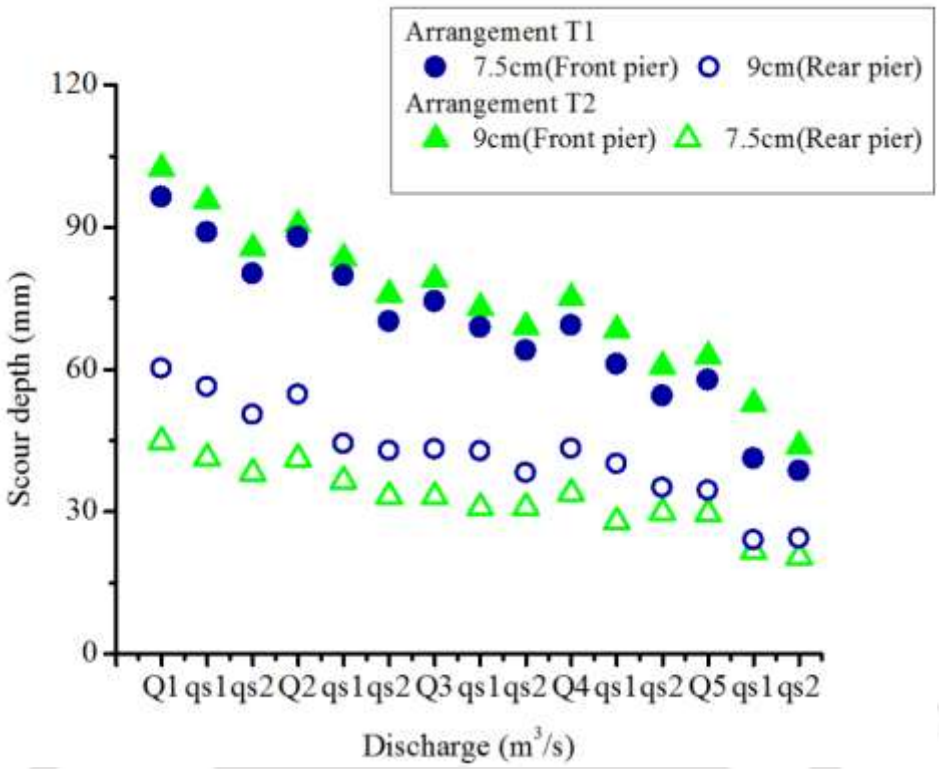


Figure 4.18 Scour depth at front pier and rear pier for arrangements T1 and T2 under no seepage, 10% seepage and 15% seepage conditions

In both the arrangements, lateral bed profiles at upstream of front piers are measured with ultrasonic ranging system at different time interval shown in Figure 4.19. From Figure 4.19, it can be observed that the scour depth is increasing with time in case of no seepage and with seepage conditions. However, the rate of increase of scour depth is decreasing gradually and reduced to about 50% after a certain period. The lateral flow through the channel boundaries in the form of downward seepage restricts the reversal flow at the upstream of piers. Hence, for both arrangements T1 and T2, the rate of increase of scour depth is lesser in case of 10% seepage condition and again reduced for 15% seepage condition. The scoured bed material is carried along the side circulations and get deposited at downstream of piers along and at both sides of the centreline. Figure 4.20 displays the graph of bed elevation along the centreline in the longitudinal direction. It can be found from Figure 4.20 that the bed elevation height at downstream of piers is increasing with increasing seepage percentage for both the arrangements T1 and T2. However, the length of deposition is decreasing with increasing seepage.

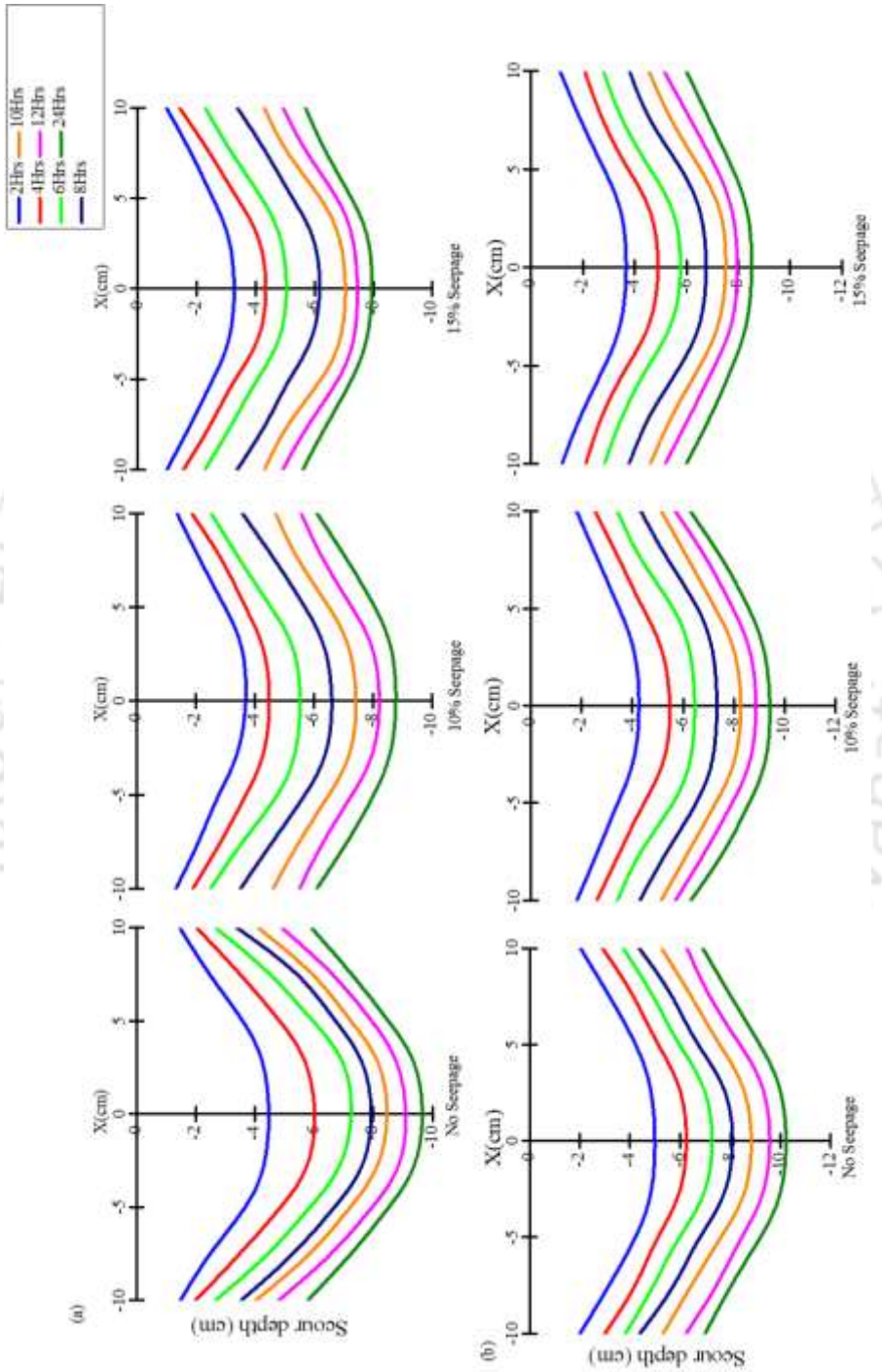


Figure 4.19 Variation of scour depth with time at upstream of (a) arrangement T1 and (b) arrangement T2

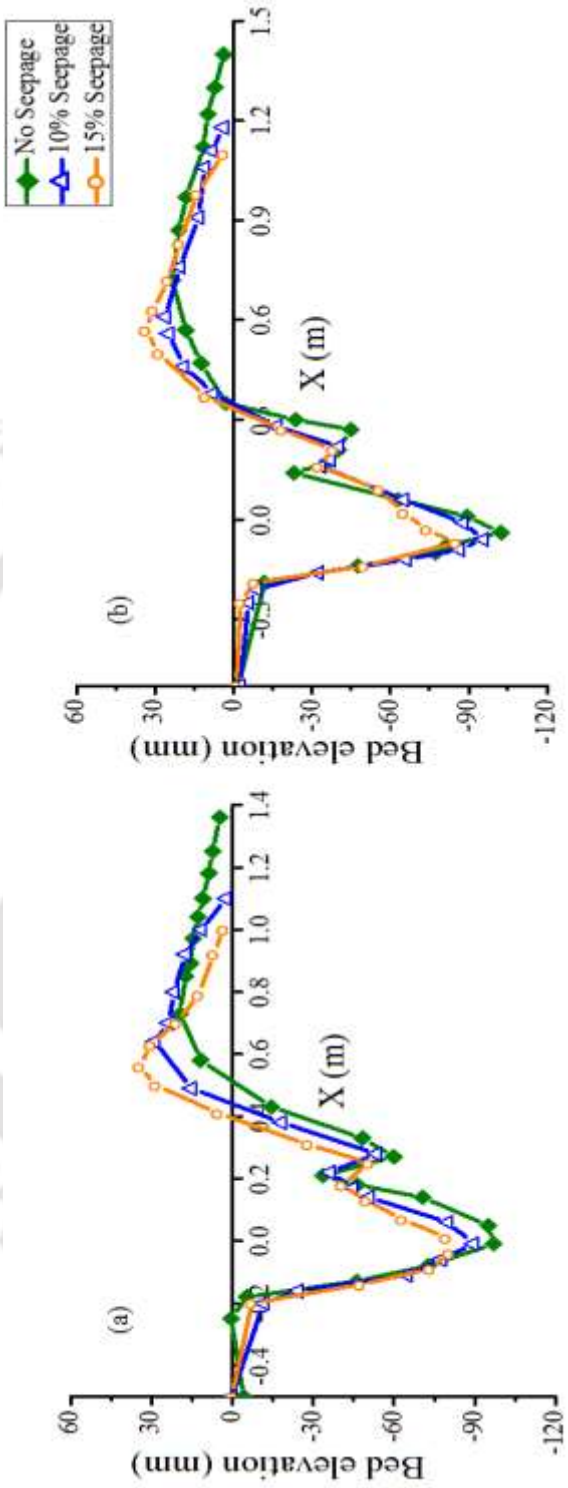


Figure 4.20 Longitudinal bed profile along the centre line for (a) arrangement T1 and (b) arrangement T2

### 4.3.9 Conclusions

The reversal flow at section A, which is mainly responsible for scouring of bed material at upstream of piers and near the free surface at section C, which keeps the sediment particles in suspension at downstream of piers are decreasing on application of downward seepage. At section B, the most complex flow pattern has been observed due to wake vortices formed at downstream of front pier and reversal flow due to presence of rear pier. At section B, with downward seepage velocity near bed is increasing. Reduction in the Reynolds shear stress with increasing seepage, near the bed at section A and near free surface at section C shows lesser erosive capacity of reversal flow at section A and weaker wake vortices at section C. At section B, the Reynolds shear stress fluctuates heavily and increases with increasing seepage percentage. The magnitude of longitudinal turbulence intensity is lesser at downstream section (C) of piers than at upstream section (A). However, the magnitude of vertical turbulence intensity is lesser at upstream section and increased at downstream sections because of increased oscillations in the wake region of piers. With downward seepage, turbulence intensity is decreasing near bed at section A, which is different from the case of plane mobile bed without piers and near free surface at section C. At section A, the positivity of $M_{30}$ and $M_{12}$ decreases with increase in seepage percentage applying lesser transport of $\overline{u'u'}$-flux and $\overline{w'w'}$-diffusion in streamwise direction. At section C, decreased negativity of $M_{30}$ and positivity of $M_{03}$ with application of downward seepage indicates lesser arrival of slower moving particles. Higher turbulent kinetic energy near the edge of the scour hole implies more erosive capacity of flow, which is decreased on application of downward seepage. In seepage runs, lesser fluxes of streamwise turbulent kinetic energy in streamwise direction and vertical kinetic energy in vertical direction indicates lower momentum exchange and leads to minimize the scouring of bed material. At downstream of piers, power spectra of velocity components shift towards lesser frequency on application of seepage. Hence, the Strouhal number is decreasing with increasing seepage that specifies reduced strength of wake vortices. In case of both arrangements T1 and T2, the scour depth is lesser at rear pie than front pier. For arrangement T1, the scour depth at rear pier is reduced by nearly 40% and near 60% in case of arrangement T2. In seepage runs, the scour depths at both piers for both the arrangements are decreasing. The rate of increase of scour depth at

arrangement T2 is more however, in both the arrangements the rate of increase in scour depth is decreasing with increasing seepage percentage. The eroded bed material is deposited at downstream of piers and height of deposition is increasing with increasing seepage percentage.

Chapter 5

# Suction Effects on Dynamics of Migrating Scour Depth and Dune-Like Bedforms at Bridge Piers[iv]

## 5.1 Introduction

In alluvial channels, celerity shows the progradation of developing bedforms along the flow. Here, dynamic characteristics of bedforms are signified by their celerity. Some of the researchers have investigated morphodynamic characteristics of bedforms from initial to equilibrium stage to understand the multifaceted splitting and merging of bedforms and stated that the change in bedform geometry affects the hydrodynamics of channel (Defina, 2003; Jerolmack and Mohrig, 2005). Recently, some investigators have performed spectral analysis of spatial and temporal bed elevations series at multiple scales (Nordin and Algert, 1966; Nikora et al., 1997; Nikora and Goring, 2001). Furthermore, Singh et al., (2011), have extensively carried out multiscale statistical analysis in migrating bedforms. In this study, we have focused on dynamic properties of migrating scour depth at piers and pdf of scour depth increments around piers for different time interval for with seepage and without seepage conditions. The scouring around bridge piers, in natural or manmade alluvial channels, demonstrate significant variability in the propagation of velocity over the range of different spatial and temporal scales. Therefore, the dynamic properties of scouring process comprehend from scale-dependant celerity of scouring around piers and the scouring is being time dependent phenomenon, we have performed wavelet analysis over the temporal bed elevation series. For particular scale, the scale dependant celerity was obtained by dividing the lag, corresponding to the maximum cross-correlation coefficient between two-bed elevation series. The scoured bed material is get deposited at downstream of piers along the centreline and dune like bedorms formed, the dynamic properties of migrating bedforms forming at downstream of single and tandem piers are also studied. The bed elevation series were recorded at a different interval of times using Ultrasonic Ranging System.

[iv] Sharma A., Chavan R. and Kumar B.- Multi-scale Statistical Characterization of Migrating Pier Scour Depth in Non-uniform Sand Bed channel, The International Journal of River Basin Management, 15, 3, 265-276, 2017

## 5.2 Results

### 5.2.1 Velocity

Figure 5.1 shows the contour of time-averaged velocity around tandem piers no seepage, 10% seepage and 15% seepage. Figure 5.1 reveals that the velocity near free surface is gradually decreasing while moving from upstream to downstream. At section A near the bed, the negative velocity that is reversal flow is observed. In between both piers, velocity is maximum near the bed and reducing gradually while moving towards the free surface. In the wake region that is at downstream of the rear pier, negative velocity occurs near free surface and turns to positive while moving towards the bed. However, the magnitude of reversal velocity is decreasing with increasing seepage percentage, which indicates that the strength of reversal flow, hence erosive capacity is reducing with increasing seepage percentage. In case of plane bed without any obstruction, the downward seepage shifts the velocity in a downward direction and results in increased velocity near the bed and subsequent increase in the movement of bed material. However, in this study, it has been observed that the downward seepage limits the reverse flow and restrains extension of scour depth.

### 5.2.2 Reynolds Shear Stress

Figure 5.2 shows a contour plot of Reynolds stresses around piers for with and without seepage conditions. Reynolds stresses are highly fluctuating around piers due to hindrance to the stream flow. From Figure 5.2, it can be perceived that at upstream of front pier Reynolds stresses are lesser near the free surface then increases towards the bed and reaches its higher value nearly at $z/h \approx 0.4$ and again becomes negative towards the bed. In between both piers, the Reynolds stresses are positive but lesser in magnitude at the surface then increasing near the bed. Reynolds stresses are negative close to free surface, became positive towards bed at section C (d/s of piers).

In seepage runs, at sections B and C, Reynolds stresses increased near the bed by 15% for 10% seepage and 24% for 15% seepage condition. The increased Reynolds stresses near the bed with seepage, suggests higher momentum exchange and sediment transport. However, at upstream section A, the magnitude of Reynolds stress is decreasing with increasing seepage percentage as downward seepage weakens the reversal flow. In

seepage runs, the decreased Reynolds stresses at bed results in lesser erosion of bed material at upstream of the pier.

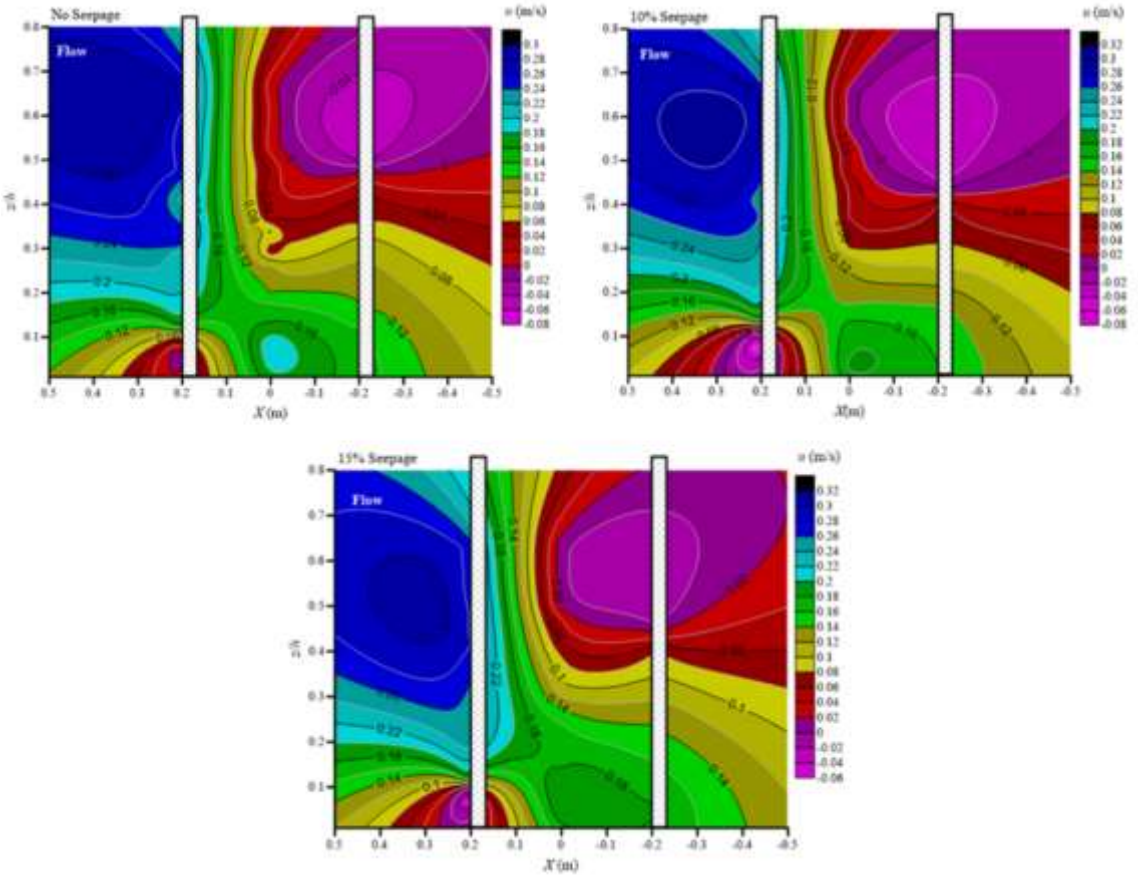


Figure 5.1 Contour of velocity profile for no seepage, 10% seepage and 15% seepage

### 5.2.3 Scale-dependent scour depth migration around tandem piers

Transportation of sediments resting on the channel boundaries in alluvial channels leads to change the morphodynamical condition of channels in terms of aggradation and degradation of channel boundaries. The presence of piers in alluvial channels cause a change in the streamflow pattern around piers. The obstruction to the flowing stream increases the shear stresses and hence scouring around the structure. A review of previous studies indicates that the flow patterns around the single pier is very complex hence, it is more complicated when two piers in tandem manner are obstructing flow. In case of tandem piers, the sour depth at the front pier is sufficiently large. The soured bed material is carried further and deposited at downstream of rear piers along and on either side of centerline.

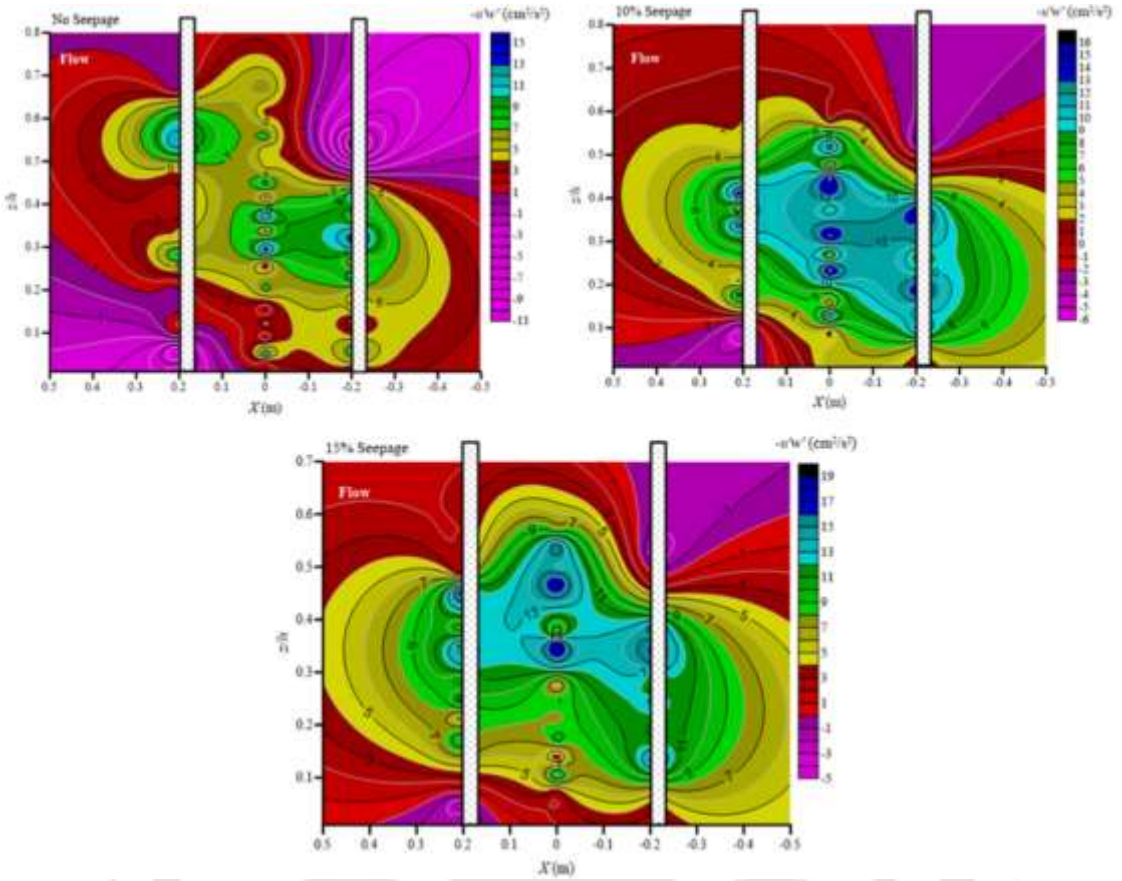


Figure 5.2 Contour of RSS for no seepage, 10% seepage and 15% seepage

The scouring around the pier is time dependent phenomenon. With time, the scour depth increases up to certain limit and then attains equilibrium condition where the resisting force of bed material exceeds the erosive capacity of flowing stream. Figure 5.3 displays the graph of lateral bed profile at upstream of piers for no seepage, 10% seepage and 15% seepage at a different time interval. The lateral bed profile was measured for 20cm transverse distance at upstream of the front pier where the scour depth is higher. Figure 5.3 shows that, firstly, the increase in scour depth is higher for all the experimental conditions and gradually the amount of growth of scour depth is reducing with time. The growth of scour is more rapid in case of no seepage runs. Further Figure 5.3 reveals that, the scour depth is higher for no seepage condition however; it is decreasing with

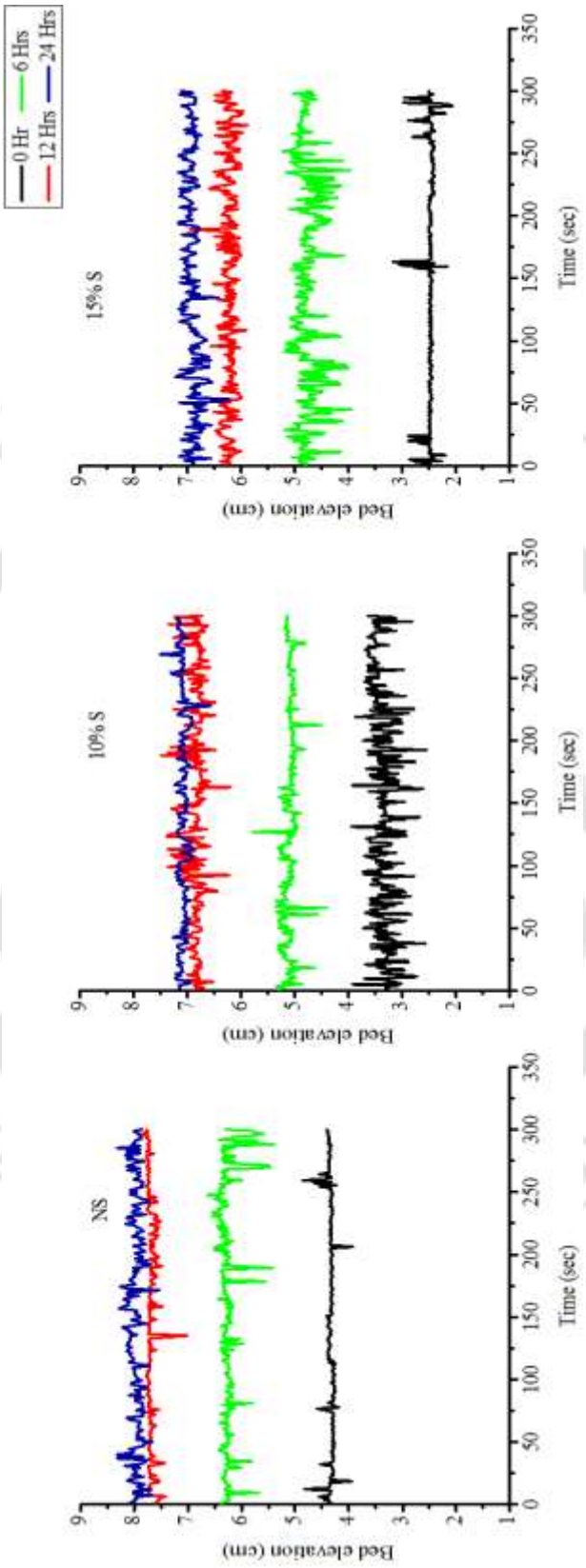


Figure 5.3 Bed elevation series at upstream of piers

increasing seepage percentage. The decrement in scour profundity with downward seepage is confirming to our findings that lesser strength of reversal flow results in lessening the scour depth (Figure 5.1 and Figure 5.2).

### 5.2.4 Wavelet Analysis

In this study to compute time dependant celerity of scouring at piers, the bed elevation was recorded for every 2s on different time spans for a single run by using transducers. For analyzing quantities that show wide disparity of physical and dynamic characteristics among various ranges of scales, wavelet transform helps to provide with a clearer and significant insight.

The wavelet transforms of signal *f (t)* is defined as integral transform with the series of functions $\psi_{a,b}(t)$;

$$W_f(a,b) = \int_{-\infty}^{+\infty} \psi_{a,b}(t) f(t) dt \tag{5.1}$$

Here, $\psi_{a,b}$ called wavelets and are obtained from mother wavelet$\psi(t)$, by translating and scaling;

$$\psi_{a,b}(t) = \frac{1}{\sqrt{a}} \psi\left(\frac{t-b}{a}\right) \tag{5.2}$$

Where, *a* and *b* are scaling and location parameter respectively and $\frac{1}{\sqrt{a}}$ is normalizing constant (Mallat, 1998; Kumar and Foufoula-Georgiou, 1997). For the invertible wavelet transform, the mother wavelet should satisfy the admissibility condition which is given by:

$$\int_{-\infty}^{+\infty} \psi_{a,b}(t) dt = 0 \tag{5.3}$$

Which indicates that, the area under the curve must be zero so that it will work like a local differencing filter. Wavelet with higher order vanishing moments, i.e.,

$$\int_{-\infty}^{+\infty} t^k \psi(t) dt = 0, (k = 0,1,2,3, \ldots\ldots, N-1 \ldots, \infty) \tag{5.4}$$

Where, N is the order of vanishing moments and are resulting in higher order vanishing filters which can remove polynomial trend of order (*N-1*) from a signal. The mother

wavelet is family of Gaussian-based wavelets of *N*th order derivatives of Gaussian function $g_0(t)$, i.e.,

$g_N(t) = (d^N/dt^N)\, g_0(t)$, (N=1,2….). It is well known that, *N=2* is Mexican hat wavelet and in this study, the wavelet coefficients were computed using Mexican hat wavelet $g_2(t)$ as the mother wavelet:

$$g_2(t) = \frac{2}{\sqrt{3}}\pi^{-1/4}(1-t^2)e^{-t^2/2} \tag{5.5}$$

In this study we are analysing temporal dataset for the scouring at piers and spatial data set for the bedfoms at the downstream side of piers so it is necessary to descritize the signals into time scales for scouring and length scale for bedforms dynamics.

Putting Eq. (7) into Eq. (3) and (4), the wavelet coefficients were found as,

$$W_f(a,b) = \frac{1}{\sqrt{a}}\int_{-\infty}^{+\infty} g_2\left(\frac{t-b}{a}\right) f(t)dt \tag{5.6}$$

The wavelet cross-covariance (WCC) between two data sets $f_1(t)$ and $f_2(t)$ were calculated as,

$$WCC_{f_1 f_2}(a,\Delta t) = \int_{-\infty}^{+\infty} W_{f_1}(a,b) W_{f_2}(a,b+\Delta t)db \tag{5.7}$$

Where, $W_{f_1}(a,b)$ and $W_{f_2}(a,b+\Delta t)$ are the wavelet coefficients of $f_1(t)$ and $f_2(t)$ respectively, at scale *a* and two adjacent locations *b* and $b+\Delta t$ respectively. The wavelet cross-correlation was calculated by normalizing it with the variance of the signals. In this study, first we found wavelet coefficient for variance of bed elevation data series, then then for a particular scale *a*, the lag corresponding to the maximum cross correlation coefficient of two series of wavelet coefficients were obtained. The time scale dependant celerity of migrating scour depth is obtained by $v_c(a,\Delta t) = L/\Delta t_{max}$, where, L is the distance between two sections where the bed elevation series are measured and $\Delta t_{max}$ is the time at which maximum cross-correlation between two signals is observed. The lag is divided by time interval of two successive data series to obtain the celerity.

Figure 5.4, displays the graph of the maximum correlation coefficient between upstream (U/S) (A) and downstream (D/S) (C) of tandem piers as a function of time scale.

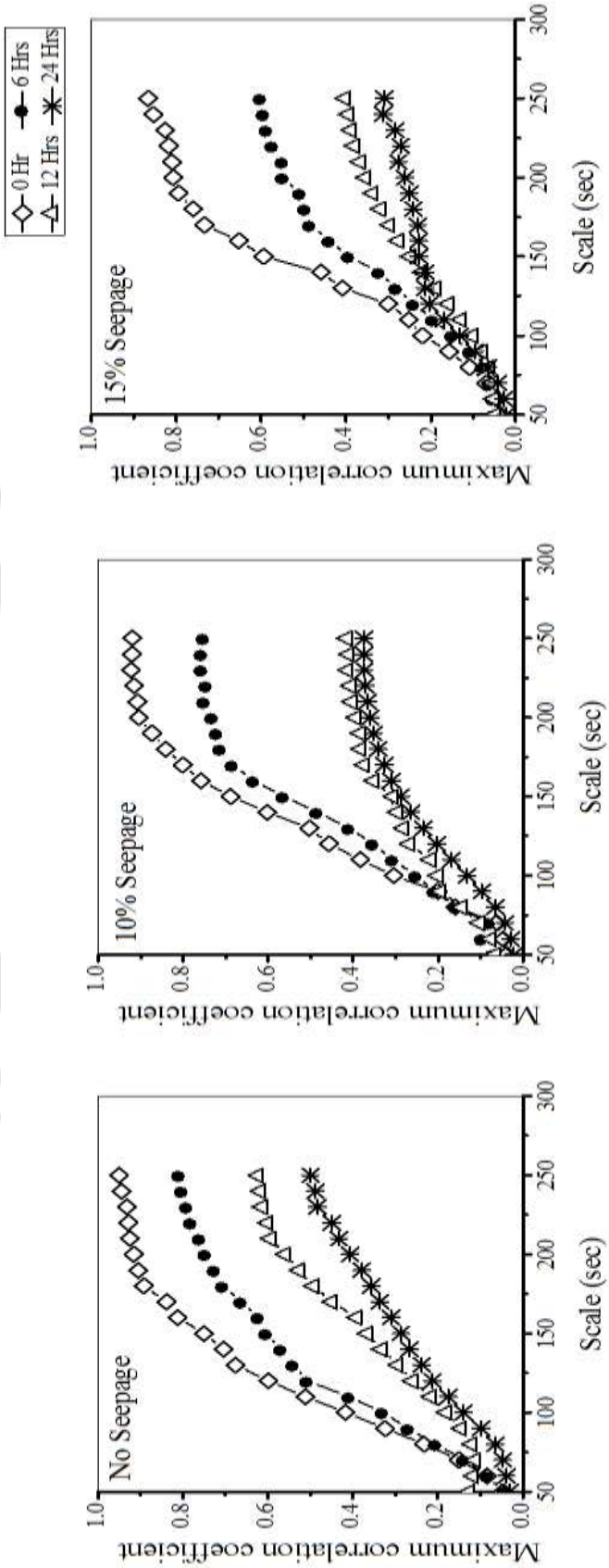


Figure 5.4 Maximum correlation coefficient at U/S-D/S of piers

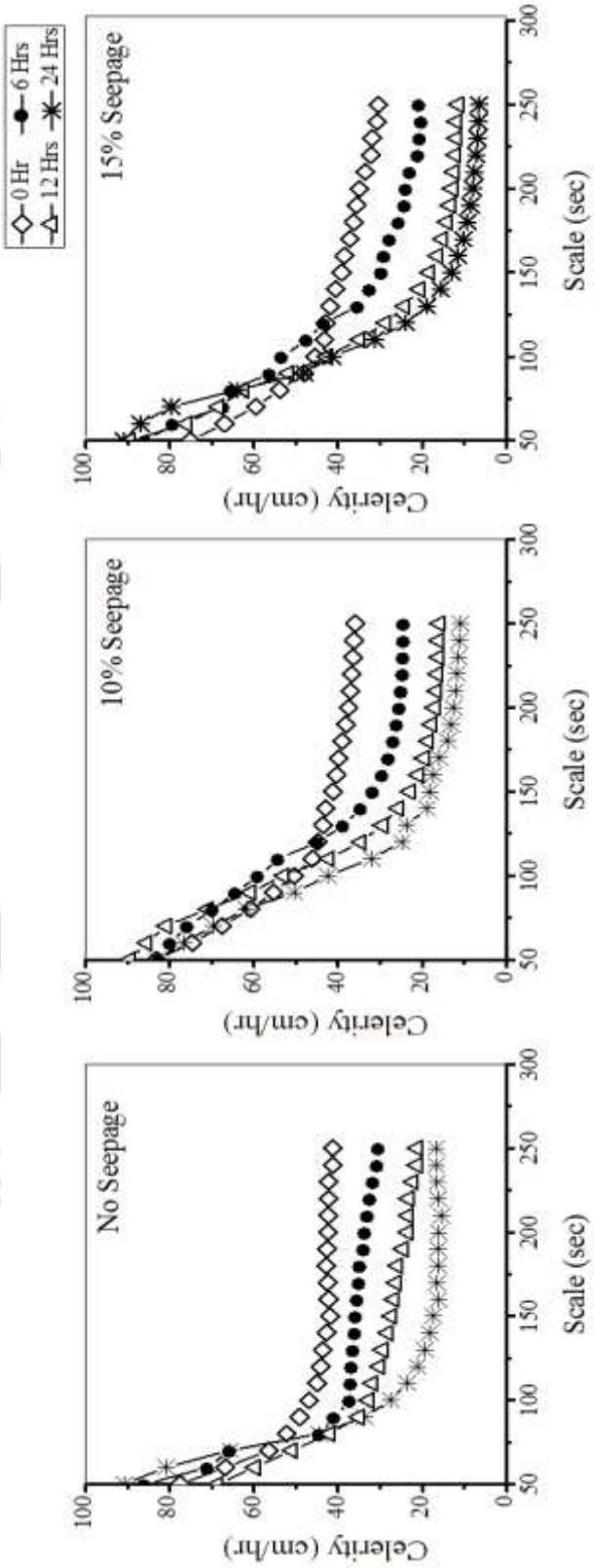


Figure 5.5 Time scale celerity at U/S-D/S of piers

From Figure 5.4, it is observed that, for smaller scales (< 60s), small values of cross-correlation coefficients (0.5-0.2) were obtained. It suggests decorrelation of these small features or linear analysis is insufficient to capture their evaluation and uncertainty in the estimation of celerity on the basis of cross-correlation analysis consequently. For the larger scales (>60s) the correlation coefficient becomes progressively larger (0.3-0.9). The lag corresponding to maximum correlation, $\Delta t_{max}$, at each scale was computed for obtaining the scale dependant celerity. Figure 5.5 shows estimated celerity for the time scale of 50- 300 s. The celerity of scour depth is gradually decreasing with increasing time scale that shows the celerity is higher for smaller time scale and vice versa. For each condition, the celerity at 0h is higher and with an increase in duration the celerity of scour hole is decreasing, which suggest that the rate of development of scour hole is diminishing with time. The increment in celerity of scour hole from 12h to 24h is quite lesser for all the three conditions; it justifies the stability or equilibrium condition of scour hole. The keen observation of Figure 5.4 shows that migration or celerity of scour hole is lesser in case of seepage runs than no seepage condition which demonstrates lesser scour depth in case of seepage runs. Statistics of celerity at U/S-D/S of tandem piers are mentioned in Table 5.1.

Similarly, in case of the single pier of diameter 75mm the measurements were taken at upstream of the pier (7.5975, 0.5), downstream of the pier (7.4025, 0.5) and at far downstream (6.7, 0.5) on the bedform behind the pier for the interval of 0hrs, 5hrs and 10hrs. Figures 5.6 and 5.7 display the results of the maximum correlation coefficient between probes placed at U/S and D/S of piers and probes located at D/S and bedform of pier as a function of time scale for no seepage and seepage runs respectively. It is clear from Figures 5.6 and 5.7 that for small value of scales (<3 sec) the small values of cross-correlation coefficients (range of 0.1-0.2) are obtained suggesting that either small scales are de-correlated or linear analysis is not sufficient to hold their evaluation for which we will not be able to get consistent measure of the celerity on the basis of a cross-correlation analysis. This type of small features may be transitory which are expected to be vanishing due to which we have to prevent any correlation between the time series data taken by probes. For large value of scales (>15 sec), the correlation coefficient gradually increases (range of 0.3-0.6).

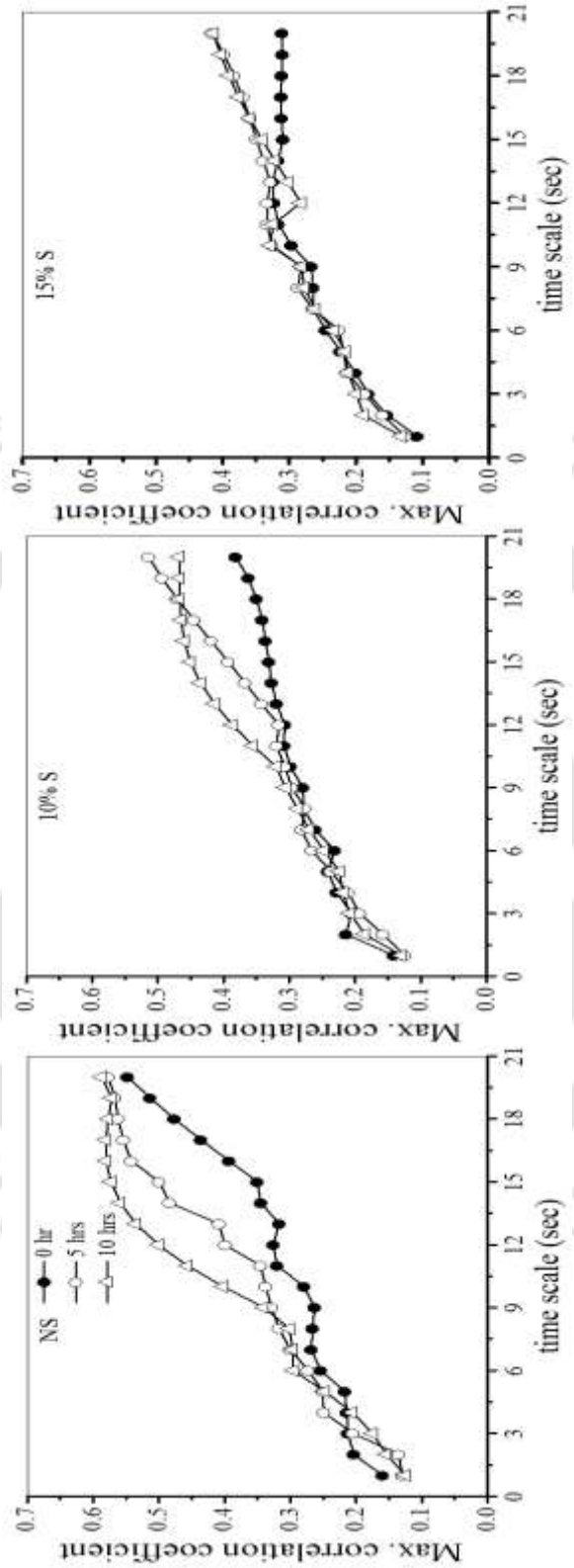


Figure 5.6 Maximum correlation coefficient at U/S-DS of pier

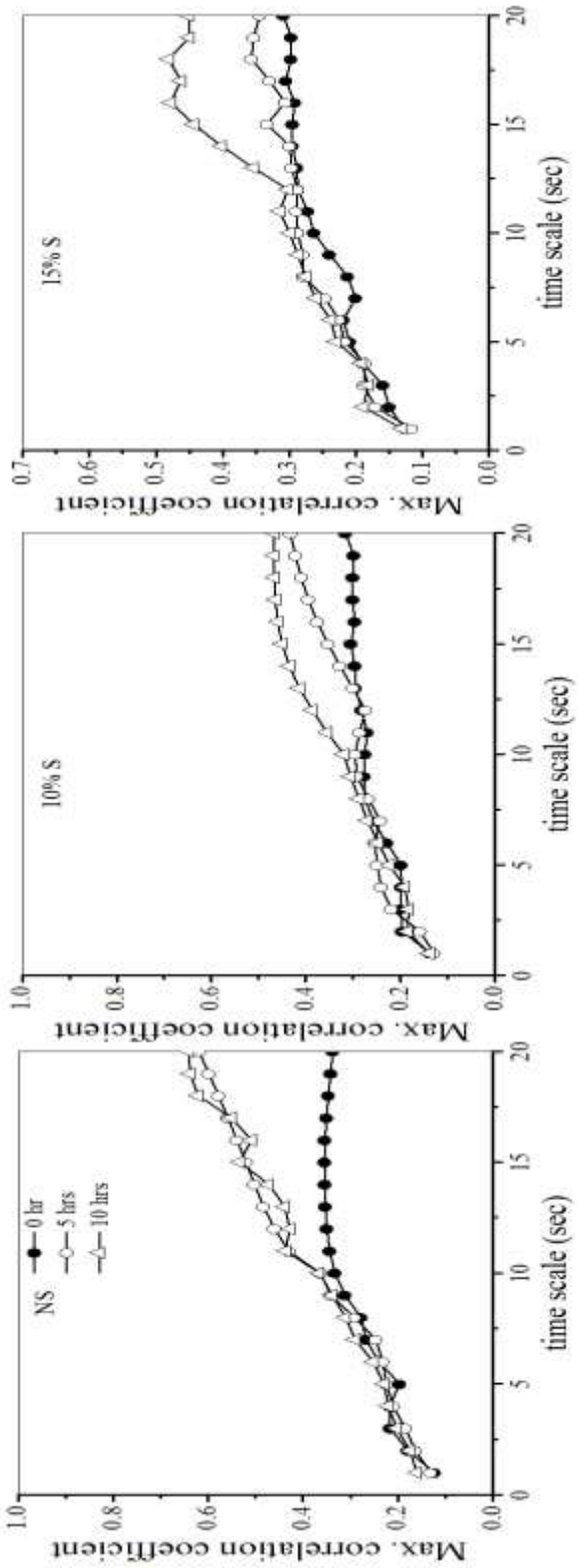


Figure 5.7 Maximum correlation coefficient at D/S-Bedform behind pier

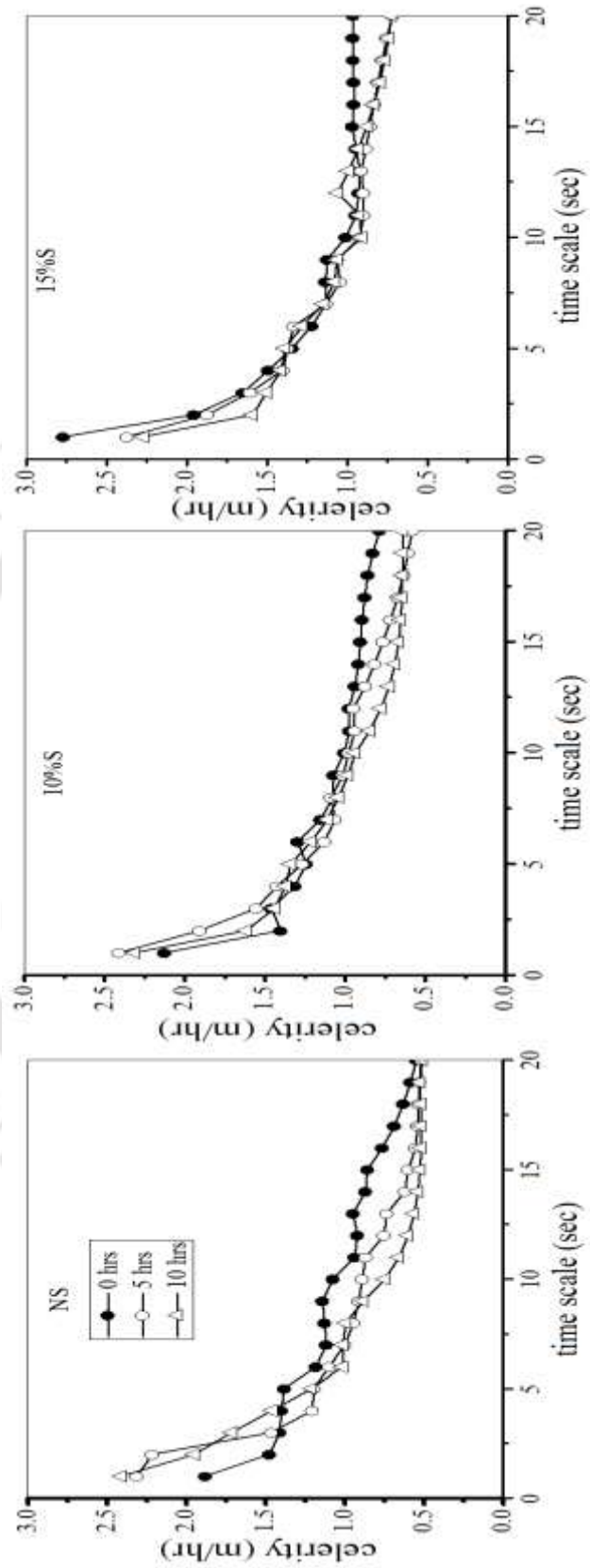


Figure 5.8 Celerity at U/S-DS of pier

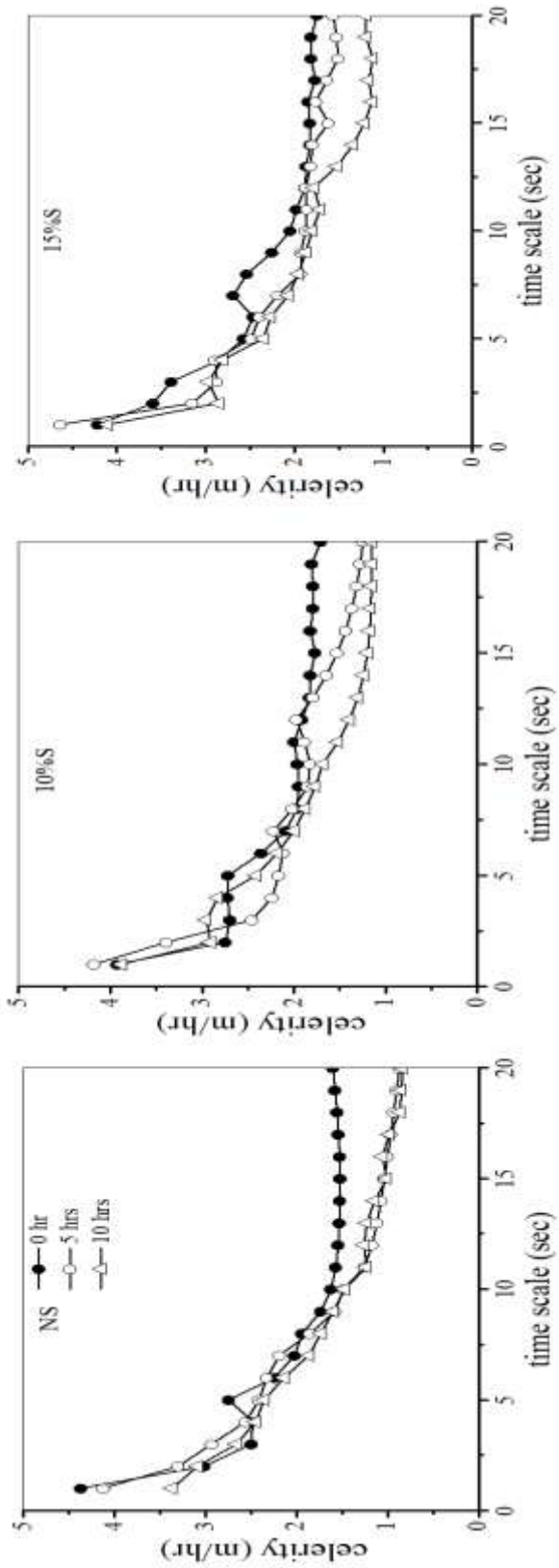


Figure 5.9 Celerity at D/S-Bedform behind pier

The position of time corresponding to maximum cross-correlation, $\Delta t_{max}$ at each scale was determined in order to estimate time scale-dependent celerity. Celerity of the scour depth ranging from a time scale of 1 sec to 20 sec was calculated using wavelet cross-correlation. Figures 5.8 and 5.9 show the estimated celerity with timescale for no seepage and seepage flow. Figures 5.8 and 5.9 indicate gradual decrease in celerity the increase of scale, i.e., higher diameter scour hole travels slowly. It is observed from Figure 5.6 that smaller scale have higher celerity as compared to larger scale. With the flow of no seepage and seepage, celerity of the scour hole has increased in the time duration of zero hour as compared to 5 hours and 10 hours. This suggest that celerity of scour hole decreases with the increase of time duration for the discharge of no seepage and seepage which justified that rate of increment of scour hole size has been decreased with the increase of time duration. Saturation level of the bed elevation with time is smaller in the case of seepage (Figures 5.6 and 5.7) which justifies a decrease in the scour hole size and consequently an increase in average bed celerity.

Table 5.1 Statistics of celerity (cm/h) at U/S-D/S of tandem piers

| | **No Seepage** | | | | **10% Seepage** | | | | **15% Seepage** | | | |
|---|---|---|---|---|---|---|---|---|---|---|---|---|
| Time scale (sec) | 0h | 6h | 12h | 24h | 0h | 6h | 12h | 24h | 0h | 6h | 12h | 24h |
| 50 | 77.56 | 85.8468 | 68.56 | 90.8468 | 83.1101 | 82.4539 | 89.4042 | 83.1101 | 74.9994 | 85.5538 | 89.6105 | 90.9994 |
| 60 | 66.78 | 70.92808 | 59.78 | 80.9280 | 74.6923 | 79.73 | 85.5341 | 76.6923 | 66.9809 | 79.1746 | 76.0945 | 86.9809 |
| 70 | 56.42776 | 65.60214 | 50.96 | 65.6021 | 67.5977 | 75.6754 | 80.8081 | 69.5977 | 59.5960 | 67.1232 | 68.3552 | 79.5960 |
| 80 | 52.21529 | 44.33474 | 42 | 44.3347 | 60.7441 | 69.6629 | 70.9278 | 61.7441 | 53.9229 | 65.2548 | 62.4330 | 63.9229 |

| | | | | | | | | | | | | |
|---|---|---|---|---|---|---|---|---|---|---|---|---|
| 90 | 49.1 | 40.7 | 35.0 | 33.7 | 55.2 | 64.3 | 60.8 | 50.2 | 48.0 | 56.1 | 51.8 | 48.0 |
| | 145 | 9067 | 829 | 906 | 696 | 118 | 619 | 698 | 525 | 276 | 439 | 525 |
| 100 | 46.8 | 37.0 | 32.7 | 27.5 | 50.4 | 58.9 | 52.8 | 42.4 | 45.3 | 53.2 | 42.7 | 41.3 |
| | 7 | 5756 | 535 | 239 | 183 | 390 | 695 | 183 | 632 | 265 | 039 | 632 |
| 110 | 45.0 | 36.7 | 31.7 | 23.5 | 46.0 | 54.0 | 42.1 | 32.0 | 43.1 | 47.3 | 34.9 | 31.1 |
| | 6848 | 7196 | 837 | 742 | 912 | 922 | 658 | 912 | 763 | 590 | 165 | 763 |
| 120 | 44.1 | 36.6 | 30.1 | 21.1 | 44.8 | 44.7 | 34.5 | 24.8 | 42.9 | 43.2 | 28.7 | 23.9 |
| | 4528 | 4643 | 727 | 052 | 079 | 985 | 608 | 079 | 080 | 100 | 664 | 080 |
| 130 | 43.5 | 36.2 | 29.4 | 19.3 | 43.6 | 38.7 | 29.4 | 23.6 | 41.9 | 35.1 | 24.1 | 18.9 |
| | 7056 | 2562 | 391 | 456 | 162 | 197 | 443 | 162 | 048 | 729 | 536 | 048 |
| 140 | 42.7 | 35.8 | 28.1 | 18.1 | 42.8 | 34.5 | 25.6 | 18.8 | 40.5 | 32.2 | 20.6 | 15.5 |
| | 2183 | 2463 | 986 | 852 | 815 | 099 | 809 | 815 | 444 | 744 | 983 | 444 |
| 150 | 41.9 | 35.6 | 27.3 | 17.3 | 41.2 | 31.5 | 22.9 | 18.2 | 39.1 | 29.5 | 18.2 | 13.1 |
| | 3021 | 1763 | 306 | 618 | 085 | 772 | 339 | 085 | 117 | 744 | 983 | 117 |
| 160 | 42.2 | 35.2 | 26.6 | 16.1 | 40.3 | 29.3 | 20.9 | 17.3 | 38.4 | 28.9 | 16.3 | 11.4 |
| | 6634 | 5229 | 611 | 699 | 820 | 603 | 540 | 820 | 789 | 069 | 651 | 789 |
| 170 | 42.4 | 34.8 | 26.1 | 16.4 | 39.9 | 27.8 | 19.5 | 15.9 | 37.1 | 27.5 | 15.2 | 10.1 |
| | 5956 | 5643 | 919 | 404 | 706 | 142 | 852 | 704 | 843 | 408 | 099 | 843 |
| 180 | 42.7 | 34.6 | 25.8 | 16.3 | 38.9 | 26.6 | 18.5 | 13.9 | 36.2 | 25.4 | 14.1 | 9.26 |
| | 8774 | 1151 | 818 | 058 | 661 | 867 | 056 | 661 | 600 | 351 | 314 | 009 |
| 190 | 42.6 | 33.7 | 24.6 | 16.2 | 38.1 | 25.8 | 17.7 | 13.1 | 35.5 | 24.0 | 13.4 | 8.55 |
| | 2116 | 1092 | 211 | 333 | 643 | 437 | 834 | 643 | 528 | 369 | 649 | 285 |
| 200 | 42.4 | 33.4 | 23.4 | 16.1 | 37.5 | 25.2 | 17.0 | 12.5 | 34.9 | 23.6 | 12.9 | 7.95 |
| | 5178 | 6341 | 517 | 103 | 413 | 247 | 96 | 413 | 586 | 930 | 015 | 863 |
| 210 | 42.3 | 32.8 | 23.3 | 15.5 | 37.0 | 24.8 | 16.5 | 12.0 | 33.5 | 22.7 | 12.4 | 7.52 |
| | 4846 | 6368 | 484 | 137 | 762 | 177 | 246 | 767 | 237 | 798 | 765 | 374 |
| 220 | 42.2 | 32.2 | 23.2 | 16.2 | 36.7 | 24.4 | 16.3 | 11.7 | 32.1 | 20.8 | 12.0 | 7.18 |
| | 8826 | 3563 | 882 | 889 | 125 | 732 | 844 | 125 | 851 | 813 | 547 | 514 |
| 230 | 42.2 | 31.4 | 22.2 | 16.3 | 36.4 | 24.3 | 16.0 | 11.4 | 31.9 | 20.3 | 11.7 | 6.90 |
| | 4526 | 8846 | 452 | 670 | 064 | 347 | 489 | 064 | 036 | 948 | 865 | 365 |

| | | | | | | | | | | | | |
|---|---|---|---|---|---|---|---|---|---|---|---|---|
| 240 | 41.2 | 30.5 | 21.2 | 16.5 | 36.1 | 24.2 | 16.1 | 11.1 | 30.6 | 20.0 | 11.8 | 6.66 |
| | 9157 | 385 | 915 | 275 | 515 | 183 | 004 | 515 | 654 | 154 | 578 | 546 |
| 250 | 41.2 | 30.2 | 21.2 | 16.5 | 35.9 | 24.2 | 15.8 | 10.9 | 30.4 | 20.6 | 11.4 | 6.46 |
| | 3405 | 4425 | 340 | 652 | 416 | 359 | 946 | 416 | 664 | 312 | 545 | 641 |
| Aver | 47.0 | 42.7 | 36.1 | 30.1 | 43.0 | 40.4 | 32.6 | 28.8 | 42.7 | 39.4 | 30.9 | 26.3 |
| age | 6658 | 1006 | 084 | 153 | 357 | 514 | 699 | 833 | 495 | 460 | 322 | 685 |
| celer | | | | | | | | | | | | |
| ity | | | | | | | | | | | | |

### 5.2.5 Pdf of scour depth increments

Most of the researchers have concentrated on characterizing the pdf of bedform fluctuations around their mean and mean bed elevation reported to be approximately Gaussian (Wong et al., 2007). However, instead of fluctuations around mean, bedform elevations ($\Delta h_x = h(t+x)-h(t)$) are more meaningful for statistical analysis as it helps in making the increments series stationary (Singh et al.,2011). In this study, we have used bedfom increments for statistical analysis. To the best of our knowledge, till date pdf's of scour depth at tandem piers is not explicitly reported before. These pdfs were computed from bed elevation series recorded by a probe placed at the centre at upstream of the front pier for different time intervals. Figure 5.10 shows semilog plots of pdfs of bed elevation at tandem piers at different times for with seepage and without seepage conditions. Pdfs have shown a similar trend for the probes at other locations but not shown here to maintain brevity of paper. At 2h the pdf is relatively narrow which becomes wider with increasing time, it signifies that pdf in some ways reflect the different phases of sediment transport during the experiments. It is observed from Figure 5.10 that initially (2h) the pdfs have heavier tails than the Gaussian pdf for all the three conditions, however with increasing the time the increments of bed elevation tend to become thinner tailed (12h). It can be justified by Figure 5.11, which shows log-log plot of the probability of exceedance of non-negative bed elevation increments. It can be observed from Figure 5.11 that the tail is heavier in case of no seepage runs than with seepage conditions and with time the pdf of bedform increments tend to become Gaussian. The thinner tail with time suggests stability of scour hole.

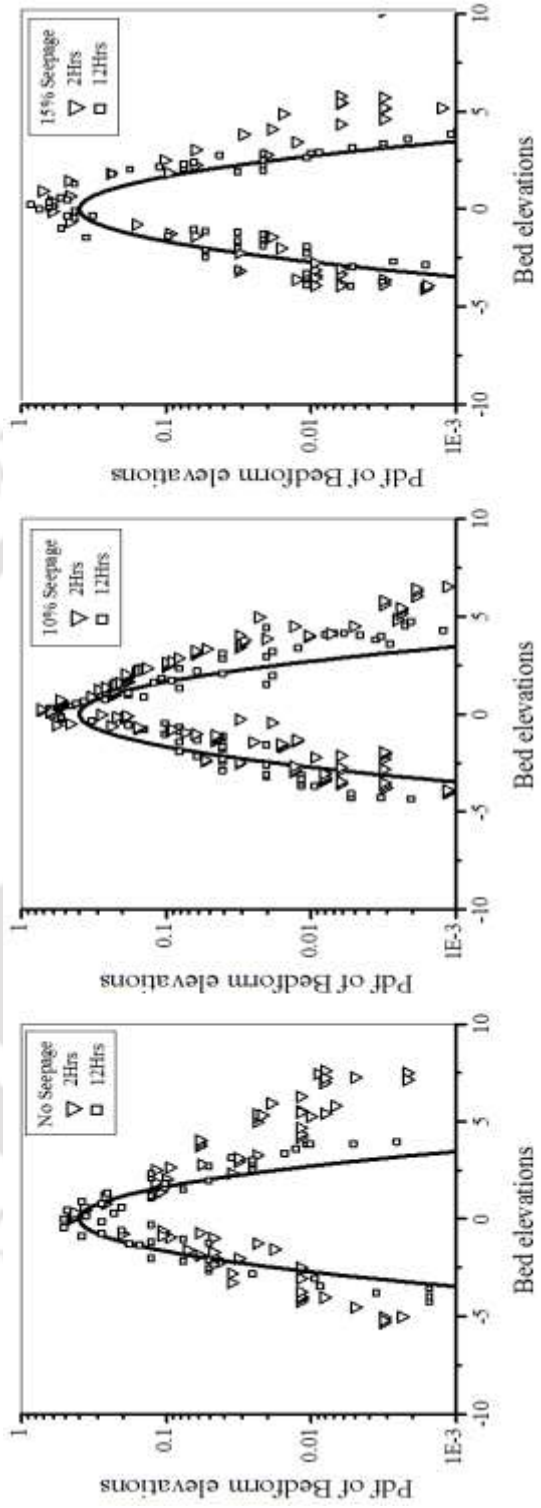


Figure 5.10 Semi log pdf of normalized bed elevations, solid line represents Gaussian distribution

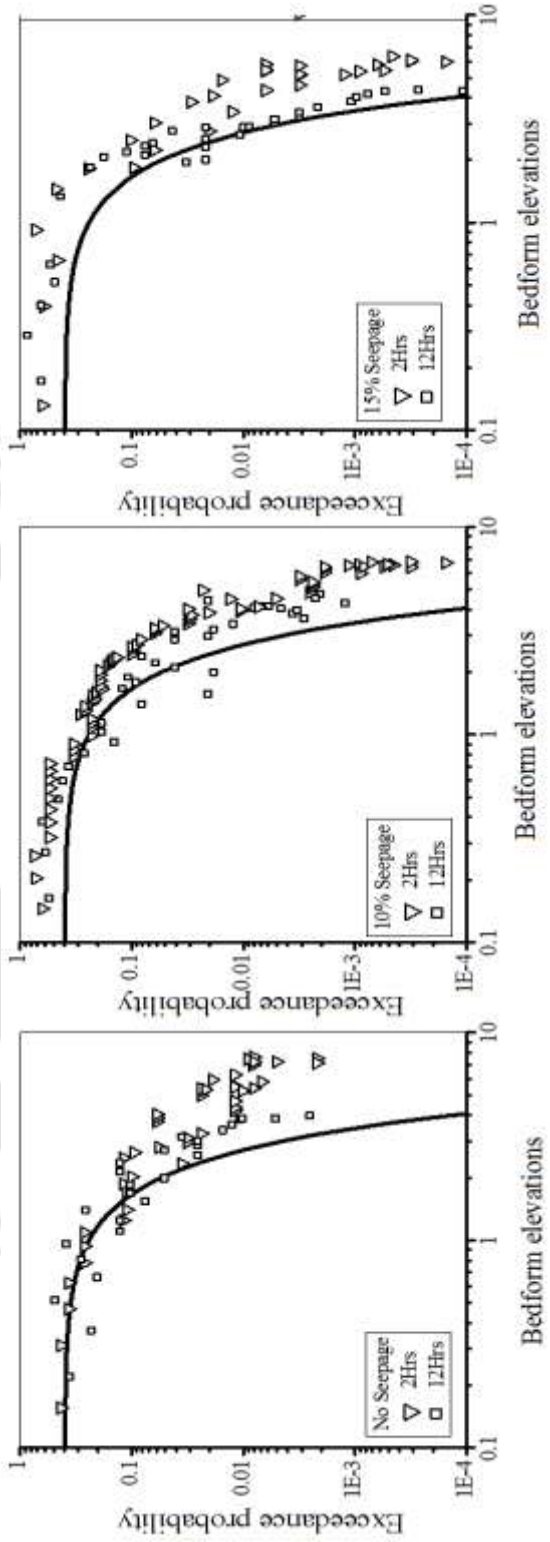


Figure 5.11 Log-log exceedance probabilities of the normalized positive increments of the bed elevation, solid line represents Gaussian distribution

### 5.2.6 Scale-dependant bedfom migration at downstream of piers

In alluvial channels with piers, the flow separation at bridge piers results in erosion of bed material. The eroded bed material is carried along the flow and are deposited at the downstream of piers along and on both sides of the centreline, producing dune like structures over there. Figure 5.12 shows a snapshot of channel bed after 24h experimental run. From Figure 5.12, it can be clearly seen that the dune-like bedforms are occurring at downstream of the piers due to sediment deposition. In our previous research (Chavan et al., 2017) we found that the height of deposition is increasing with increasing seepage percentage however the length of deposition is decreasing with downward seepage. While analysing the dynamic properties of migrating scour depth, one simply cannot avoid the dune like structures forming at downstream of piers.

Figure 5.12 Snapshot of channel bed after scouring

Most studies to date have concentrated on the statistical analysis of bedfoms on the plane bed (Singh et al., 2011, Patel et al., 2017). In this study, we have devised the effect of main channel flow with or without downward seepage on migrating dune like structure forming at downstream of tandem piers. First, the bed elevation series data is discretized into length scale. We found out the wavelet coefficients for variance of bed elevation data series and lab corresponding to a maximum cross-correlation coefficient of two series of wavelet coefficients for a particular scale is obtained. Thereafter, length scale dependent

celerity is computed by dividing the lag by the time interval between the two consecutive data series. The celerity of migrating dune structure from a length scale of 10mm-100mm is calculated using wavelet cross-correlation. The celerity with various length scale for the different time interval is shown in Figure 5.13. The celerity of dune structure is more during 2-12 hrs, for past 12 hrs that is 12-24hrs the celerity is decreased. Figure 5.13 also reveals that, up to certain length scale (<50mm) celerity is decreasing rapidly and then attain constancy at larger length scales (50-100mm) of bedforms. This can be hypothesized that the resistance to the flow is governed by the scale structures of bedforms which inhibits further sediment transport at larger scales (Bennett, 1995). For the same length scales of bedforms, celerity is decreasing with the application of downward seepage which might be the reason behind the higher height of deposition in case of seepage runs than no seepage condition. Statistics of celerity at bedforms behind piers for different time interval are mentioned in Table 5.2. Exceedance of probabilities of normalized bedform at downstream of tandem piers, for all the experimental runs have been found out and compared with a Gaussian distribution. Figure 5.14 displays the graph of exceedance probability of bedform elevations for no seepage, 10% seepage and 15% seepage conditions. It has been observed that in each experimental condition, for initial 2 hrs the pdf of bedform elevations is having heavier tails, however the tails of pdf are becoming thinner during with time (12 hrs) and getting closer towards the Gaussian distribution curve. This suggests that the equilibrium condition of dune like bedform structure at downstream of piers.

Table 5.2 Statistics of celerity (mm/h) at Dune like bedforms for different time interval

| | **No Seepage** | | **10% Seepage** | | **15% Seepage** | |
|---|---|---|---|---|---|---|
| **Length scale (mm)** | **2-12Hrs** | **12-24Hrs** | **2-12Hrs** | **12-24Hrs** | **2-12Hrs** | **12-24Hrs** |
| 10 | 98.3379 | 63.2265 | 113.3651 | 114.376 | 133.301 | 126.260 |
| 15 | 66.5859 | 39.9022 | 78.21538 | 44.3493 | 97.3631 | 48.6797 |
| 20 | 59.8936 | 31.5925 | 67.10986 | 29.0464 | 74.8852 | 31.4227 |
| 25 | 55.5777 | 22.4739 | 57.84939 | 19.8178 | 57.7824 | 21.0993 |

| | | | | | | |
|---|---|---|---|---|---|---|
| 30 | 49.9273 | 16.1076 | 46.71249 | 13.7127 | 42.3903 | 14.4356 |
| 35 | 44.8029 | 12.3193 | 37.59381 | 10.1317 | 32.5099 | 10.6145 |
| 40 | 40.9059 | 10.0205 | 31.27481 | 8.05867 | 26.6017 | 8.42786 |
| 45 | 38.0444 | 8.59919 | 27.0822 | 6.81472 | 22.9664 | 7.12239 |
| 50 | 35.9004 | 7.68012 | 24.21544 | 6.02441 | 20.6046 | 6.29548 |
| 55 | 34.2909 | 7.07766 | 22.27956 | 5.50829 | 19.0383 | 5.7556 |
| 60 | 33.0651 | 6.66941 | 20.95392 | 5.161 | 17.238 | 5.39232 |
| 65 | 32.1155 | 6.40102 | 20.00205 | 4.92228 | 16.8528 | 5.1442 |
| 70 | 31.7508 | 6.26404 | 19.48407 | 4.77374 | 16.6049 | 4.9912 |
| 75 | 31.4546 | 6.18417 | 19.12464 | 4.67989 | 16.4858 | 4.89484 |
| 80 | 31.3072 | 6.1532 | 18.93973 | 4.62835 | 16.4696 | 4.54232 |
| 85 | 31.3279 | 6.16042 | 18.86085 | 4.60973 | 16.6119 | 4.52413 |
| 90 | 31.5929 | 6.22814 | 18.98791 | 4.63434 | 16.8019 | 4.45104 |
| 95 | 32.0407 | 6.30936 | 19.1585 | 4.66966 | 16.9883 | 4.48867 |
| 100 | 32.3159 | 6.38995 | 19.32686 | 4.71582 | 16.7845 | 4.33819 |
| Average Celerity | 42.6967 | 16.5136 | 35.81771 | 15.8229 | 35.6990 | 14.9937 |

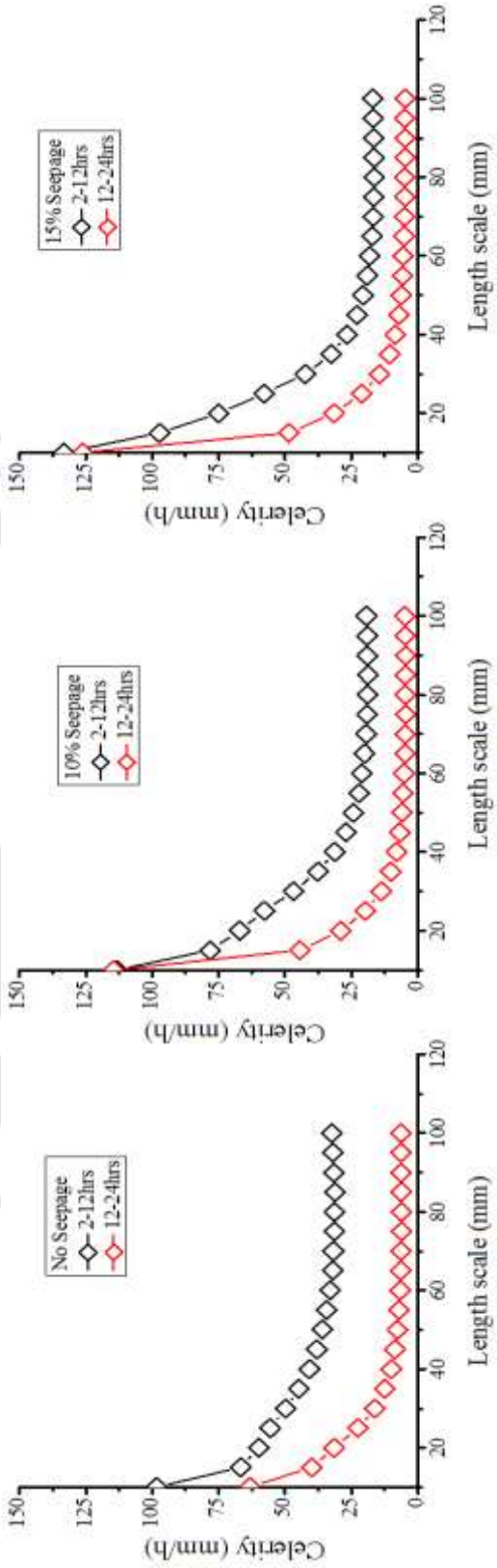


Figure 5.13 Length scale celerity at dune-like Bedforms

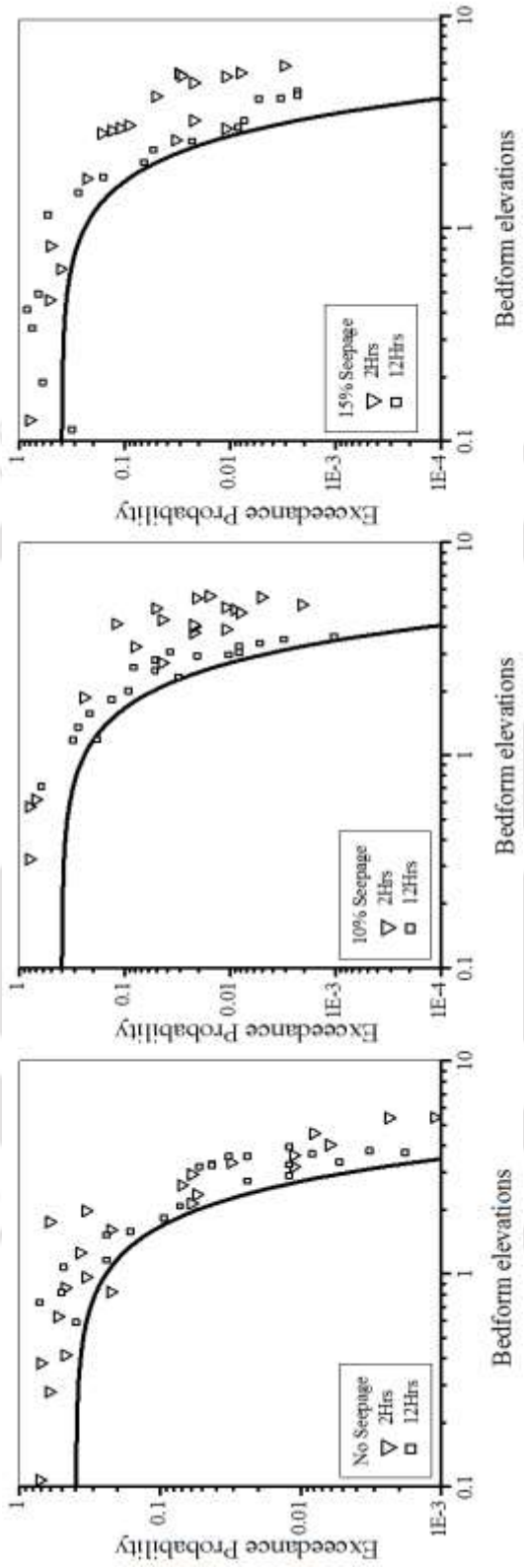


Figure 5.14 Log-log exceedance probability of bedform elevations at downstream of piers, solid line represents Gaussian distribution

## 5.3 Conclusions

Various results showing velocity, RSS around tandem piers for all the three conditions are presented. The reverse velocity is observed close to the bed at upstream section A and close to free surface at downstream section C. The reversal flow is found to be decreased with increasing downward seepage. In between both piers, velocity is higher near the bed and decreasing gradually towards free surface. Wake region of the front pier is clogged by the rear pier. At the downstream of rear pier, wake vortices are prevailing. RSS is found to be negative near the bed at upstream of the front pier and near the free surface at downstream of the rear pier. The magnitude of RSS is higher at section B and C. Reynolds stresses are fluctuating heavily at section C. Lesser magnitude of Reynolds stresses at upstream of piers in seepage runs, signifies that downward seepage impedes the reversal flow which is mainly responsible for scouring at bridge piers. Scour depth at piers is found to be higher in no seepage condition. With time, the rate of increase of scour depth is reducing. The wavelet-based scale dependant correlation analysis is done to estimate the celerity of migrating scour depth at piers and dune like bedforms behind the piers. Results of this study have revealed that the celerity of scour depth increases initially and then decreases gradually with time. At downstream of piers it has been observed that celerity of bedfomrs is decreasing with time, however in case of seepage runs average celerity of bedform for the same length scale is found to be increased initially and then gradually decreasing with increasing length scale. The reduction in celerity shows the dominance of larger bedforms in case of seepage runs. We have also presented the evidence that pdf of bed elevation increments are asymmetric and having heavier positive tails than a Gaussian distribution and with increasing time, the tails became thinner.

# Chapter 6

# Conclusions and Recommendations

In the history of bridge failure, scour around the bridge piers has been reported as main cause of failure. Many researchers have been attempted to estimate the maximum scour depth around bridge piers and mechanism of scour. No work has devised the effect of downward seepage on scour depth and flow field around piers. Additionally, the flow field around tandem piers considering effect of suction is not well investigated. Thus a detailed study on scour and flow around single and tandem bridge piers in seepage affected alluvial channels has been carried out.

An experimental study has been carried out on two types of non-uniform sands of median diameter 0.395mm and 0.5mm for no seepage, 10% seepage and 15% seepage conditions. The effect of the size of pier, arrangements of the piers (single or tandem), effect of sediment characteristics were considered for investigation of scour depth and flow around bridge piers. Important conclusions are drawn from the present study are presented below:

## 6.1 Effect of Downward Seepage on Turbulent Flow Field and Bed Morphology around Bridge Piers

- At upstream of the piers the strong reversal flow confirmed with the negative streamwise velocity is reduced with downward seepage.
- The vertical profile of its longitudinal velocity component at upstream of the pier, after eliminating the negative velocities occurring in the separation region near the bed, can be well explained by the logarithmic law of the wall for the inner region.
- The secondary currents are more significant at downstream of the pier because the maximum velocity occurs closer to the bed. Increase in percentage of seepage increases velocity, Reynolds stress at downstream of pier near the bed region.
- The wake behind piers is stronger in case of no seepage runs and becoming weaker with the application of downward seepage.
- At the upstream of the pier within the scour hole, the contribution of inward and outward interaction events towards the Reynolds stresses is more as the flow is

not able to move the particles further and they are lifted up by the flow and returned back to the bed. With downward seepage near the edge of scour hole sweep events are dominant. In the wake region of the pier, particles are remained in suspensions and transported along the flow due to the dominance of ejection events.

- The diminishing reversal flow at upstream of piers with downwards seepage results in lesser scour depth in case of seepage runs than no seepage conditions.
- Towards the start of scour, the rate of expansion in scour depth is progressively and gradually diminishes with development in time.
- The height of dunes at rear side of pier is lesser in case of no seepage runs and increases with increasing seepage percentage.
- Finally, the new empirical relationships are developed for prediction of scour depth at upstream of piers and prediction of dune morphology behind piers.

### 6.2 Hydrodynamics and Morphology around Tandem Piers in Alluvial Channel with Downward Seepage

- The reversal flow at upstream of piers near the bed and at downstream of piers near the free surface is decreasing with increasing seepage percentage.
- In the case of tandem piers, the wake region is stronger at downstream of rear pier than in between both piers.
- The streamwise flux and vertical flux of Reynolds stresses are lesser in case of seepage runs than no seepage conditions.
- Turbulent kinetic energy is observed to be higher near the edge of the scour hole as the scouring capacity of the flow is more at the edge of scour hole and decreased in magnitude in case of seepage runs.
- With increasing seepage percentage, lesser fluxes of streamwise and vertical turbulent kinetic energy in streamwise direction and vertical turbulent kinetic energy in vertical direction been observed.
- The lesser strength of wake region at downstream of piers with the application of downwards seepage has been confirmed with lesser Strouhal number in case of seepage runs.

- In the case of tandem piers with equal diameter, the scour depth at front piers is two times greater than the scour depth at the rear pier. However, in the case of tandem piers with different diameters, for the arrangement of 75mm front and 90mm rear pier, and 90mm front and 75mm rear pier, the scour depth at rear pier is reduced by nearly 40% and 60% than the scour depth at the front pier, respectively.

### 6.3 Suction Effects on Dynamics of Migrating Scour Depth and Dune- Like Bedforms at Bridge Piers

- The celerity of scour depth is increasing initially and then decreasing with the time that confirms the diminishing erosive capacity of flowing stream consequently, the rate of increase in scour depth is more initially and reducing with time.
- At downstream of piers, reduced celerity shows the dominance of larger bedforms in case of seepage runs, indicating bedforms of all length scales move at a slower speed in the case of a higher percentage of seepage.
- Analysis of dimensionalized probability distribution functions and logarithmic exceedance probability show occurrence of larger bed elevation fluctuations.

### 6.4 Recommendations of Future Research

The present research confirmed notable progress in the understanding of flow structures and bed morphology around single piers and tandem piers in seepage affected alluvial channels, opens the door for future investigators to explore many other aspects of scour around bridge piers.

- In the present study, circular piers were used; however in actual practices many different shapes of piers are used. The future investigators can further investigate the effect of shape of piers on scour depth and turbulent flow characteristics.
- In the present study, only two seepage percentages are used 10% and 15% downward seepage. Further study can be done by applying the various percentage of seepage. Additional experiments can be conducted over a larger range of velocities, pier diameter and channel sizes.
- The angle of attack is another important parameter and needs to be considered during the experiments. In the present study, only zero angle of attack was

employed. However, the variation of the angle of attack is strongly recommended to be taken into account for future research to investigate its interference effects on the horseshoe vortex system.

- In the case of tandem piers, further investigation can be done by changing the spacing between piers and studying the influence of spacing between piers on scour depths. The new empirical relationships can be developed for scour around tandem piers with incorporating downward seepage parameter and spacing between piers.
- Although the experimental investigations can provide comparatively more precise and accurate results, they are costly and more time consuming. From the economic point of view, research on bridge scouring based on the finite element numerical modelling using verified software packages is highly recommended for future research in this area. Nonetheless selected field results or laboratory tests are required to validate the numerical outputs.

# References


Aghaee-Shalmani, Y., & Hakimzadeh, H. (2015). Experimental investigation of scour around semi-conical piers under steady current action. European Journal of Environmental and Civil Engineering, 19(6), 717-732.

Ahmad M (1953, August) Experiments on design and behaviour of spur dikes. In Proceedings: Minnesota International Hydraulic Convention (pp. 145-159). ASCE

Ahmed, F., & Rajaratnam, N. (1998). Flow around bridge piers. Journal of Hydraulic Engineering, 124(3), 288-300.

Al-Shukur, A. H. K., & Obeid, Z. H. (2016). Experimental Study of Bridge Pier Shape to Minimize Local Scour. International Journal of Civil Engineering and Technology, 7(1), 162-171.

ANCID (2006). Australian Irrigation Water Provider Benchmarking Data Report for 2004-2005, Australian National Committee on Irrigation and Drainage, Canberra.

Ansari, S. A., Kothyari, U. C., & Ranga Raju, K. G. (2002). Influence of cohesion on scour around bridge piers. Journal of Hydraulic Research, 40(6), 717-729.

Ardiclioglu, M., & Ozturk, O. (2006). Numerical and experimental determination of boundarylayer thickness. WSEAS Transactions on Systems, 5(5), 1186-1189.

Ataie-Ashtiani, B., & Beheshti, A. A. (2006). Experimental investigation of clear-water local scour at pile groups. Journal of Hydraulic Engineering, 132(10), 1100-1104.

Ataie-Ashtiani, B., & Aslani-Kordkandi, A. (2013). Flow field around single and tandem piers. Flow, turbulence and combustion, 90(3), 471-490.

Ataie-Ashtiani, B., Baratian-Ghorghi, Z., & Beheshti, A. A. (2010). Experimental investigation of clear-water local scour of compound piers. Journal of Hydraulic Engineering, 136(6), 343-351.

Baker, C. J. (1979). The laminar horseshoe vortex. Journal of fluid mechanics, 95(2), 347-367.

Baker, C. J. (1980). The turbulent horseshoe vortex. Journal of Wind Engineering and Industrial Aerodynamics, 6(1-2), 9-23.

Baker, C. J. (1981). New design equations for scour around bridge piers. Journal of Hydraulic Engineering, 107(4), 507-511.

Beg, M. (2010). Characteristics of developing scour holes around two piers placed in transverse arrangement. In Scour and Erosion (pp. 76-85).

Beg, M., & Beg, S. (2015). Scour hole characteristics of two unequal size bridge piers in tandem arrangement. ISH Journal of Hydraulic Engineering, 21(1), 85-96.

Bennett, J. P. (1995). Algorithm for resistance to flow and transport in sand-bed channels. Journal of Hydraulic Engineering, 121(8), 578-590.

Blench T (1969) Mobile-bed fluviology, University of Alberta Press, Edmonton, Canada

Breusers, H. N. C., Nicollet, G., & Shen, H. W. (1977). Local scour around cylindrical piers. Journal of Hydraulic Research, 15(3), 211-252.

Brunke, M., & Gonser, T. O. M. (1997). The ecological significance of exchange processes between rivers and groundwater. Freshwater biology, 37(1), 1-33.

Carlson, R. A., & Petrich, C. R. (1999). New York Canal geologic cross-section, seepage gain/loss data, and ground water hydrographs: compilation and interim findings. Treasure Valley Hydrologic Project Open File Report.

Chabert J, Engeldinger P (1956). Etude des affouillements autour des piles des ponts. Laboratoire National d'Hydraulique, Chatou, France (In French)

Chavan, R., Sharma, A., & Kumar, B. (2017). Effect of downward seepage on turbulent flow characteristics and bed morphology around bridge piers. Journal of Marine Science and Application, 16(1), 60-72.

Cheremisinoff, P.N., Cheremisinoff, N.P. and Cheng, S.L. (1987). Hydraulic mechanics 2. Civil Engineering Practice, T echnomic Publishing Company, Inc., Lancaster, Pennsylvania, U.S.A., 780.

Chiew, Y. M. (1984). Local scour at bridge piers (Doctoral dissertation, ResearchSpace@ Auckland).

Chiew Y M, Melville B W (1987) Local scour around bridge piers. Journal of Hydraulic Research, 25(1), 15-26.

Chitale S V (1962) “Scour at bridge crossings.” Trans. Am. Soc. Civ. Eng., 127(1), 191–196

Coleman, S. E., & Melville, B. W. (2001). Case study: New Zealand bridge scour experiences. Journal of Hydraulic Engineering, 127(7), 535-546.

Coleman, S. E. (2005). Clearwater local scour at complex piers. Journal of Hydraulic Engineering, 131(4), 330-334.

Cao, D., & Chiew, Y. M. (2013). Suction effects on sediment transport in closed-conduit flows. Journal of Hydraulic Engineering, 140(5), 04014008.

Chang, W. Y., Lai, J. S., & Yen, C. L. (2004). Evolution of scour depth at circular bridge piers. Journal of Hydraulic Engineering, 130(9), 905-913.

Chen, X., & Chiew, Y. M. (2004). Velocity distribution of turbulent open-channel flow with bed suction. Journal of Hydraulic Engineering, 130(2), 140-148.

Cheng, N. S., & Chiew, Y. M. (1998). Turbulent open-channel flow with upward seepage. Journal of Hydraulic Research, 36(3), 415-431.

Cheng, N. S., & Chiew, Y. M. (1999). Incipient sediment motion with upward seepage. Journal of Hydraulic Research, 37(5), 665-681.

Chiew, Y. M. (1984). Local scour at bridge piers (Doctoral dissertation, ResearchSpace@ Auckland).

Chiew, Y. M. (2004). Local scour and riprap stability at bridge piers in a degrading channel. Journal of Hydraulic Engineering, 130(3), 218-226.

Chiew, Y. M., & Melville, B. W. (1987). Local scour around bridge piers. Journal of Hydraulic Research, 25(1), 15-26.

Chiew, Y. M., & Lim, F. H. (2000). Failure behavior of riprap layer at bridge piers under live-bed conditions. Journal of Hydraulic Engineering, 126(1), 43-55.

Defina, A. (2003). Numerical experiments on bar growth. Water Resources Research, 39(4).

Deshpande, V., & Kumar, B. (2016). Turbulent flow structures in alluvial channels with curved cross-sections under conditions of downward seepage. Earth Surface Processes and Landforms, 41(8), 1073-1087.

Deshpande, V., & Kumar, B. (2016). Advent of sheet flow in suction affected alluvial channels. Environmental Fluid Mechanics, 16(1), 25-44.

Devi, T. B., & Kumar, B. (2015). Turbulent flow statistics of vegetative channel with seepage. Journal of Applied Geophysics, 123, 267-276.

Dey, S. (1999). Time-variation of scour in the vicinity of circular piers. Proceedings of the Institution of Civil Engineers-Water Maritime and Energy, 136(2), 67-75.

Dey, S., Bose, S. K., & Sastry, G. L. (1995). Clear water scour at circular piers: a model. Journal of Hydraulic Engineering, 121(12), 869-876.

Dey, S., Das, R., Gaudio, R., & Bose, S. (2012). Turbulence in mobile-bed streams. Acta Geophysica, 60(6), 1547-1588.

Dey, S., & Raikar, R. V. (2007). Characteristics of horseshoe vortex in developing scour holes at piers. Journal of Hydraulic Engineering, 133(4), 399-413.

Dey, S., & Sarkar, A. (2006). Scour downstream of an apron due to submerged horizontal jets. Journal of hydraulic engineering, 132(3), 246-257.

Dukker, P., Bhutta, M. N., Peter, R., & Javed, I. (1994). Seepage losses from the Lower gugera Branch Canal. Punjab, Pakistan, IWASRI, Publication, 134.

Elhimer, M., Harran, G., Hoarau, Y., Cazin, S., Marchal, M., & Braza, M. (2016). Coherent and turbulent processes in the bistable regime around a tandem of cylinders including reattached flow dynamics by means of high-speed PIV. Journal of Fluids and Structures, 60, 62-79.

Elsabaie, I. H. (2013) 'An Experimental Study of Local Scour around Circular Bridge Pier in Sand Soil', International Journal of Civil & Environmental Engineering IJCEE-IJENS, 13(01).

Ettema, R. (1980). Scour at bridge piers (No. 216 Monograph).

Ettema, R., Constantinescu, G., & Melville, B. (2011). Evaluation of bridge scour research: Pier scour processes and predictions (No. NCHRP Project 24-27 (01)).

Euler, T., & Herget, J. (2012). Controls on local scour and deposition induced by obstacles in fluvial environments. Catena, 91, 35-46.

Ettema R, Melville B W, Constantinescu G (2011) Evaluation of bridge scour research: Pier scour processes and predictions. Washington, DC: Transportation Research Board of the National Academies

Fipps, G. (2000). Potential water savings in irrigated agriculture for the Rio Grande Planning Region (Region M). Texas Cooperative Extension, Texas A&M University System.

Francalanci, S., Parker, G., & Solari, L. (2008). Effect of seepage-induced nonhydrostatic pressure distribution on bed-load transport and bed morphodynamics. Journal of Hydraulic Engineering, 134(4), 378-389.

Garde, R. J., & Kothyari, U. C. (1998). Scour around bridge piers. Proceedings-Indian National Science Academy PART A, 64, 569-580.

Garde, R. J., & Raju, K. R. (2000). Mechanics of sediment transportation and alluvial stream problems. Taylor & Francis.

Goring, D. G., & Nikora, V. I. (2002). Despiking acoustic Doppler velocimeter data. Journal of Hydraulic Engineering, 128(1), 117-126.

Grimaldi, C., Gaudio, R., Calomino, F., & Cardoso, A. H. (2009). Countermeasures against local scouring at bridge piers: slot and combined system of slot and bed sill. Journal of Hydraulic Engineering, 135(5), 425-431.

Hancu, S. (1971). Sur le calcul des affouillements locaux dams la zone des piles des ponts. In XIV IAHR Congress.

Hannah, C.R.: Scour at pile groups. New Zealand, Christchurch, Univ. of Canterbury, Civil Engineering Dept., Research Rep. No. 28-3 (1978)

Huang, R. F., Hsu, C. M., & Lin, W. C. (2014). Flow characteristics around juncture of a circular cylinder mounted normal to a flat plate. Experimental Thermal and Fluid Science, 55, 187-199.

Inglis, C. C. (1949). The behaviour and control of rivers and canals (with the aid of models) (No. 13). Yeravda Prison Press.

IRC:5 (1998) Standard specifications and code of practice for road bridgessection- I. Indian Roads Congress, Jamnagar House, New Delhi

IRC:78 (2000) Standard specifications and code of practice for road bridges, section-VII. Indian Roads Congress, Jamnagar House, New Delhi

Istiarto, I. (2001). Experiments on flow around a cylinder in a scoured channel bed. International Journal of Sediment Research: English version, (4), 431-444.

Istiarto, I. (2001). Flow around a cylinder in a scoured channel bed (Doctoral dissertation, PhD-thesis).

Izadinia, E., Heidarpour, M., & Schleiss, A. J. (2013). Investigation of turbulence flow and sediment entrainment around a bridge pier. Stochastic environmental research and risk assessment, 27(6), 1303-1314.

Jain, S. C., & Fischer, E. E. (1979). Scour around bridge piers at high Froude numbers. Report. no. FHWA-RD-79-104. Washington, DC, USA: Federal Highway Administration.

Jain, S. C. (1981). Maximum clear-water scour around circular piers. Journal of the Hydraulics Division, 107(5), 611-626.

Jerolmack, D. J., & Mohrig, D. (2005). A unified model for subaqueous bed form dynamics. Water Resources Research, 41(12).

Johnson P A, Torrico E F (1994) Scour around wide piers in shallow water. Transportation Research Record, (1471)

Jones, J. S., Alqalam, K., Gratton, B., & Summers, B. (1995). Effect of the 1994 Southeast Flooding on the Highway System in Georgia. In unpublished handout presented at the 1995 ASCE Hydraulics Division Conference, San Antonio, TX.

Jones, J. B., & Mulholland, P. J. (1999). Streams and ground waters. academic press.

Jueyi, S. U. I., Afzalimehr, H., Samani, A. K., & Maherani, M. (2010). Clear-water scour around semi-elliptical abutments with armored beds. International Journal of sediment research, 25(3), 233-245.

Karambas, T. V. (2003). Modelling of infiltration-exfiltration effects of cross-shore sediment transport in the swash zone. Coastal Engineering Journal, 45(01), 63-82.

Keshavarzi, A., Shrestha, C. K., Zahedani, M. R., Ball, J., & Khabbaz, H. (2017, June). Experimental study of flow structure around two in-line bridge piers. In Proceedings of the Institution of Civil Engineers-Water Management, 1-17.

Kinzli, K. D., Martinez, M., Oad, R., Prior, A., & Gensler, D. (2010). Using an ADCP to determine canal seepage loss in an irrigation district. Agricultural water management, 97(6), 801-810.

Kirkil, G., Constantinescu, S. G., & Ettema, R. (2008). Coherent structures in the flow field around a circular cylinder with scour hole. Journal of Hydraulic Engineering, 134(5), 572-587.

Kirkgöz, M. S., & Ardiçlioğlu, M. (1997). Velocity profiles of developing and developed open channel flow. Journal of Hydraulic Engineering, 123(12), 1099-1105.

Kothyari, U. C. 2008.Bridge scour: status and research challenges. ISH Journal of Hydraulic Engineering, 14(1), 1-27.

Kothyari U C, Garde R C J, Ranga Raju K G (1992) Temporal variation of scour around circular bridge piers. Journal of Hydraulic Engineering, 118(8), 1091-1106

Kothyari, U. C., Ranga Raju, K. G., & Garde, R. J. (1992). Live-bed scour around cylindrical bridge piers. Journal of Hydraulic Research, 30(5), 701-715.

Kothyari, U. C. and Kumar, A. (2012) 'Temporal variation of scour around circular compound piers', Journal of Hydraulic Engineering. American Society of Civil Engineers, 138(11), 945–957.

Kumar, P., & Foufoula-Georgiou, E. (1997). Wavelet analysis for geophysical applications. Reviews of geophysics, 35(4), 385-412.

Kumar, A., & Kothyari, U. C. (2011). Three-dimensional flow characteristics within the scour hole around circular uniform and compound piers. Journal of Hydraulic Engineering, 138(5), 420-429.

Krishnamurthy, K., & Rao, S. (1969). Theory and experiment in canal seepage estimation using radioisotopes. Journal of Hydrology, 9(3), 277-293.

Krogstad, P. Å., & Kourakine, A. (2000). Some effects of localized injection on the turbulence structure in a boundary layer. Physics of Fluids, 12(11), 2990-2999.

Lacey G (1930) STABLE CHANNELS IN ALLUVIUM (INCLUDES APPENDICES). In Minutes of the Proceedings of the Institution of Civil Engineers (Vol. 229, No. 1930, pp. 259-292)

Lagasse, P. F., & Richardson, E. V. (2001). ASCE compendium of stream stability and bridge scour papers. Journal of Hydraulic Engineering, 127(7), 531-533.

Laursen, E. M., & Toch, A. (1956). Scour around bridge piers and abutments (Vol. 4). Ames, IA: Iowa Highway Research Board.

Lee, S. O. (2006). Physical modeling of local scour around complex bridge piers (Doctoral dissertation, Georgia Institute of Technology).

Lee, S. O. and Sturm, T. W. (2009) 'Effect of sediment size scaling on physical modeling of bridge pier scour', Journal of Hydraulic Engineering. American Society of Civil Engineers, 135(10), 793–802.

Li, J. (2017). Assessing the accuracy of predictive models for numerical data: Not r nor r2, why not? Then what?. PloS one, 12(8), e0183250.

Lu, Y., & Chiew, Y. M. (2007). Seepage effects on dune dimensions. Journal of Hydraulic Engineering, 133(5), 560-563.

Lu, S. S., & Willmarth, W. W. (1973). Measurements of the structure of the Reynolds stress in a turbulent boundary layer. Journal of Fluid Mechanics, 60(3), 481-511.

Maclean, A. G. (1991). Open channel velocity profiles over a zone of rapid infiltration. Journal of Hydraulic Research, 29(1), 15-27.

Maclean, A. G. (1991). Bed shear stress and scour over bed-type river intake. Journal of Hydraulic Engineering, 117(4), 436-451.

Maclean, A. G., & Willetts, B. B. (1986). Measurement of boundary shear stress in non-uniform open channel flow. Journal of Hydraulic Research, 24(1), 39-51.

Maity, H. and Mazumder, B. S. (2012) 'Contributions of burst-sweep cycles to Reynolds shear stress over fluvial obstacle marks generated in a laboratory flume', International Journal of Sediment Research, 27(3), 378–387.

Maity, H., & Mazumder, B. S. (2014). Experimental investigation of the impacts of coherent flow structures upon turbulence properties in regions of crescentic scour. Earth Surface Processes and Landforms, 39(8), 995-1013.

Mallat, S. (1999). A wavelet tour of signal processing. Academic press.

Marsh, N. A., Western, A. W., & Grayson, R. B. (2004). Comparison of methods for predicting incipient motion for sand beds. Journal of Hydraulic Engineering, 130(7), 616-621.

Martin, C. A., & Gates, T. K. (2014). Uncertainty of canal seepage losses estimated using flowing water balance with acoustic Doppler devices. Journal of hydrology, 517, 746-761.

Masjedi, A., Bejestan, M. S., & Esfandi, A. (2010). Experimental study on local scour around single oblong pier fitted with a collar in a 180 degree flume bend. International Journal of Sediment Research, 25(3), 304-312.

Mazumder, B. S., Maity, H., & Chadda, T. (2011). Turbulent flow field over fluvial obstacle marks generated in a laboratory flume. International Journal of Sediment Research, 26(1), 62-77.

Melville, B. W. (1975). Local scour at bridge sites (Doctoral dissertation, ResearchSpace@ Auckland).

Melville, B. W., & Chiew, Y. M. (1999). Time scale for local scour at bridge piers. Journal of Hydraulic Engineering, 125(1), 59-65.

Melville, B. W., & Coleman, S. E. (2000). Bridge scour. Water Resources Publication.

Melville, B. W., & Raudkivi, A. J. (1977). Flow characteristics in local scour at bridge piers. Journal of Hydraulic Research, 15(4), 373-380.

Melville, B. W., & Sutherland, A. J. (1988). Design method for local scour at bridge piers. Journal of Hydraulic Engineering, 114(10), 1210-1226.

Mohamed T A, Noor M J M M, Ghazali,A H, Huat B B (2005) Validation of some bridge pier scour formulae using field and laboratory data. Am J Environ Sci, 1(2), 119-125

Nikora, V. I., & Goring, D. G. (2001). Extended self-similarity in geophysical and geological applications. Mathematical geology, 33(3), 251-271.

Nikora, V. I., Sukhodolov, A. N., & Rowinski, P. M. (1997). Statistical sand wave dynamics in one-directional water flows. Journal of Fluid Mechanics, 351, 17-39.

Nazariha, M. (1996). Design relationships for maximum local scour depth for bridge pier groups. University of Ottawa (Canada).

Nezu, I., Nakagawa, H., & Jirka, G. H. (1994). Turbulence in open-channel flows. Journal of Hydraulic Engineering, 120(10), 1235-1237.

Nordila A, Ali T, Faisal A, Badrunnisa Y (2014) Local Scour at Wide Bridge Piers. In International Journal of Engineering Research and Technology, 3(1).

Nordin, C. F., & Algert, J. H. (1966). Spectral analysis of sand waves. Journal of the Hydraulics Division, 92(5), 95-114.

Oldenziel, D. M., & Brink, W. E. (1974). Influence of suction and blowing on entrainment of sand particles. Journal of the Hydraulics Division, 100(7), 935-949.

Oliveto, G., & Hager, W. H. (2002). Temporal evolution of clear-water pier and abutment scour. Journal of Hydraulic Engineering, 128(9), 811-820.

Oliveto, G., & Hager, W. H. (2014). Morphological evolution of dune-like bed forms generated by bridge scour. Journal of Hydraulic Engineering, 140(5), 06014009.

Pagliara, S., & Carnacina, I. (2010). Temporal scour evolution at bridge piers: Effect of wood debris roughness and porosity. Journal of Hydraulic Research, 48(1), 3-13.

Palau-Salvador, G., Stoesser, T., & Rodi, W. (2008). LES of the flow around two cylinders in tandem. Journal of Fluids and Structures, 24(8), 1304-1312.

Parola, A. C., Mahavadi, S. K., Brown, B. M., & El Khoury, A. (1996). Effects of rectangular foundation geometry on local pier scour. Journal of Hydraulic Engineering, 122(1), 35-40.

Pasiok, R., & Stilger-Szydło, E. (2010). Sediment particles and turbulent flow simulation around bridge piers. Archives of Civil and Mechanical Engineering, 10(2), 67-79.

Patel, M., Majumder, S., & Kumar, B. (2017). Effect of seepage on flow and bedforms dynamics. Earth Surface Processes and Landforms.

Patel, M., Deshpande, V., & Kumar, B. (2015). Turbulent characteristics and evolution of sheet flow in an alluvial channel with downward seepage. Geomorphology, 248, 161-171.

Prinos, P. (1995). Bed-suction effects on structure of turbulent open-channel flow. Journal of Hydraulic Engineering, 121(5), 404-412.

Qadar, A. (1981, September). The vortex scour mechanism at bridge piers. In Institution of Civil Engineers, Proceedings, Pt2 (Vol. 71).

Qi, M., Chiew, Y. M., & Hong, J. H. (2012). Suction effects on bridge pier scour under clear-water conditions. Journal of Hydraulic Engineering, 139(6), 621-629.

Rao, A. R., & Sitaram, N. (1999). Stability and mobility of sand-bed channels affected by seepage. Journal of Irrigation and Drainage Engineering, 125(6), 370-379.

Rao, A. R., & Sreenivasulu, G. (2009). Design of plane sand-bed channels affected by s

Rao, A. R., Sreenivasulu, G., & Kumar, B. (2011). Geometry of sand-bed channels with seepage. Geomorphology, 128(3), 171-177.eepage. Periodica Polytechnica. Civil Engineering, 53(2), 81.

Raja, R. K., Kumar, A., & Chhabra, S. S. (1983). Estimation of Seepage Losses from an Unlined Channel-A Field Study by Nuclear Techniques. In Proceeding (Vol. 2).

Raudkivi, A. J., & Ettema, R. (1983). Clear-water scour at cylindrical piers. Journal of Hydraulic Engineering, 109(3), 338-350.

Richardson E V, Davis S R (2001) HEC-18. Evaluating Scour at 'Bridges. Hydraulic Engineering Circular, (18)

Said, N. M., Mhiri, H., Bournot, H., & Le Palec, G. (2008). Experimental and numerical modelling of the three-dimensional incompressible flow behaviour in the near wake of circular cylinders. Journal of Wind Engineering and Industrial Aerodynamics, 96(5), 471-502.

Salim, M., & Jones, J. S. (1996). Scour around exposed pile foundations. In North American Water and Environment Congress & Destructive Water (pp. 2202-2211). ASCE.

Sarkar, K., Chakraborty, C., & Mazumder, B. S. (2015). Spacetime dynamics of bed forms due to turbulence around submerged bridge piers. Stochastic environmental research and risk assessment, 29(3), 995-1017.

Schloeder, C. A., Zimmerman, N. E., & Jacobs, M. J. (2001). Comparison of methods for interpolating soil properties using limited data. Soil Science Society of America Journal, 65(2), 470-479.

Sharma, H. D., & Chawla, A. S. (1975). Manual of canal lining. Central Board of Irrigation and Power, New Delhi.

Shen HW, Schneider VR, Karaki S (1969) Local scour around bridge piers. J Hydraul Div 95(6):1919–1940

Sheppard, D. M., Melville, B., & Demir, H. (2013). Evaluation of existing equations for local scour at bridge piers. Journal of Hydraulic Engineering, 140(1), 14-23.

Shirhole, A. M. and Holt, R. C. (1991) 'Planning for a comprehensive bridge safety program', Transportation Research Record, 1290, 39–50.

Singh, A., Lanzoni, S., Wilcock, P. R., & Foufoula-Georgiou, E. (2011). Multiscale statistical characterization of migrating bed forms in gravel and sand bed rivers. Water Resources Research, 47(12).

Smith, D. W. (1976, August). Bridge failures. In Institution of Civil Engineers, Proceedings (Vol. 60, No. Pt 1).('Smith1976', no date)

Soltani-Gerdefaramarzi, S., Afzalimehr, H., Chiew, Y. M., & Gallichand, J. (2014). Reduction of pier scour using bed suction and jet injection. Proceedings of the Institution of Civil Engineers, 167(2), 105.

Soltani-Gerdefaramarzi, S., Afzalimehr, H., Chiew, Y. M., Gallichand, J., & Ghasemi, M. (2013). Turbulent characteristics in flow subjected to bed suction and jet injection as a pier-scour countermeasure. International Journal of Hydraulic Engineering, 2(5), 93-100.

Sreenivasulu, G., Kumar, B., & Rao, A. R. (2011). Variation of stream power with seepage in sand-bed channels. Water SA, 37(1), 115-119.

Sumer, B. M., Christiansen, N., & Fredsøe, J. (1997). The horseshoe vortex and vortex shedding around a vertical wall-mounted cylinder exposed to waves. Journal of Fluid Mechanics, 332, 41-70.

Sumer, B. M., & Fredsøe, J. (2006). Hydrodynamics around cylindrical structures.

Sumner, D. (2010). Two circular cylinders in cross-flow: a review. Journal of Fluids and Structures, 26(6), 849-899.

Tanida, Y., Okajima, A., & Watanabe, Y. (1973). Stability of a circular cylinder oscillating in uniform flow or in a wake. Journal of Fluid Mechanics, 61(4), 769-784.

Tanji, K. K., & Kielen, N. C. (2002). Agricultural drainage water management in arid and semi-arid areas. FAO.

Turner, I. L. (1995). Simulating the influence of groundwater seepage on sediment transported by the sweep of the swash zone across macro-tidal beaches. Marine Geology, 125(1-2), 153-174.

USACE, H. (1982). Hydrologic analysis of ungaged watersheds using HEC-1. US Army Corps of Engineers Hydrologic Engineering Center, TD-15, Davis, CA, USA.

Watters, G. Z., & Rao, M. V. (1971). Hydrodynamic effects of seepage on bed particles. Journal of the Hydraulics Division, 97(3), 421-439.

Willetts, B. B., & Drossos, M. E. (1975). Local erosion caused by rapid forced infiltration. Journal of the Hydraulics Division, 101(ASCE# 11796 Proceeding).

Wong, M., Parker, G., DeVries, P., Brown, T. M., & Burges, S. J. (2007). Experiments on dispersion of tracer stones under lower-regime plane-bed equilibrium bed load transport. Water Resources Research, 43(3)

Wu, B., Molinas, A., & Julien, P. Y. (2004). Bed-material load computations for nonuniform sediments. Journal of hydraulic engineering, 130(10), 1002-1012.

Yanmaz, A. M., & Altinbilek, H. D. G. ˇ. A. (1991). Study of time-depenbent local scour around bridge piers. Journal of Hydraulic Engineering, 117(10), 1247-1268.

Yong, Z., Zhi, Z., Li, Z., & Tianlin, W. (2015). Turbulence model investigations on the boundary layer flow with adverse pressure gradients. Journal of Marine Science and Application, 14(2), 170-174.

# Appendix A

## Scour and Flow characteristics around Oblong Bridge Piers in Seepage Affected Alluvial Channels[v]

### 1 Introduction

The vortex system around the pier, which consists of horseshoe vortex at upstream of pier, wake vortices at downstream of the pier, trailing vortices and bow wave is depending upon size and shape of the piers (Al-Shukur et al., 2016). Jueyi et al., 2010 have conducted laboratory experiments to compare scour depth around semi-elliptical and semi-circular abutments with armoured beds. The researchers have found that the scour depth at semi-elliptical abutment is lesser than the scour depth at semi-circular abutments. Al-Shukur et al. (2016) have carried out an experimental investigation using ten different shapes of piers and found that scour depth is minimum for streamline shapes where maximum for the rectangular pier. As scour around piers is the result of complex interaction between turbulent flow and bed material so, the study of turbulent flow statistics around piers gives more insight in the process of scouring (Ahmed and Rajaratnam, 1998). This section focuses on the effect of shape pier on turbulent flow characteristics and bed geometry around piers for that experimentation has been carried out using oblong piers and the obtained results are then compared with the circular one. Two types of piers were used, i.e. circular and oblong piers. Diameter of the circular pier was 75mm, whereas, oblong pier of width 75mm, length 225mm and 270mm were used. The results obtained for circular piers are already mentioned in chapter 1, so to maintain the brevity of the research some of the figures are not repeated here.

[v]Rutuja Chavan, B. Venkataramana, P. Acharya and Bimlesh Kumar- Comparison of Scour and Flow characteristics around Circular and Oblong Bridge piers in Seepage affected Alluvial Channel, Journal of Marine Science and Application (accepted for publication).

## 1.2 Results

### 1.2.1 Scour Geometry

Figure 1 shows a snapshot of scoured bed around circular and oblong piers. The contour profile of bed morphology around oblong and circular piers for with seepage and without seepage condition are shown in figures 2 and 3 respectively. It can be observed from figures 2 and 3 that the scoured region is large for circular pier than oblong pier. The scour depth at oblong pier is reduced by 15% than the scour depth at circular pier under the same experimental conditions. The diameter of scour hole is more in case of circular pier than oblong pier and that too for every experimental condition. However, the deposition height and deposition length at downstream of pier is also greater for circular pier.

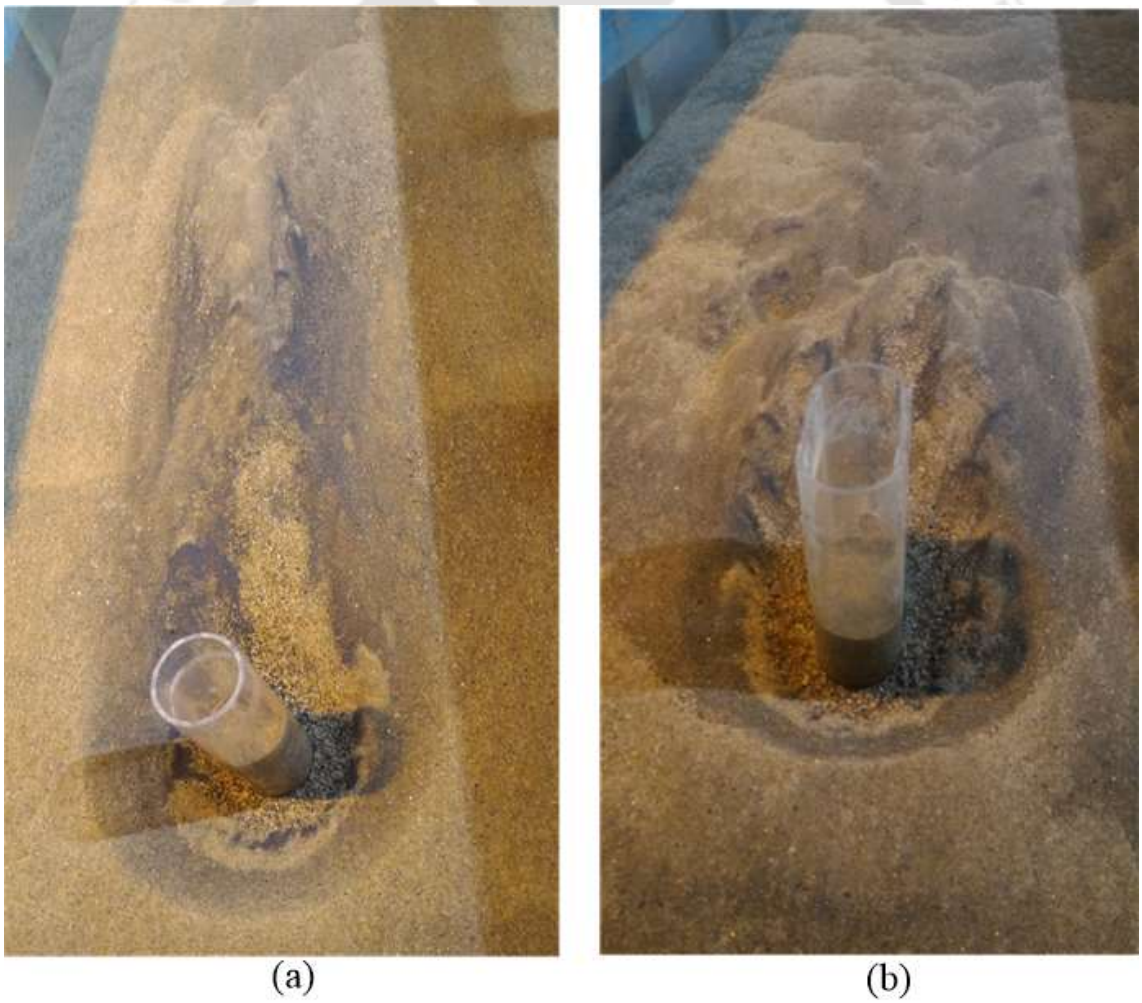


Figure 1 Snapshot of scour hole around (a) circular pier and (b) oblong pier

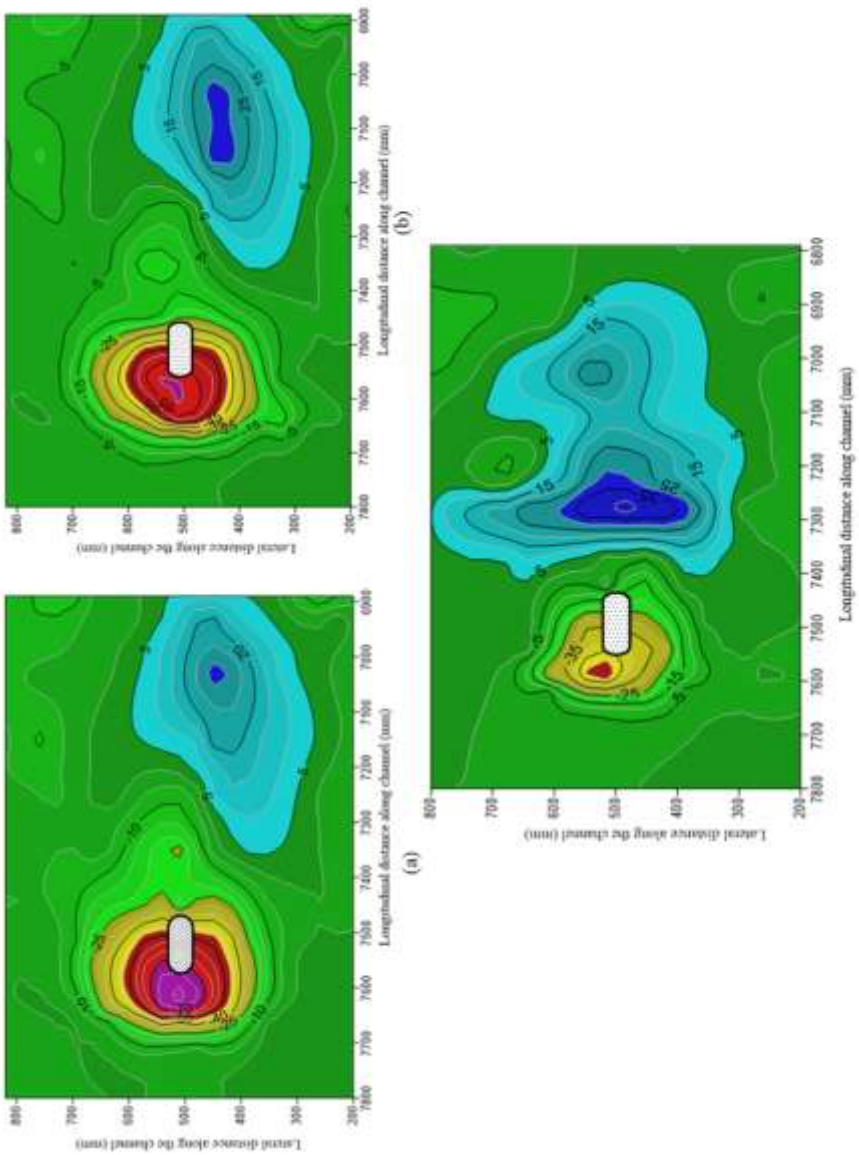

Figure 2 Contour diagram of scour around oblong pier, (a) No Seepage, (b) 10% Seepage, (c) 15% Seepage (Scour depth in mm)

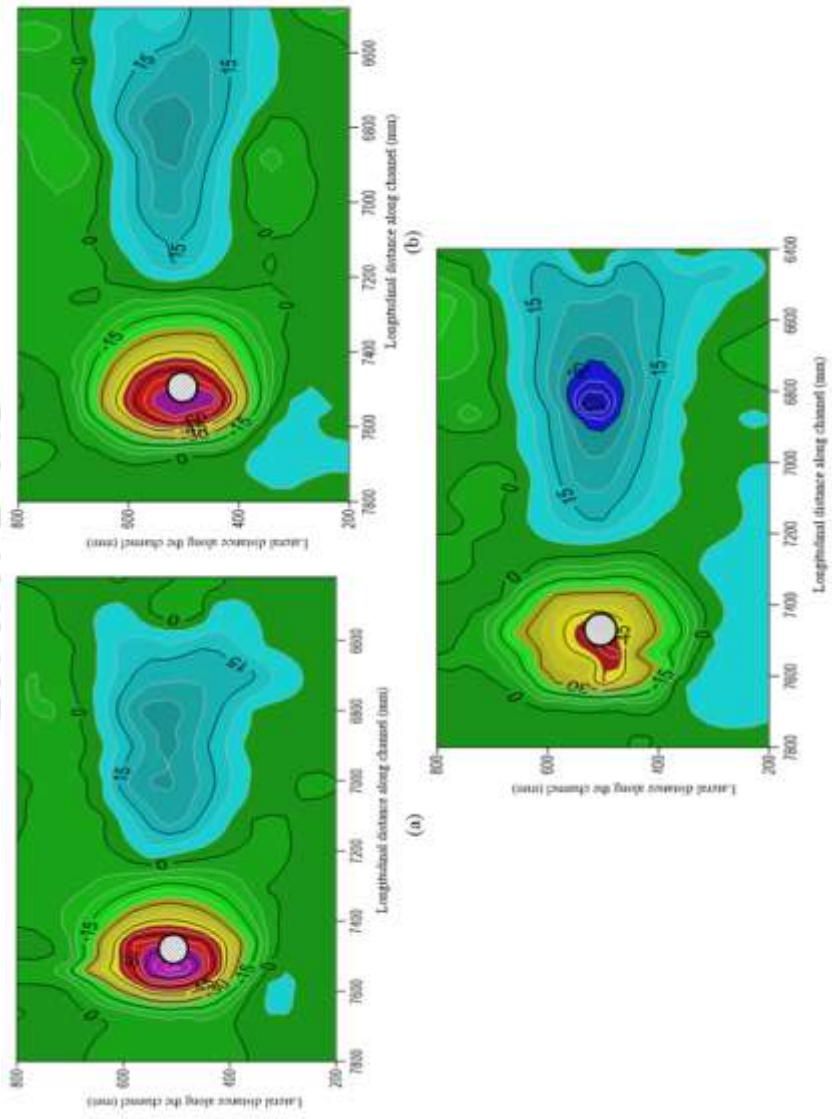

Figure 3 Contour diagram of scour around circular pier, (a) No Seepage, (b) 10% Seepage, (c) 15% Seepage (Scour depth in mm)

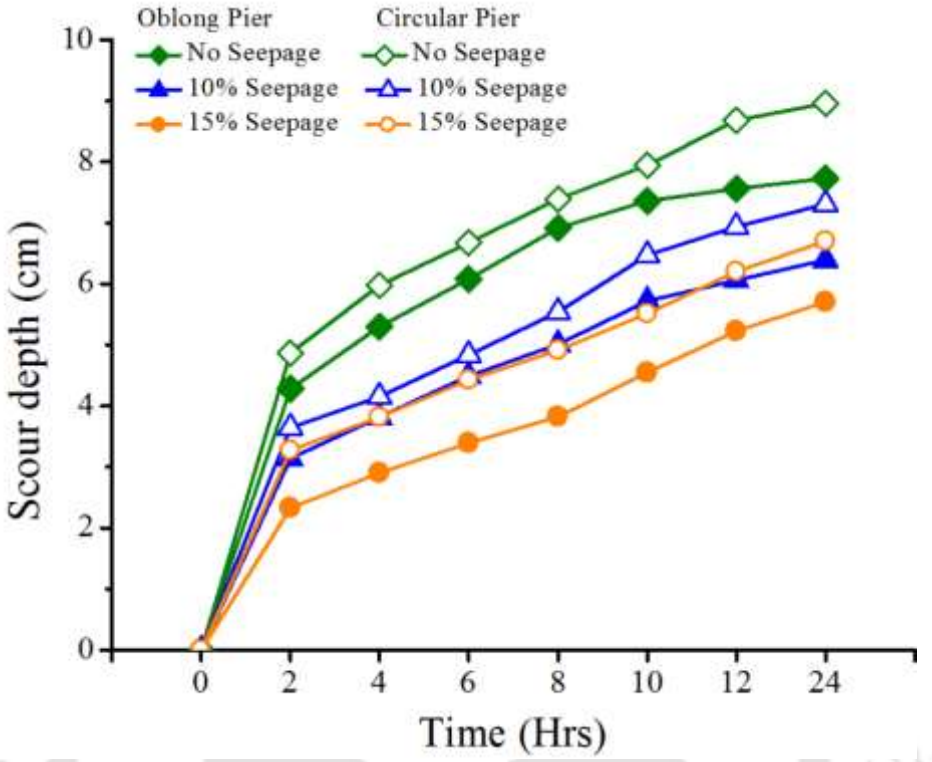


Figure 4. Development of Scour depth with time at oblong pier and circular pier

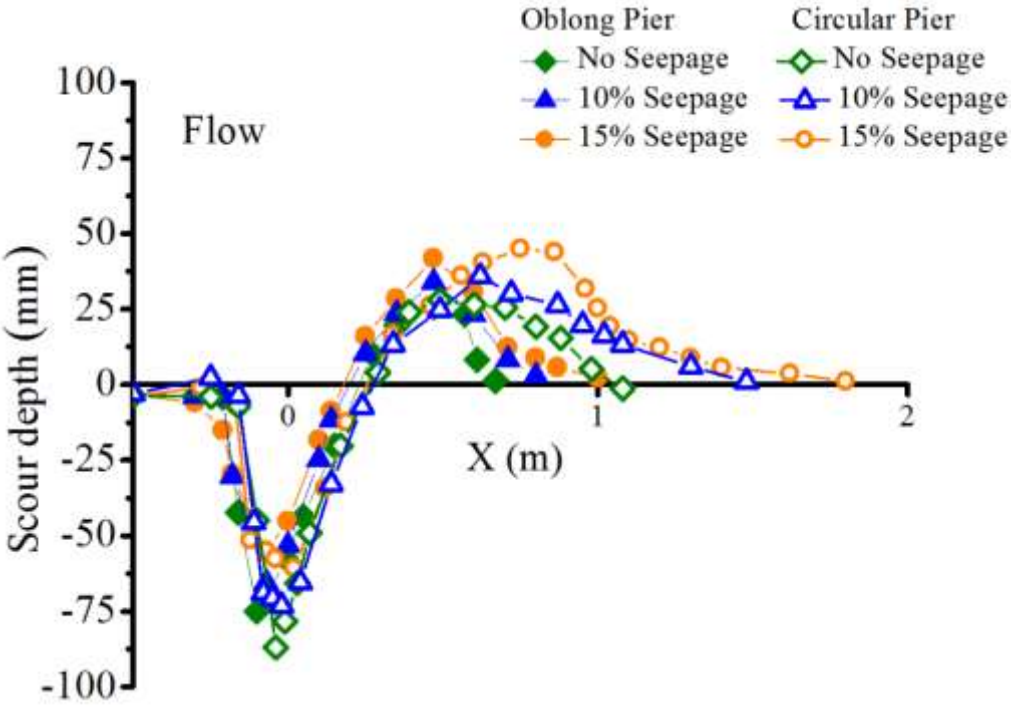


Figure 5. Bed profile along the centre line at oblong pier and circular pier

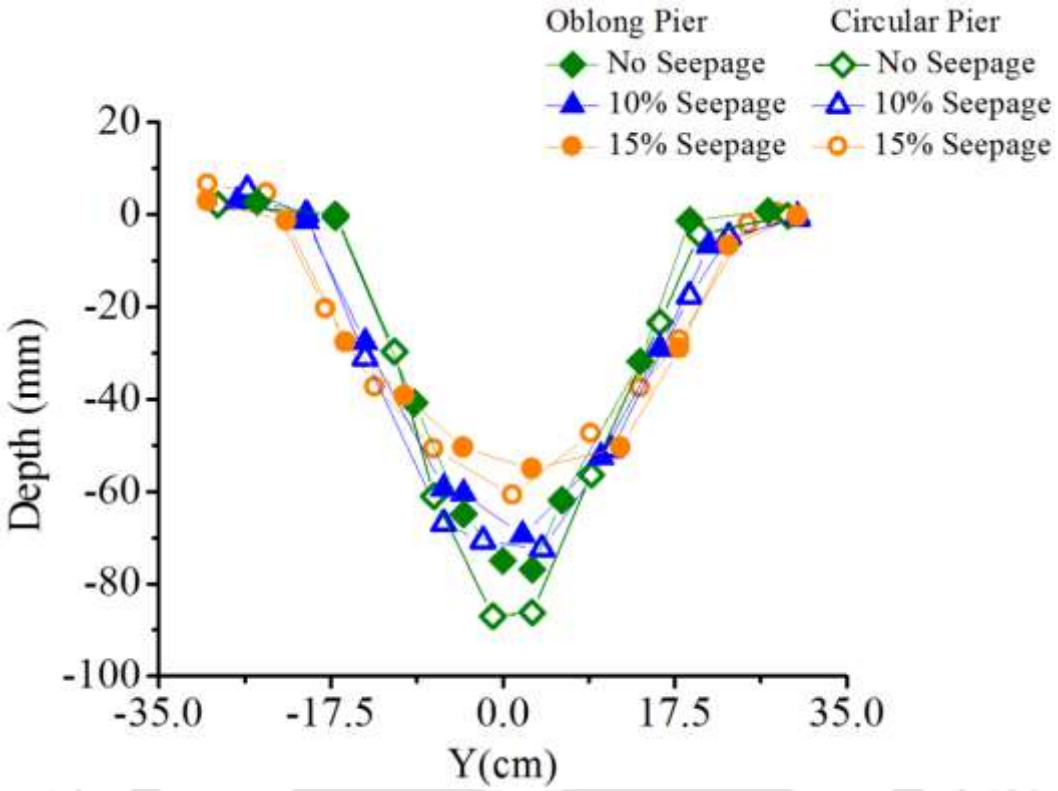


Figure 6. Lateral bed profile at upstream of oblong pier and circular pier

Scouring around piers is a time depending phenomenon. Scour depth at piers is increasing gradually with increasing time. After a certain limit, equilibrium sets between the erosive capacity of flowing stream and extent of bed material to get eroded. Figure 4 shows graph of scour depth with respect to time. From figure 4, it can be observed that the scour depth is increasing with increase in time, however the rate of increase of scour depth is more in no seepage runs than in seepage runs (Chavan et al. 2017). Initially, the rate of increase of scour depth is more and reduces gradually with increase in time such that, nearly after 12 hours, an equilibrium condition is reached.

The scoured bed material is deposited at downstream of piers along and at sides of centerline. Figure 5 shows bed elevation along the centerline in the longitudinal direction. Close observation of figure 5 shows that scour depth at upstream of the pier is lesser for oblong pier than circular pier in all experimental conditions. However, scour depth at oblong pier is more in case of no seepage condition and reduced by 15% in case of 10% seepage condition and again reduced by 25% for 15% seepage condition. Similarly, for circular pier in case of 10% seepage and 15% seepage conditions, the scour depth is

reduced by 17% and 29% respectively. The scoured bed material is deposited further at downstream of pier along and at sides of the centerline and produce hump at rear side of pier. For both shapes of pier, the height of deposition is increased with increased seepage percentage. At downstream of oblong pier, height of deposition is increased by 30% in case of 10% seepage condition and again increased by 50% in case of 15% seepage. For circular pier, deposition height is increase by 32% on application of 10% seepage and 70% in case of 15% seepage. With time, the vortex around pier increased in longitudinal and lateral direction too.

Figure 6 shows lateral bed profile at upstream of oblong and circular pier for no seepage, 10% seepage and 15% seepage condition. Close observation of figure 6 shows that depth of scour hole at upstream of piers are decreasing with downward seepage however, width of scour hole is increasing with increase in downward seepage. For circular pier, width of scour hole is increased in 10% seepage run by 25% and again increased by 36% in 15% seepage run. For oblong pier, scour hole width is increased by 28% in case of 10% seepage condition and again increase by 44% for 15% seepage condition. From figure 6, it is also observed that, width of scour hole is lesser for oblong pier than circular pier. The percentage reduction of scour characteristics in oblong pier than circular pier is mentioned in table 1.

As the shape of pier plays an important role in scouring around pier, so in this study it is observed that oblong shape of pier can be protecting measure against scour in comparison with circular one. However, for both of the shapes of pier the scour depth is reducing with application of downward seepage.

Table 1. Table showing percentage difference of scour characteristics between circular and oblong piers

| **Scour Characteristics** | **% Reduction for oblong pier** | | |
|---|---|---|---|
| | **No Seepage** | **10% Seepage** | **15% Seepage** |
| Scour depth | 15 | 13 | 13 |
| Scour width | 21 | 22 | 20 |
| Deposition height | 7.5 | 6.8 | 7.2 |
| Deposition length | 52 | 55.6 | 49 |

### 1.2.2 Velocity

For oblong pier, measurements were taken at upstream A (7.6725, 0.5) and downstream B (7.3275, 0.5). Figure 7 shows velocity profile around oblong pier for no seepage and seepage conditions. Stremwise velocity is negative near the bed at upstream of piers (figure 7) due to reversal flow near the bed at upstream of pier. With application of downward seepage, the reversal velocity is decreasing. From figure 7 it can be observed that the reversal velocity near the bed is more in no seepage runs and lessens for 10% seepage and again decrease in case of 15% seepage runs. At upstream of pier the downward seepage impedes the reversal flow hence, the velocity near the bed at upstream of pier is decreasing with application of downward seepage. At downstream of pier, reversal flow can be found near free surface due to wake vortices forming at downstream of pier. At downstream section of circular pier, streamwise velocity is negative near free surface then increasing gradually with moving towards bed (Izadinia et al., 2013). With downward seepage, reversal velocity near free surface is decreasing whereas near the bed, velocity is increasing with increasing seepage percentage. While flow separation at upstream of oblong pier, the flow becomes streamline while moving along the sides of pier which results in diminishing the strength of wake vortices at downstream of oblong pier. Therefore, at downstream of oblong pier, near the free surface the velocity is less positive unlike the circular pier.

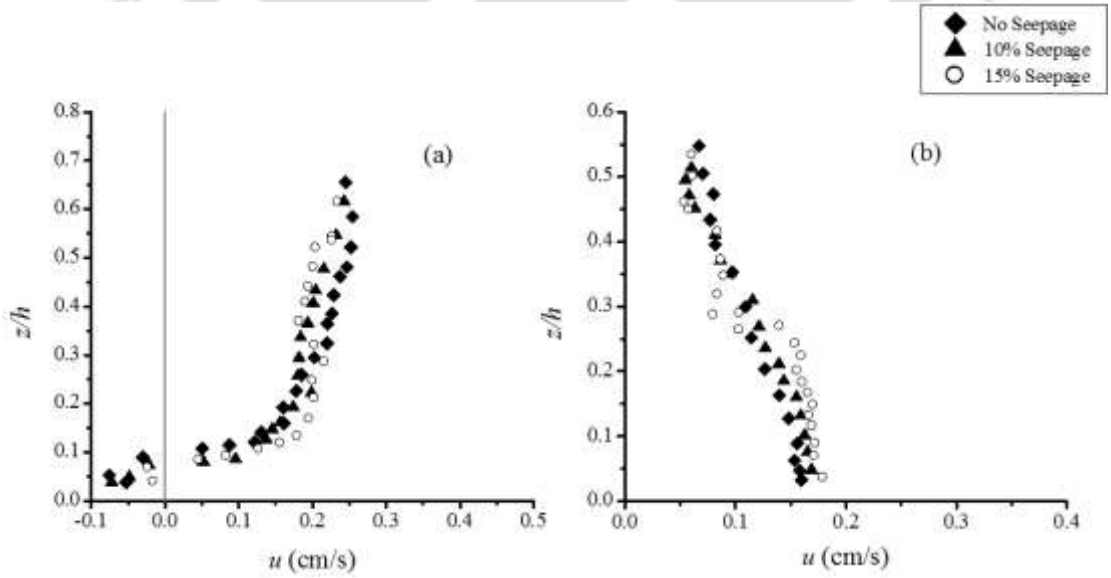


Figure 7. Velocity profiles around oblong pier at sections (a) Upstream A, (b) Downstream B

### 1.2.3 Reynolds Shear Stress

From figure 8, it can be observed that Reynolds stress are negative near the bed and strength of Reynolds stress is decreasing with increasing seepage percentage. At downstream of oblong piers Reynolds stresses are less positive, which shows the lesser strength of wake vortices at downstream of oblong piers than circular pier.

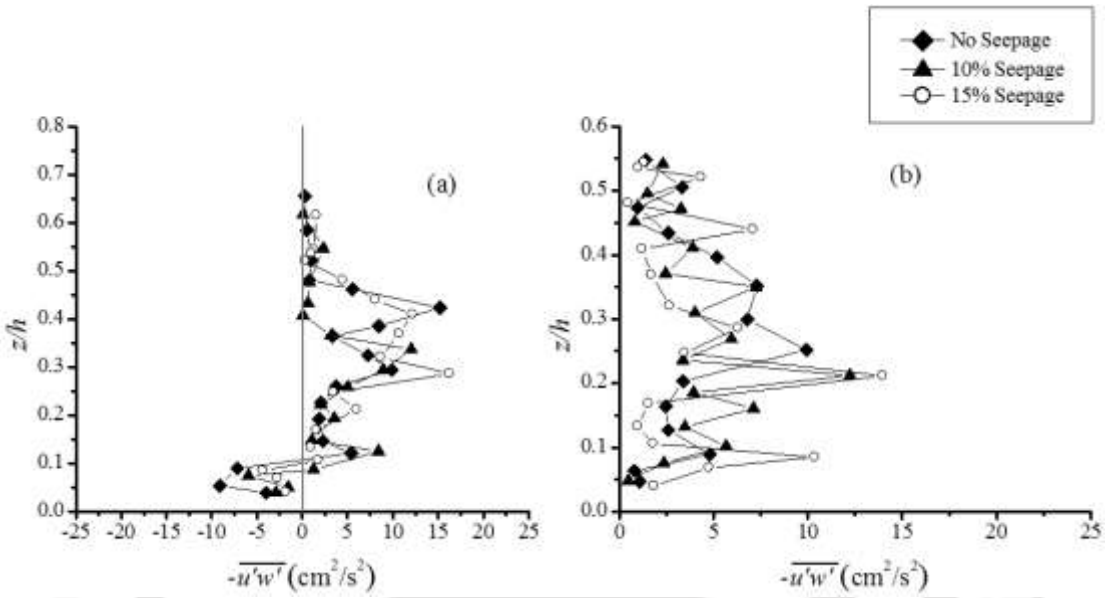


Figure 8. RSS profiles around oblong pier at sections (a) Upstream A, (b) Downstream B

### 1.2.4 Turbulent Kinetic Energy

Vertical profile of turbulent kinetic energy (TKE) at upstream (A) and downstream (B) of the oblong pier and circular for no seepage, 10% seepage and 15% seepage runs are depicted in figure 9. From figure 9, it can be seen that TKE is highly fluctuating due to flow separation. At upstream of both piers, TKE is lesser near free surface and increasing gradually away from free surface attends maximum value near the edge of the scoured region and again decreasing towards the bed. At upstream section near the bed region, the magnitude of TKE is more for no seepage condition and decreasing with increasing seepage percentage as downward seepage lessens the strength of reversal flow, which results in a decrement of TKE. Separation of flow and strong pressure gradient at upstream of pier leads to enhance kinetic energy at the edge of scour hole and consequently increase the rate of scouring (Maity and Mazumder, 2012). At downstream section (B), TKE is fluctuating heavily, having a maximum value near free surface and

then decreasing with moving towards the bed. The TKE fluctuations and magnitude of TKE are significantly higher at downstream of the circular pier.

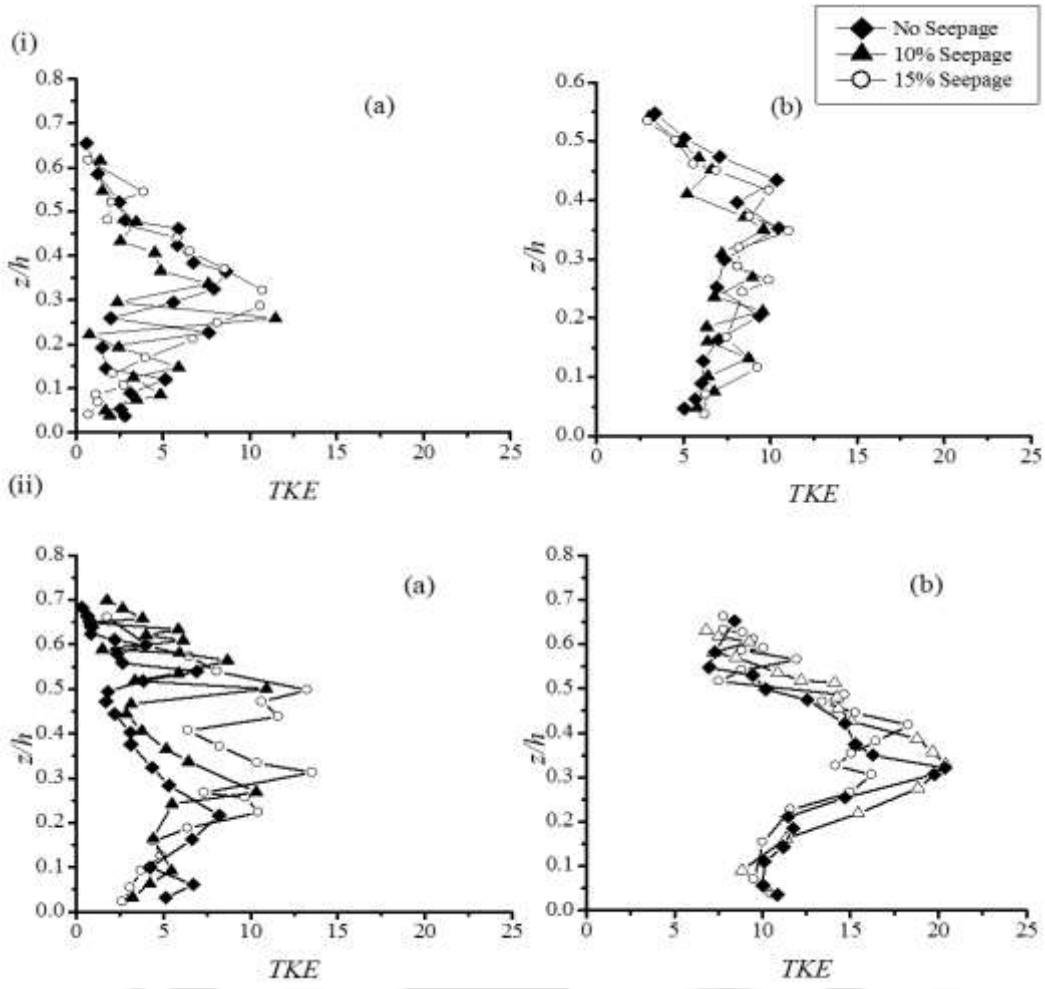


Figure 9. Vertical distribution of turbulent kinetic energy at (i) oblong pier and (ii) circular pier at sections (a) Upstream A, (b) Downstream B

### 1.2.5 Power Spectra Analysis

The Strouhal number for both the piers calculated from the power spectra analysis are mentioned in table 2. From table 2, it can be observed that Strouhal number is lesser in case of the oblong pier and more for the circular pier. The strength of vorticity is more at downstream of the circular pier than the oblong pier. However, with the application of downward seepage strength of wake vortices is decreasing for both circular and oblong piers. Comparing both oblong and circular piers, the wake of oblong pier is quite weaker than circular pier which indicates that the capacity of wake vortices to scour the bed material at downstream of oblong pier is lesser than the capacity of wake vortices at

downstream of the circular pier. In case of the oblong pier as the flow hits the pier, it separates in the form of downflow along upstream face of pier and side circulations along sides of the pier. The sides of the oblong pier are straight unlike the circular pier, which curtails the turbulence at sides of the pier and make the flow streamline. When this streamlined flow reached at the downstream of pier it creates lesser turbulence because of which the strength of wake vortices is reduced at downstream of the oblong pier. The capacity of wake vortices to erode the bed material at downstream of both oblong and circular piers, diminishes with the application of downward seepage.

Table 2. Strouhal number at downstream of piers

| Case | Circular Pier | | Oblong Pier | |
|---|---|---|---|---|
| | Near free surface | Near bed | Near free surface | Near bed |
| **No Seepage** | 0.23 | 0.14 | 0.22 | 0.12 |
| **10% Seepage** | 0.20 | 0.12 | 0.19 | 0.10 |
| **15% Seepage** | 0.18 | 0.11 | 0.16 | 0.08 |

**1.3 Conclusions**

The scour depth and width of scour hole is greater at circular pier than the oblong pier. The extent of deposited bed material is more at downstream of the circular pier. So oblong bridge pier can be used instead of circular bridge pier as protecting measure against scour. With the application of downward seepage, the scour depth is reducing for both the piers. However, the width of scour hole and deposition height at downstream of piers are increasing with increasing downward seepage for both types of piers. Reversal flow at upstream of both piers diminishes with seepage. Wake vortices at downstream of the oblong pier are weaker than the wake vortices at the circular pier.

# Appendix **B**

## Wavelet Based Semblance Analysis at Single Piers[vi]

The important of Similarity measures are increasing continuously in order to compare the multiple signals from different field. The measure of Semblance analysis gives similarity between two datasets based on correlations between their phase angles in terms of frequency. Cooper and Cowan (2008) have used wavelet built semblance analysis for comparing series of synthetic data. However, to the best of our knowledge, semblance analysis on the sediment transport mechanics remains to be explored. Thus we have done wavelet based semblance analysis on the pier scouring process for both no seepage and seepage condition. In the present study, we have calculated semblance using CWT because CWT based semblance analysis permits the local phase interactions between the two signals in terms of both scale and time. The details about the continuous wavelet transform are already explained in chapter 5. The process of comparison between two time series datasets using CWT can be expressed as (Torrence and Compo, 1998)

$$W_{f1,2} = W_{f1} \times W_{f2} \tag{1}$$

The quantity $W_{f1,2}$ is a complex nature with an amplitude $X$ and local phase θ is given by

$$X = \left| W_{f1,2} \right| \tag{2}$$

$$\theta = \tan^{-1}\left\{ \mathrm{Im}aginary(\mathrm{W}_{f1,2}) / \mathrm{Re}al(\mathrm{W}_{f1,2}) \right\} \tag{3}$$

When the local phase θ of two datasets are calculated, the semblance at each frequency were measures as (Cooper and Cowan, 2008)

$$S = \cos^{n}(\theta) \tag{4}$$

Where n is an odd number. The advantage of using S compared with θ is that the values of S will be varied from -1 to 1. Values of $S=-1$ and $S=1$ indicates inversely correlation

[vi]Sharma A., Chavan R. and Kumar B.- Multi-scale Statistical Characterization of Migrating Pier Scour Depth in Non-uniform Sand Bed channel, The International Journal of River Basin Management, 15, 3, 265-276, 2017

and perfectly correlation between two datasets respectively while *S=0* represent un-correlation between signals. Because S and θ gives information of phase angles only rather than amplitude, the advantage of comparison of two signals using S and θ is that, they (signals) are not necessary to require the same units. The absence of amplitude information leads to noise sensitivity for which we can further expressed as

$$D = \cos^n(\theta)\left|W_{f1} \times W_{f2}\right| \tag{5}$$

When *n*=1, the value of *D* is approximately equal to the vector dot product of two wavelet coefficient for each scale and position. *D* indicates the information of amplitude *X* with information of phase *S* that can be beneficial if the phase correlations of the higher amplitude components of the signal are of the best noticeable. The CWT based semblance analysis is estimated in terms of both scale and position. This allows the varying phase relationships of two signals to be imagined and studied. In the present study, semblance analysis is done for two datasets at the sections A, B and C of the pier, which contains velocity time series and bed elevation time series.

In first dataset of Figures 1, 2 and 3, the real part of the complex CWT indicates the occurring of velocity time series for the duration of the dataset. In the second dataset of Figures 1, 2 and 3, the time series of bed elevation exist but this dataset differs in phase angle from those in the first dataset in terms of position. Figures 1, 2 and 3 shows the semblance *S* and dot product *D* (calculated with *n* = 1) for flow of no seepage and seepage. Figure 1(a) show the red region at shorter wavelength component representing a positive correlation between the signals (*S* = 1) and inversely correlated (*S*=-1) at the longer wavelength component while at mid portion of wavelength component, the phase relationship between the two signals were changed due to semblance becomes correlated, uncorrelated or inversely correlated in terms of position. Figures 1(b) and 1(c) show a broad blue patch running throughout wavelength representing a negative correlation between the signals for corresponding wavelength and times. The result suggested that at upstream of pier, time series datasets of velocity and bed elevation shows the perfectly correlated for most of the wavelength component while at downstream of the pier, the data sets is uncorrelated. Figure 3 and 3 shows the semblance analysis at sections A, B and D of pier when seepage is applied in the downward direction. Figure 2(a) and 3(a) shows the blue region at shorter wavelength component representing a negative

correlation between the signals for corresponding wavelength and perfectly correlated at the longer wavelength component. Figure 2(b), 2 (c), 3(b) and 3(c) shows the correlation between two data sets are correlated, uncorrelated or inversely correlated in terms of position. Thus under the application of seepage, the result for semblance at upstream of pier is quite opposite as compared to no seepage runs while at the downstream of the pier, the results is slightly matching with no seepage runs. There is improvement in the simplicity of plot when information of amplitude is incorporated concurrently. However, if we will interest to compute the phase relationship of signals corresponding to small values of amplitude, then displaying this plot might not be the correct way. The longitudinal defining restrictions of this methodology are scale dependant that is visible longitudinal deviations in semblance is sharper at lower wavelengths as compared to higher wavelengths. These happen because of wavelet transform nature. As $n>1$, the spreading in the areas of positive and negative correlation is gradually decreased. The higher values of $n$ will have a tendency to grind down the degree of these areas mainly at higher wavelengths creating the selection of a best value dependant on the signals.

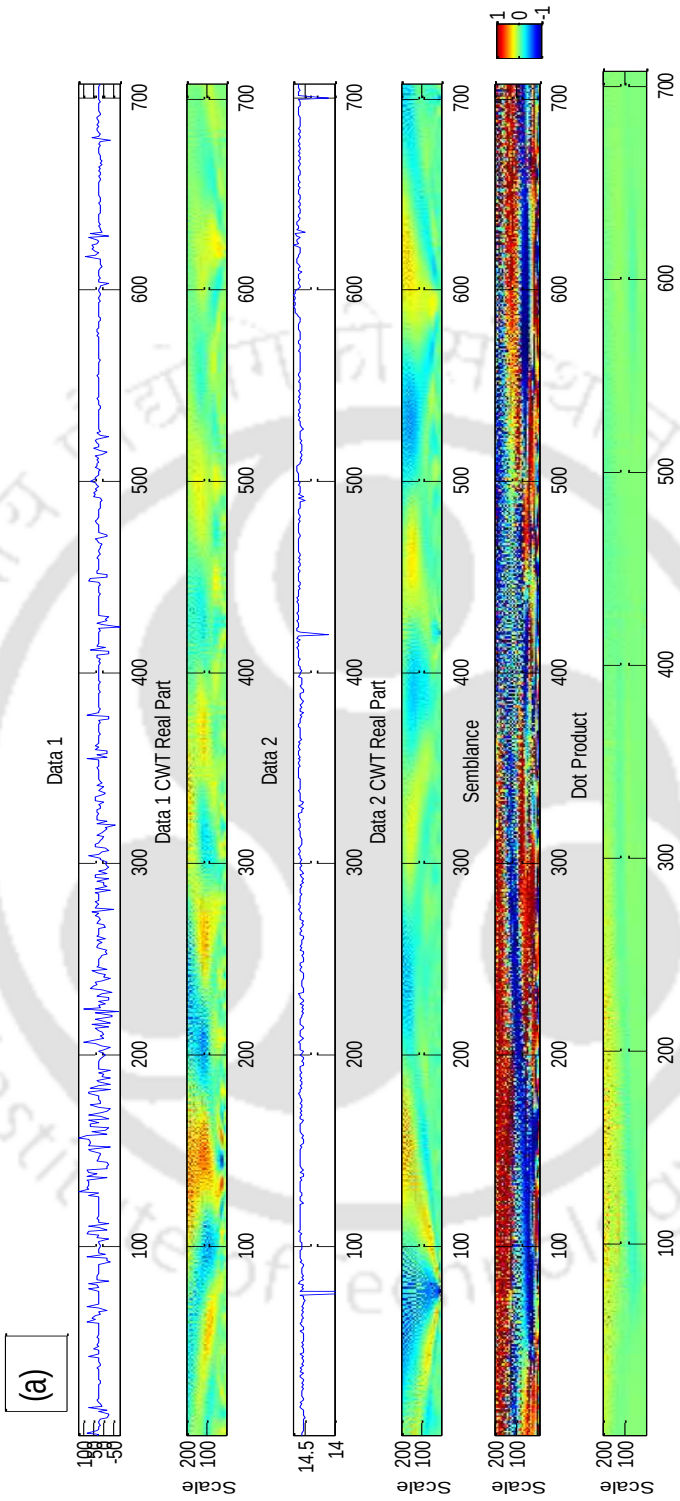

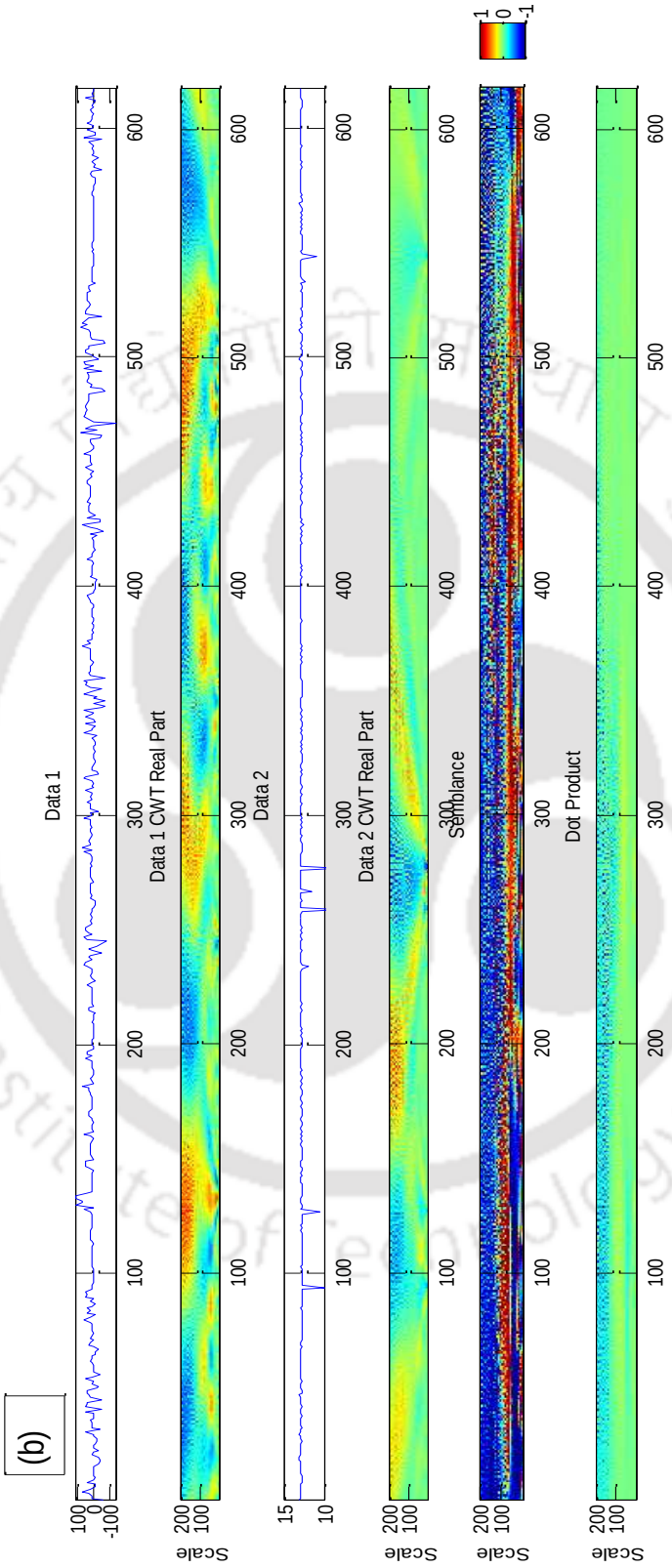

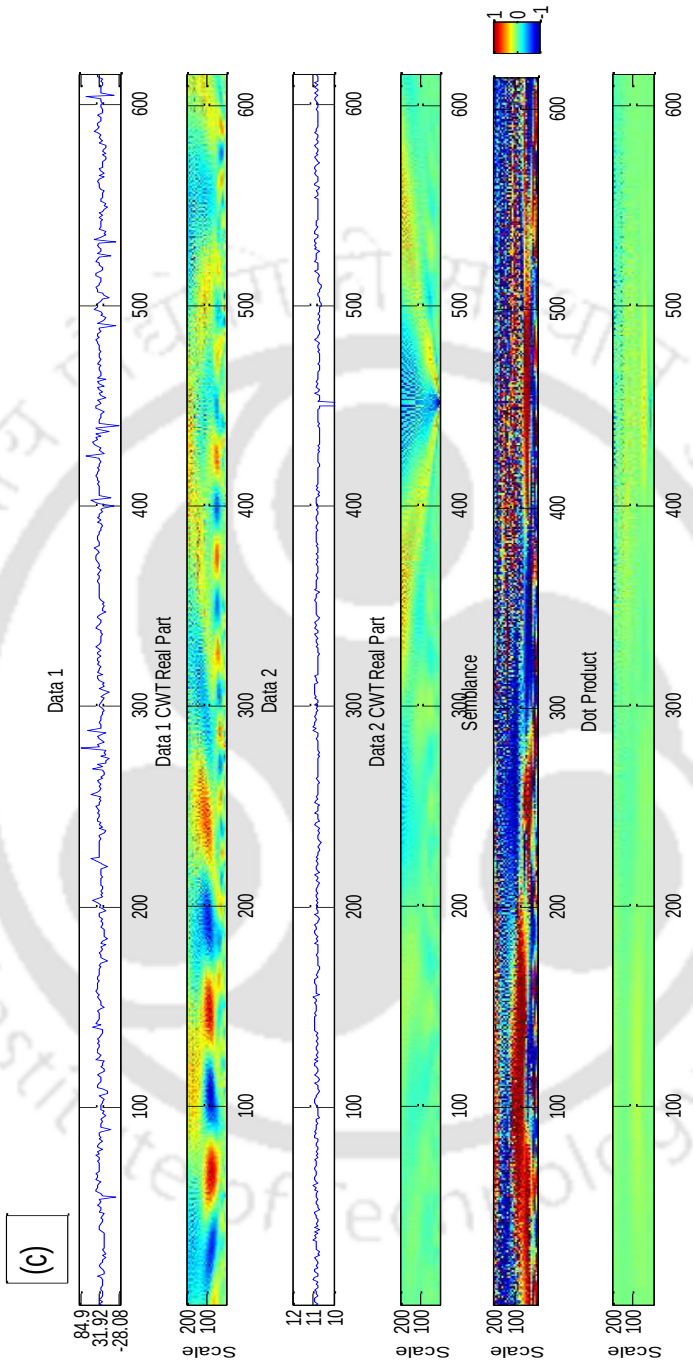


Figure 1 Semblance analysis at (a) Section A (upstream of pier) (b) Section B (downstream of pier) and (c) Section D (dune like bedform) for no seepage case

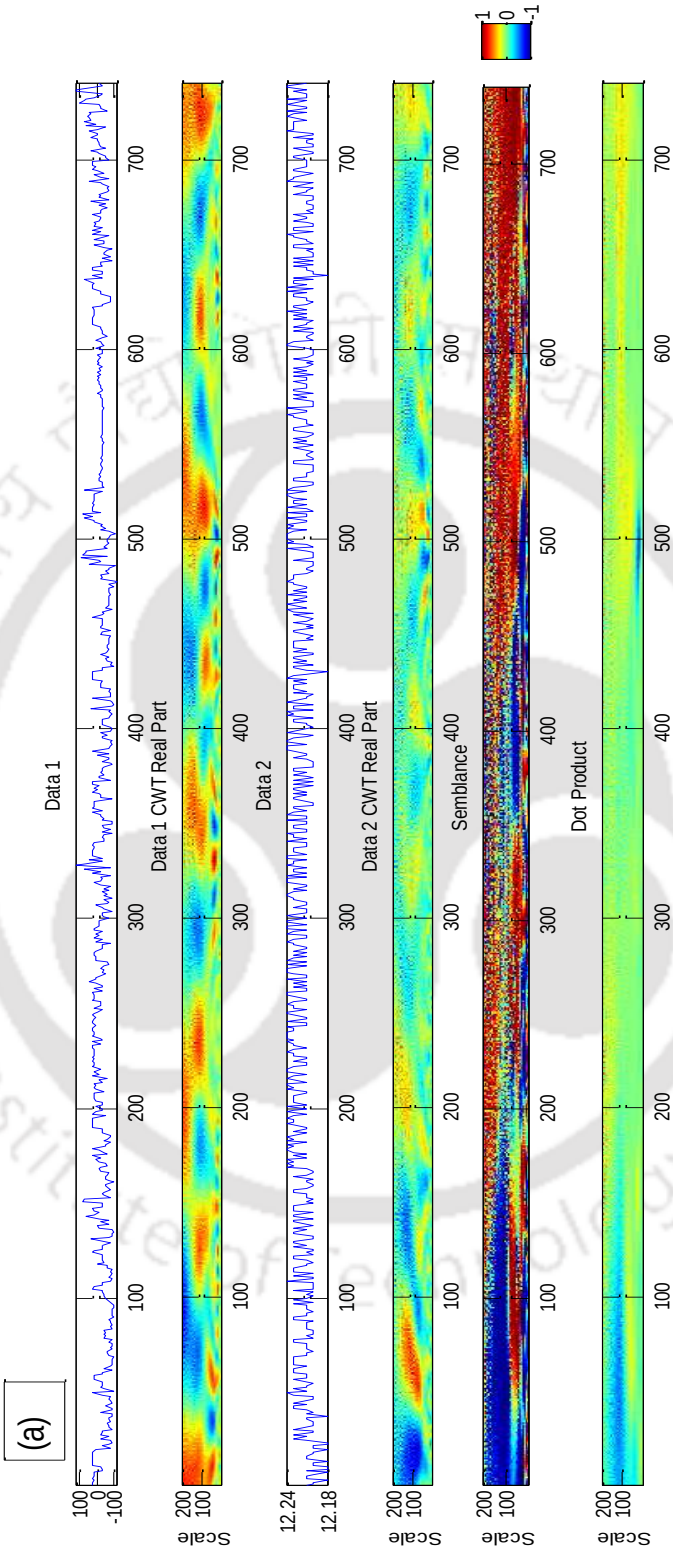

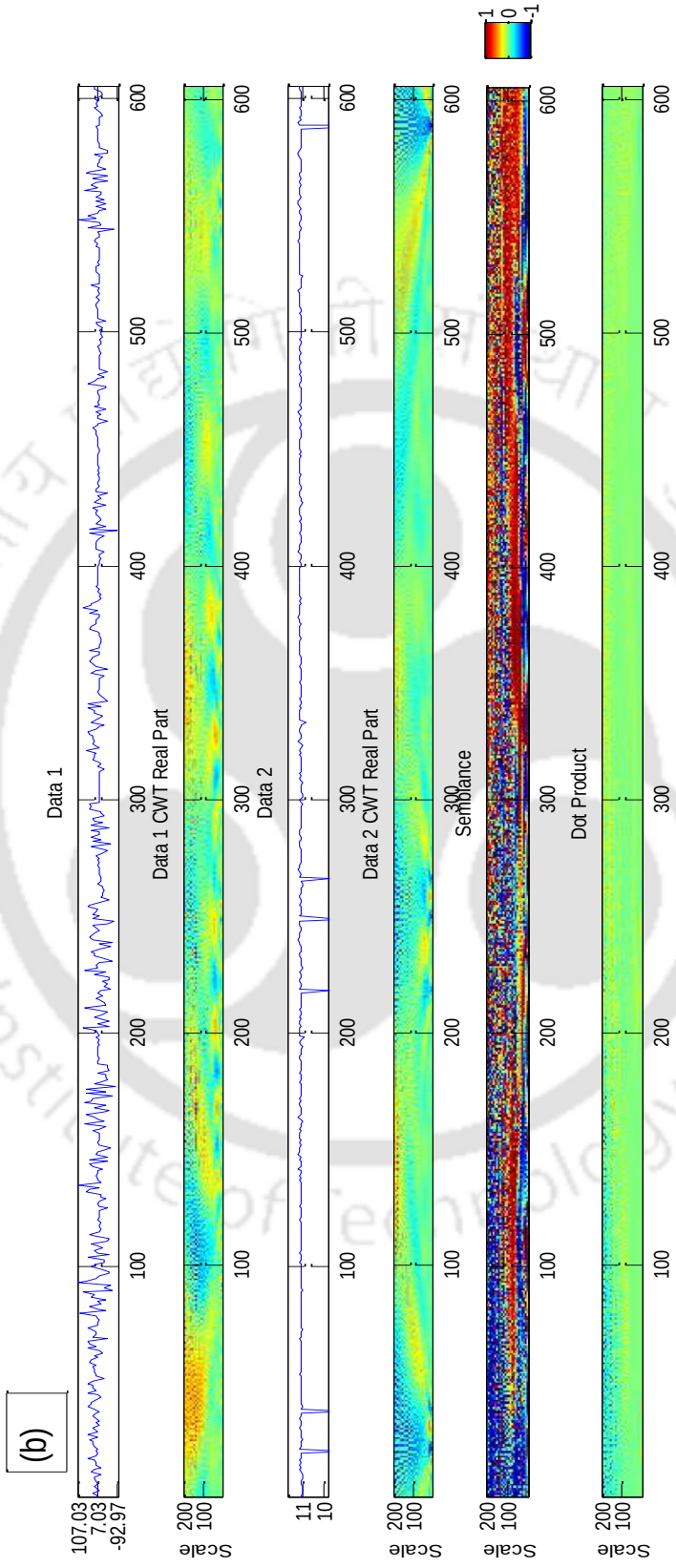

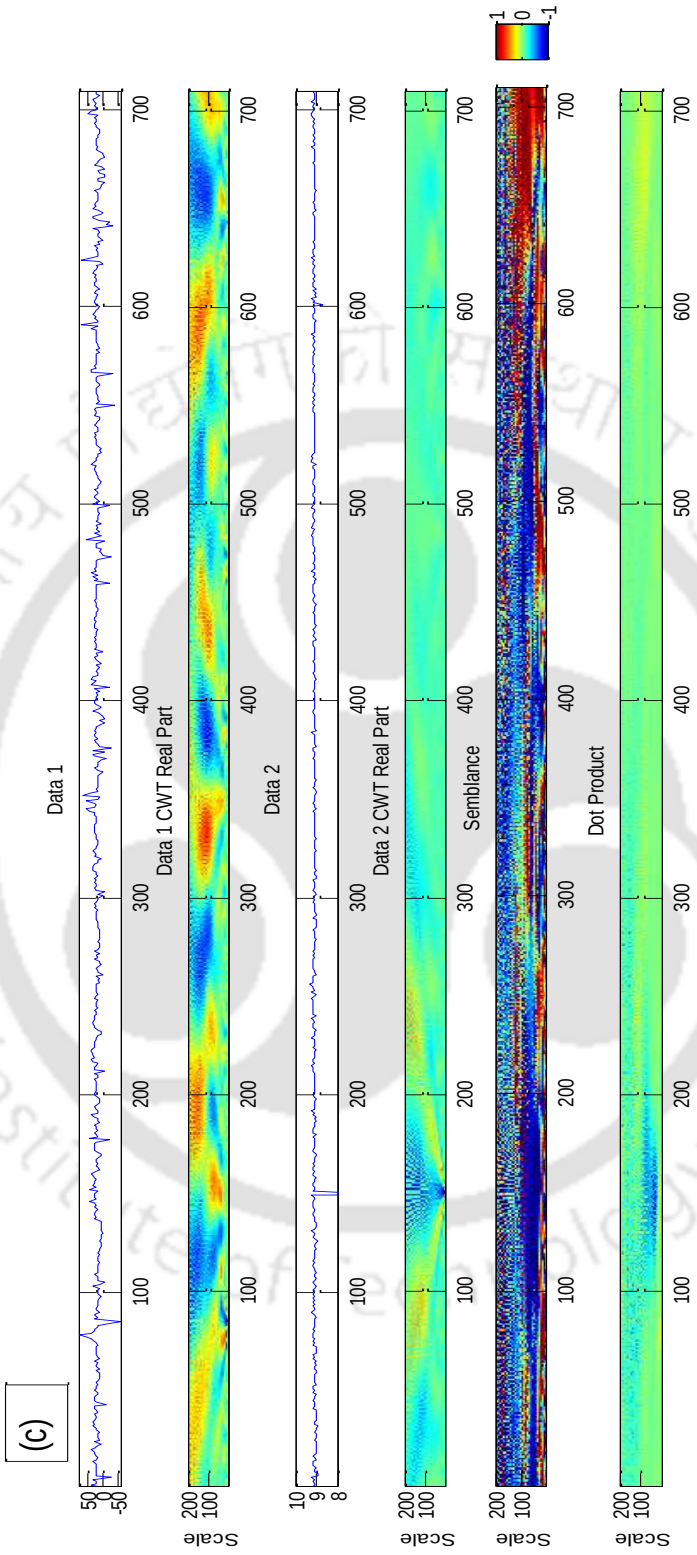


Figure 2 Semblance analysis at (a) Section A (upstream of pier) (b) Section B (downstream of pier) and (c) Section D (dune like bedform) for 10% seepage case

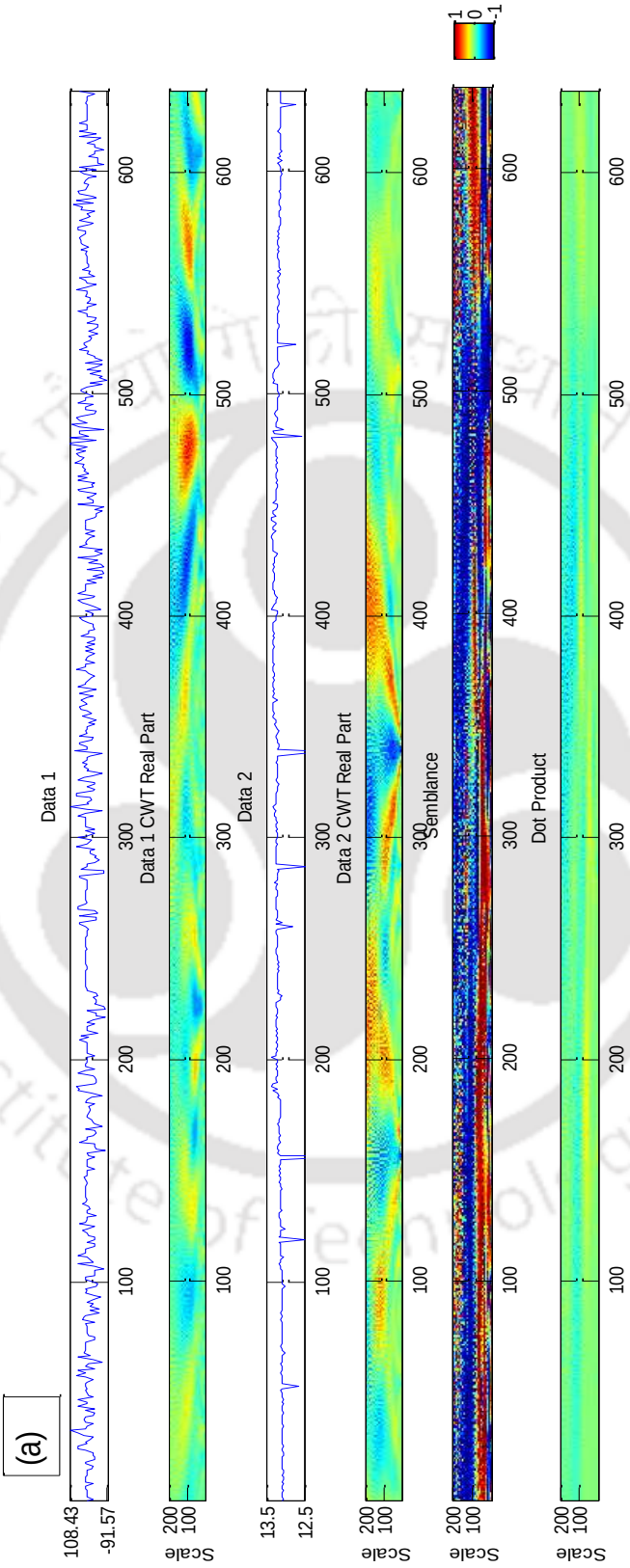

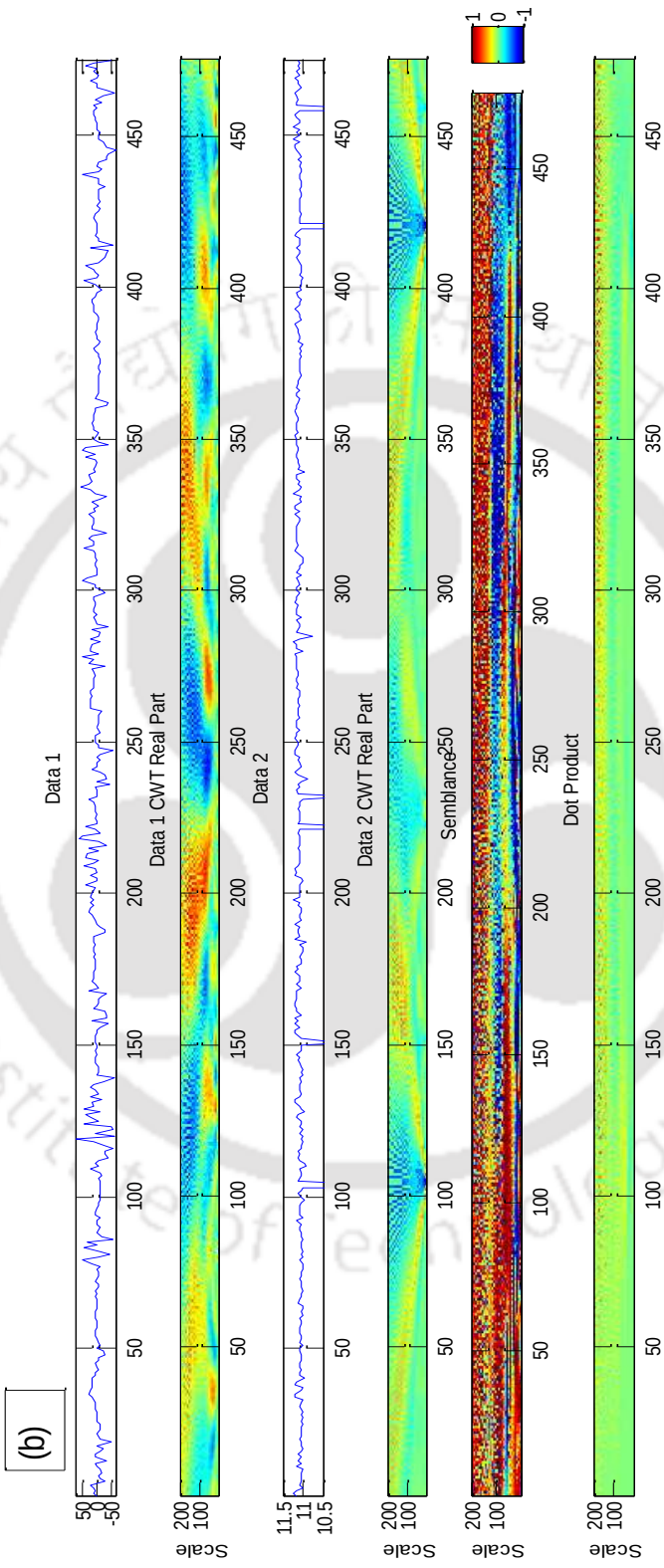

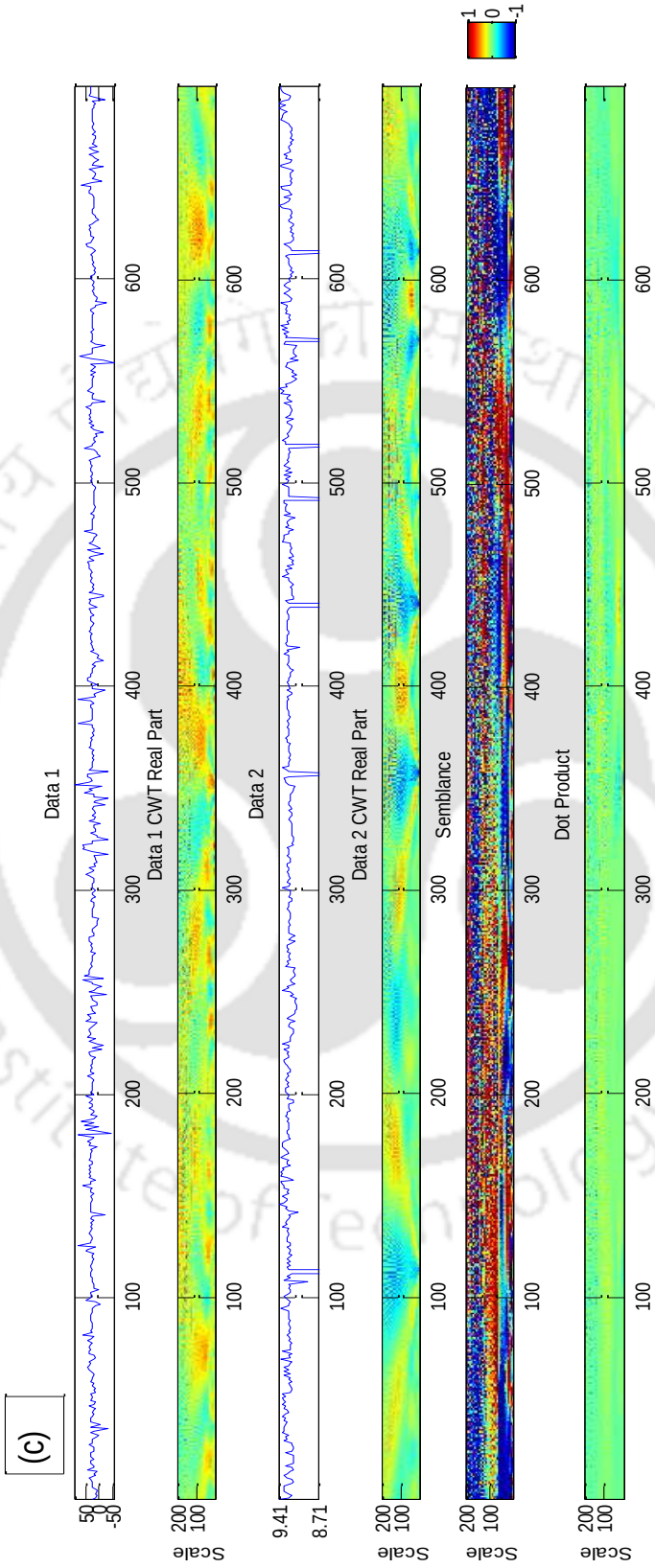


Figure 3 Semblance analysis at (a) Section A (upstream of pier) (b) Section B (downstream of pier) and (c) Section D (dune like bedform) for 15% seepage case

# Appendix C

## Experimental results of scour depth and dune geometry around single bridge pier

| Sr. No | Pier Dia(mm) | $\sigma_g$ | Q ($m^3/s$) | Seepage% | $H_D$ (mm) | $X_D$ (m) | ds/D |
|---|---|---|---|---|---|---|---|
| 1 | 75 | 1.65 | 0.032 | 0 | 16.65 | 0.65 | 0.78373 |
| 2 | 75 | 1.65 | | 0.1 | 23.42 | 0.59 | 0.5616 |
| 3 | 75 | 1.65 | | 0.15 | 26.39 | 0.49 | 0.46813 |
| 4 | 75 | 1.65 | 0.034 | 0 | 23.88 | 0.75 | 0.92333 |
| 5 | 75 | 1.65 | | 0.1 | 27.97 | 0.69 | 0.82827 |
| 6 | 75 | 1.65 | | 0.15 | 31.59 | 0.59 | 0.75587 |
| 7 | 75 | 1.65 | 0.036 | 0 | 27.92 | 1.09 | 1.03493 |
| 8 | 75 | 1.65 | | 0.1 | 32 | 0.85 | 0.9444 |
| 9 | 75 | 1.65 | | 0.15 | 35.46 | 0.65 | 0.8848 |
| 10 | 75 | 1.65 | 0.038 | 0 | 30.12 | 1.3 | 1.17 |
| 11 | 75 | 1.65 | | 0.1 | 34.5 | 1.15 | 1.0464 |
| 12 | 75 | 1.65 | | 0.15 | 38.79 | 0.93 | 0.94787 |
| 13 | 75 | 1.65 | 0.04 | 0 | 32.29 | 1.2 | 1.20347 |
| 14 | 75 | 1.65 | | 0.1 | 34.98 | 1.12 | 1.17613 |
| 15 | 75 | 1.65 | | 0.15 | 36.95 | 1.06 | 1.08453 |
| 16 | 90 | 1.65 | 0.032 | 0 | 20.52 | 0.68 | 0.69778 |
| 17 | 90 | 1.65 | | 0.1 | 24.85 | 0.61 | 0.59522 |
| 18 | 90 | 1.65 | | 0.15 | 29.65 | 0.53 | 0.48844 |
| 19 | 90 | 1.65 | 0.034 | 0 | 26.36 | 0.8 | 0.86278 |
| 20 | 90 | 1.65 | | 0.1 | 30.36 | 0.7 | 0.75967 |
| 21 | 90 | 1.65 | | 0.15 | 35.02 | 0.63 | 0.67389 |
| 22 | 90 | 1.65 | 0.036 | 0 | 26.77 | 0.96 | 0.91756 |
| 23 | 90 | 1.65 | | 0.1 | 30.5 | 0.72 | 0.84133 |
| 24 | 90 | 1.65 | | 0.15 | 33.39 | 0.6 | 0.76211 |
| 25 | 90 | 1.65 | 0.038 | 0 | 28.01 | 1.38 | 1.00889 |
| 26 | 90 | 1.65 | | 0.1 | 33.26 | 1.27 | 0.91811 |
| 27 | 90 | 1.65 | | 0.15 | 37.2 | 1.02 | 0.84822 |
| 28 | 90 | 1.65 | 0.04 | 0 | 30.97 | 1.26 | 1.11878 |
| 29 | 90 | 1.65 | | 0.1 | 35.56 | 1.18 | 1.03478 |
| 30 | 90 | 1.65 | | 0.15 | 38 | 1.12 | 0.96844 |
| 31 | 75 | 1.85 | 0.032 | 0 | 14.03 | 0.52 | 0.66813 |

| | | | | | | | |
|---|---|---|---|---|---|---|---|
| 32 | 75 | 1.85 | | 0.1 | 20.75 | 0.44 | 0.5156 |
| 33 | 75 | 1.85 | | 0.15 | 24.32 | 0.32 | 0.40693 |
| 34 | 75 | 1.85 | 0.034 | 0 | 21.96 | 0.72 | 0.79147 |
| 35 | 75 | 1.85 | | 0.1 | 25.69 | 0.6 | 0.6104 |
| 36 | 75 | 1.85 | | 0.15 | 28.13 | 0.48 | 0.48093 |
| 37 | 75 | 1.85 | 0.036 | 0 | 23.89 | 0.9 | 0.90707 |
| 38 | 75 | 1.85 | | 0.1 | 27.16 | 0.78 | 0.76867 |
| 39 | 75 | 1.85 | | 0.15 | 30.87 | 0.62 | 0.64133 |
| 40 | 75 | 1.85 | 0.038 | 0 | 24.94 | 0.99 | 1.01493 |
| 41 | 75 | 1.85 | | 0.1 | 29.92 | 0.82 | 0.89587 |
| 42 | 75 | 1.85 | | 0.15 | 32.69 | 0.7 | 0.79147 |
| 43 | 75 | 1.85 | 0.04 | 0 | 26.5 | 1.12 | 1.1592 |
| 44 | 75 | 1.85 | | 0.1 | 30.79 | 0.89 | 0.9756 |
| 45 | 75 | 1.85 | | 0.15 | 34.39 | 0.75 | 0.81027 |
| 46 | 90 | 1.85 | 0.032 | 0 | 18.77 | 0.55 | 0.61233 |
| 47 | 90 | 1.85 | | 0.1 | 23.17 | 0.49 | 0.50389 |
| 48 | 90 | 1.85 | | 0.15 | 27.89 | 0.38 | 0.40578 |
| 49 | 90 | 1.85 | 0.034 | 0 | 22.45 | 0.74 | 0.69978 |
| 50 | 90 | 1.85 | | 0.1 | 26.17 | 0.62 | 0.58111 |
| 51 | 90 | 1.85 | | 0.15 | 30.3 | 0.48 | 0.47922 |
| 52 | 90 | 1.85 | 0.036 | 0 | 25.56 | 0.93 | 0.77911 |
| 53 | 90 | 1.85 | | 0.1 | 29.31 | 0.69 | 0.67856 |
| 54 | 90 | 1.85 | | 0.15 | 32.79 | 0.54 | 0.61467 |
| 55 | 90 | 1.85 | 0.038 | 0 | 27.04 | 0.98 | 0.88856 |
| 56 | 90 | 1.85 | | 0.1 | 30.62 | 0.8 | 0.7469 |
| 57 | 90 | 1.85 | | 0.15 | 34.48 | 0.64 | 0.69244 |
| 58 | 90 | 1.85 | 0.04 | 0 | 28.35 | 1.02 | 0.966 |
| 59 | 90 | 1.85 | | 0.1 | 33.07 | 0.81 | 0.813 |
| 60 | 90 | 1.85 | | 0.15 | 36.93 | 0.69 | 0.67522 |